(2)

NASA-CR-159640

COST ITEM $13.00

DO NOT DESTROY
RETURN TO LIBRARY

NASA CR-159640
ERR-FW-2014

EXPERIMENTAL INVESTIGATION OF A 0.15-SCALE MODEL OF A CONFORMAL VARIABLE-RAMP INLET FOR THE F-16 AIRPLANE

by J. E. Hawkins

GENERAL DYNAMICS
Fort Worth Division

14 OCT 1981
MCDONNELL DOUGLAS
RESEARCH & ENGINEERING LIBRARY
ST. LOUIS

prepared for

NATIONAL AERONAUTICS AND SPACE ADMINISTRATION

NASA Lewis Research Center

LM133933E

M80-16210

NASA CR-159640
ERR-FW-2014

EXPERIMENTAL INVESTIGATION OF A 0.15-SCALE MODEL OF A CONFORMAL VARIABLE-RAMP INLET FOR THE F-16 AIRPLANE

by J. E. Hawkins

GENERAL DYNAMICS
Fort Worth Division

prepared for

NATIONAL AERONAUTICS AND SPACE ADMINISTRATION

NASA Lewis Research Center

1. Report No.
NASA CR-159640

2. Government Accession No.

3. Recipient's Catalog No.

4. Title and Subtitle
Experimental Investigation of a 0.15-Scale Model of a Conformal Variable-Ramp Inlet for the F-16 Airplane

5. Report Date
March 1980

6. Performing Organization Code
-

7. Author(s)
J. E. Hawkins

8. Performing Organization Report No.

9. Performing Organization Name and Address
General Dynamics
Fort Worth Division, P. O. Box 748
Fort Worth, Texas 76101

10. Work Unit No.

11. Contract or Grant No.

12. Sponsoring Agency Name and Address
National Aeronautics and Space Administration
Washington, D. C. 20546

13. Type of Report and Period Covered
Contractor Report

14. Sponsoring Agency Code

15. Supplementary Notes
Final report. Project Manager, Robert W. Cubbison, Wind Tunnel and Flight Division, NASA Lewis Research Center, Cleveland, Ohio 44135

16. Abstract
A 0.15-scale model of a proposed conformal variable-ramp inlet for the F-16 Multirole Fighter was tested from Mach 0.8 to 2.2 at a wide range of angles of attack and sideslip. Inlet ramp angle was varied to optimize ramp angle as a function of engine airflow, Mach number, angle of attack, and angle of sideslip. Several inlet configuration options were investigated to study their effects on inlet operation and to establish the final flight configuration. These variations were cowl sidewall cutback, cowl lip bluntness, boundary-layer bleed, and first-ramp leading-edge shape. Diagnostic and engine-face instrumentation were used to evaluate inlet operation at various inlet stations and at the inlet/engine interface. Pressure recovery and stability of the inlet were satisfactory for the proposed application. On the basis of an engine stability audit of the worst-case instantaneous distortion patterns, no inlet/engine compatibility problems are expected for normal operations.

17. Key Words (Suggested by Author(s))
Air induction systems; Air inlets; Engine inlets; Inlet flow; Inlets; Intake systems; Pressure recovery; Supersonic inlets

18. Distribution Statement
Unclassified - Unlimited

19. Security Classif. (of this report)
Unclassified

20. Security Classif. (of this page)
Unclassified

21. No. of Pages
213

22. Price*

* For sale by the National Technical Information Service, Springfield, Virginia 22161

NASA-C-168 (Rev. 10-75)

FOREWORD

The author wishes to acknowledge the efforts of Mr. D. E. Banducci and Mr. G. E. Lovett of ARO, Inc., NASA Ames Division, who conducted the test; Mr. Dennis Sedlock of the Air Force Flight Dynamics Laboratory, who performed the screening of the dynamic inlet distortion data; and Mr. F. B. Thompson and Mr. L. A. Hayward of the Pratt & Whitney Aircraft Group, Government Products Division, who performed the engine stability audits.

Mr. David N. Bowditch, Chief of the Propulsion Aerodynamics Branch, Wind-Tunnel and Flight Test Division of the NASA Lewis Research Center, was instrumental in arranging for the required test time in the Ames 6- x 6-foot Wind Tunnel.

The requirements of NASA Policy Directive NPD 2220.4 regarding the use of SI Units have been waived in accordance with the provisions of paragraph 5d of that Directive by the Director of Lewis Research Center.

Page intentionally left blank

Page intentionally left blank

TABLE OF CONTENTS

TABLE OF CONTENTS (CONT'D)

SUMMARY

A 0.15-scale model of a proposed variable-ramp inlet configuration for the F-16 Multirole Fighter was tested in the NASA Ames 6- x 6-foot wind tunnel in August and September of 1977. This test was in support of a General Dynamics funded program to design, build, and flight test a prototype variable-geometry inlet configuration on the F-16 airplane. The test was sponsored by the NASA Lewis Research Center with the belief that the data would be relevant to the general field of inlet technology.

The purpose of the test was to: (1) substantiate a 2-ramp conformal inlet design concept; (2) establish a viable flight test configuration; and (3) obtain documentation of inlet total pressure recovery and distortion from Mach 0.8 to the inlet design Mach number of 2.2. These objectives were accomplished.

A forebody flow field survey was made at the beginning of the test to determine flow conditions at the inlet. At a free-stream Mach number of 2.2 with a nominal cruise angle of attack (α), local Mach number was found to be 0.07 higher than freestream. No other flow-field anomalies were found.

The performance of the final inlet test configuration, which was designated Conformal IIIB, was equal to or better than predicted. Inlet ramp angle was varied to optimize ramp angle as a function of engine airflow, Mach number, angle of attack, and angle of sideslip. On the basis of an engine stability audit of the worst-case instantaneous distortion patterns, no inlet/engine compatibility problems are expected for normal operations.

Several inlet configuration options were investigated to study their effects on inlet operation and to establish the final flight configuration. These variations were cowl sidewall cutback, cowl lip bluntness, boundary-layer bleed, and first-ramp leading-edge shape.

Cowl cutback provided an improvement in subcritical stability at some conditions, and a blunter cowl lip provided slightly improved performance at high angles of attack at subsonic speeds.

Inlet throat bleed equal to approximately 4% of design engine airflow at Mach 2.2 gave satisfactory inlet performance and stability. The proposed airplane bleed louver design provided the required bleed flow.

First-ramp leading-edge shape variation did not affect inlet performance, so the basic first-ramp design was selected for the flight configuration.

1. INTRODUCTION

The basic F-16 inlet is a fixed-geometry, normal-shock inlet designed for low cost, minimum complexity, and optimum performance in the subsonic-to-Mach 1.6 speed region. These design criteria have been realized in both prototype and production F-16 aircraft.

Advanced versions of the aircraft are being studied that place emphasis on airplane performance to Mach 2.2; therefore, a more sophisticated inlet type must be considered. A relatively simple double-ramp design with a variable second ramp will provide adequate pressure recovery to Mach 2.2 and can be incorporated on the airplane with only minor modifications to the existing aircraft.

Airplane integration has been enhanced and airplane drag and stability optimized by conformal shaping of the inlet. A candidate conformal design was evolved from design studies and force model tests that will minimize airplane drag and the effects on airplane lateral directional stability. With this design, a significant increase in supersonic capability can be realized without significantly affecting subsonic and transonic performance.

This report presents the results of a test in the NASA Ames 6- x 6-foot wind tunnel to substantiate the proposed conformal variable-ramp design. The test was conducted from 11 August 1977 to 21 September 1977 using a 0.15-scale model of the proposed inlet on the F-16A. This test was in support of a larger program, funded by General Dynamics, to design, build, and flight test a prototype configuration on an F-16A airplane. The overall purpose of the test was to select a viable flight test configuration from the model variations provided and to document its internal performance in terms of pressure recovery and distortion.

This test was performed with the support and under the auspices of the NASA/Lewis Research Center with the belief that the data would be relevant to the general field of inlet technology. The conformal inlet design is a modification to a more conventional two-dimensional configuration designed and tested by General Dynamics under contract with the Air Force Flight Dynamics Laboratory (Configuration A-3-3 of Reference 1).

Specific test objectives, which were successfully accomplished, were:

- Definition of the inlet flow field in terms of local Mach number, total pressure, and flow angularity.
- Evaluation of the effects of the first-ramp leading-edge sweep and selection of the optimum design.
- Evaluation of the effects of cowl sidewall cutback and cowl lip bluntness and selection of the optimum design.
- Evaluation of the effects of throat slot bleed and substantiation of the airplane bleed exit design.
- Documentation of the performance and stability characteristics of the selected flight test configuration and definition of the optimum second-ramp angle schedule as a function of Mach number, angle of attack, and engine corrected airflow.

The NASA Ames test designation was 260-1-66. Data were obtained at Mach 0.8, 1.3, 1.6, 2.0, and 2.2 at a Reynolds number of 1.5×10^6 per foot. Angle of attack was varied from -10° to $+30^\circ$ at Mach 0.8, -5° to $+25^\circ$ at Mach 1.3, and -2° to $+20^\circ$ at Mach 1.6, 2.0, and 2.2. Angle of sideslip was varied from 0° to 10° at Mach 0.8 and 1.3 and from 0° to 5° at Mach 1.6, 2.0, and 2.2. Approximately 1050 data points were recorded during 208 runs.

The first part of the test was devoted to a flow field survey; the second part to evaluating configuration variables with throat total pressure instrumentation; and the final part to performance documentation of the selected configuration without throat instrumentation. Performance documentation included the recording of time-variant (6700 Hz) engine-face total pressure data for use in inlet/engine compatibility assessment.

This report presents a complete summary and discussion of the steady-state test results as computed at NASA Ames during the test and the results of a subsequent analysis of the time-variant data for inlet/engine compatibility assessment.

Computed steady-state parameters include engine corrected airflow, inlet capture area ratio, total pressure recovery, various distortion parameters, turbulence index, and static- and total-pressure distributions.

The analysis of the time-variant data consisted of analog screening of the data to define the maximum instantaneous distortion values followed by an engine stability audit of selected points by the engine manufacturer.

Also included in this report are descriptions of the test facility, model, model instrumentation, and test procedure.

2. SYMBOLS

A	Area, in.^{2}
A_i	Inlet capture area (highlight area), in.^{2}
A_{oi}	Inlet captured flow area referenced to free-stream conditions, in.
BL	Buttock line, in.
℄	Centerline
ΔP_{t_2}	Maximum compressor-face total pressure minus minimum compressor-face total pressure
FS	Fuselage station, in.
K_{a2}	Pressure distortion factor for engine fan based on the 40 total-pressure probes at the compressor face (see Appendix C)
$K_{a2})_{limit}$	Instantaneous screening limit of fan distortion factor as defined by Pratt and Whitney Aircraft (see Appendix C)
K_{C_2}	Pressure distortion factor for the engine high compressor (see Appendix C)
$K_{C_2})_{limit}$	Instantaneous screening limit of engine high-compressor distortion factor as defined by Pratt and Whitney Aircraft (see Appendix C)
LE	Leading edge
M	Mach number
M_L	Local Mach number
M_o	Freestream Mach number
P	Static pressure
P_T	Total pressure

$P_{T_{BL}}$	Bleed cavity total pressure
P_{T_L}	Local total pressure
P_{T_0}	Freestream total pressure
$P_{T_{rms}}$	Average compressor-face turbulence (40-probe average)
$\bar{P}_{T_2}$	Average compressor-face total pressure (40-probe average)
T_{T_2}	Total temperature of airflow at compressor face, ^{o}R
W	Airflow, lbm/sec
WL	Waterline
W_{c2}	Full-scale engine corrected airflow, $W \sqrt{\theta_2} / \delta_2$, lbm/sec
W_{BL}	Inlet throat slot bleed flow, lbm/sec
W_2	Engine compressor-face airflow, lbm/sec
α (or ALPHA)	Angle of attack, degrees, measured between waterline plane and freestream direction. Positive α is nose up.
β (or BETA)	Angle of sideslip, degrees, measured between buttock-line plane and freestream direction. Positive β is nose left.
δ_2	Relative pressure at compressor face, $\bar{P}_{T_2}$ (psia)/14.696
θ_2	Relative temperature at compressor face, T_{T_2} (^{o}R)/518.7
θ_{R2}	Second-ramp angle relative to a waterline, deg.

3. TEST FACILITY

The test program was conducted in the NASA/Ames Research Center's 6- x 6-foot supersonic wind tunnel. This is a closed-circuit single-return tunnel. It has an asymmetric, continuously variable, sliding-block nozzle, and a test section with perforated floor and ceiling to permit transonic testing. An 8-stage axial-flow compressor driven by two electric motors provides airflow at Mach numbers from 0.55 to 2.2. Details of the tunnel test section are shown in Figure 3-1. The tunnel operating characteristics are given in Figure 3-2.

The facility also has schlieren and shadowgraph systems, which were utilized advantageously during the test.

4. MODEL DESCRIPTION

The test article was a 0.15-scale model of the General Dynamics F-16A modified to incorporate a variable-geometry inlet. The general arrangement of the model and its features are shown in Figures 4-1 through 4-5. The installation in the Ames 6- x 6-foot tunnel is shown in Figures 4-6, 4-7 and 4-8.

The model consists of a forebody, boundary-layer diverter, primary inlet, subsonic duct, engine compressor-face rake, and a remotely actuated throttle plug for the primary inlet. Airplane lines are simulated to Fuselage Station (FS) 242 externally and to the engine-face instrumentation plane at FS 358.22 internally. The lines for the F-16A forebody and for the diverter, inlet, and subsonic duct of the selected inlet configuration are given in Figures 4-9 through 4-13. The selected configuration has been designated as Conformal IIIB.

The proposed inlet is a 3-shock external-compression design with a fixed first ramp, a variable-angle second ramp, and a variable-angle subsonic duct ramp. The design of the inlet is based on that of the A-3-3 inlet configuration of Reference 1. The A-3-3 inlet, a conventional rectangular inlet, was modified into a curved cross-section for better integration with the airframe. The modified inlet conforms closely to the shape of the lower fuselage and blends smoothly into the existing airplane lines with an acceptable distribution of total cross-sectional area. Sections cut through the ramp surface are circular arcs with a common center on the airplane centerline (B.L.O.). The inlet sideplates are formed along radial lines through this center (Figure 4-10). The frontal profile of the cowl lip is a semi-elliptical shape, tangent to the sidewalls, with approximately the same lower contour as the fuselage profile into which it fairs.

The first ramp leading edge and the first-ramp/second-ramp intersection of the inlet were tailored to the cowl leading edge in the following manner:

(1) The flow was assumed two-dimensional along radial planes passing through the center of curvature of the frontal trace of the first-ramp leading edge.

(2) The first ramp and second ramp leading edges were then located to place the oblique shocks at the same position relative to the cowl lip as at B.L.0.

Two first-ramp configurations, shown in Figure 4-14, were evaluated during the test. The basic ramp design has a constant 6° wedge angle in all radial planes and a leading edge swept to place the oblique shock at a constant distance forward of the cowl lip, as described in the preceding paragraph. Sweeping the ramp leading-edge introduces three-dimensional effects into the flow, which increase the effective ramp angle and flow compression as the sweep angle increases. An alternate first ramp was designed, considering the effects of leading-edge sweep, in an attempt to provide a constant static pressure rise in all radial planes. To accomplish this, the wedge angle of the alternate ramp decreased in the outward direction as leading-edge sweep increased. Also, the leading-edge sweep of the alternate ramp was made less than that of the basic ramp, as shown in Figure 4-14.

The variable second ramp and the subsonic duct ramp are mechanically linked together in a fixed geometric relationship and are positioned by a single actuator in the proposed flight configuration. This relationship between the second ramp and subsonic duct was maintained in the test model. On the model, variation of the second-ramp angle was produced by wedge-shaped blocks placed under the ramps (Figure 4-5). Blocks were provided for second-ramp angles (θ_{R2}) of 4°, 6°, 8°, 10°, 12°, 14°, 16°, 17°, 18°, 18.8°, and 20°.

Four cowl lip variations were evaluated during the test by means of interchangeable cowl lip inserts (Figures 4-1 and 4-5). The four designs are shown in Figure 4-15. Two degrees of lip bluntness were evaluated, and each of these designs was tested with a basic and a cutback cowl profile. The purpose of the blunter lip was to reduce the possibility of lip flow separation at high angles of attack at subsonic speeds. The purpose of the cutback cowl profile was to increase the subcritical stable range of the inlet by allowing corner spillage at low airflows, thereby reducing the forward movement of the normal shock ahead of the cowl lip.

Inlet ramp boundary-layer control is provided by boundary-layer removal through a slot at the inlet throat between the trailing edge of the second ramp and leading edge of the subsonic duct ramp. Two methods of metering the boundary-layer bleed were provided. During the diagnostic phase of testing, the bleed air was discharged through orifice plates at the base of the model diverter (Figure 4-1) to provide an accurate measurement of bleed rate. Design bleed rates of 0, 2.5, and 5% of total engine airflow were provided by this method. During the documentation test phase, the boundary-layer bleed air was discharged through low-angle louver-type flush exits on either side of the nacelle. The location of the louvers is shown in Figures 4-1 and 4-3; louver detail is given in Figure 4-16. These bleed exits simulated the proposed flight configuration and were tested to substantiate the design. The basic louver design exit area was 68 in.^{2}, full scale (34 in.^{2} per side). This was reduced approximately 25% to 50 in.^{2} for the selected configuration by closing off the aft set of louvers on the model.

A thin tension strut is located in the inlet near the throat at Buttock Line (BL) 0.00. Strut detail is given in Figure 4-17. The strut has a double-wedge cross-section swept forward toward the top to minimize blockage. All test runs were made with the strut in place as there was no evidence that it had any adverse effect on inlet flow quality.

The fiberglass subsonic duct consists of three sections with breaks at FS 196.3, 247.2, and 354.9. FS 243 is a manufacturing break in the F-16 inlet duct, and the lines for the variable ramp inlet aft of FS 243 are identical with the F-16A. The subsonic duct area distribution is given in Figure 4-18.

A compressor-face rake and remotely actuated mass flow plug attaches to the subsonic duct at FS 354.9. The calibrated flow plug provides a range of engine-face corrected airflows from 0 to approximately 255 lb/sec, full scale.

The model was tested with a measured diverter height of 0.48 in. (3.2 in. full scale), which is 12% greater than the flight-configuration design value of 2.86 in. At the model test conditions, this resulted in a model fuselage boundary-layer thickness to diverter-height ratio equal to that of the full-scale vehicle at approximately a 75,000-foot altitude.

Airplane environmental control system (ECS) air inlets are located on both sides of the model in the diverter at FS 215 (Figure 4-1). The airflow through these inlets was unmetered and ducted overboard.

The model was mounted to an auxiliary pitch and yaw mechanism provided by General Dynamics. This in turn was mounted to the 6- x 6-foot tunnel sting support (Figures 4-6, 4-7, and 4-8). The auxiliary pitch/yaw mechanism was set up to give a pitch (α) range of -2° to +33° and a yaw (β) range of -10° to +10°. The tunnel pitch mechanism was used to extend the angle-of-attack range from -2° to -10°. Additional model and model installation information can be found in Reference 2.

5. MODEL INSTRUMENTATION

The model was instrumented with steady-state and high-response static and total pressure instrumentation to determine inlet performance in terms of engine-face total pressure recovery and distortion and to provide static and total pressure surveys on the forebody, at the inlet throat, and at various stations throughout the inlet.

The location and type of model instrumentation used is shown in Figure 5-1. The upper part of Figure 5-1 shows the installation of the flow-field rake on the airplane forebody with the inlet and duct sections removed. The lower part of Figure 5-1 highlights the composite model instrumentation and gives reference to instrumentation details shown in Figures 5-2 through 5-9.

The 9-element cone-probe flow-field rake (Figure 5-1) was utilized to define the flow field near the inlet leading-edge station in terms of flow angularity, local Mach number, and total pressure recovery. The model nose probe (Figure 5-1) was similar to the production airplane nose probe but was modified slightly to incorporate a steady-state total pressure and high-response transducer to monitor tunnel total pressure and turbulence level.

A cowl lip total-pressure rake, shown in Figure 5-2, defines the oblique shock locations relative to the cowl lip at the outboard station shown. The rake was installed on the basic cowl only. Pressure data from this rake were obtained during Runs 11 through 27.

Three total-pressure probes were installed at the entrance to the bleed louvers on the left side of the model and three static pressure taps were installed externally (both sides) to provide a pressure ratio for measuring bleed flow rate (Figure 5-3).

Static pressure taps were installed on the first and second ramps (Figure 5-4) to provide complete measurements over the area of the ramp for both flow field and structural loads analyses.

The model throat-rake instrumentation (Figure 5-5) was used to define total pressure and distortion at the inlet throat plane. These rakes were removed for the performance documentation phase of the test.

Static pressure taps were located in the duct from the throat to the compressor face (Figure 5-6), on the diverter (Figure 5-7), and at the base of the diverter (Figure 5-7) for bleed-flow measurement during the early phase of the test. This bleed-flow measurement at the base of the diverter was believed to be more accurate than that obtained with the louvers because of the predictable flow coefficient (0.98) of the diverter orifice-plate exits. The louver bleed data were compared with the diverter bleed data to establish confidence in the louver bleed measurement.

Engine-face total-pressure recovery and distortion were determined from the 40-probe rake shown in Figure 5-8. The side-by-side high-response/steady-state probes were located on centroids of equal area, as shown in the figure. Kulite high-response differential transducers were mounted in the tips of the larger probes with a protective screen and a silicone sealer (RTV) coating to protect the pressure-sensitive element. The high-response data were acquired with a 0- to 6700 Hz minimum fidelity range, which corresponds to a frequency range from 0 to 1000 Hz for the full-scale inlet. The flow plug base pressures from which mass flow was determined are shown in Figure 5-9.

All steady-state pressures were measured with a scanivalve mounted to the model's mid-support beam. The scanivalve was furnished by the test facility. A maximum of 132 steady-state pressures could be measured at one time, which necessitated alternate hookups to measure all model pressures. The instrumentation schedule used, which can be correlated with the test log (Appendix A), is given in Figure 5-10.

The leads from the high-response transducers were routed from the model through the tunnel support strut to a High-Response Data Acquisition System (HRDAS) provided and operated by General Dynamics. These data were recorded on magnetic tape for post-test analysis to assess inlet/engine compatibility. In addition, the signal from each high-response transducer was connected to a true rms meter in the HRDAS and the measured rms value was transmitted to the tunnel's data system for normalizing and on-line printout. Also, an average compressor face rms value, obtained from a 40-channel rms-averaging circuit in the HRDAS, was transmitted to the tunnel's data system for normalizing and on-line printout. A complete description of the HRDAS is given in Reference 3.

Dual slideware linear potentiometers were used to provide position indication and servosystem feedback for both the auxiliary pitch and yaw system and the flow-plug unit.

The steady-state and rms pressure data were used to compute corrected airflows, capture area ratios, total pressure recovery, various distortion parameters, turbulence index, and static- and total-pressure distributions. Additional instrumentation and data reduction information can be found in References 2 and 3.

6. TEST PROCEDURE

The complete as-run test program is given in Appendix A. With the exception of Runs 1 through 4, the test was conducted at a nominal Reynolds number of 1.5×10^6 per foot. Runs 1 through 3 were made at Mach 1.6 and Run 4 at Mach 2.0 at a Reynolds number of 2.3×10^6 per foot. Unsatisfactory tunnel operation due to tunnel overheating was encountered at Mach 2.0 as well as at Mach 2.2 at this higher total pressure level. No further testing was attempted at these higher Reynolds number/Mach number combinations. Model blockage prevented tunnel operation at Mach 0.9 and 1.2 but satisfactory operation was achieved at Mach 0.8 and 1.3.

During the flow-field survey phase of the test (Runs 1 through 10), tunnel conditions were established and the model pitched through the angle-of-attack range at a constant sideslip angle. During the inlet test phase (Runs 11 through 208) the same procedure was followed with inlet airflow being varied at each model attitude setting. Data were taken at five to six throttle settings that varied engine corrected airflow from values greater than the design engine airflow to either the minimum engine airflow or the inlet stability limit. The inlet stability limit was determined for all α / β settings during the performance documentation phase of the test at Mach 1.6, 2.0, and 2.2. No stability limits were found for the subsonic and transonic test conditions.

In general, dynamic data were recorded at the nominal engine airflow during the configuration study phase of the test and for all data points during the performance documentation phase of the test. Approximately 30 seconds of dynamic data were recorded for each data point following the steady-state data scan.

At supersonic speeds, a shadowgraph of the inlet shock system projected on a ground-glass screen was used in evaluation of inlet operation during the test and in definition of the inlet stability limit. Schlieren photographs were taken for selected points during the configuration study phase of the test to provide a permanent flow visualization record.

7. RESULTS AND DISCUSSION

A summary and discussion of the test results are presented in the following subsections. The forebody flow-field characteristics are summarized; performance of the configuration selected for full-scale development is presented, including an assessment of inlet/engine compatibility; and the effects of the various configuration perturbations investigated are shown.

7.1 Flow-Field Characteristics

The results of the forebody flow-field survey, in terms of flow angularity, local Mach number and local total pressure recovery, are summarized in Figures 7-1 through 7-5. Data at angles of attack (α) of -2, +1, +10, and +20° at Mach 2.2 are shown in Figures 7-1 through 7-4, respectively. In each of these figures data are given at angles of sideslip (β) of 0° and 5°. Since the flow survey only covered the left side of the inlet face, leeward and windward data were obtained by testing at both positive and negative β. The flow survey results for Mach 1.6 and 2.0, at a nominal cruise α of +1° and 0° β, are summarized in Figure 7-5.

These data show that the average inlet-face local Mach number is about 0.07 Mach higher than freestream Mach number at Mach 2.2 and +1° α, but about the same as freestream Mach at Mach 1.6 and 2.0. The forebody lines provide for a slight re-expansion of the flow (about 1°) at +1° α and, therefore, a slightly higher Mach number might be predicted.

The total pressure loss due to the forebody is small at all α's, with the lowest pressures being along the airplane centerline and nearest the fuselage. Note that total pressure recoveries greater than unity were calculated for some probes. Cone-probe theory, rather than a calibration, was used in reducing the data, which possibly contributed to this anomaly.

Flow angularity is, as expected, highest away from the body centerline. A favorable effect of the forebody is the reduction of flow angularity at the inlet at positive α.

7.2 Selected Configuration - Steady-State Performance

The configuration selected for full-scale development and performance documentation, designated configuration Conformal IIIB, is described by Figures 4-10 through 4-13. Its steady-state performance characteristics are described in Subsections 7.2.1 through 7.2.8.

7.2.1 Effect of Airflow at $\beta = 0^\circ$

The effects of engine-face corrected airflow on inlet performance as a function of Mach number, α , and inlet second-ramp angle (θ_{R2}) at zero sideslip are shown in Figures 7-6 through 7-10. Performance is given in terms of average compressor-face total pressure recovery, average turbulence, max - min distortion, inlet capture area ratio, fan distortion index K_{a2}, and high-compressor distortion index K_{c2}.

At Mach 0.8 (Figure 7-6) the effects of airflow are small at all values of α with no evidence of inlet choking up to the maximum airflow tested (about 248 lb/sec). The effect of ramp angle change from 4° to 6° at $+1^\circ$, $+20^\circ$, and $+30^\circ \alpha$ is also small. The large value of K_{a2} at the lower airflows is a characteristic of the parameter and is not indicative of a high distortion level.

At Mach 1.3 (Figure 7-7) performance is about the same as at Mach 0.8. No significant effect of ramp angle variation from 4° to 8° is evident.

At Mach numbers 1.6, 2.0, and 2.2 (Figures 7-8, 7-9, and 7-10, respectively), the corrected airflow for critical inlet operation is a strong function of second-ramp angle and is reasonably well defined. Supercritical inlet operation is characterized by a sharp reduction in pressure recovery and an increase in turbulence and distortion. At these Mach numbers, the minimum airflow at which data were obtained represents the inlet low airflow-stability (buzz) limit. One important effect of increasing ramp angle at Mach 1.6 and above is to extend the stable range of the inlet to lower airflows. The minimum stable range exists at the highest Mach number. Positive α has a favorable effect on stable range and overall inlet performance.

The maximum ramp angle available during the test was 20°. It is possible that an increased stable range might have been obtained at Mach 2.2 with a slightly higher ramp angle.

These data show that for best matching of engine airflow requirements with the inlet operating characteristics, an inlet control system that positions the second-ramp angle as a function of Mach number and engine corrected airflow is required. The effect of angle of attack on optimum ramp angle at a given corrected airflow is not significant and, therefore, it would probably not be necessary to include α effects in scheduling ramp position.

7.2.2 Effect of Airflow at $\beta \neq 0^0$

The effect of airflow on inlet performance at 5^o and 10^o β at Mach 0.8 and 1.3 and at 5^o at Mach 1.6, 2.0, and 2.2 is shown in Figures 7-11 through 7-17. The data shown are for the ramp angle giving near-optimum performance at the design airflow for each Mach number. In each figure, α is an independent variable. These data show that the largest performance degradation with sideslip occurs at negative α. A reduced subcritical stable range also occurs at Mach 1.6 to 2.2 and at -2^o and $+1^o$ α. The effect of β is small at high α.

7.2.3 Effect of Angle of Attack (α)

The effect of α on inlet performance is summarized in Figure 7-18 for each of the test Mach numbers. These data are shown at the nominal design airflow and ramp angle, with α as an independent variable. The data show the degradation in inlet performance at low and negative α when coupled with β, particularly at Mach 2.0 and 2.2.

7.2.4 Bleed Characteristics

The inlet boundary-layer bleed system characteristics, in terms of bleed weight-flow ratio (W_{BL}/W_2) and bleed exit total pressure recovery, are presented in Figures 7-19 through 7-22. The effect of engine corrected airflow at $+1^o$ α for Mach 0.8, 1.3, 1.6, 2.0, and 2.2 is shown in Figure 7-19. Data are presented for each ramp angle tested at each Mach number. The effects of α, β, and Mach number are summarized in Figures 7-20, 7-21, and 7-22.

As shown in Figure 7-19, bleed flow increases with decreasing engine airflow particularly at supersonic Mach numbers because of the increase in throat static pressure and consequent increase in bleed exit total pressure recovery. The corrected airflow at which the inlet terminal shock moves forward of the bleed slot is characterized by a sharp increase in bleed flow ratio and bleed exit pressure recovery.

The effect of α (Figure 7-20) is generally to increase bleed flow. There is no significant effect of β (Figure 7-21).

The change in bleed flow ratio and pressure recovery with Mach number is summarized in Figure 7-22. These data are for $+1^{\circ}$ α , design airflow, and the selected ramp angle shown. Bleed flow ratio is less than 1% of engine airflow at Mach 0.8 and increases to about 4% at Mach 2.2.

7.2.5 Compressor-face Total Pressure Distribution

Compressor-face steady-state total pressure and turbulence distributions, as determined from the 40 compressor-face probes, are presented in Figures 7-23 through 7-27 for selected α and β at each test Mach number. The data are shown at the nominal design airflow and the selected ramp angle for each Mach number. Average pressure recovery and turbulence values are shown in the center of each map.

As would be expected from the data presented in Subsections 7.2.1, 7.2.2, and 7.2.3, the worst patterns are generated at low α coupled with β .

7.2.6 Throat Total-Pressure Distribution

Inlet throat total-pressure surveys were made for the Conformal IIIB configuration at Mach numbers 0.8, 1.6, 2.0, and 2.2. The survey stations are described in detail in Section 5. The data are summarized in Figures 7-28 through 7-31 and, as with the compressor-face maps, the data are shown for design airflow and ramp angle.

The throat survey data were obtained with the throat slot bleed exhausting through fixed orifices at the base of the model rather than through the nacelle louvers as during the performance documentation phase of the test. Comparable bleed rates were provided, however, so it is believed that the throat survey data are typical of what would have been obtained employing the louver bleed exhaust. The effect of the different bleed systems on inlet performance is discussed in Subsection 7.4.4.

The data show uniform pressure profiles at the throat at Mach 0.8 with the lowest energy air being closest to the ramp surface (A, C, G, and H rakes in Figure 7-28). A small amount of lower cowl lip flow separation is seen on the B rake at +30° α and 0° β and to a slightly greater extent at +25° α and 10° β .

At the supersonic Mach numbers (Figures 7-29, 7-30, and 7-31) a reasonably uniform total-pressure distribution is obtained with the lowest pressure recovery being measured next to the ramp surface. Slightly lower pressures are measured on the G and H rakes as the flow moves downstream in the duct and negotiates the expansion on the aft ramp and the adverse pressure gradient of the duct. Some indication of flow separation is given by the H rake at Mach 2.0 and +15° α (Figure 7-30) and at Mach 2.2 at all α's (Figure 7-31). At Mach 2.2 the profiles are less uniform than at Mach 1.6 and 2.0 with more effect of α and β being present.

One significant observation from these data is that high pressure recoveries are realized at the outboard corner of the inlet as well as at the centerline up to Mach 2.2. These high pressure recoveries could not be confidently predicted prior to the test.

7.2.7 Ramp and Duct Static Pressure Distribution

The steady-state static pressure distribution on the first and second ramps, aft ramp, and inlet sideplate are summarized in Figure 7-32. As in the preceding section, data are presented for design airflow and matching ramp angle at Mach numbers 0.8, 1.6, 2.0, and 2.2.

The forward ramps were instrumented with 3 rows (at BL 0, 11.33, and 22.0) of static pressures and the aft ramp with 2 rows (at BL 2.5 and 17.3) to evaluate both the stationwise and spanwise static pressure distributions on the compression surfaces and to provide loads data for structural design.

At Mach 1.6, 2.0, and 2.2, the stationwise static pressure distribution is about as predicted by plane-shock theory at low α . No significant spanwise pressure gradient is present such as might be generated by the ramp curvature and swept ramp leading edge. This further substantiates the simplified two-dimensional design approach used for the inlet design.

7.2.8 Schlieren Photographs

Inlet flow behavior at supersonic speeds was monitored visually during the test by projecting a shadowgraph image on a ground-glass screen placed in front of the tunnel Schlieren window. A permanent flow-visualization record was made by taking Schlieren still photographs at selected test conditions. The photographs presented in Figure 7-33 show the effect of α at design airflow and the effect of airflow at $+1^{\circ}\alpha$ at Mach 1.6, 2.0, and 2.2. Although the photographs are less than definitive, they do provide a gross inidcation that the inlet shock structure is well behaved for the conditions shown. The degree of movement of the normal shock forward of the cowl lip as airflow is reduced can also be determined.

7.3 Selected Configuration - Assessment of Inlet/Engine Compatibility

On the basis of the steady-state data already presented, certain test points were selected for analysis of the time-variant compressor-face data for an assessment of inlet/engine compatibility. The selected data were processed in accordance with the engine manufacturer's recommendations for determining the worst-case instantaneous distortion pattern utilizing the 40 time-variant compressor-face total-pressure readings. These procedures are described in Reference 3. This processing was performed by the AFFDL Internal Aerodynamics Group on their DYNADEC System. The criterion for determining the worst-case pattern is the Pratt and Whitney Aircraft (P&WA) fan distortion index K_{a2}. This index is a measure of the combined effect of radial and circumferential distortion on fan stability.

Seventy test conditions, listed in Figure 7-34, were processed on DYNADEC. The resulting worst-case patterns from 24 of these conditions were then submitted to P&WA for a comprehensive stability audit at selected altitudes. Figure 7-35 is a listing of the test parameters for these 24 patterns and the altitudes at which they were audited. The 24 patterns are given in Appendix B.

The stability audit results, which according to P&WA are accurate to approximately ±3%, are summarized in Figures 7-36 through 7-40. The stability-audit ground rules are given in Figure 7-41. Figure 7-36 shows the stall margin remaining for standard-day conditions at intermediate altitudes. Positive stall margins are shown for all conditions audited. At Mach 2.2 the effect of $5^{\circ}\beta$ is to reduce stall margin to near zero at $+1^{\circ}\ \alpha$.

Figure 7-37 shows stall margin remaining for a standard day at high-altitude conditions. Negative margins are predicted at Mach 0.8 at all α / β combinations and at Mach 1.3 at negative α and non-zero β conditions.

Stall margin remaining is plotted as a function of altitude in Figure 7-38 to better define the predicted altitude limit for positive stall margin at Mach 0.8.

The effect of ambient temperature on stall margin, shown in Figure 7-39, was also predicted. Atmospheres colder than standard significantly reduce the stall margin remaining at Mach 1.3 to 2.2 at the altitudes audited. The effect of a hot atmosphere also reduced stall margin at Mach 0.8. The effects of hot-day conditions were not determined at the other Mach numbers but previous stability audits for the basic F-16 inlet (Reference 4) show that hot-day conditions provide increased stall margin at supersonic speeds.

The stability audit results for the Conformal IIIB inlet, shown in Figure 7-40, were compared with audit results for the basic F-16 fixed geometry inlet at comparable flight conditions. In general, the two inlets are comparable in terms of fan stall margin remaining.

In summary, the stability audit results indicate that there are no F100(3)/F-16 compatibility problems unique to the variable-geometry inlet, but that areas of potential engine/inlet incompatibility exist for some cold day and high-altitude transonic operating conditions.

7.4 Effect of Configuration Variables

Several configuration variables were investigated early in the test to provide a firm basis for selecting a viable flight test configuration. The variables evaluated were cowl sidewall cutback, cowl lip bluntness, throat bleed, bleed exhaust, and first-ramp leading-edge shape. With the exception of cowl lip bluntness, the investigations were made at Mach 2.2. Lip bluntness effects were evaluated at Mach 0.8 and Mach 2.2.

The effects of these test variables on inlet performance are discussed in the following subsections.

7.4.1 Effect of Cowl Sidewall Cutback

The effect of cowl sidewall cutback on the selected inlet performance parameters and throat-pressure distribution at Mach 2.2 is shown in Figures 7-42 through 7-45. Cowl geometry is described in Figure 4-15. Figure 7-42 shows the effect of airflow for the basic and cutback cowls (basic lip) at -2° and $+1^\circ$ α. The cutback cowl had a greater subcritical stable range than the basic cowl at -2° α, but a smaller stable range at 1° α. Pressure recovery at cruise conditions (1° α and $W_{C2} = 162$ lb/sec) is slightly higher for the cutback cowl.

A comparison of throat total pressures for the two cowls (for design airflow) at $\alpha = -2^\circ$ and 1° is given in Figure 7-43. It was expected that the greatest effect of the more aft location of the normal shock produced by the cutback cowl would be reflected in the location of the slipline resulting from the intersection of the oblique and normal shocks, as indicated by throat rakes B, D, and F. At 1° α, a slightly improved throat pressure distribution is achieved with the cutback cowl on rakes B and D, but not on the other rakes.

The effects of sidewall cutback on the performance of the blunt-lip cowl are shown for $\alpha = 1^\circ$ in Figure 7-44. The cutback cowl provided only slightly better performance. Pressure distributions on the throat rakes for the two cowls are very similar, as is shown in Figure 7-45.

As indicated by the above discussion, the cutback and basic cowls had very similar characteristics. The cutback cowl was selected as the preferred configuration on the basis of its slight performance advantage at 1° α and on the test engineer's evaluation of inlet shock stability as shown on the shadowgraph screen during the test.

7.4.2 Effect of Cowl Lip Bluntness

The effect of cowl lip bluntness on inlet performance is shown in Figure 7-46 where the performance of the basic cutback cowl is compared with the blunt-lip cutback cowl. Basic and blunt lip geometry are given in Figure 4-15.

At Mach 2.2 the performance differences between the basic and blunt lips are small. Shadowgraph images showed that the blunt lip cowl is slightly more stable at subcritical airflow. The lower maximum capture-area ratio of the blunt-lip cowl is due to the larger inlet capture area, A_i. Similarly, at Mach 0.8 (Figure 7-46b) the effects of lip bluntness on compressor-face performance are small, with the blunt lip being slightly better. The blunt lip improves the throat pressure distribution at high α , as shown in Figure 7-47, but as noted above, the effects on compressor-face performance are small.

7.4.3 Effect of Throat Bleed

Throat bleed was varied to evaluate inlet performance at design bleed rates of 0, 2½%, and 5% of design engine airflow at Mach 2.2. The diverter base bleed exits shown in Figure 4-1 were utilized during these runs. The test results are summarized in Figures 7-48, 7-49, and 7-50. The actual bleed rates, 4.3% and 6.2% as shown in the figures, were greater than the design values.

Zero throat bleed resulted in unacceptable compressor-face performance (Figure 7-48) and possibly separated flow conditions in the inlet throat and on the aft ramp (Figure 7-49). Bleed rates of 4.3% and 6.2% show approximately equal performance, with the higher bleed rate providing a slightly better subcritical stability margin. The effect of α at design engine airflow is shown in Figure 7-50. The nominal bleed rates of 4.3% and 6.2% show approximately equal performance at all α 's.

On the basis of these data, the nominal bleed of 4.3% was used for the remainder of the test.

7.4.4 Evaluation of Airplane Bleed Exhaust Louvers

Flush nacelle louvers for discharge of the throat bleed air were tested and compared with the more accurately calibrated diverter bleed exits to substantiate the proposed airplane configuration. The first runs were made with a basic set of louvers designed to provide a bleed flow of 2½% of engine airflow. The bleed louvers were not calibrated and the bleed rate through the louvers is based on an estimated flow coefficient. As with the diverter bleed, measured bleed was higher than predicted. The estimated flow coefficient may have been too high. However, the bleed system pressure recovery was lower than that obtained with the diverter bleed system, leading to the conclusion that the actual bleed flow was higher. The louvers were subsequently modified (by reducing their flow area) to achieve approximately the same bleed pressure recovery as the selected diverter base bleed.

Performance of the basic and modified louvers is shown and compared with the diverter base bleed in Figures 7-51 and 7-52. Compressor-face pressure recovery, bleed-flow ratio, and bleed pressure recovery are presented as a function of engine corrected airflow in Figure 7-51 and as a function of α in Figure 7-52 ($\beta = 0^{\circ}$ and $\beta = -5^{\circ}$). It should be noted that the data for the modified louvers are with the throat rakes removed from the inlet, which could have a small favorable effect on compressor-face pressure recovery.

On the basis of these data and the performance data in Subsections 7.2 and 7.3, it was concluded that the modified louver configuration is a viable bleed exhaust system and is adequately sized.

7.4.5 Effect of Alternate First Ramp

A basic and alternate first ramp (Figure 4-14) were tested to determine the effects of ramp angle and leading-edge sweep on inlet performance. The results are summarized in Figures 7-53, 7-54, and 7-55. Figure 7-53 shows inlet performance as a function of engine corrected airflow; Figure 7-54 shows a comparison of throat total pressure distribution at design airflow; and Figure 7-55 shows a comparison of ramp static-pressure distribution at design airflow. All of these data are for Mach 2.2 and $+1^{\circ}$ α .

As can be seen from the data, there was no appreciable difference in performance between the two designs except for the greater stability range of the basic ramp. As a result, the basic ramp was chosen for the flight configuration.

8. CONCLUSIONS

The overall purpose of the test, to select and document the performance of a viable flight test configuration, was accomplished. Inlet performance, for the range of test conditions covered, was equal to or better than predicted. Specific conclusions drawn from analysis of the data are follows:

1. The measured forebody local Mach number ahead of the inlet, at nominal cruise α (1^{o}) at Mach 2.2, is approximately 0.07 higher than the inlet design Mach number of 2.2.

2. The selected inlet configuration, designated Conformal IIIB, is a viable flight test configuration and will provide performance equal to or better than the design goals. On the basis of an engine stability audit of worst-case instantaneous distortion patterns and a comparison with the F-16 fixed-geometry inlet, no inlet/engine compatibility problems are expected for normal inlet and engine operation.

3. Cowl sidewall cutback had a stabilizing effect on the inlet at subcritical airflows. The cutback allowed additional side spillage behind the terminal shock, lessening the forward movement of the shock at low airflows.

4. The cowl lip with increased bluntness improved the pressure distribution at the inlet throat at high angles of attack at subsonic speeds, but the effect on compressor-face performance was small.

5. Inlet throat bleed, approximately equal to 4% of design engine airflow at Mach 2.2, provides satisfactory inlet performance and stability. The airplane bleed louver design with 50 in.^{2} exit area will provide the required bleed flow.

6. The basic first-ramp design provided satisfactory inlet operation. An alternate design, with reduced leading-edge sweep, did not show any improvement in ramp pressure distribution or inlet performance and had a reduced range of stable airflow.

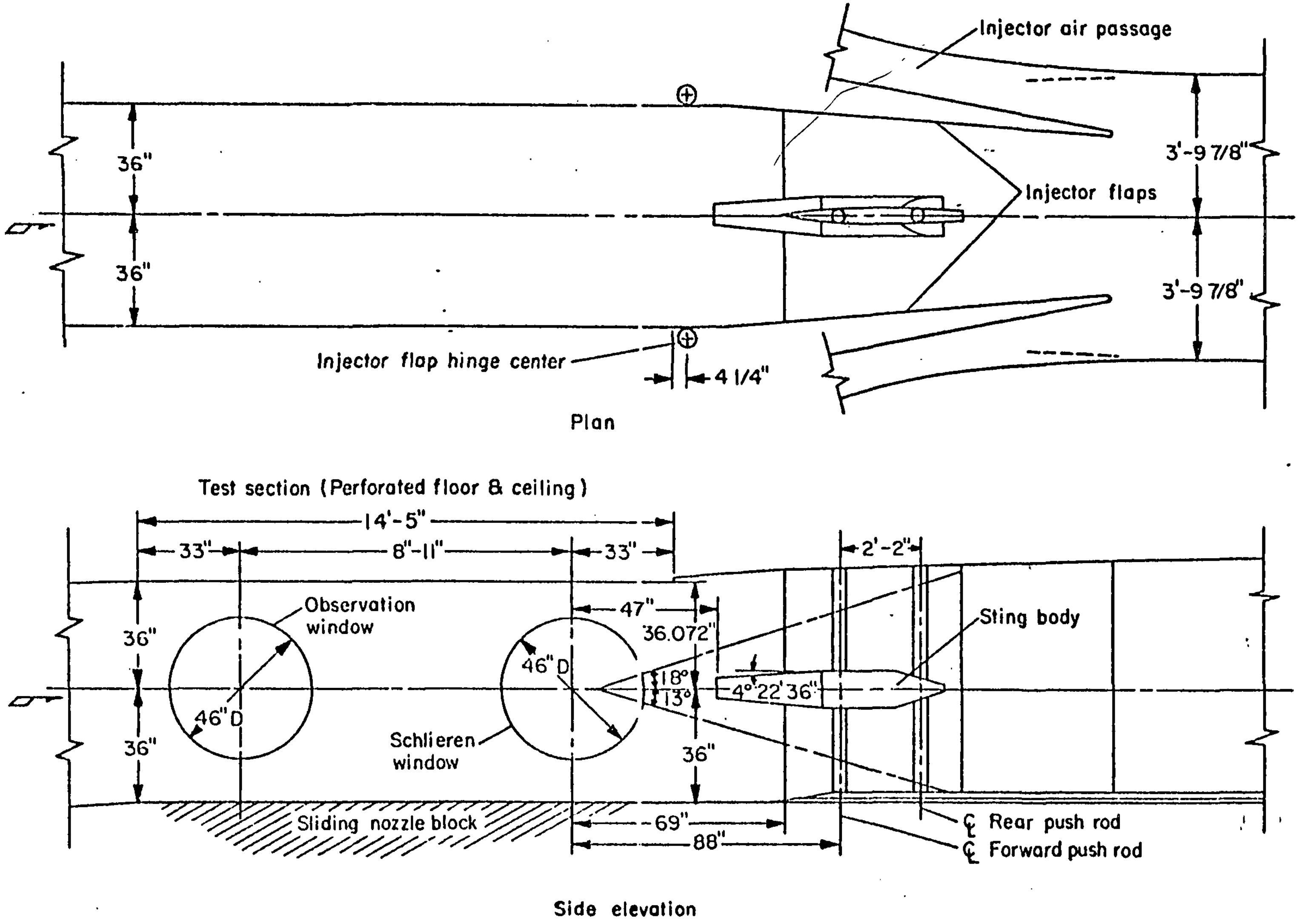

Figure 3-1 Ames 6- by 6-Foot Supersonic Wind Tunnel Test Section and Model-Support System Details

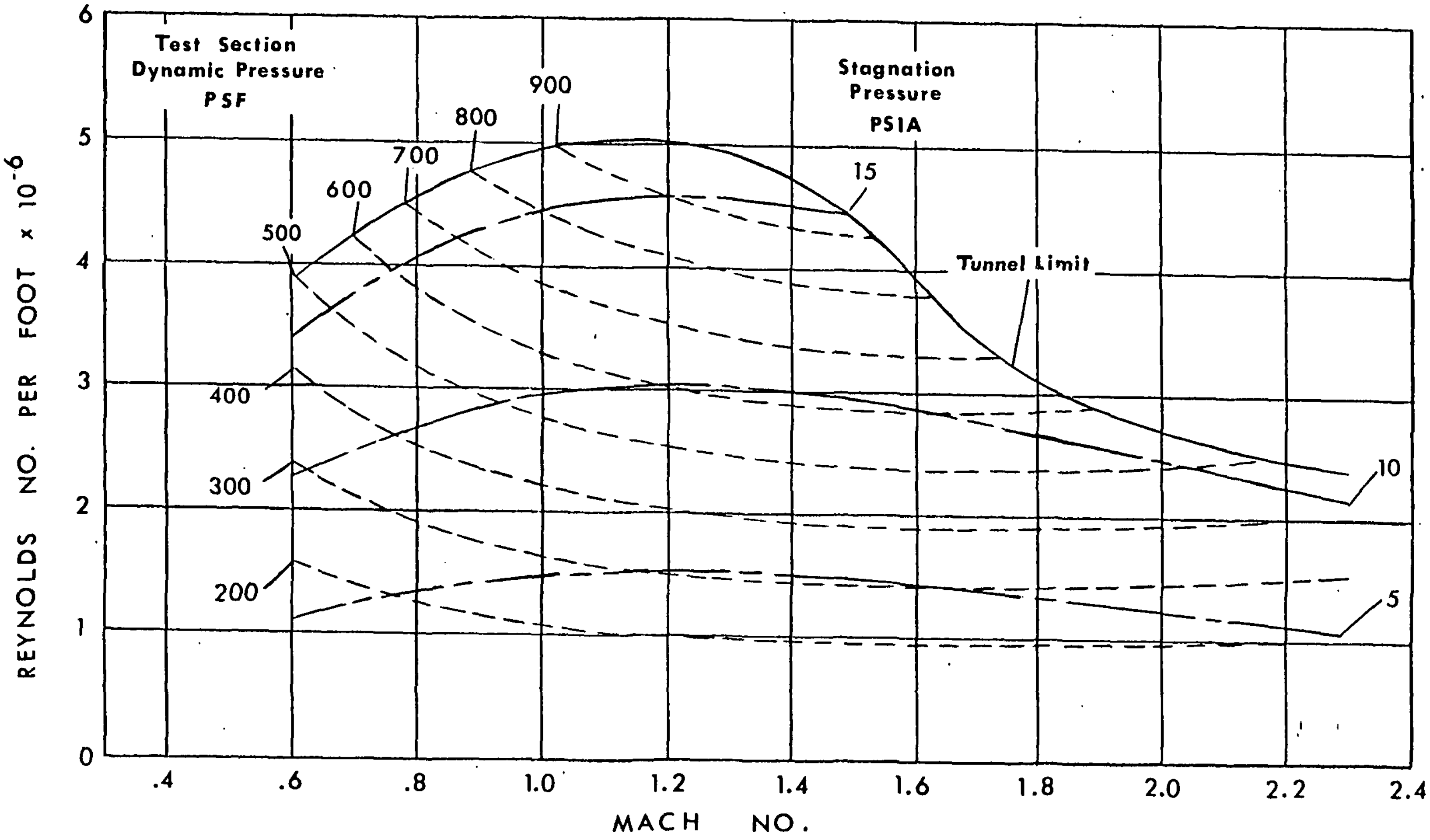

Figure 3-2 Operating Characteristics of the Ames 6- by 6-Foot Supersonic Wind Tunnel With Stagnation Temperature 560°R

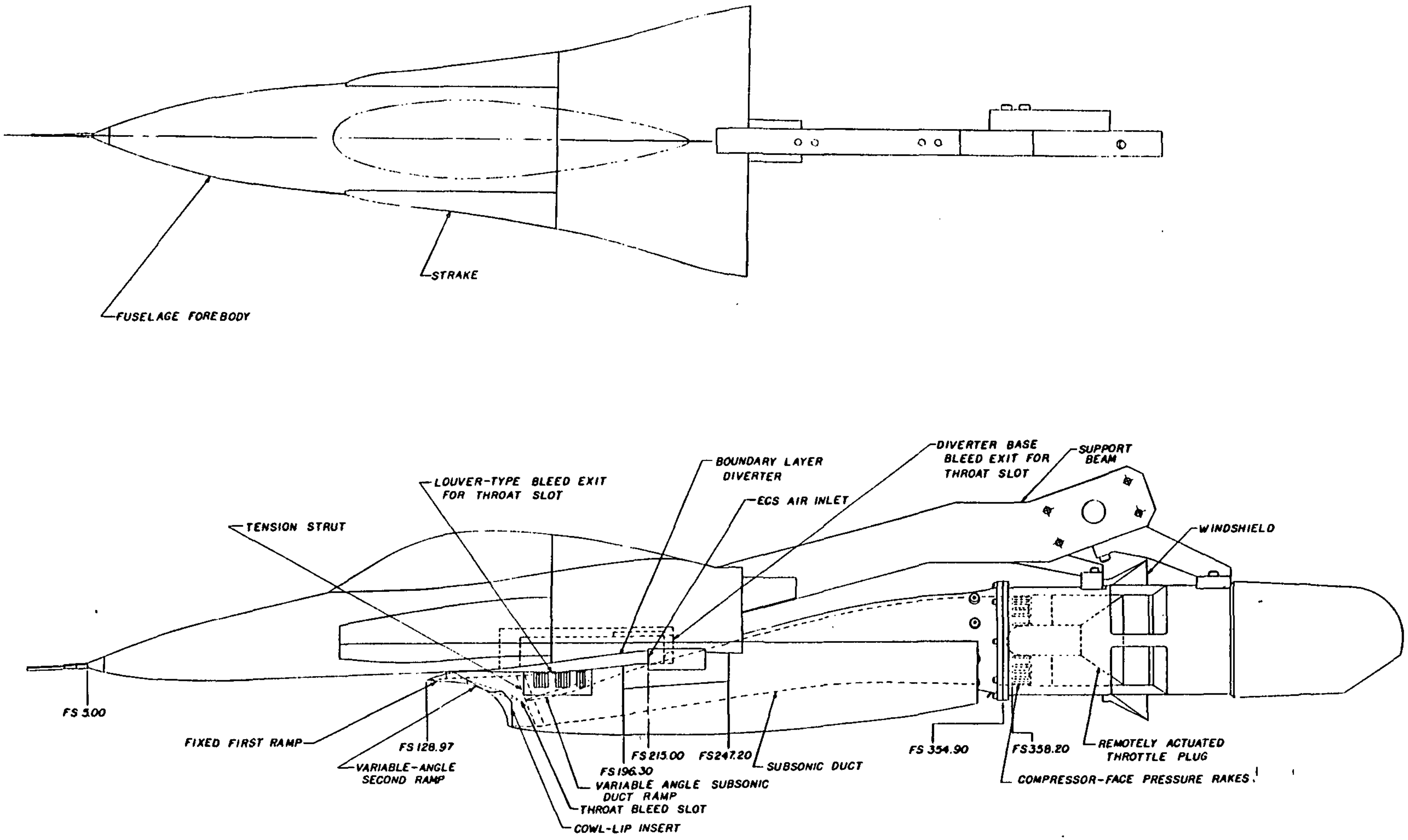

Figure 4-1 0.15-Scale Model General Arrangement

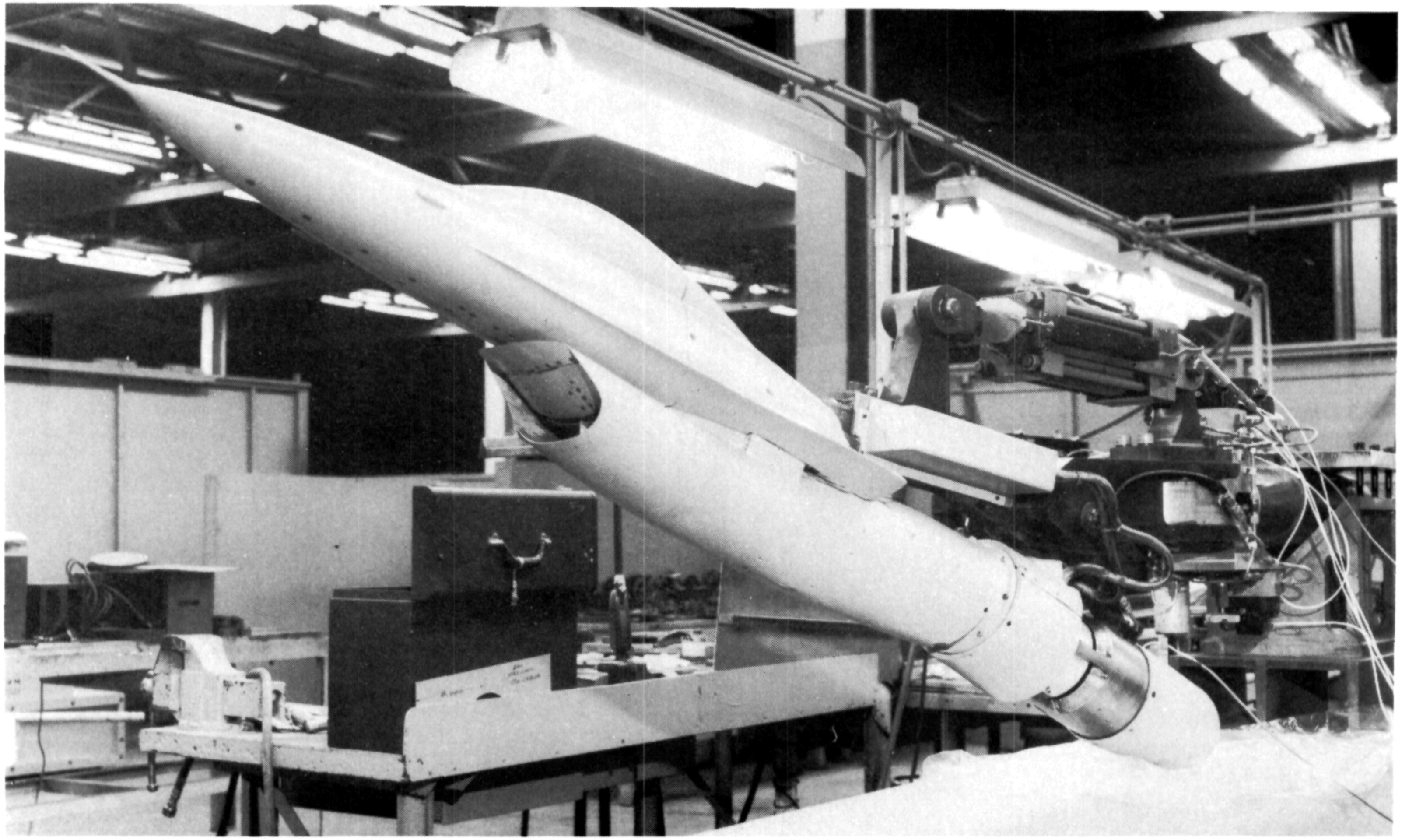

Figure 4-2 Assembled Model

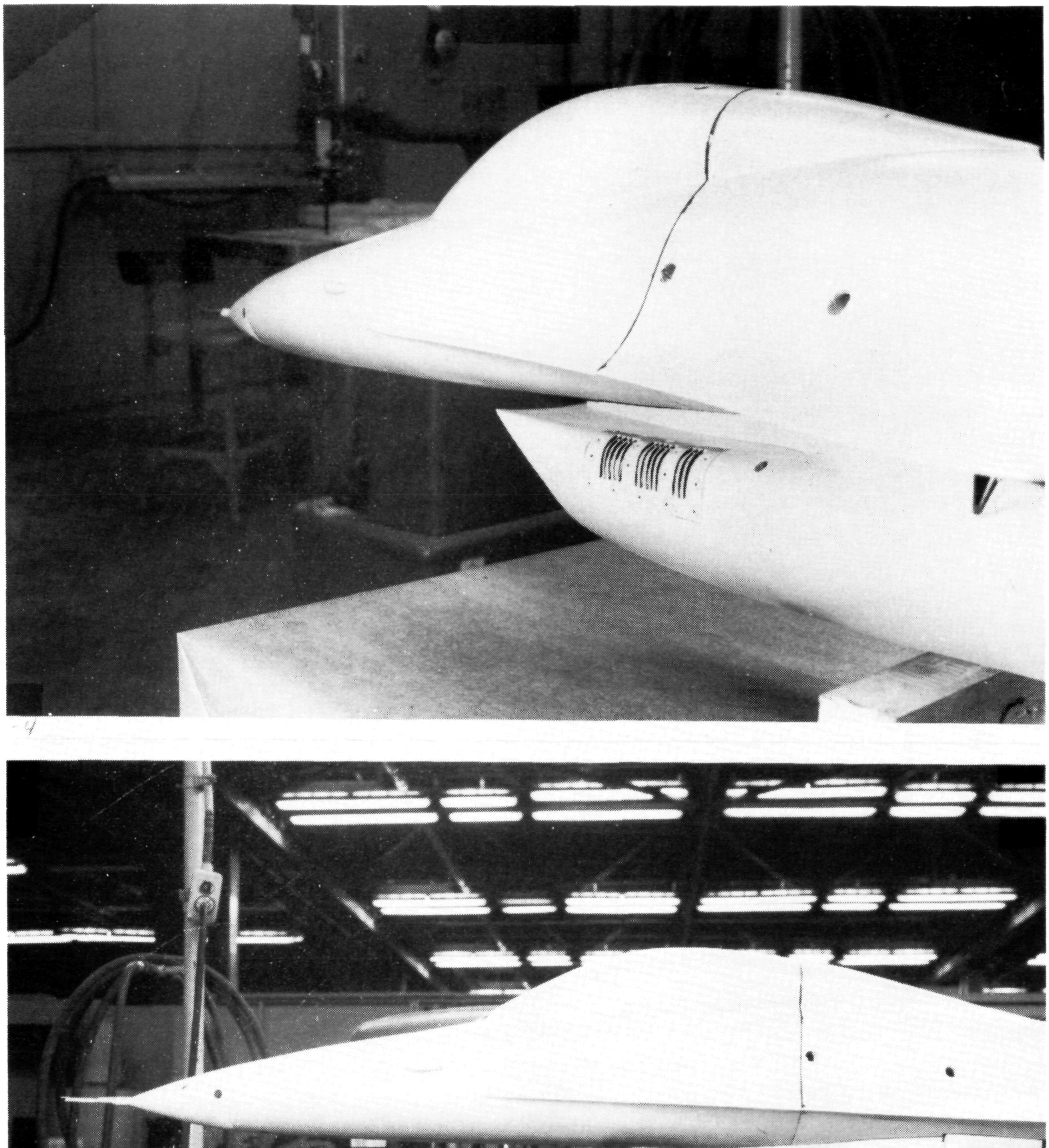

Figure 4-3 Bleed Louver and Diverter Installation

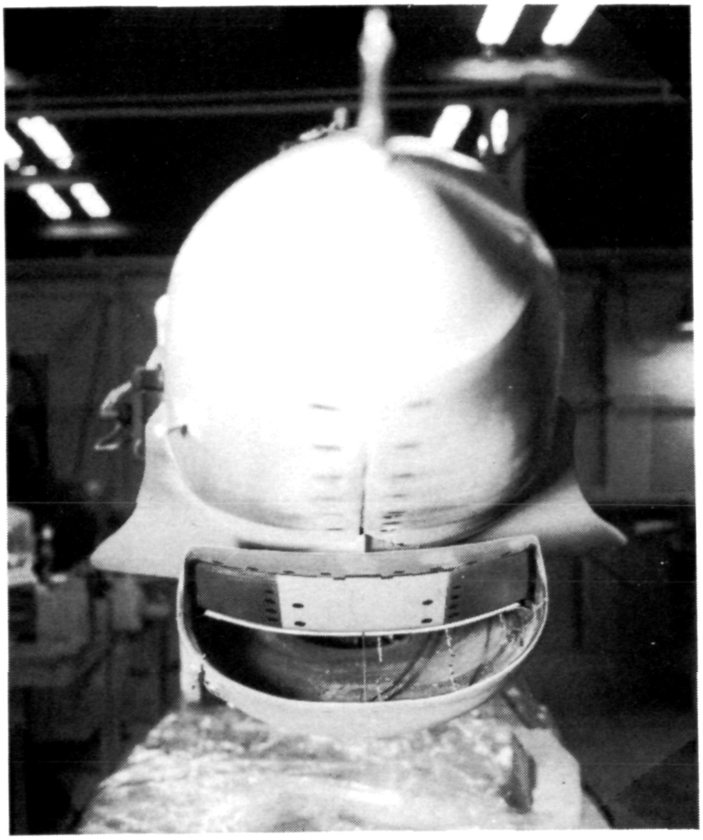

Figure 4-4 Inlet Detail Showing Throat Instrumentation

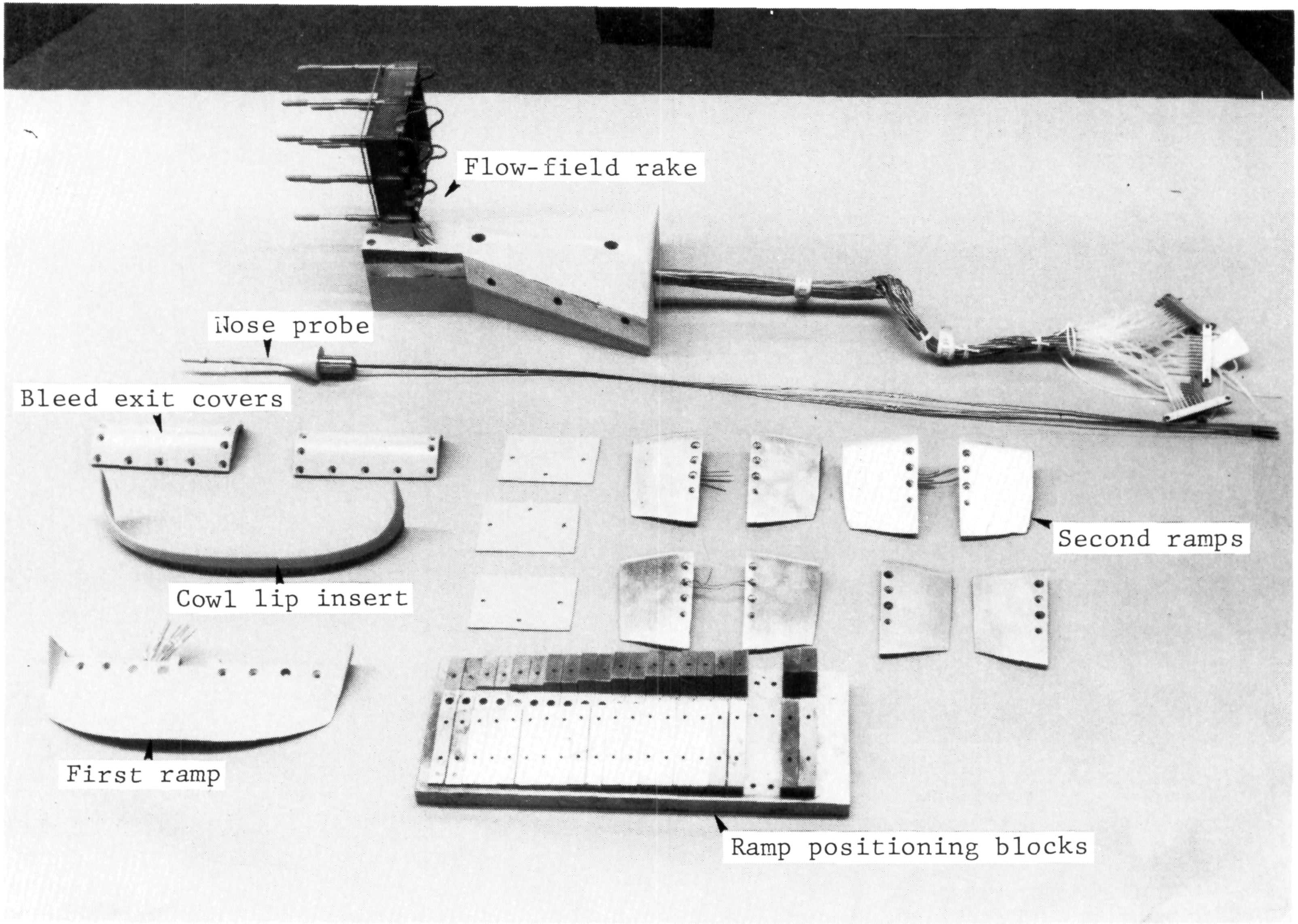

Figure 4-5 Inlet Components

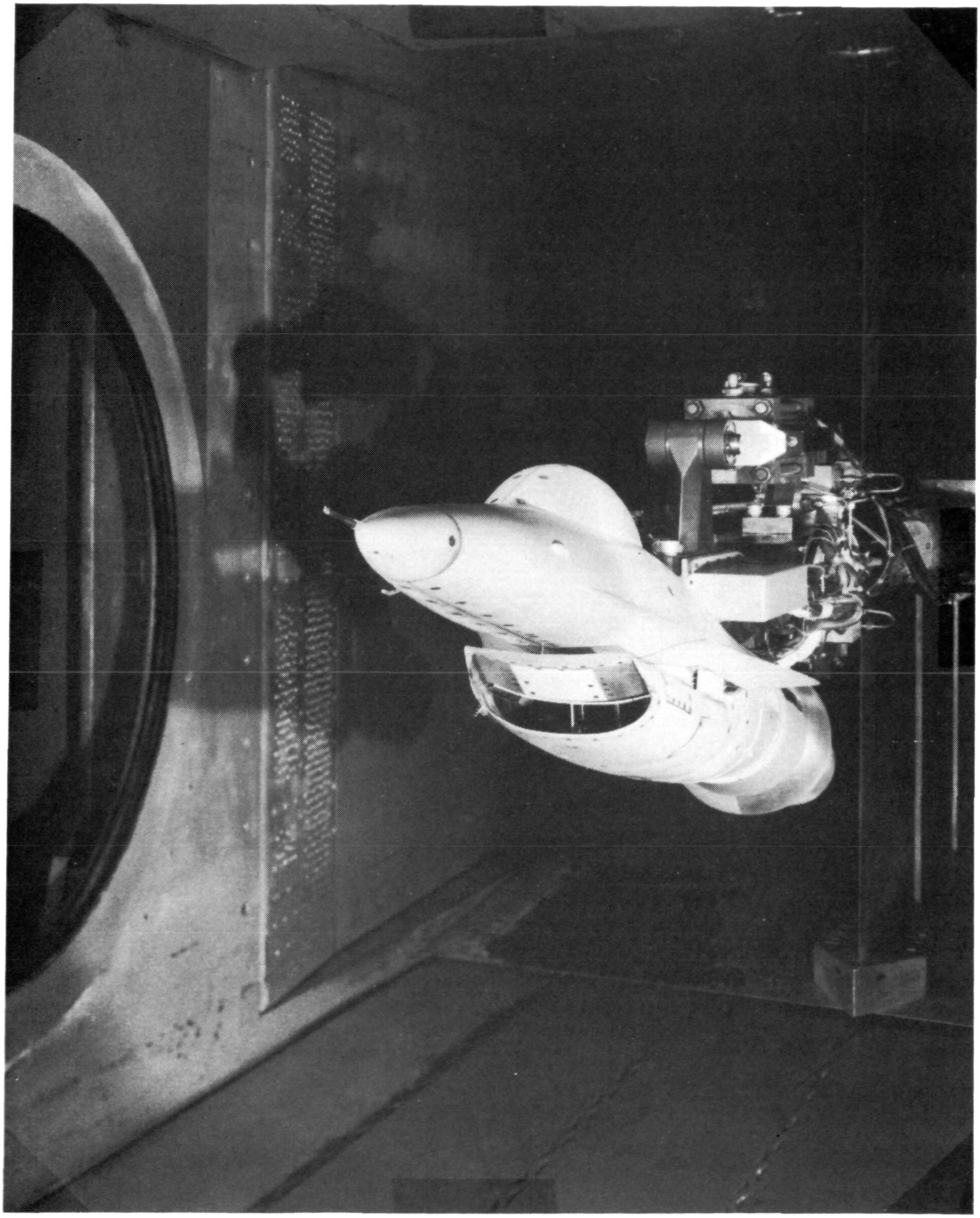

Figure 4-6 Model Installation - Front View

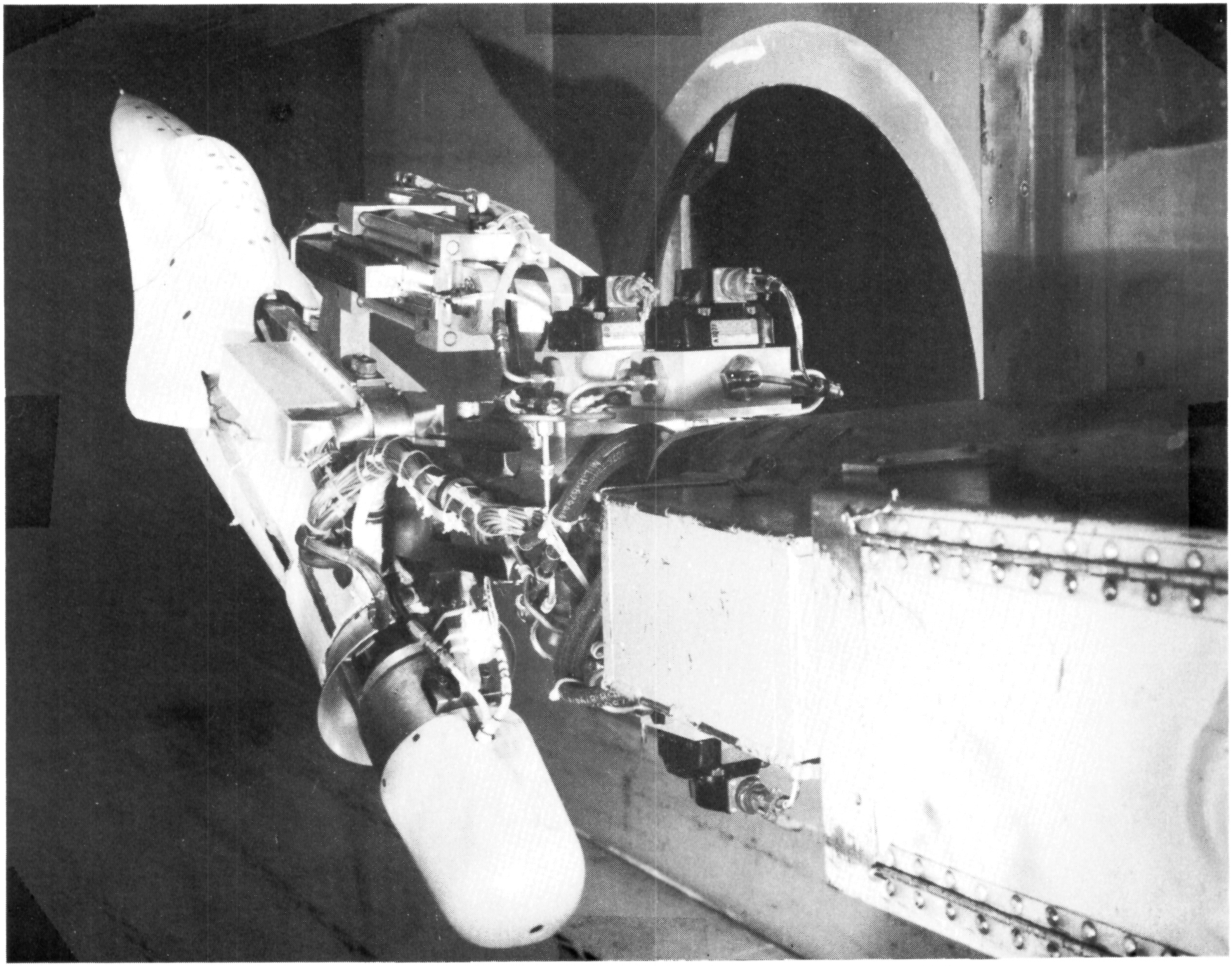

Figure 4-7 Model Installation - Rear View

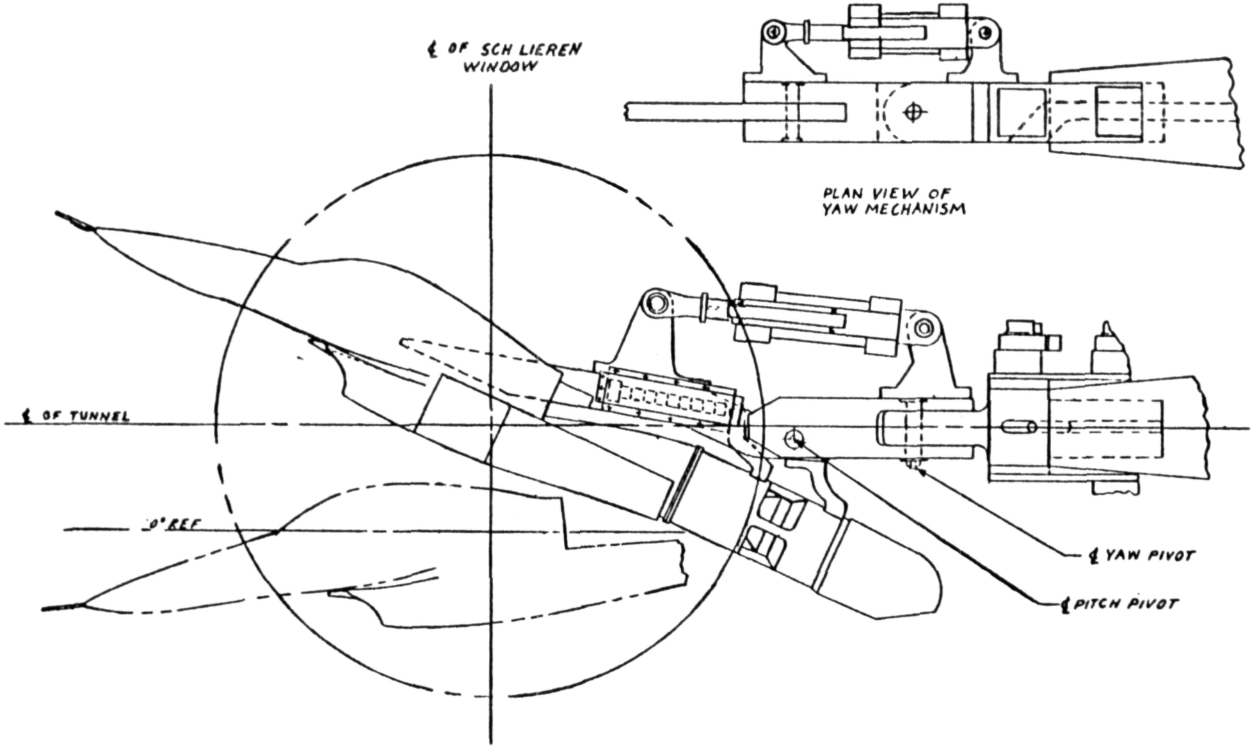

Figure 4-8 Tunnel Installation and Support System

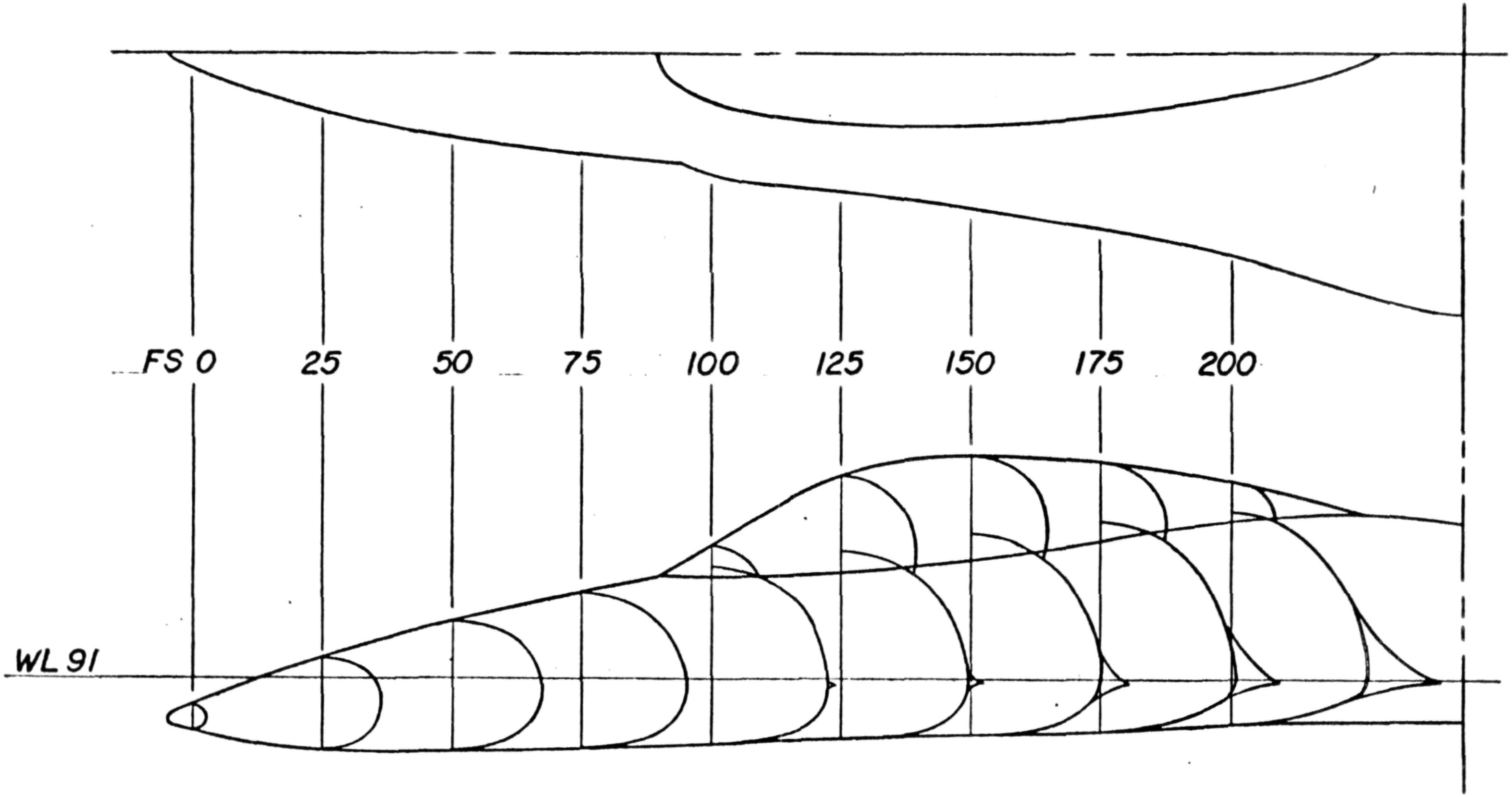

Figure 4-9 F-16A Forebody Lines

Figure 4-10 Conformal IIIB Inlet Leading Edge Lines

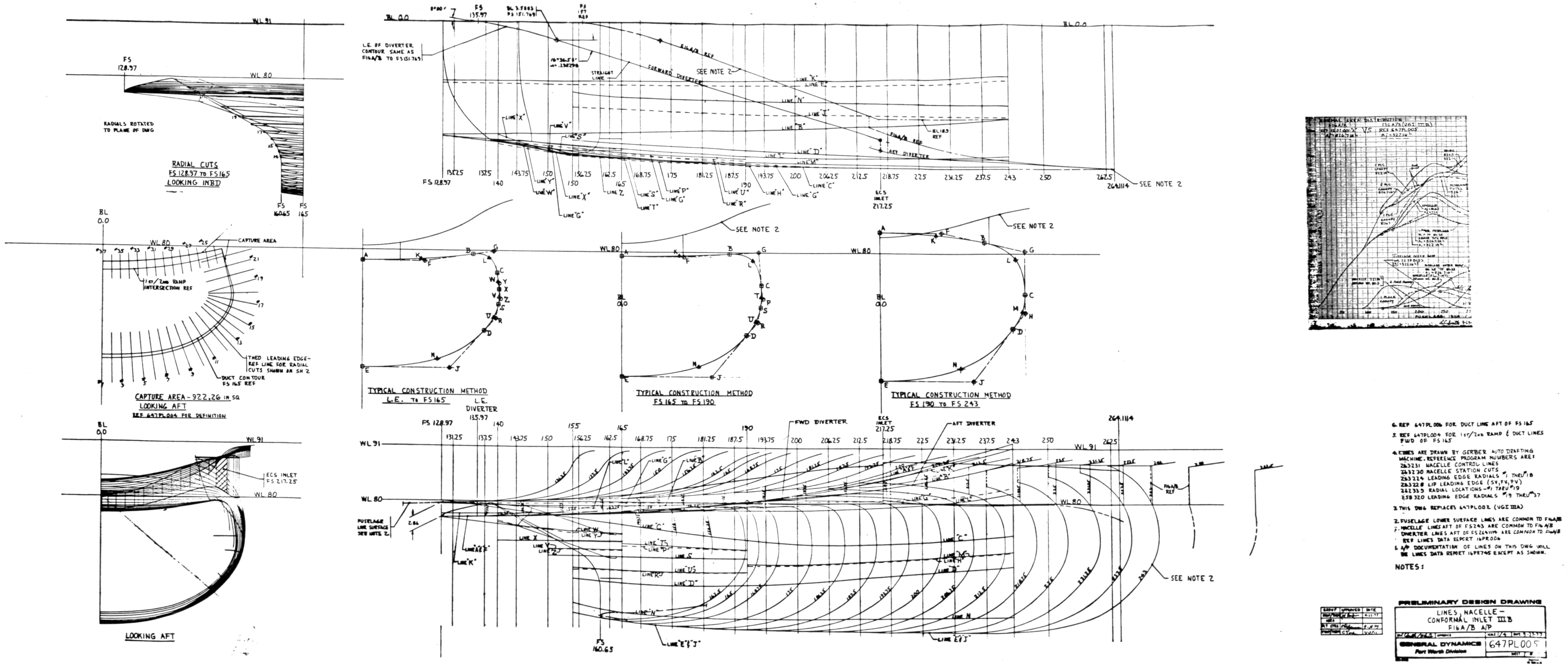

6. REF 647PL006 FOR DUCT LINE AFT OF FS 165
5. REF 647PL004 FOR 1ST/2ND RAMP & DUCT LINES FWD OF FS 165
4. LINES ARE DRAWN BY GERBER AUTO DRAFTING MACHINE. REFERENCE PROGRAM NUMBERS ARE:
   263231 NACELLE CONTROL LINES
   263230 NACELLE STATION CUTS
   263224 LEADING EDGE RADIALS #1 THRU #18
   263228 LIP LEADING EDGE (SV, FV, PV)
   262339 RADIAL LOCATIONS - #1 THRU #19
   258320 LEADING EDGE RADIALS #19 THRU #37
3. THIS DWG REPLACES 647PL002 (VGI IIIA)
2. FUSELAGE LOWER SURFACE LINES ARE COMMON TO F16A/B
   NACELLE LINES AFT OF FS243 ARE COMMON TO F16 A/B
   DIVERTER LINES AFT OF FS264.1114 ARE COMMON TO F16A/B
   REF LINES DATA REPORT 16PR006
1. A/P DOCUMENTATION OF LINES ON THIS DWG WILL BE LINES DATA REPORT 16PR745 EXCEPT AS SHOWN.

NOTES:

PRELIMINARY DESIGN DRAWING

LINES, NACELLE -
CONFORMAL INLET IIIB
F16A/B A/P

SCALE 1/4 DATE 5-27-77

GENERAL DYNAMICS
Fort Worth Division

647PL005

Figure 4-11 Conformal IIIB Nacelle Lines

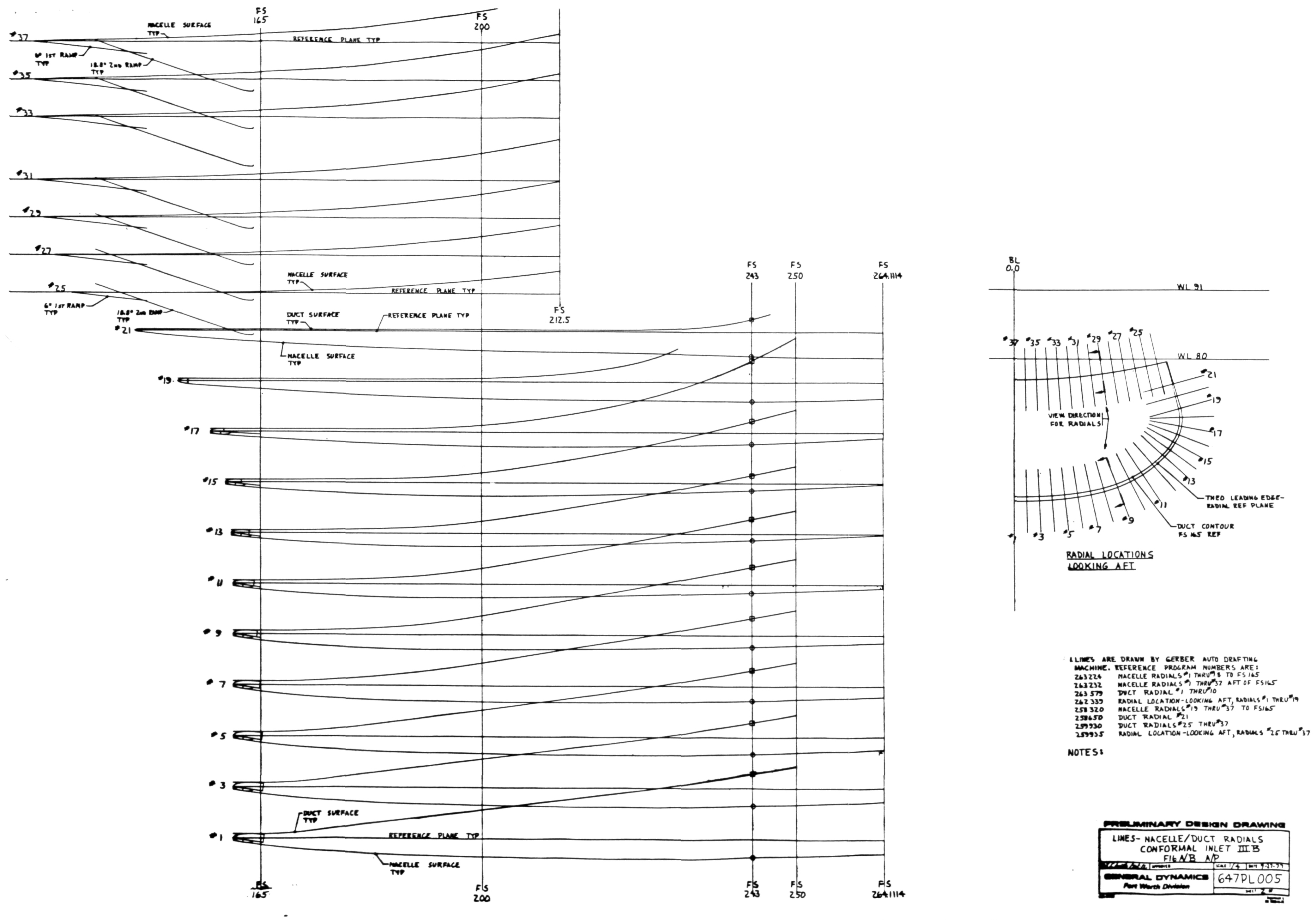

LINES ARE DRAWN BY GERBER AUTO DRAFTING MACHINE. REFERENCE PROGRAM NUMBERS ARE:

263224 NACELLE RADIALS #1 THRU #18 TO FS 165
263232 NACELLE RADIALS #1 THRU #37 AFT OF FS165
263579 DUCT RADIAL #1 THRU #10
262339 RADIAL LOCATION-LOOKING AFT, RADIALS #1 THRU #19
258320 NACELLE RADIALS #19 THRU #37 TO FS165
258650 DUCT RADIAL #21
259930 DUCT RADIALS #25 THRU #37
259935 RADIAL LOCATION-LOOKING AFT, RADIALS #25 THRU #37

NOTES:

PRELIMINARY DESIGN DRAWING
LINES- NACELLE/DUCT RADIALS
CONFORMAL INLET IIIB
F16 A/B A/P
SCALE 1/4 DATE 9-27-77
GENERAL DYNAMICS
Fort Worth Division
647PL005

Figure 4-12 Conformal IIIB Nacelle/Duct Radials

RHO VALUE DEFINITION

SEGMENT	ORIGIN	RHO VALUE	SLOPE TANGENT	TERMINATION	RHO VALUE	SLOPE TANGENT
1	FS 165	.74900	0.00	FS 237.5	.74900	0.00
2	FS 165	.705946	0.00	FS 243	.74011	0.00
3	FS 165	.74011	0.00	FS 243	.74011	0.00
4	FS 165	.74900	0.00	FS 243	.74900	0.00
5	FS 165	.70000	0.00100	FS 243	.74011	0.00
6	FS 169.8	.74610	0.00	FS 202.33	.74360	-.00012
7	FS 169.8	.74610	0.00	FS 202.33	.74360	-.00012
8	FS 202.33	.74360	-.00012	FS 243	.74011	0.00

2ND RAMP/AFT DIFFUSER MECHANISM DATA

REF PROGRAM ~ P25375C

2ND RAMP ANGLE	POINT "A" (2ND RAMP) FS	POINT "A" (2ND RAMP) WL	POINT "B" (AFT DIFFUSER) FS	POINT "B" (AFT DIFFUSER) WL
4°	165.68884	76.99847	165.01416	77.86727
5°	165.70626	76.62395	165.03273	77.49363
6°	165.71714	76.24918	165.05460	77.12726
7°	165.72148	75.87427	165.07962	76.76759
8°	165.71928	75.49935	165.10768	76.41365
9°	165.71053	75.12453	165.13873	76.06423
10°	165.69524	74.74991	165.17279	75.71792
11°	165.67341	74.37562	165.20996	75.37322
12°	165.64506	74.00176	165.25040	75.02852
13°	165.61019	73.62846	165.29433	74.68214
14°	165.56880	73.25582	165.34209	74.33221
15°	165.52092	72.88396	165.39410	73.97663
16°	165.46656	72.51300	165.45096	73.61289
17°	165.40573	72.14304	165.51348	73.23775
18°	165.33845	71.77419	165.58188	72.84670
18.8°	165.28000	71.48000	165.64460	72.51782
20°	165.18464	71.04031	165.75157	71.98296
20.8°	165.11596	70.74834	165.83797	71.57821

5. DUCT IS COMMON TO F16A/B FROM FS243 AFT
4. LINES ARE DRAWN BY GERBER AUTO DRAFTING MACHINE. REFERENCE PROGRAM NUMBERS ARE:

255778A	4° 2ND RAMP POSITION AIRFLOW DUCT SECTIONS
255782C	18.8° 2ND RAMP POSITION AIRFLOW DUCT SECTIONS
255781A	18.8° 2ND RAMP POSITION DUCT SECTIONS
255780B	4° 2ND RAMP POSITION DUCT SECTIONS
255773B	BASIC F16A/B FS243 AFT
255779B	CONTROL LINES FS165-FS243
250176B	CONTROL LINES FS130-FS165

3. THIS DWG REPLACES DUCT LINES DWG NR 647PL003
2. REF 647PL005 FOR NACELLE LINES.
1. REF 647PL004 FOR 1ST/2ND RAMP AND DUCT SURFACE FWD OF FS165.
NOTES:

PRELIMINARY DESIGN DRAWING

LINES - DUCT
CONFORMAL INLET IIIB
F16A/B A/P

GENERAL DYNAMICS
Fort Worth Division

647PL006

Figure 4-13 Conformal IIIB Duct Lines

1ST RAMP L.E. GEOMETRY			
BASIC	ALT	COMMON	
STA	STA	BL	WL
19.346	19.346	0	11.505
19.348	19.348	0.522	11.514
19.365	19.365	1.044	11.543
19.430	19.425	1.566	11.589
19.570	19.543	2.088	11.651
19.837	19.733	2.610	11.733
20.246	20.013	3.132	11.834
20.799	20.351	3.579	11.937

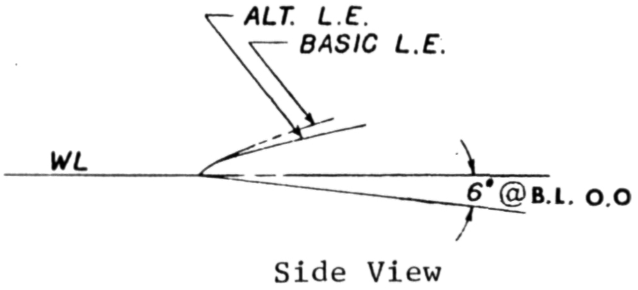

Side View

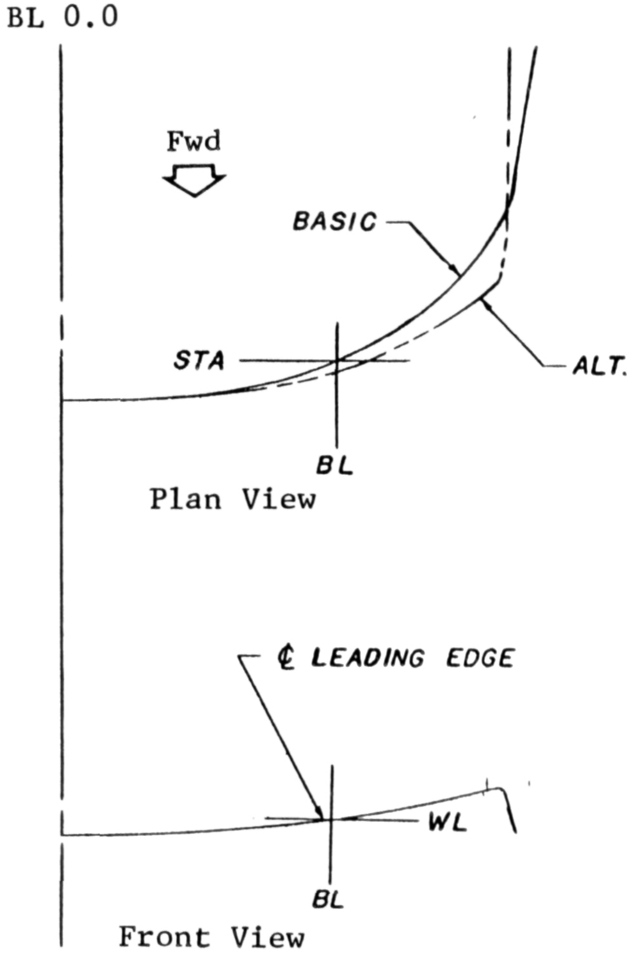

Plan View

Front View

Figure 4-14 Basic and Alternate First Ramp Leading-Edge Geometry

BASIC LIP GEOMETRY					
Radial	∠1	A	B	C	D
1	8.000°	.600	2.400	.400	1.600
2	↓	↓	↓	↓	↓
3					
4					
5					
6					
7					
8					
9					
10					
11					
12					
13	8.000°	.600	2.400		
14	7.505°	.594	2.374		
15	6.170°	.574	2.297		
16	4.272°	.542	2.169		
17	2.226°	.498	1.992		
18	0.613°	.442	1.768	.400	1.600
19	0.000°	.380	1.520	.380	1.520
22	0.000°	.060	.240	.130	0.520

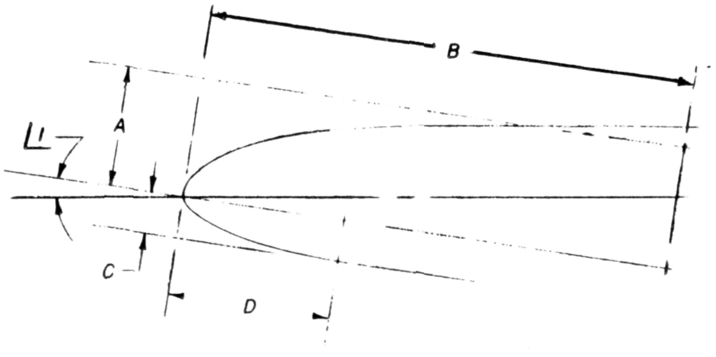

Section A-A (Typical)

BLUNT LIP GEOMETRY					
Radial	∠1	A	B	C	D
1	8.000°	1.200	4.800	0.400	1.600
2	↓	1.196	4.784	↓	↓
3		1.183	4.733		
4		1.162	4.647		
5		1.131	4.525		
6		1.092	4.366		
7		1.044	4.177		
8		0.992	3.967		
9		0.938	3.750		
10		0.883	3.530		
11		0.825	3.300		
12	8.000°	0.763	3.050		
13	7.505°	0.703	2.810		
14	7.000°	0.665	2.660		
15	6.125°	0.623	2.490		
16	4.875°	0.578	2.310		
17	3.225°	0.523	2.070		
18	1.000°	0.450	1.800	0.400	1.600
19	0.000°	0.380	1.520	0.380	1.520
22	0.000°	0.130	0.520	0.130	0.520

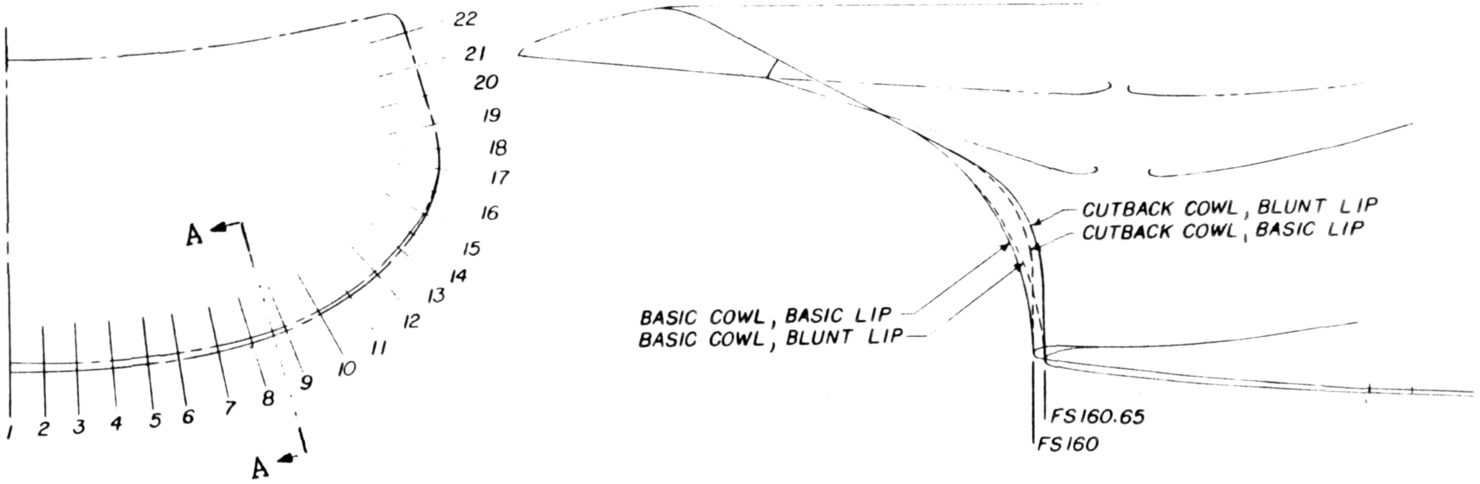

Figure 4-15 Inlet Cowl Lip Variations

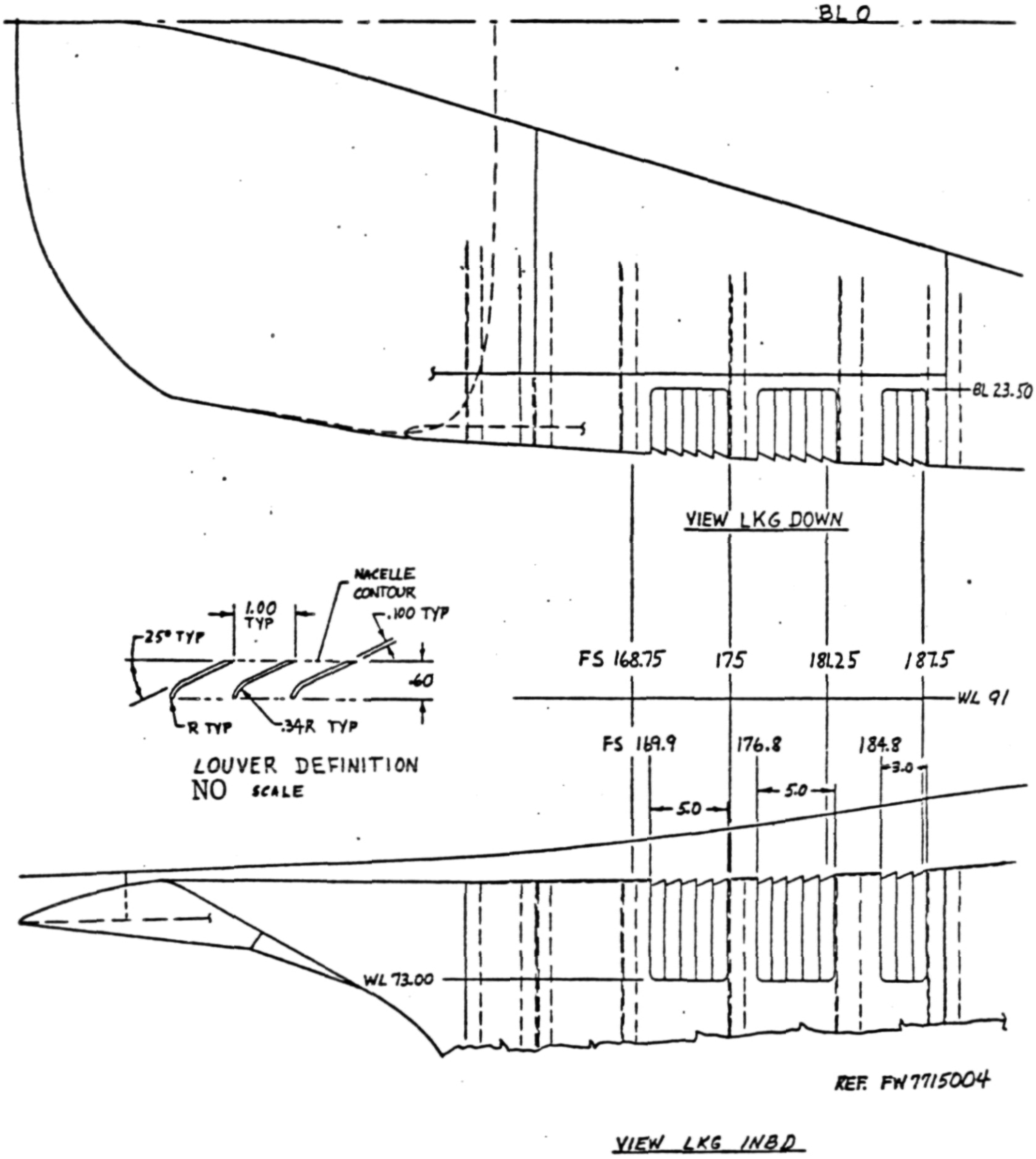

Figure 4-16 Bleed Louver Detail

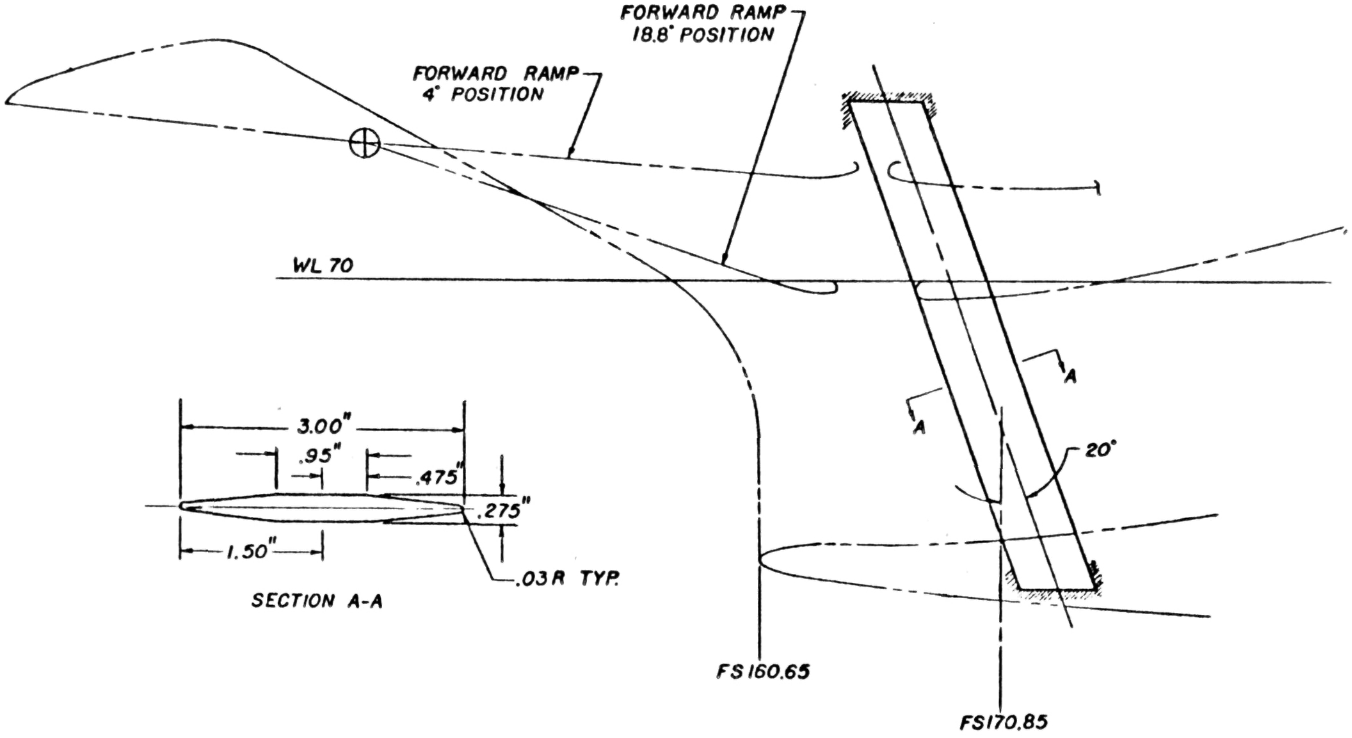

Figure 4-17 Tension Strut Detail

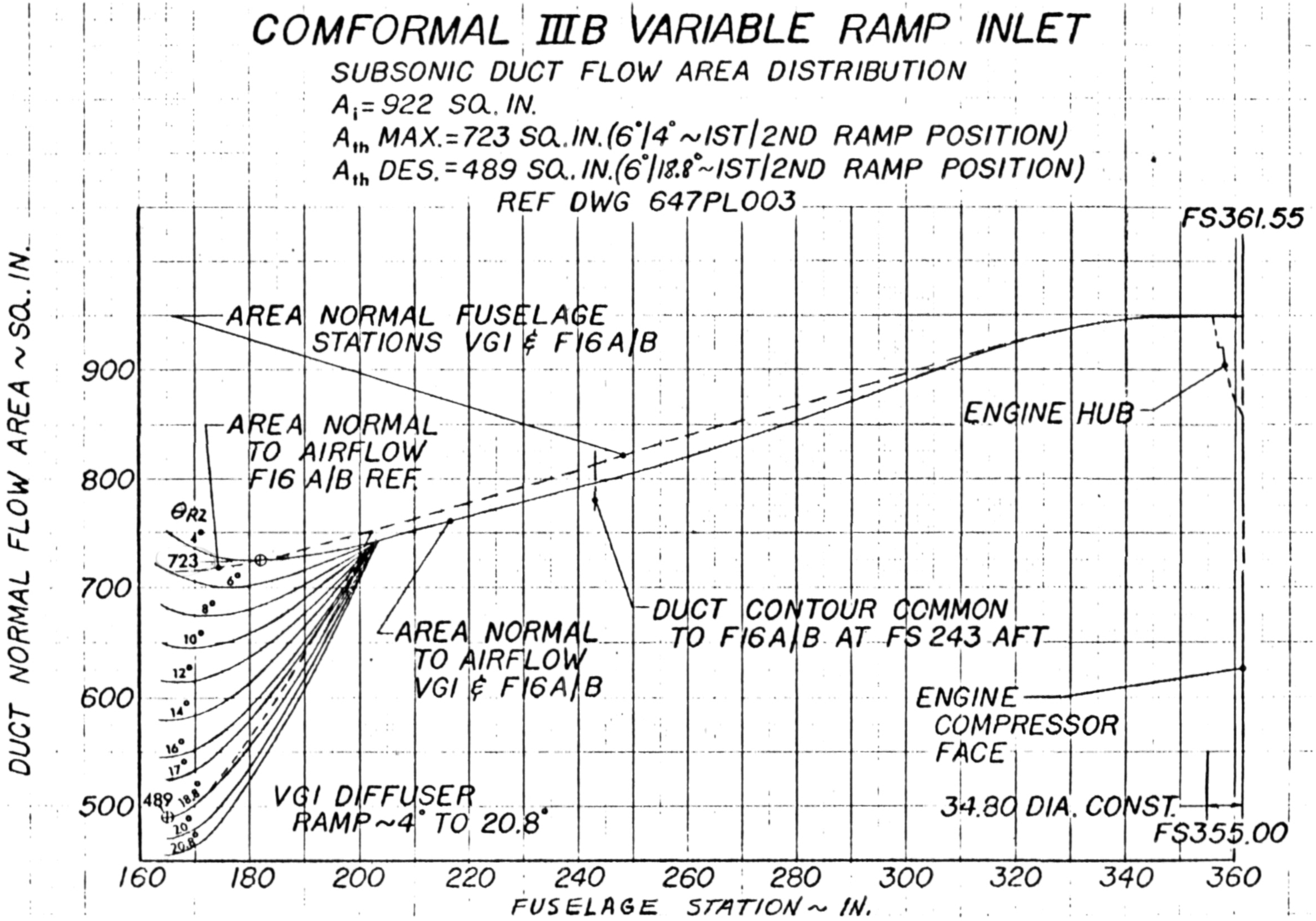

Figure 4-18 Conformal IIIB Subsonic Duct Flow Area Distribution

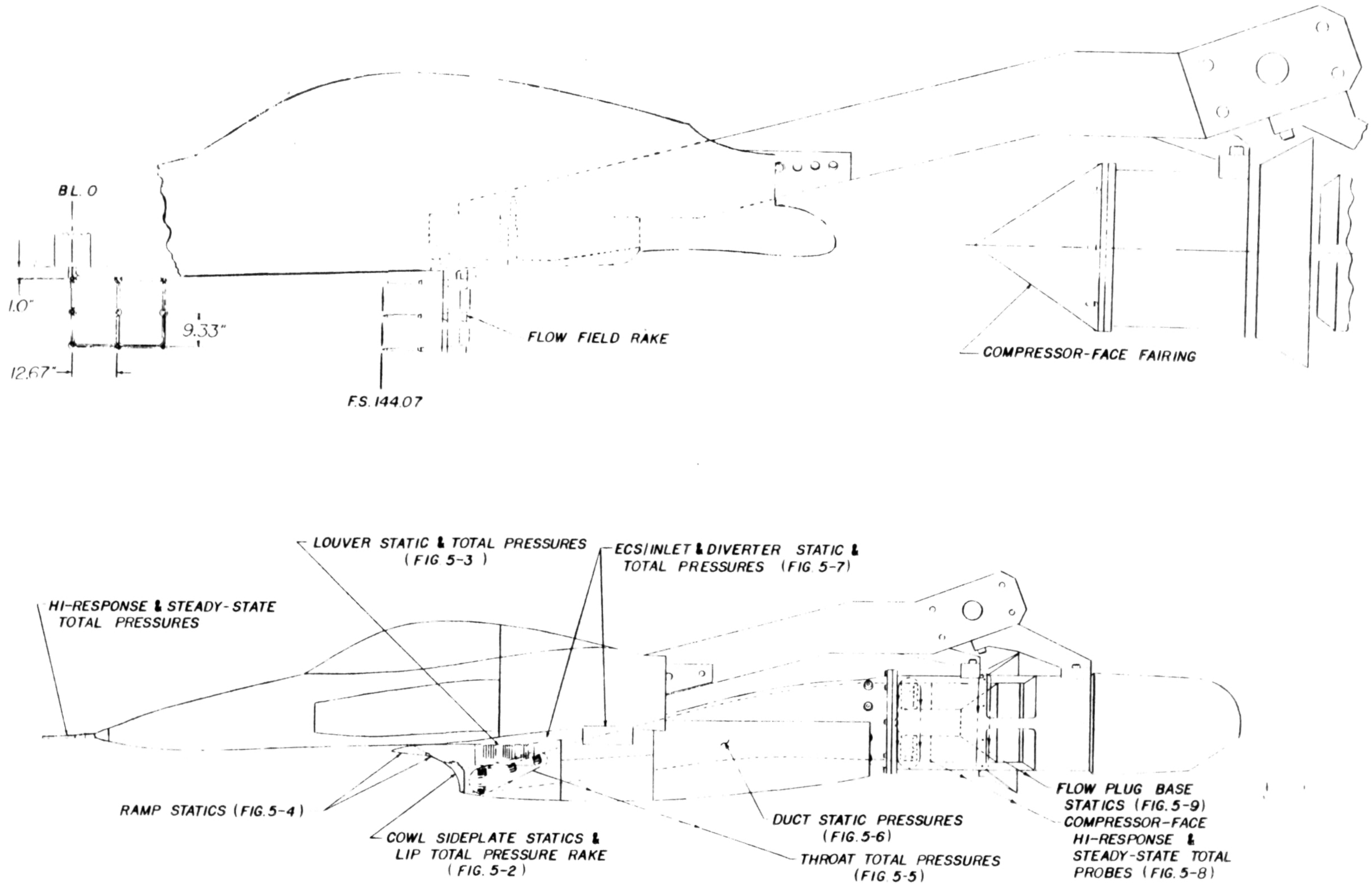

Figure 5-1 Model Instrumentation

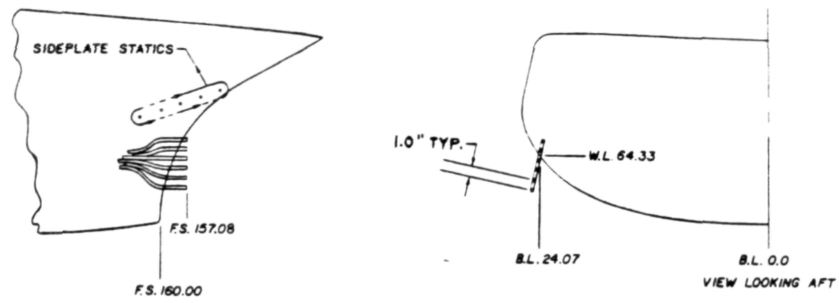

Figure 5-2 Cowl Lip Rake and Sideplate Statics

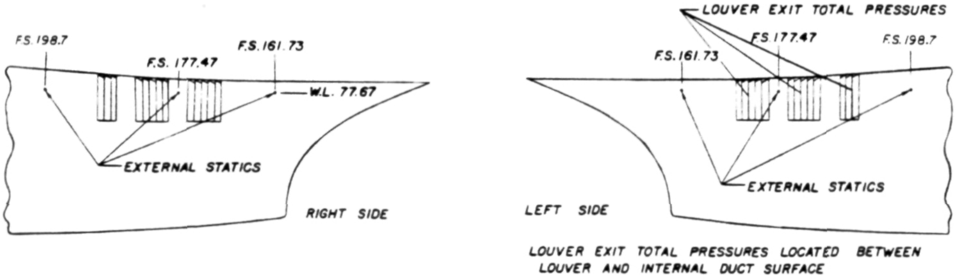

Figure 5-3 Bleed Louver Instrumentation

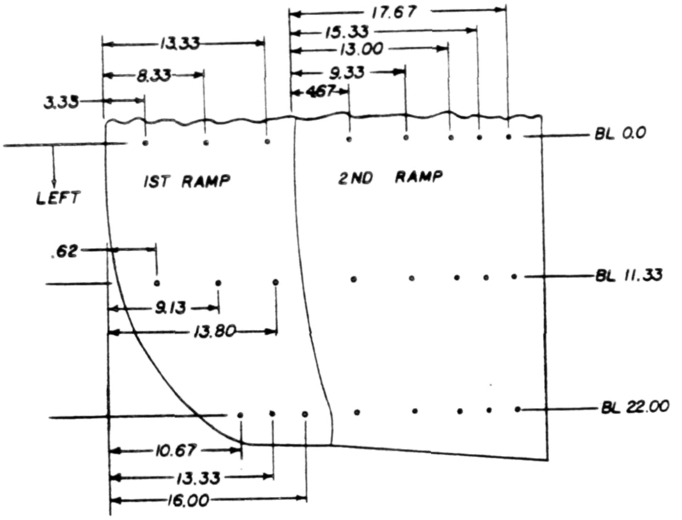

Figure 5-4 First and Second Ramp Statics

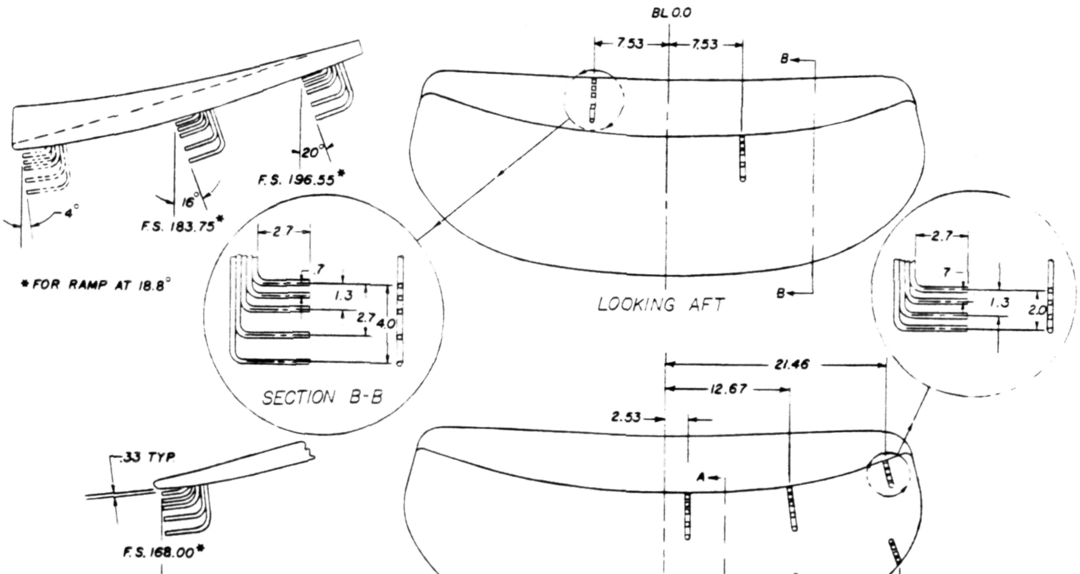

Figure 5-5 Throat Rake Instrumentation

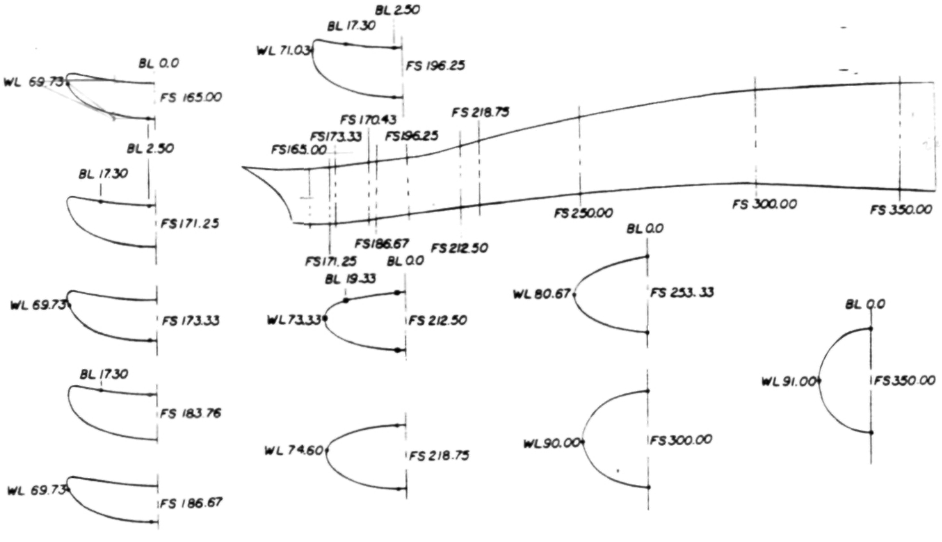

Figure 5-6 Subsonic Duct Static Instrumentation

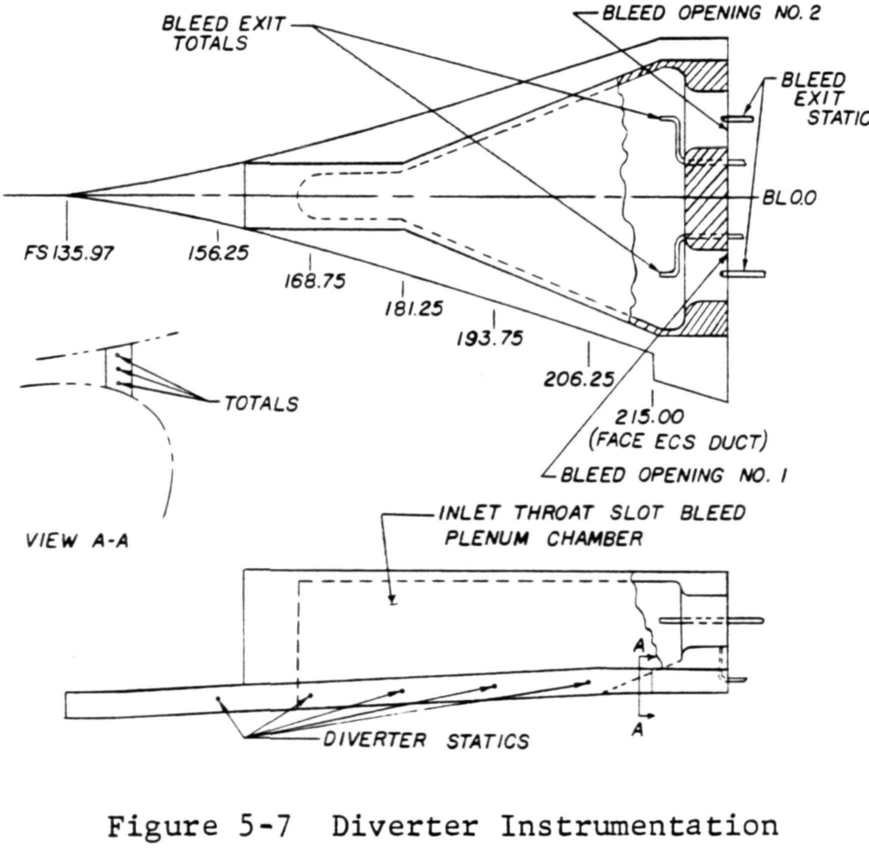

Figure 5-7 Diverter Instrumentation

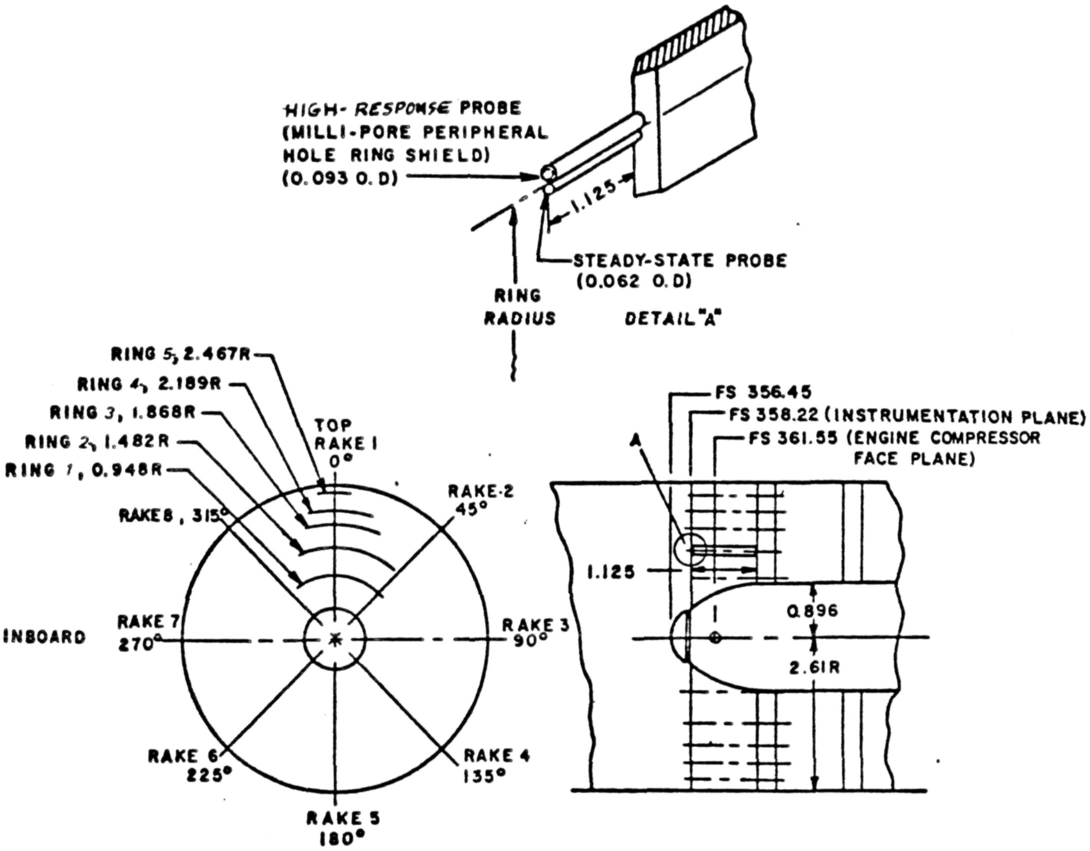

FS IN INCHES (FULL SCALE)
DIMENSIONS IN INCHES (MODEL SCALE)

Figure 5-8 Compressor-Face Rake Instrumentation

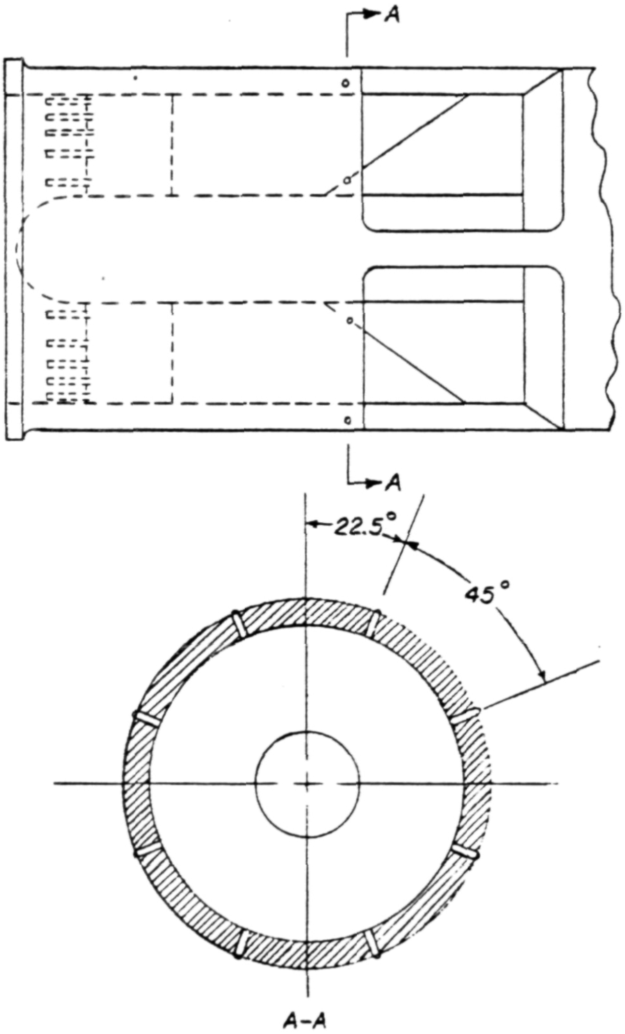

Figure 5-9 Flow Plug Base Statics

		SCHEDULE			
Inst. & Location	No. Tubes	A	B	B'	C
Cone probe rakes	10 T(Total)	A			
	40 S(Static)	A			
1st ramp statics	3 S		B		C
	6 S		B	B'	C
Cowl lip rake	6 T		B	B'	
2nd ramp statics	15 S		B	B'	C
Aft ramp statics	6 S		B	B'	C
Throat bleed orifice	2 T		B		C
	2 S		B	B'	C
Throat rakes	28 T		B	B'	
Aft ramp rakes	10 T		B	B'	
Sideplate statics	5 S		B		C
Comp. face totals & statics	40 T		B	B'	C
	8 S		B	B'	C
Nose boom total	1 T		B	B'	C
Duct statics	20 S				C
Bleed louver totals	3 T			B'	C
ECS subinlet	3 T				C
Bleed louver exit statics	6 S			B'	C
Diverter statics	5 S				C

Figure 5-10 Model Pressure Instrumentation Schedule

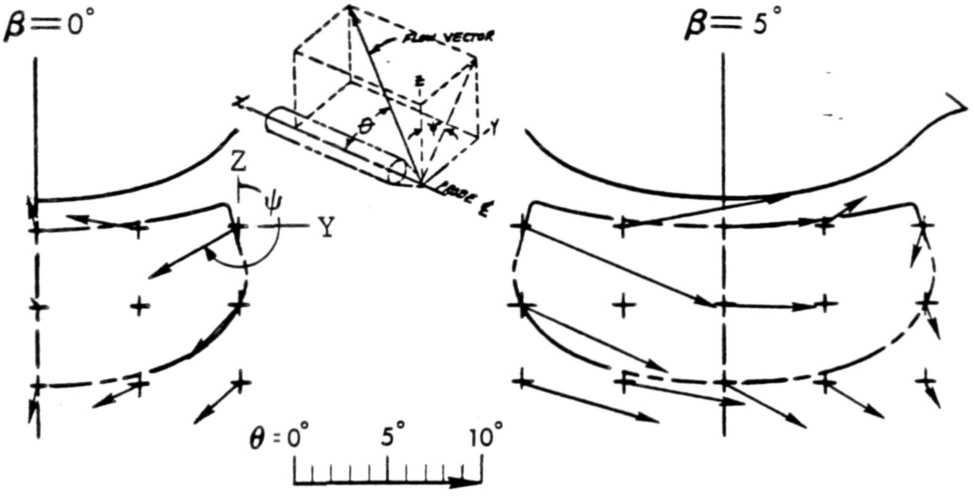

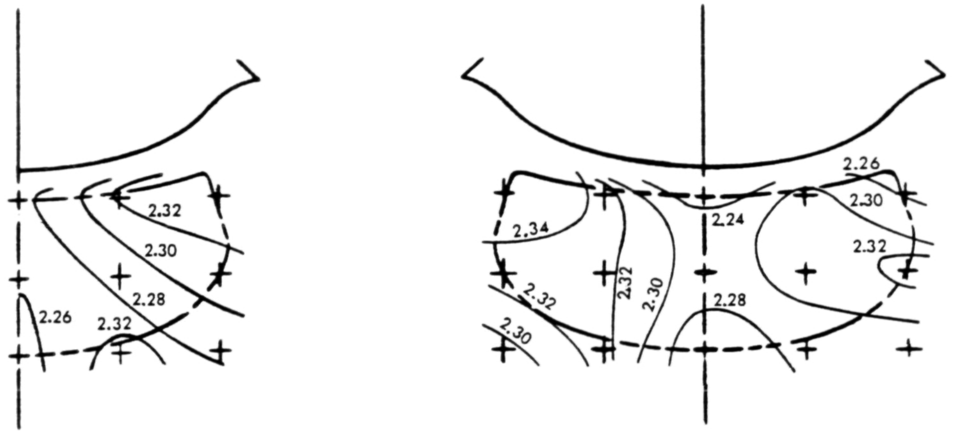

M_{Local}

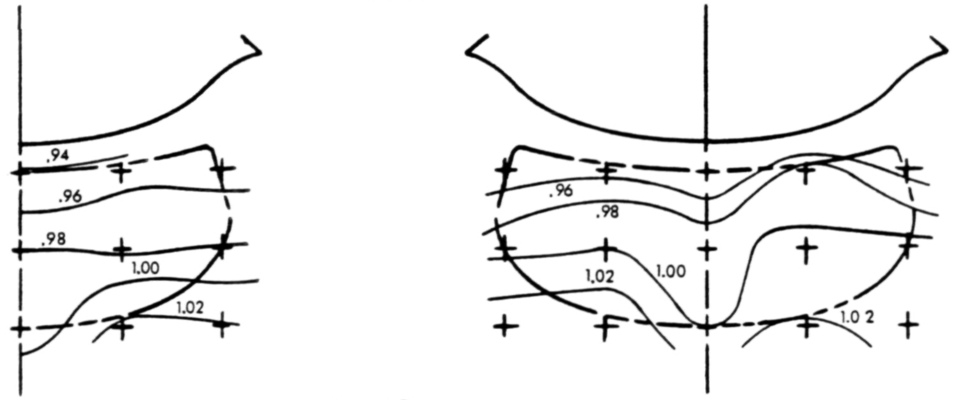

P_{TL}/P_{TO}

Figure 7-1 Forebody Flow Field Characteristics, $M_0 = 2.2$, $\alpha = -2^{\circ}$

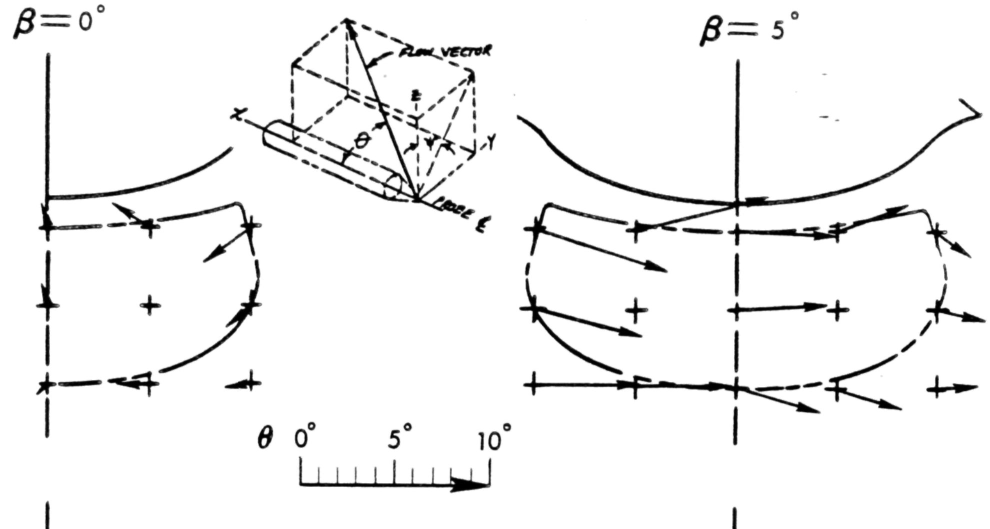

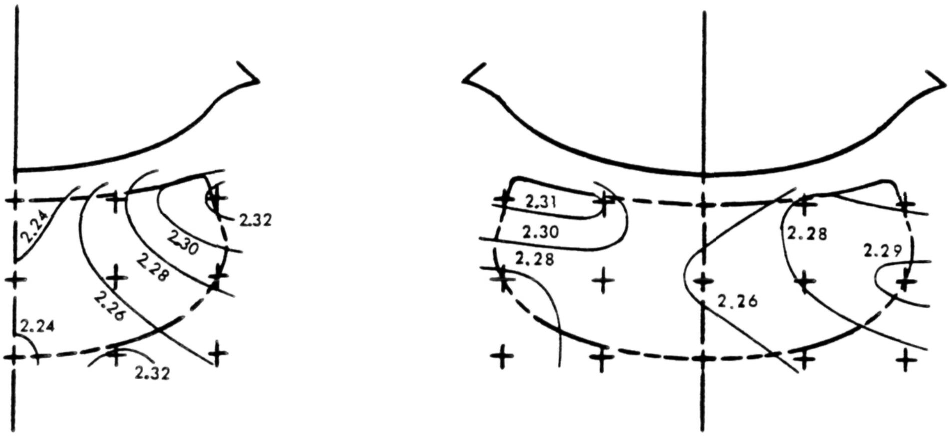

M_{Local}

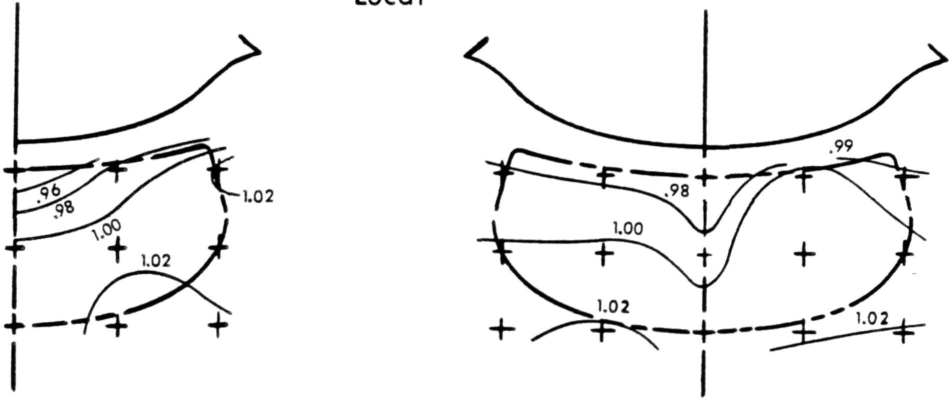

P_{TL} / P_{TO}

Figure 7-2 Forebody Flow Field Characteristics, $M_O = 2.2$, $\alpha = 0.4^{\circ}$, (1° Nominal)

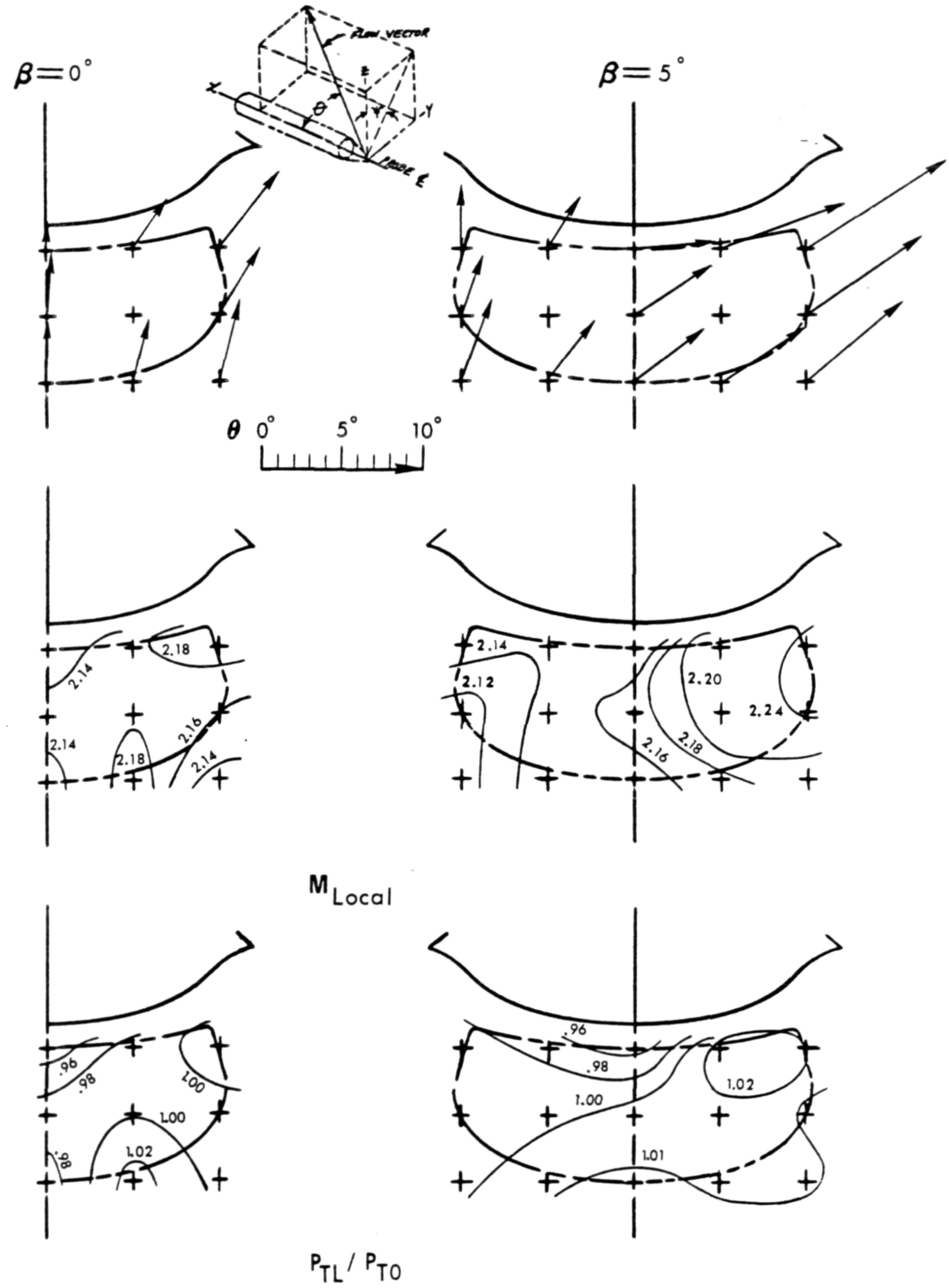

Figure 7-3 Forebody Flow Field Characteristics, $M_O = 2.2$, $\alpha = 10^O$

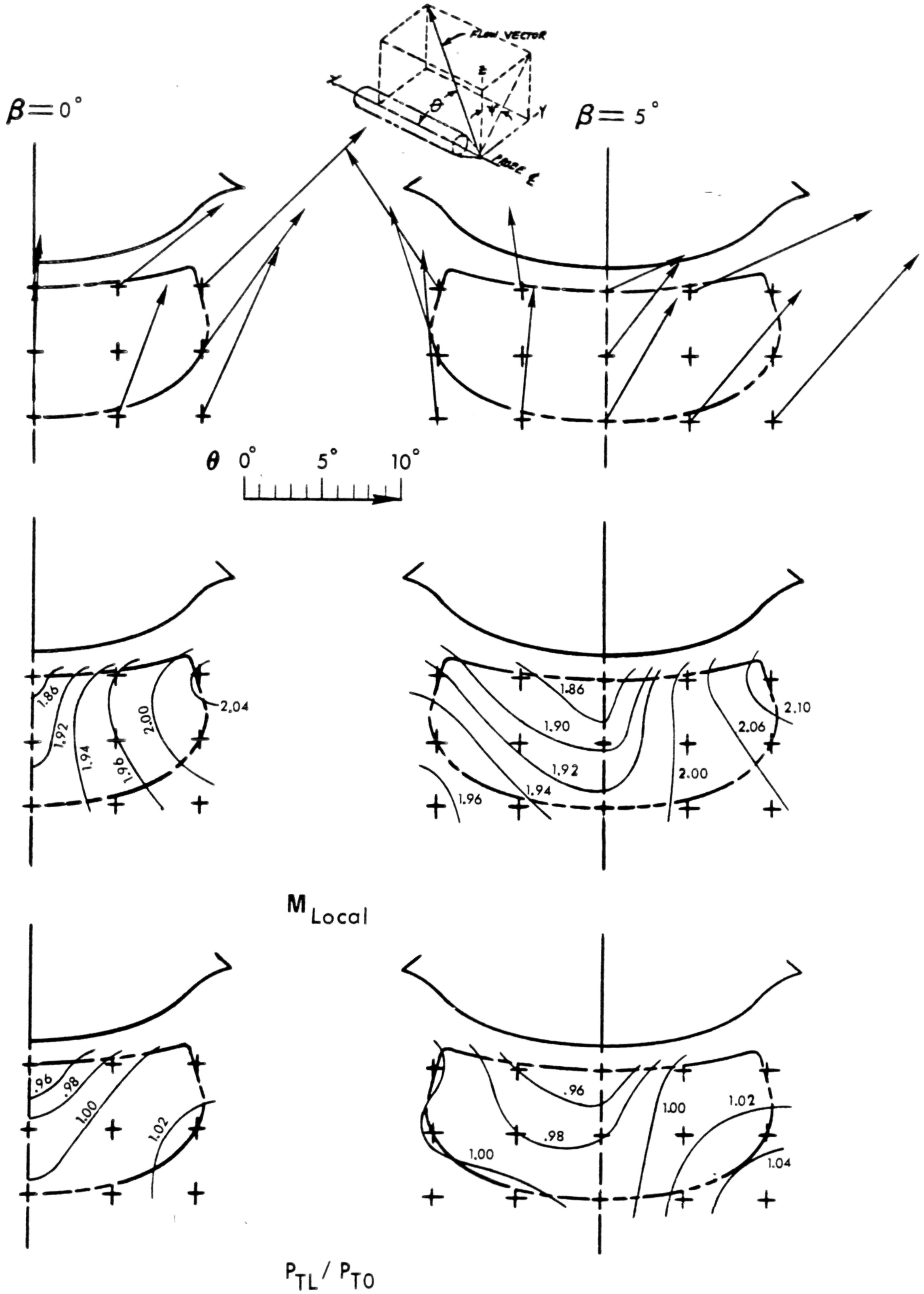

Figure 7-4 Forebody Flow Field Characteristics, $M_o = 2.2$, $\alpha = 20^\circ$

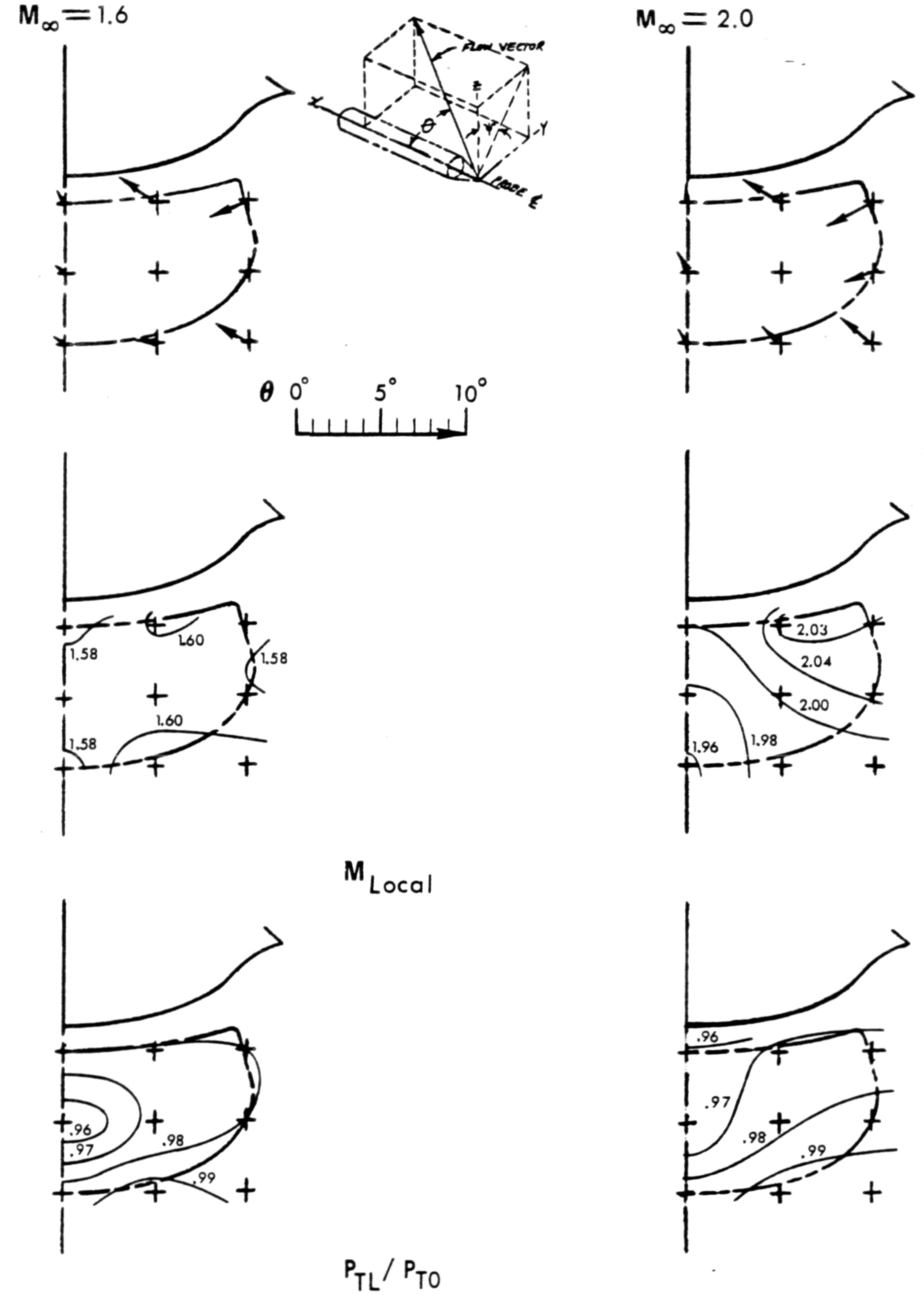

Figure 7-5 Forebody Flow Field Characteristics, M_o = 1.6 and 2.0, $\alpha = 1^o$, $\beta = 0^o$

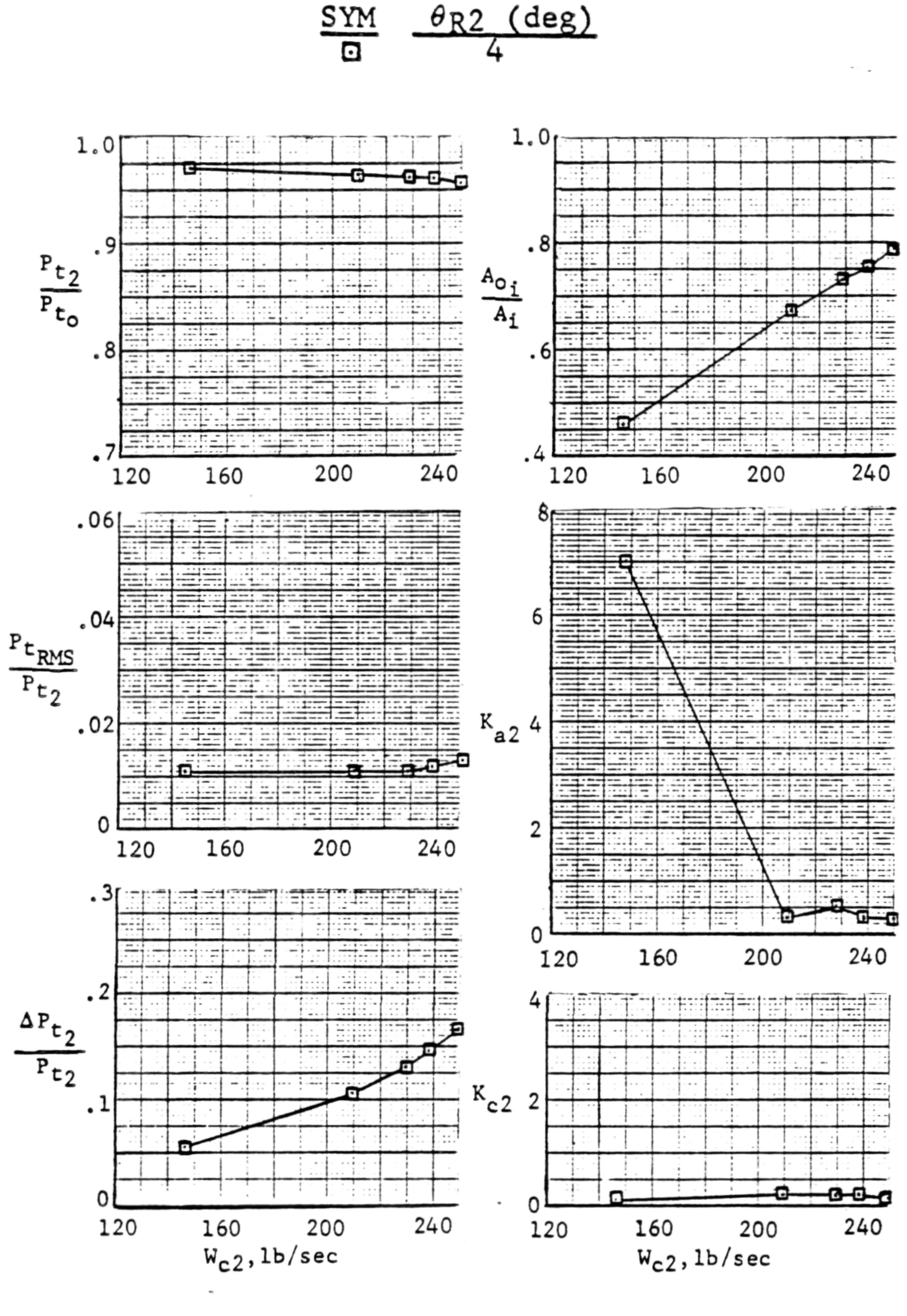

(a) $\alpha = -10^\circ$

Figure 7-6 Effect of Airflow on Steady-State Performance, $M_o = 0.8$, $\beta = 0^\circ$

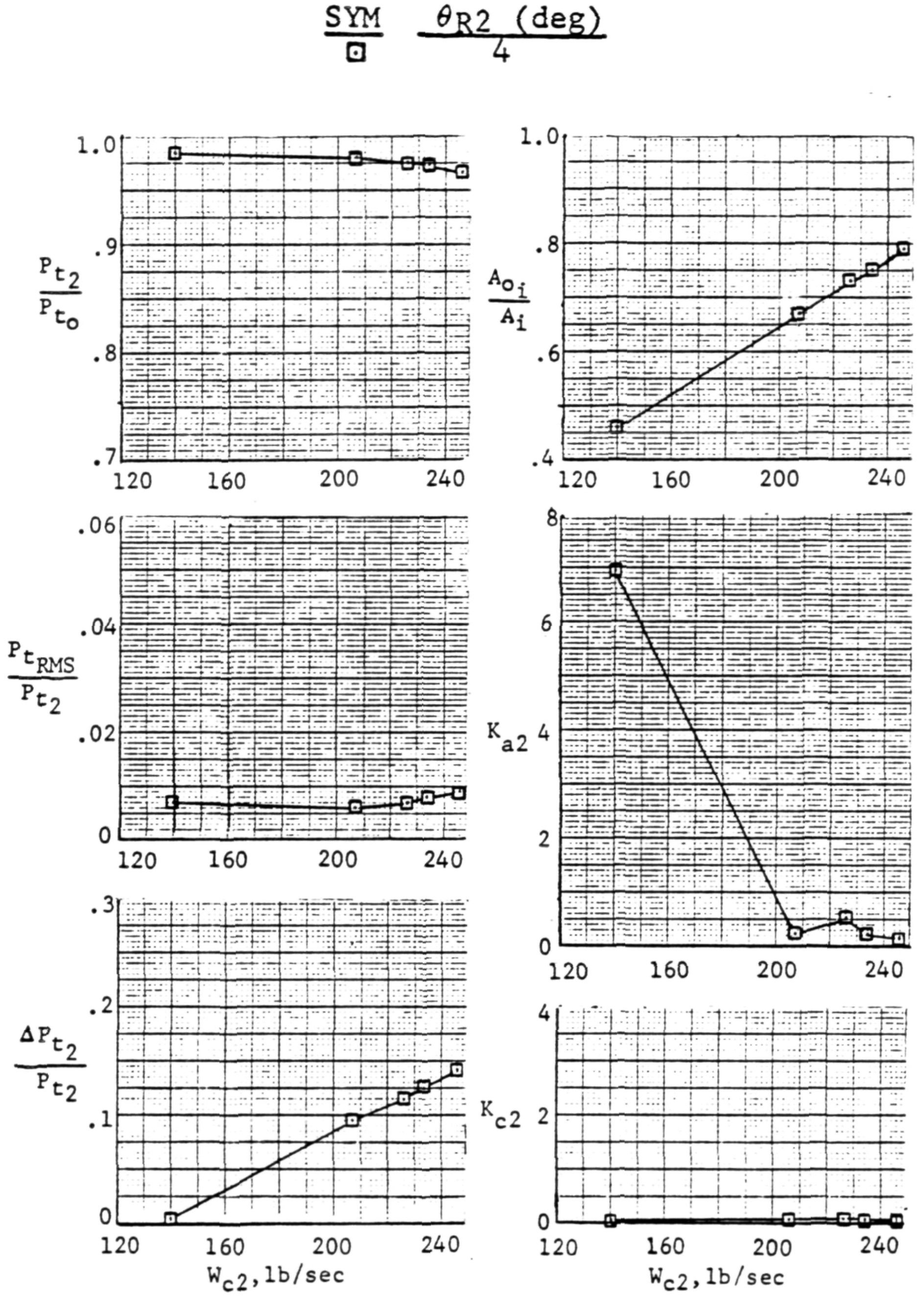

(b) $\alpha = -5^{\circ}$

Figure 7-6 (Cont'd)

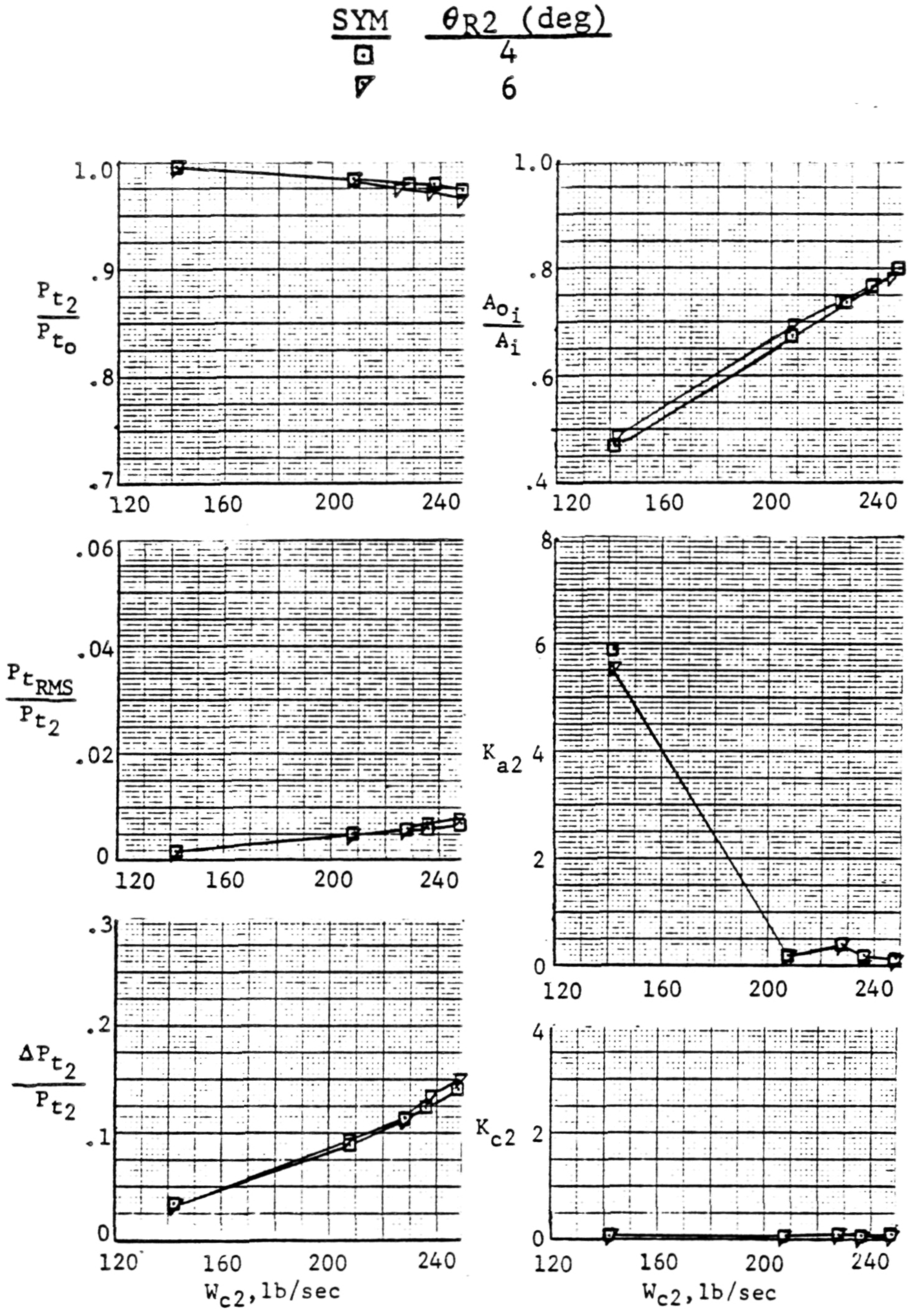

(c) $\alpha = 1^{\circ}$

Figure 7-6 (Cont'd)

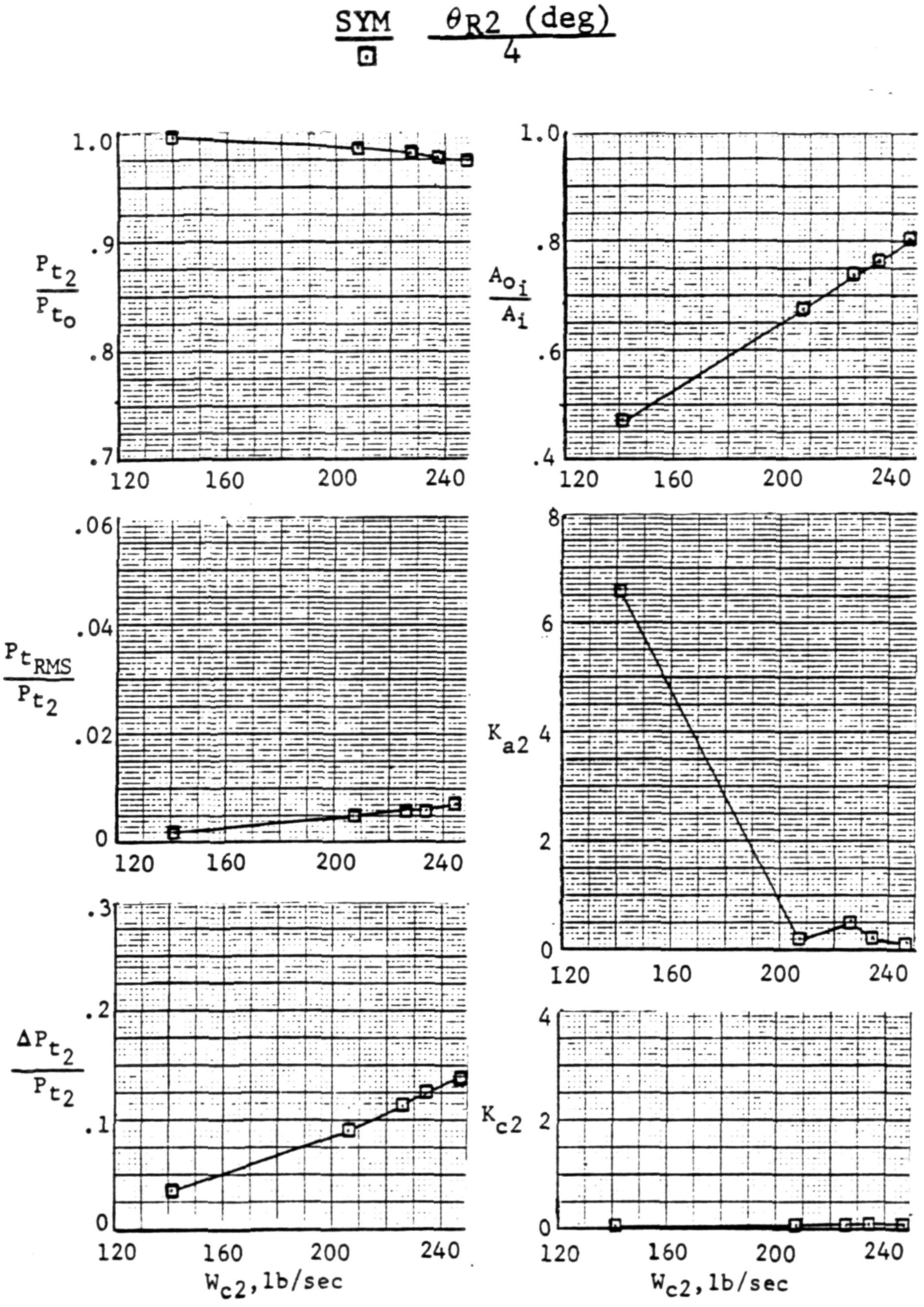

(d) $\alpha = 6^{o}$

Figure 7-6 (Cont'd)

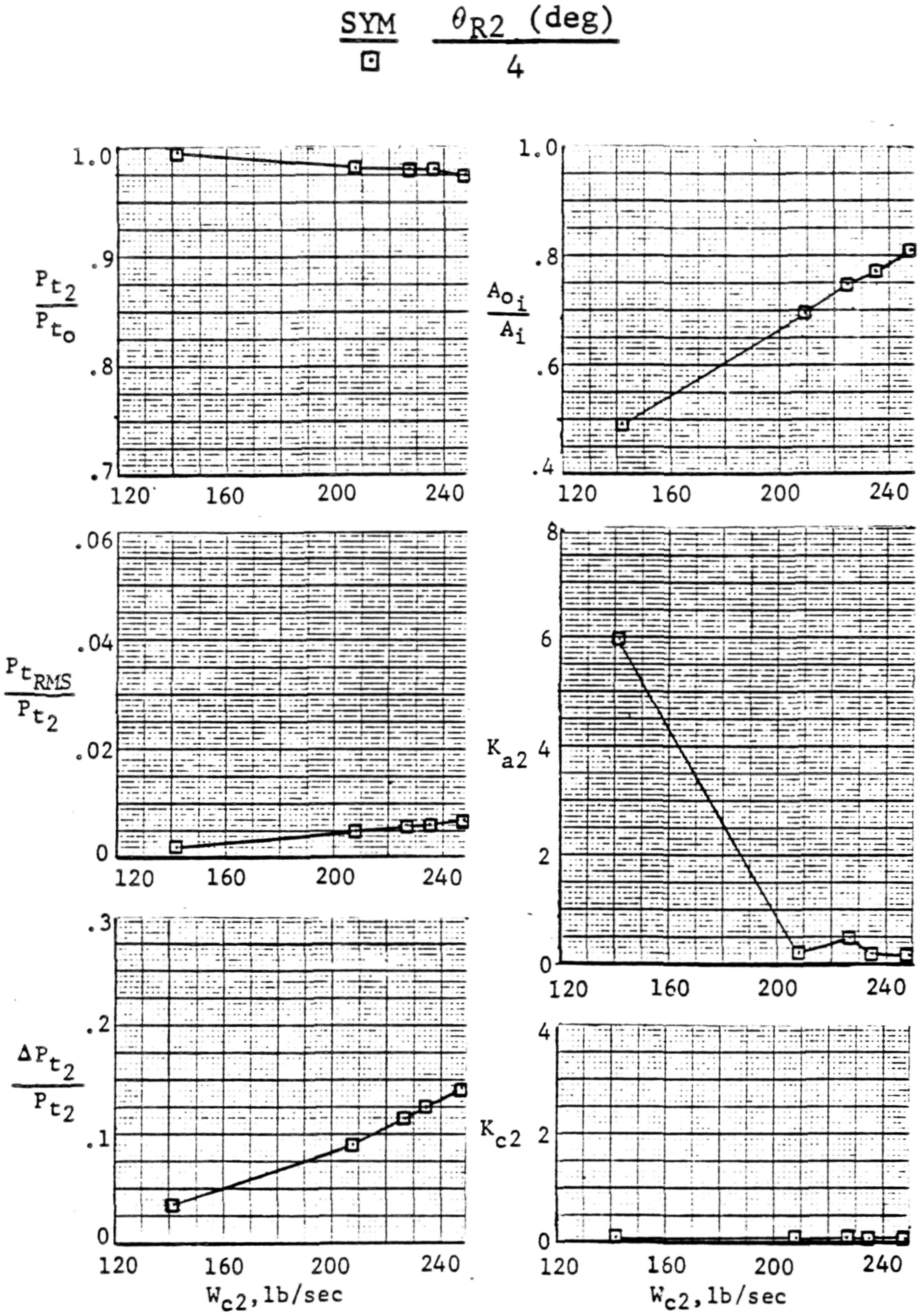

(e) $\alpha = 15^{\circ}$

Figure 7-6 (Cont'd)

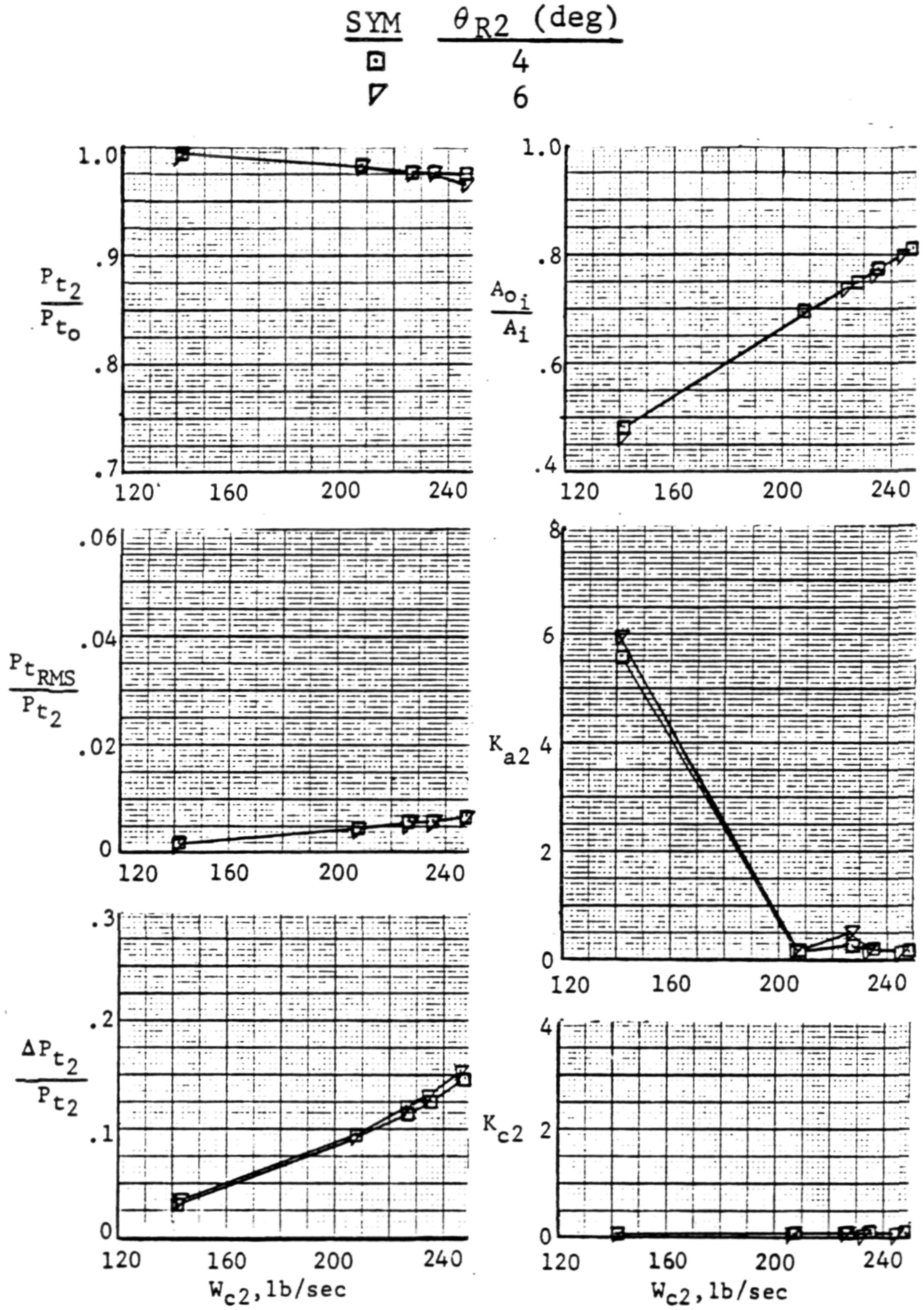

(f) $\alpha = 20^{\circ}$

Figure 7-6 (Cont'd)

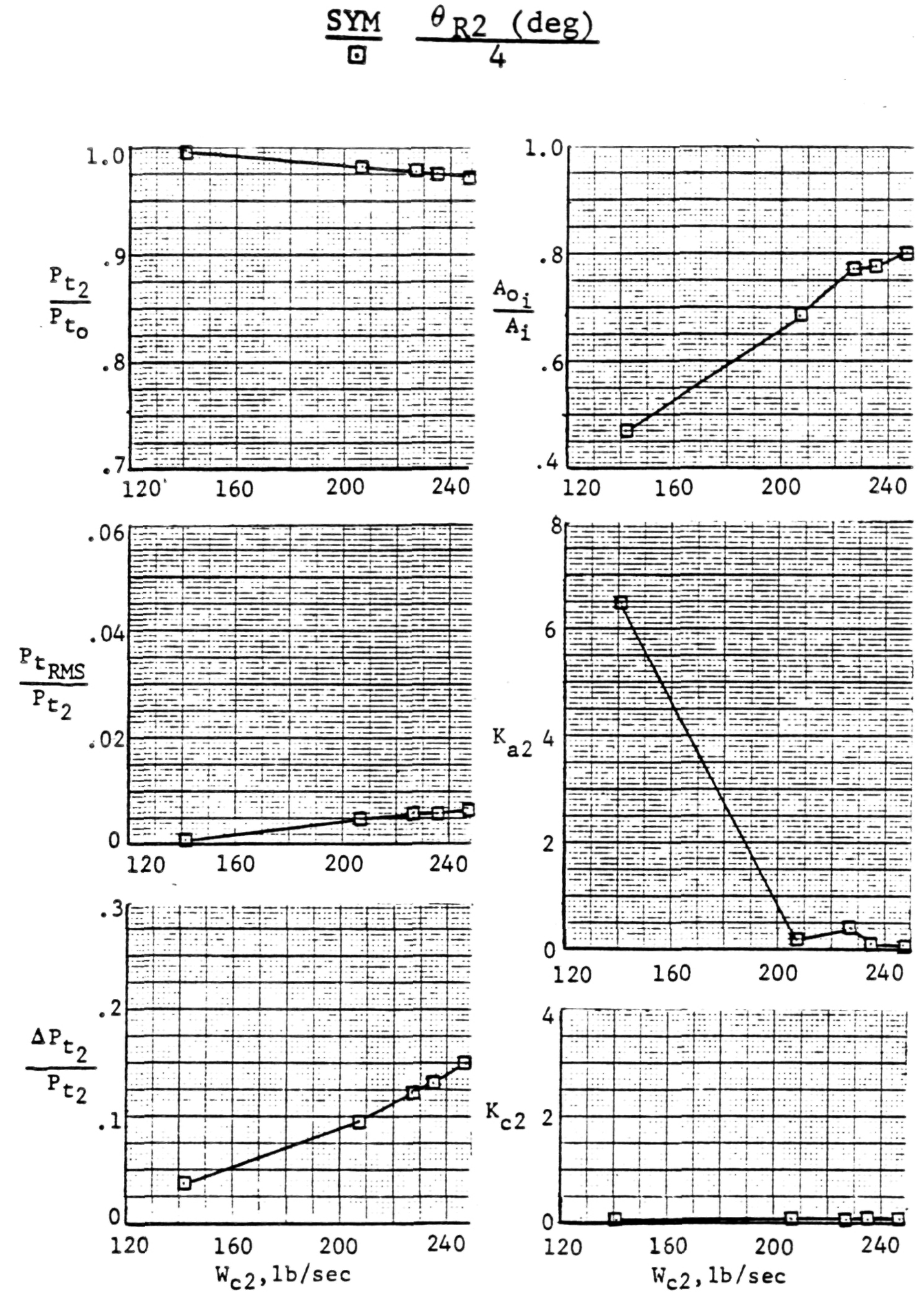

(g) $\alpha = 25^{\circ}$

Figure 7-6 (Cont'd)

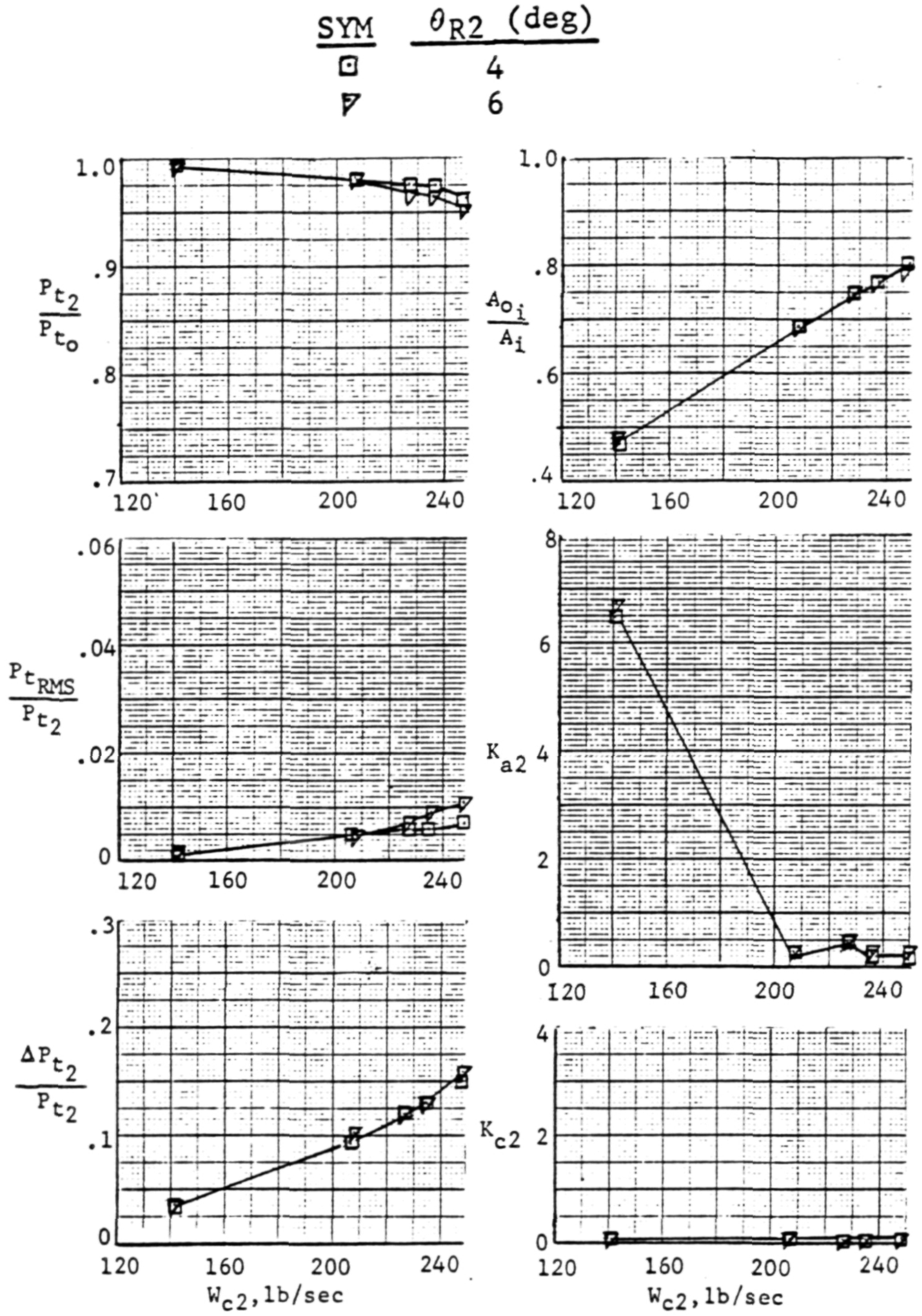

(h) $\alpha = 30^{\circ}$

Figure 7-6 (Concl)

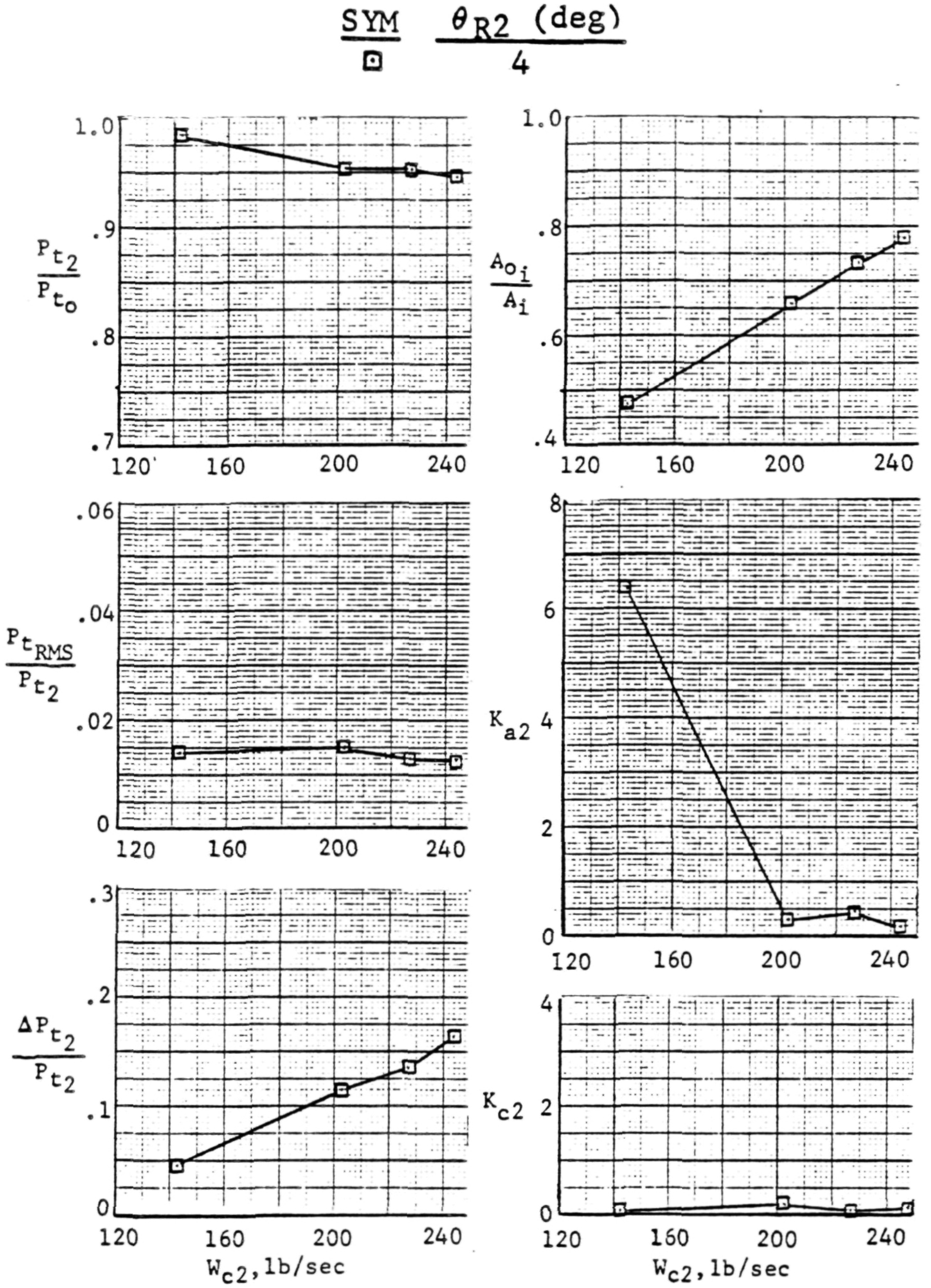

(a) $\alpha = -5^{\circ}$

Figure 7-7 Effect of Airflow on Steady-State Performance, $M_o = 1.3$, $\beta = 0^{\circ}$

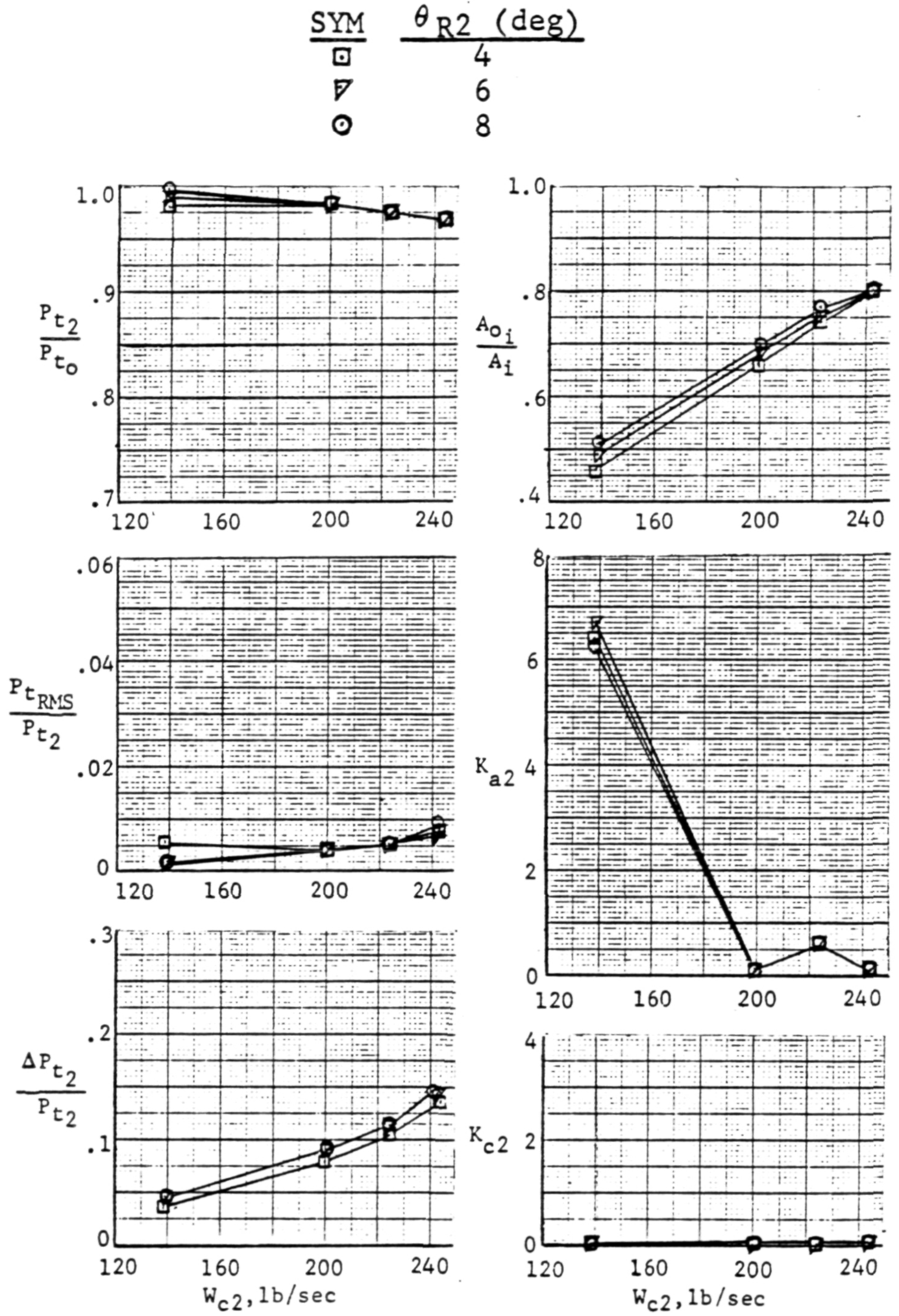

(b) $\alpha = 1^{o}$

Figure 7-7 (Cont'd)

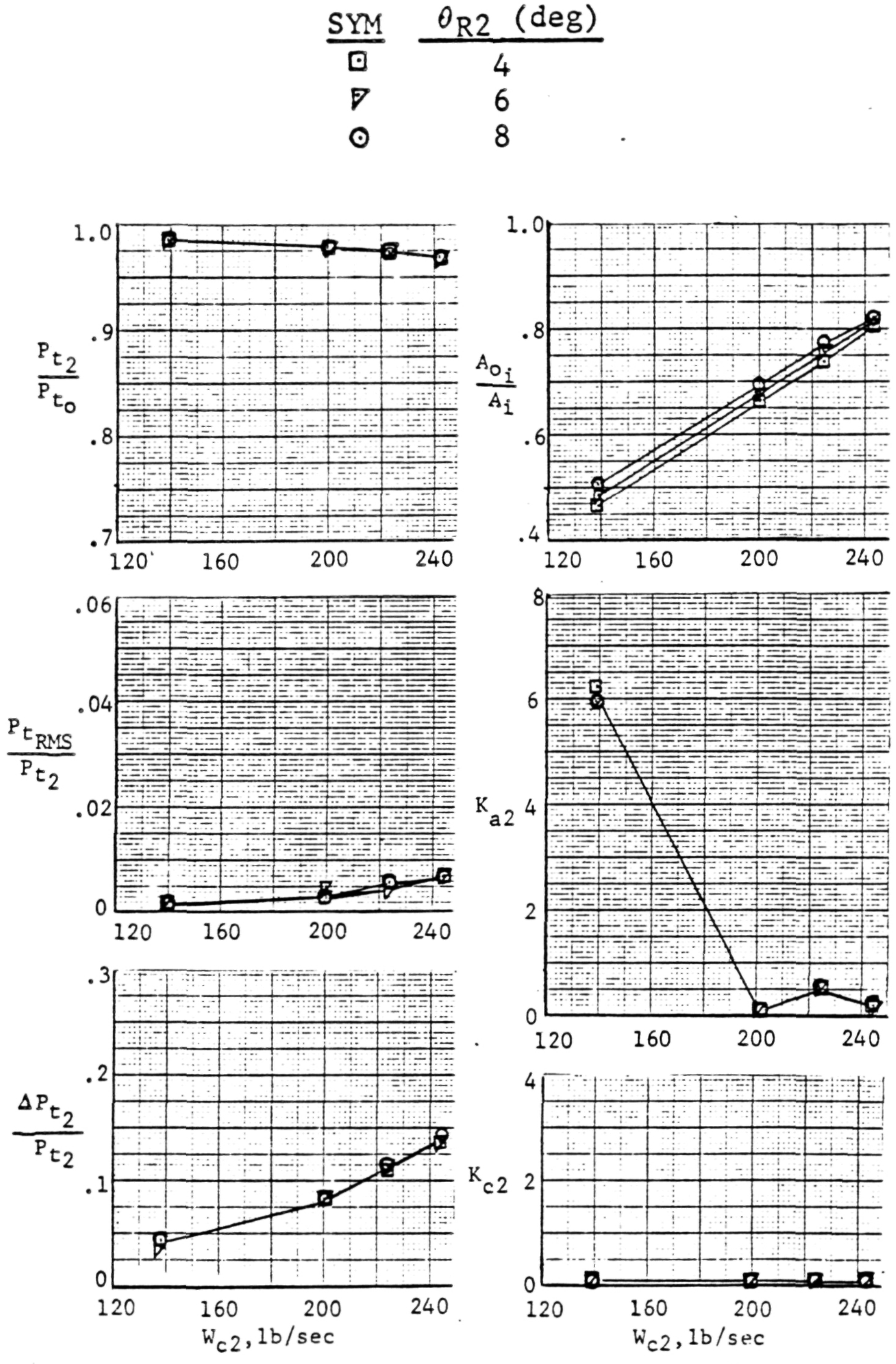

(c) $\alpha = 6^\circ$

Figure 7-7 (Cont'd)

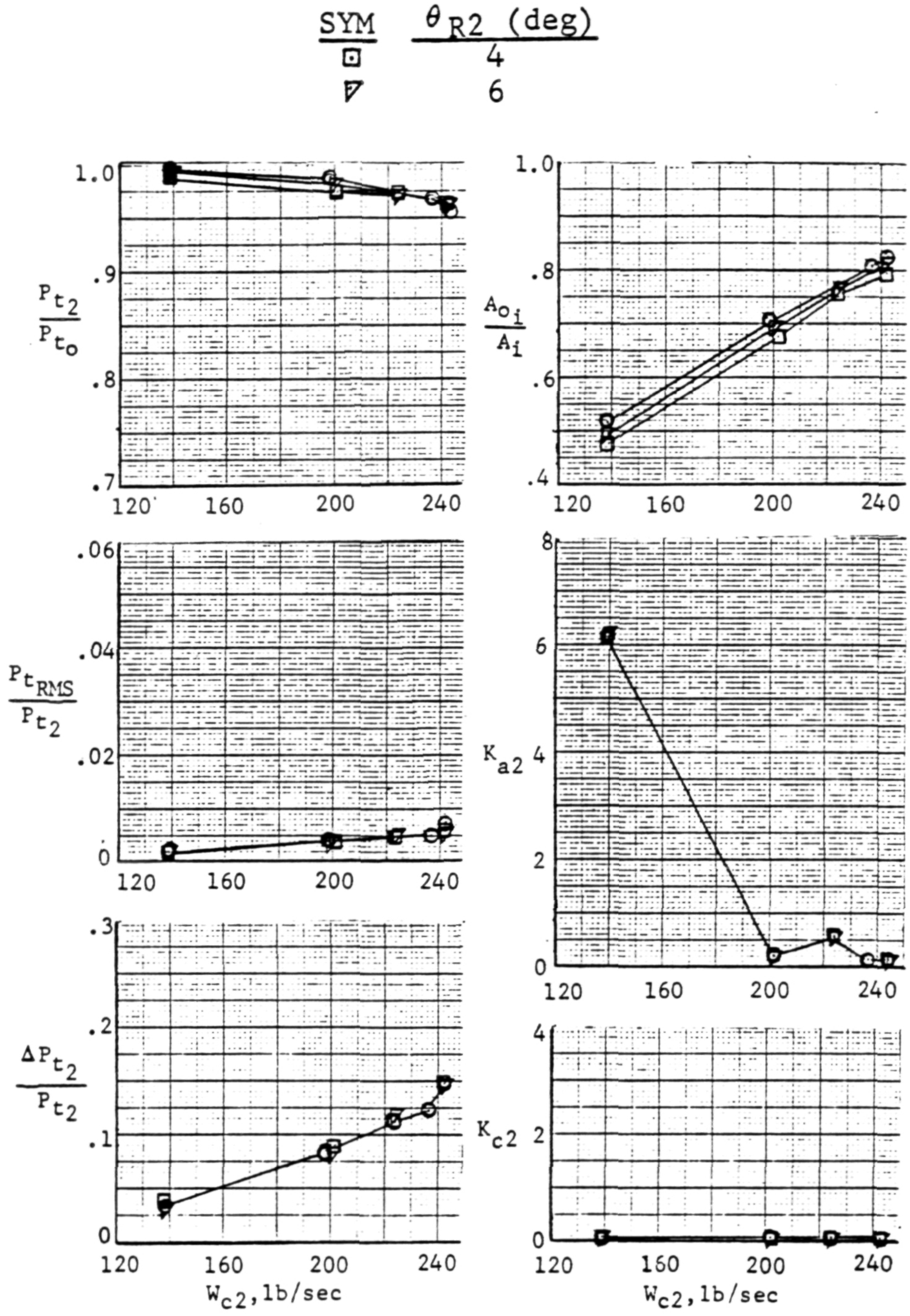

(d) $\alpha = 15^{\circ}$

Figure 7-7 (Cont'd)

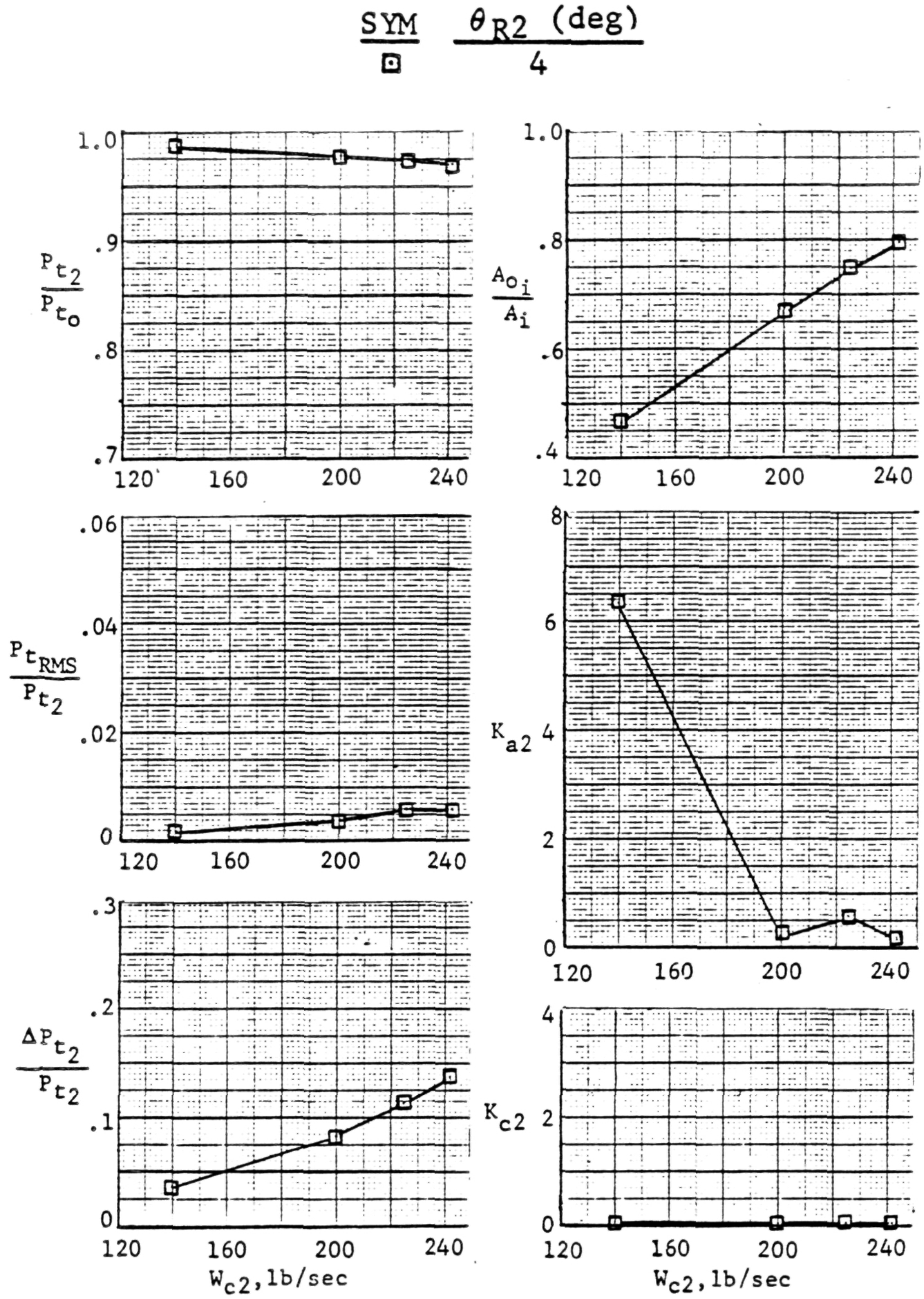

(e) $\alpha = 20^\circ$

Figure 7-7 (Cont'd)

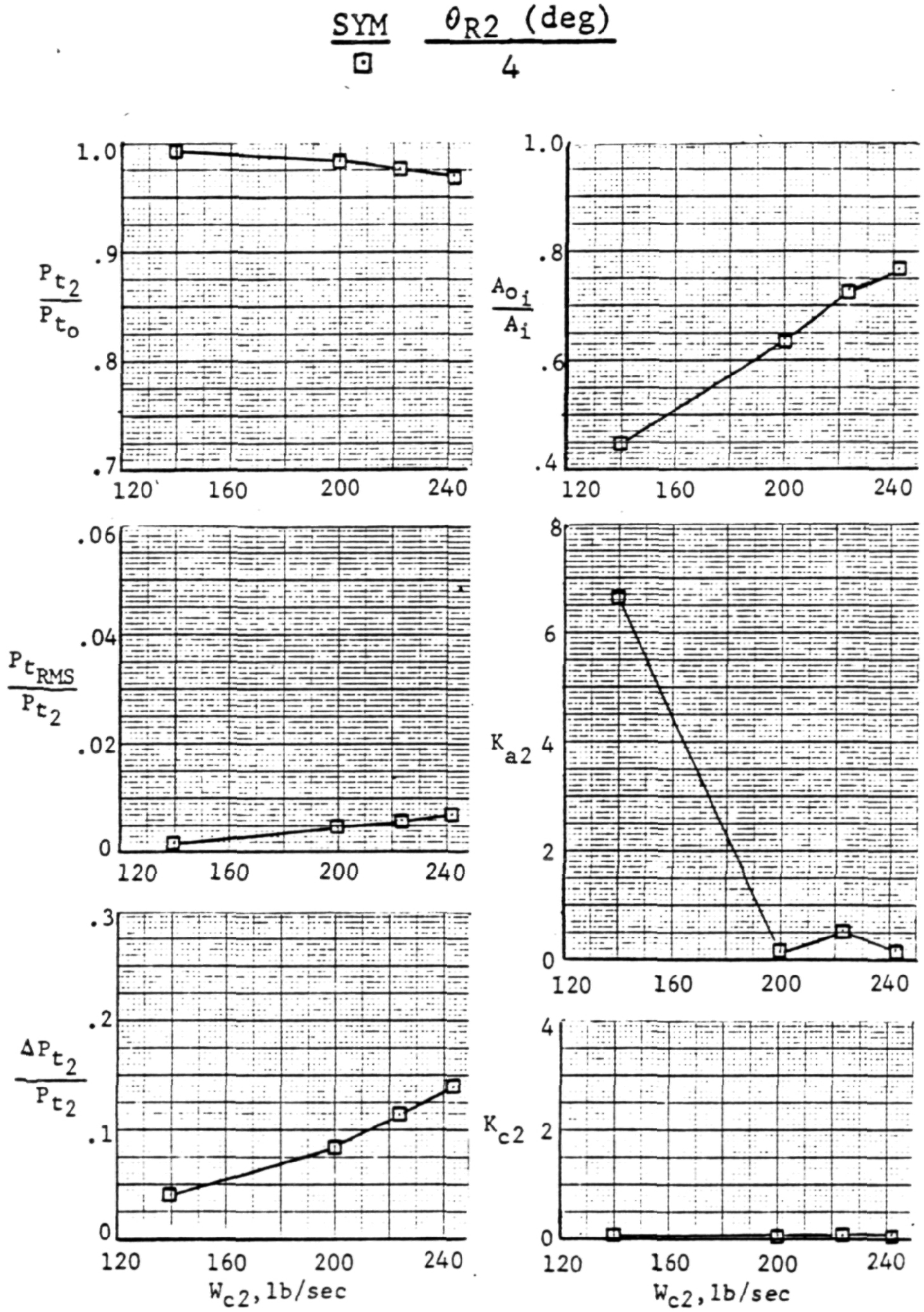

(f) $\alpha = 25^{\circ}$

Figure 7-7 (Concl)

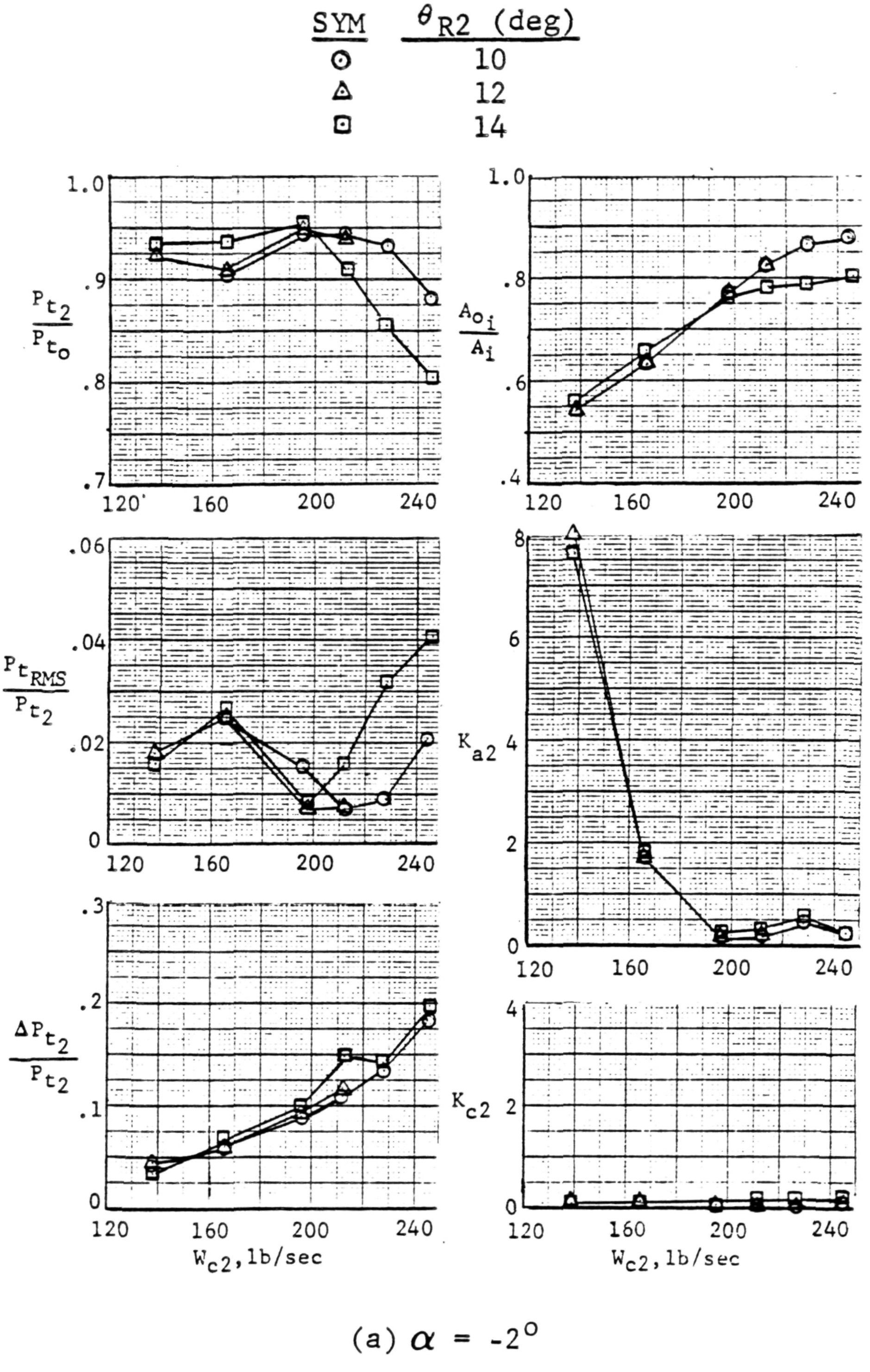

(a) $\alpha = -2^\circ$

Figure 7-8 Effect of Airflow on Steady-State Performance, $M_0 = 1.6$, $\beta = 0^\circ$

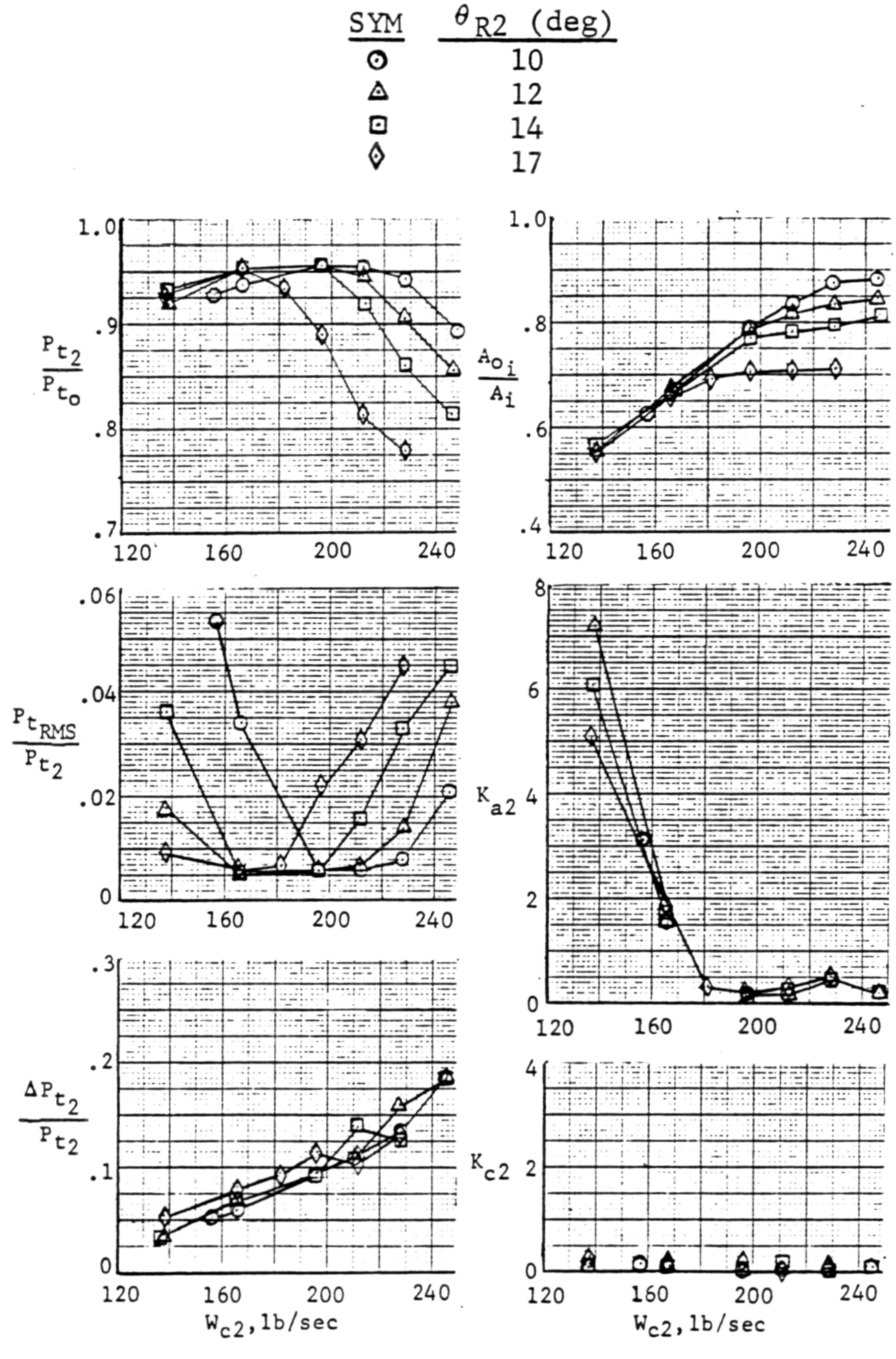

(b) $\alpha = 1^{o}$

Figure 7-8 (Cont'd)

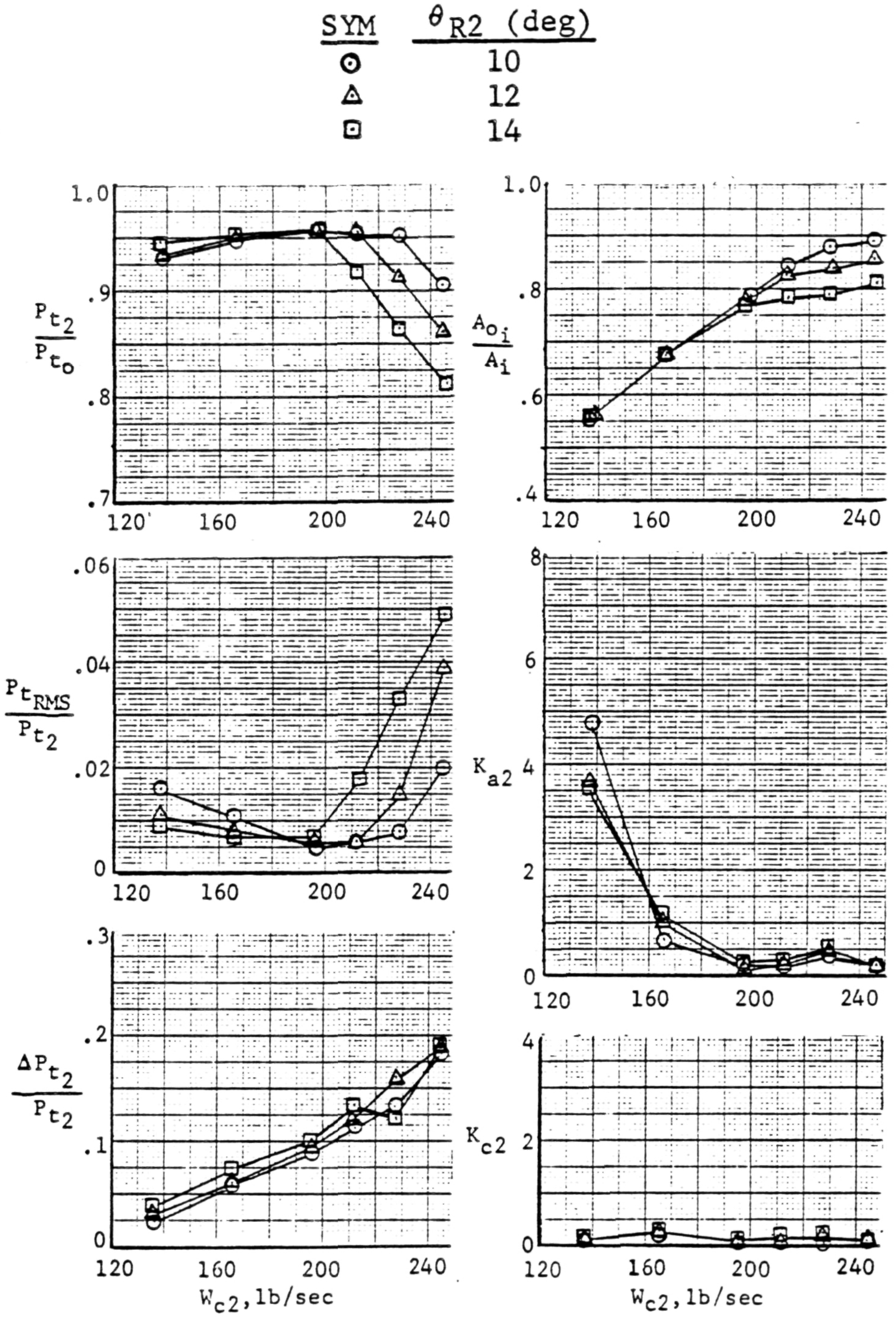

(c) $\alpha = 6^{\circ}$

Figure 7-8 (Cont'd)

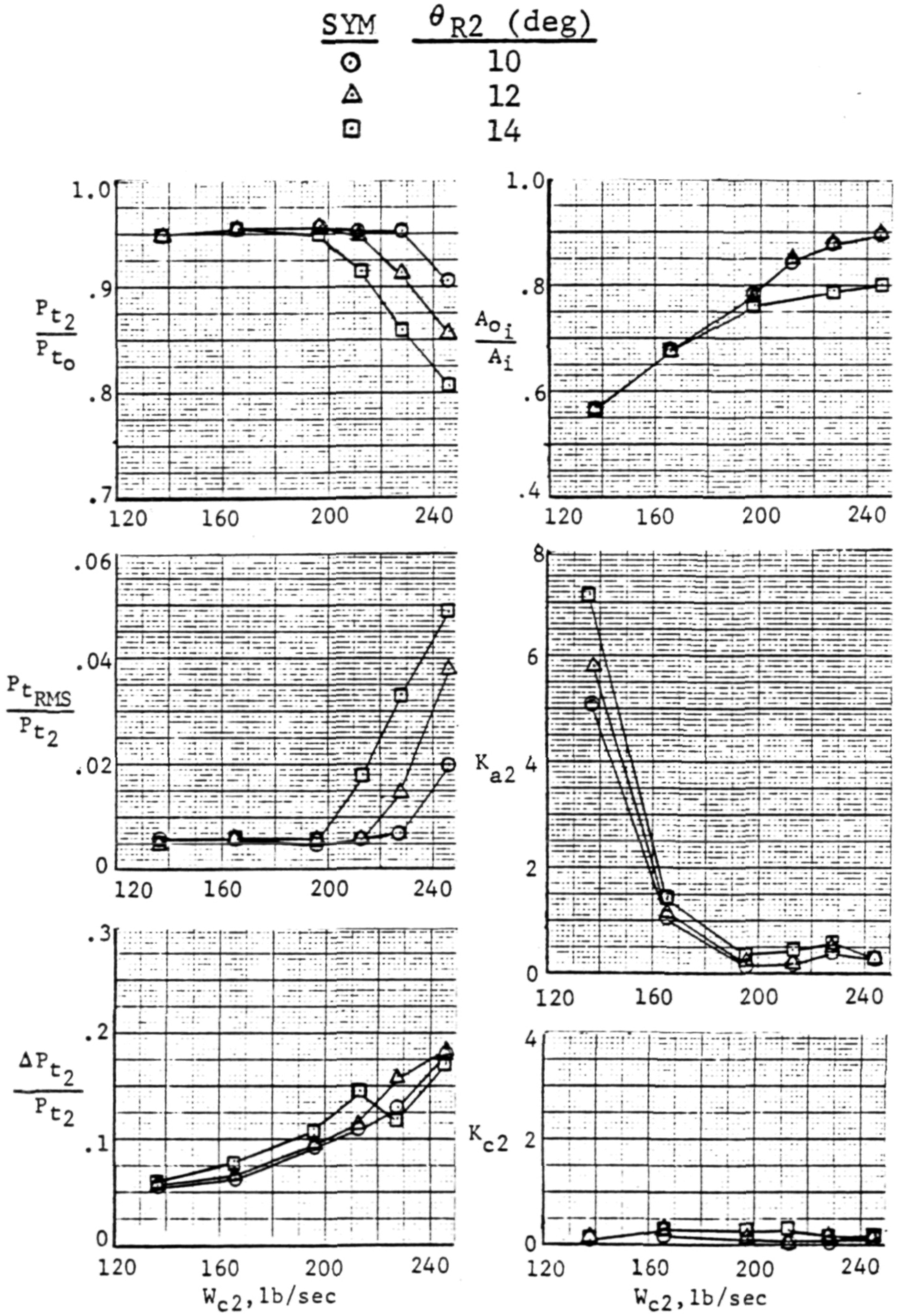

(d) $\alpha = 10^{\circ}$

Figure 7-8 (Cont'd)

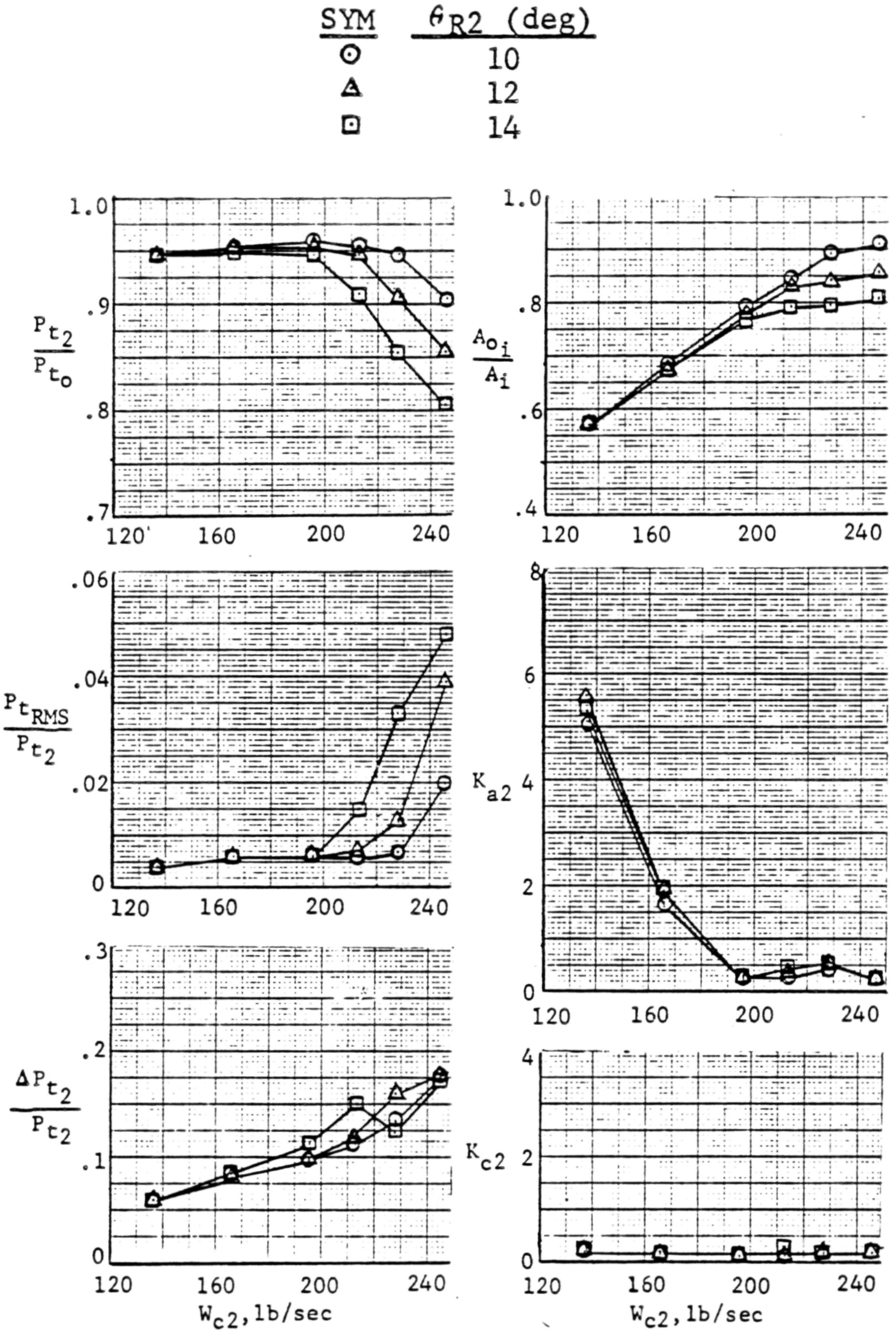

(e) $\alpha = 15^{\circ}$

Figure 7-8 (Cont'd)

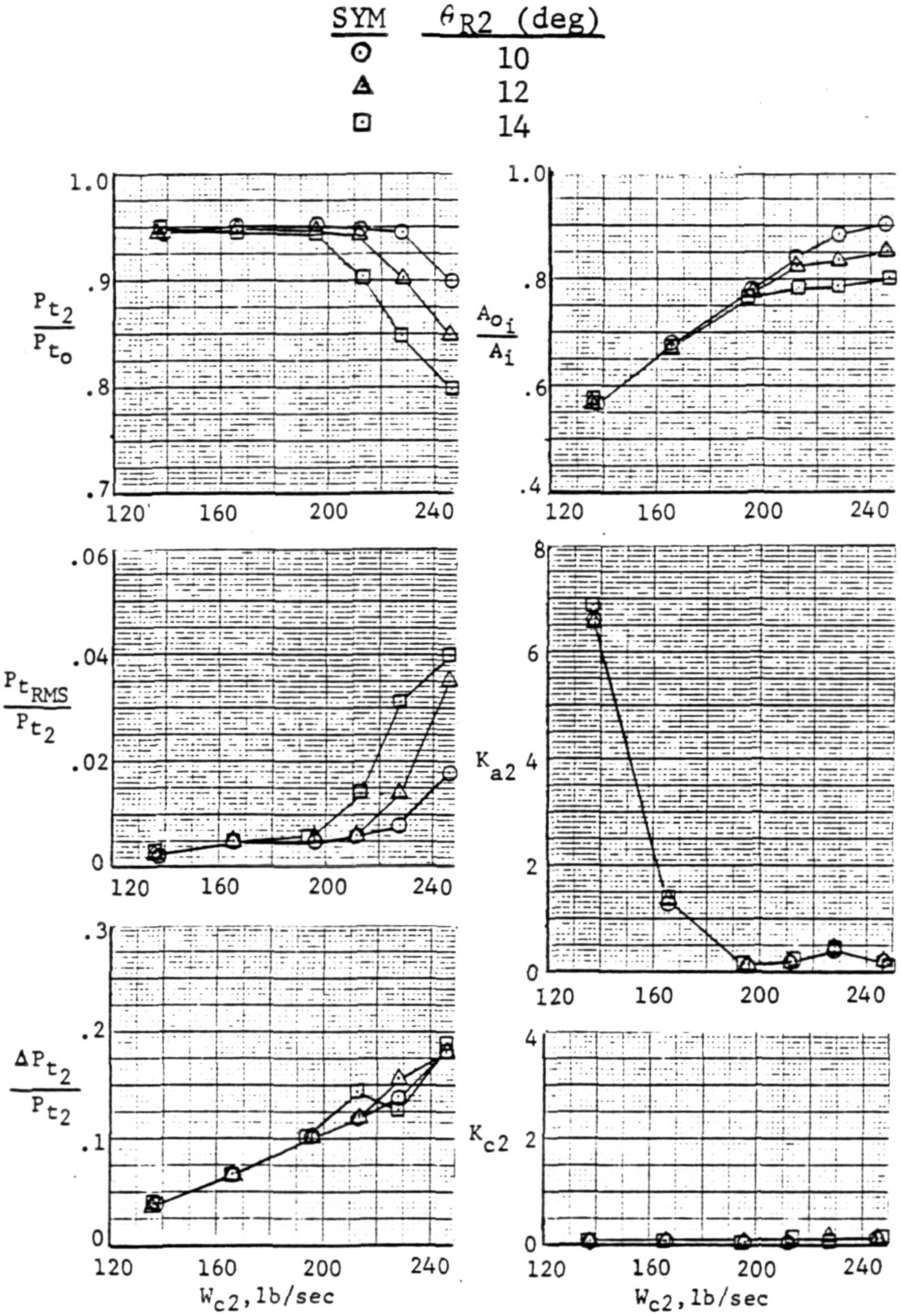

(f) $\alpha = 20^{\circ}$

Figure 7-8 (Concl)

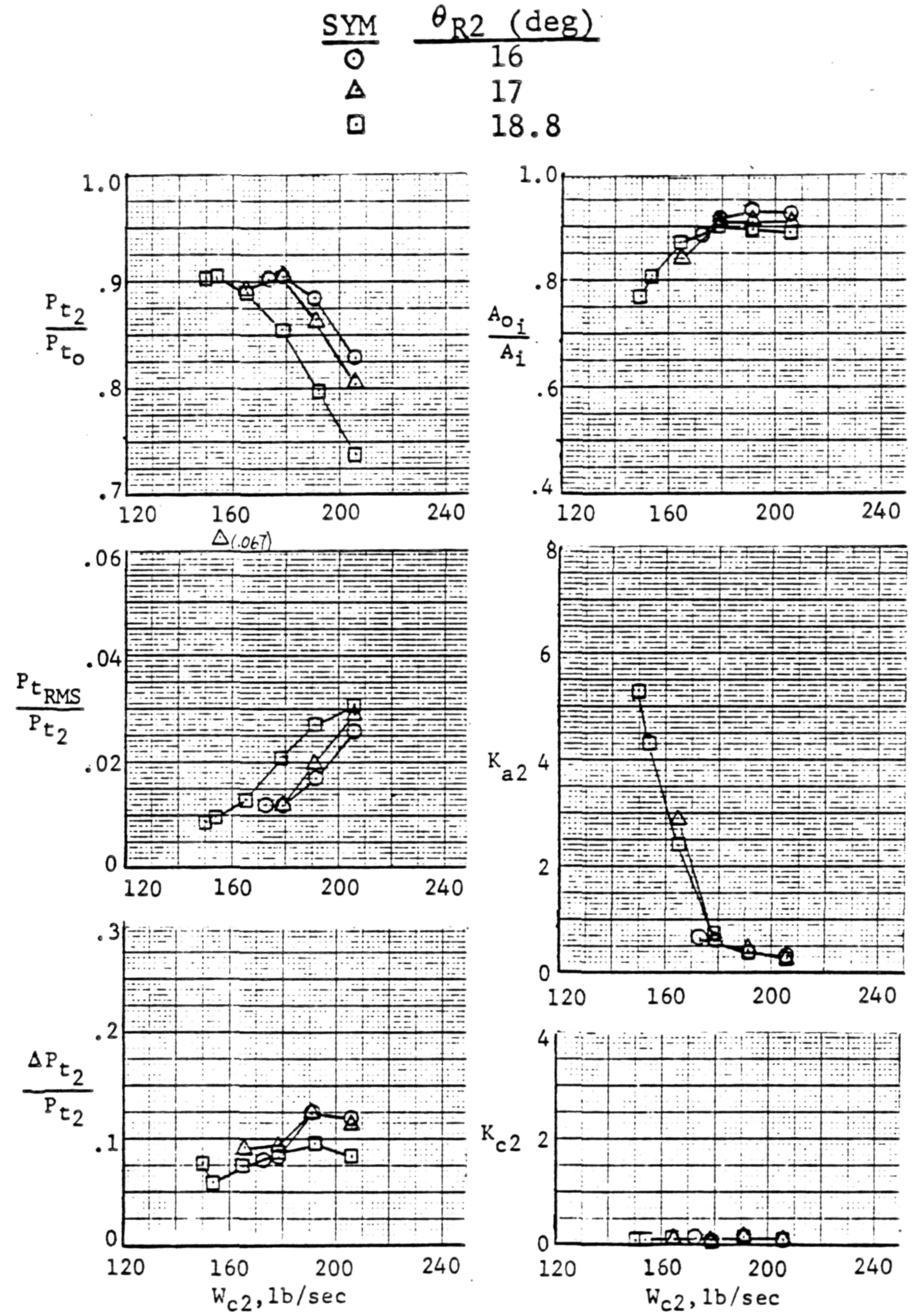

(a) $\alpha = -2^\circ$

Figure 7-9 Effect of Airflow on Steady-State Performance, $M_o = 2.0$, $\beta = 0^\circ$

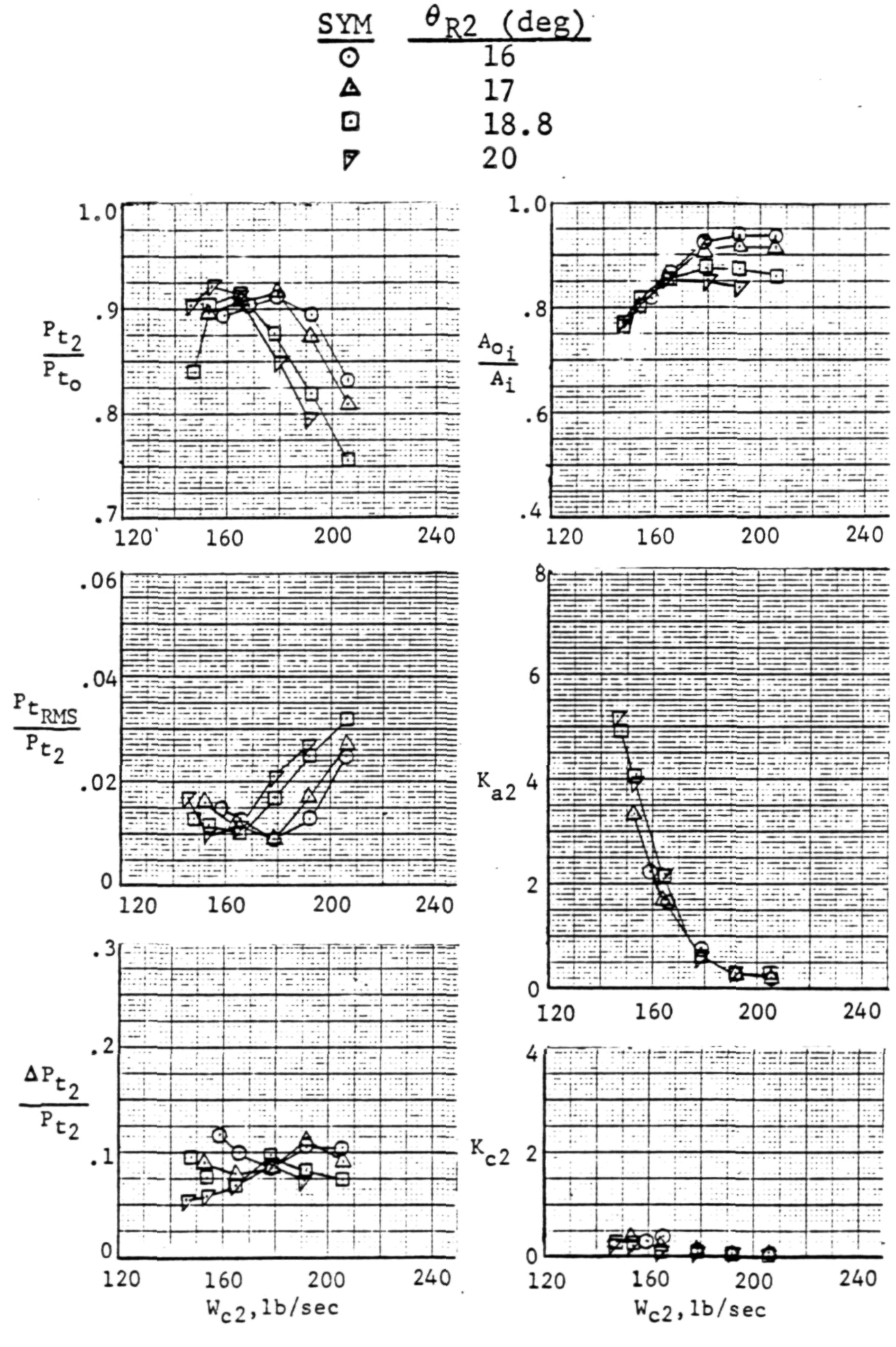

(b) $\alpha = 1^{\circ}$

Figure 7-9 (Cont'd)

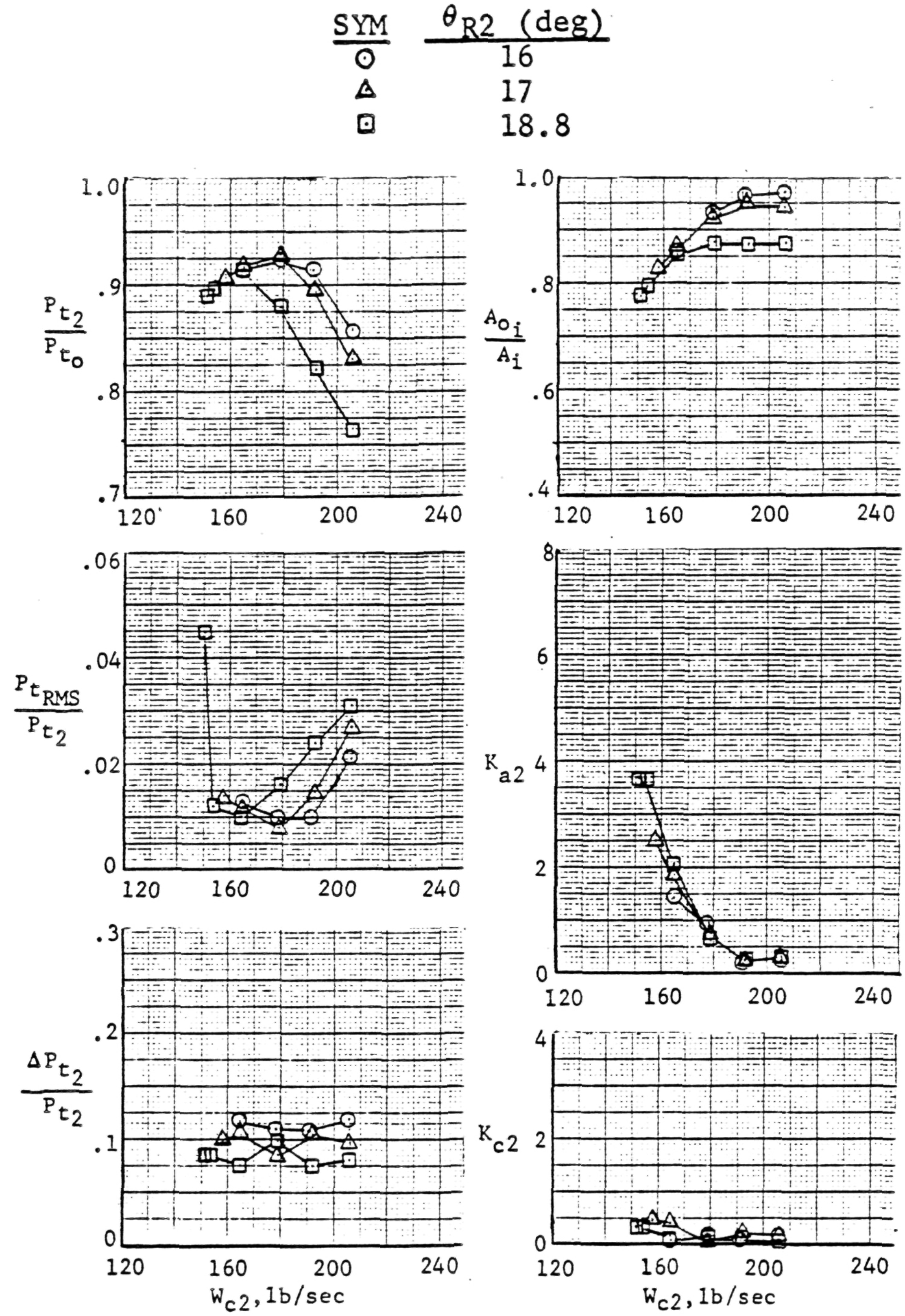

(c) $\alpha = 6^{\circ}$

Figure 7-9 (Cont'd)

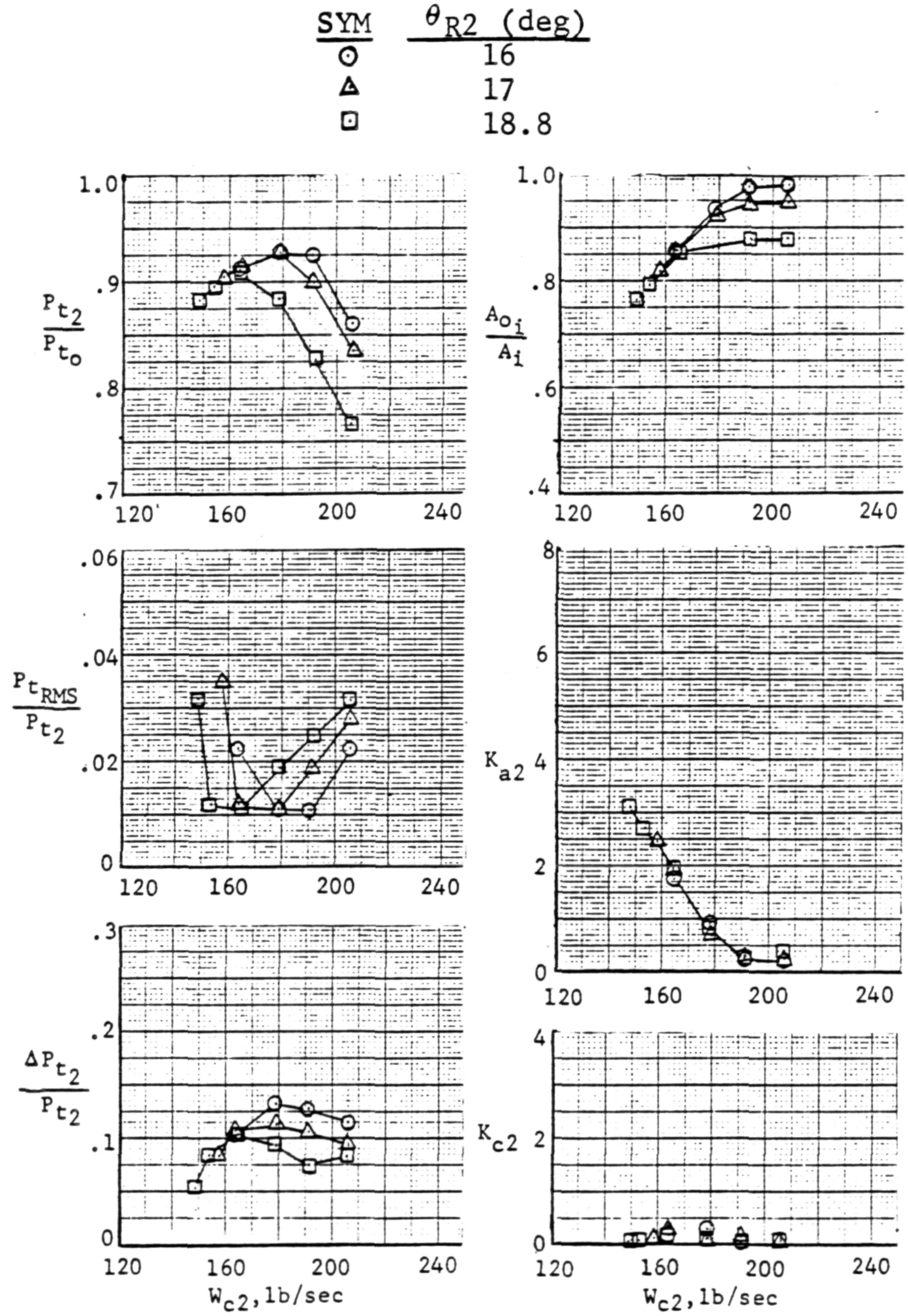

(d) $\alpha = 10^o$

Figure 7-9 (Cont'd)

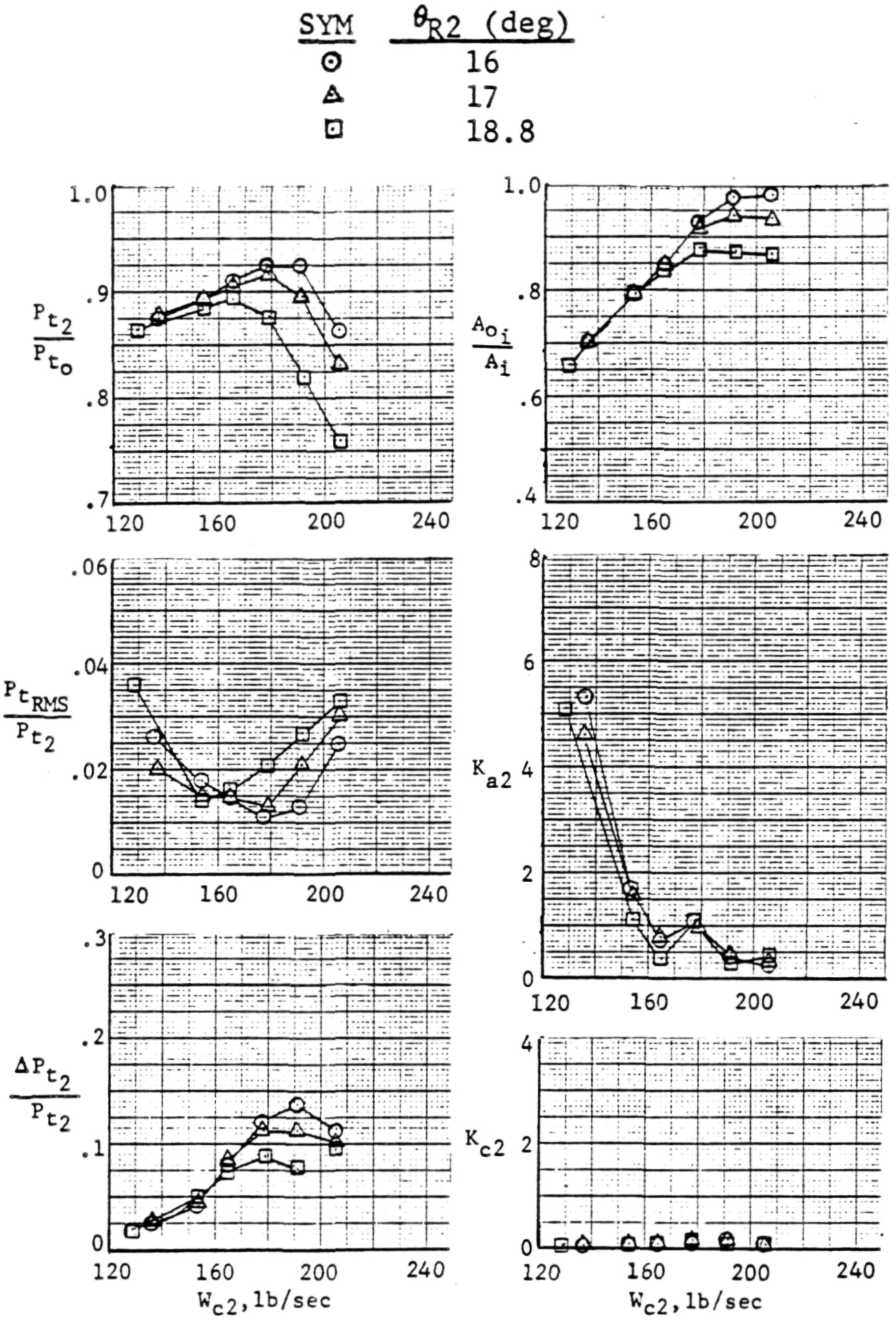

(e) $\alpha = 15^{\circ}$

Figure 7-9 (Cont'd)

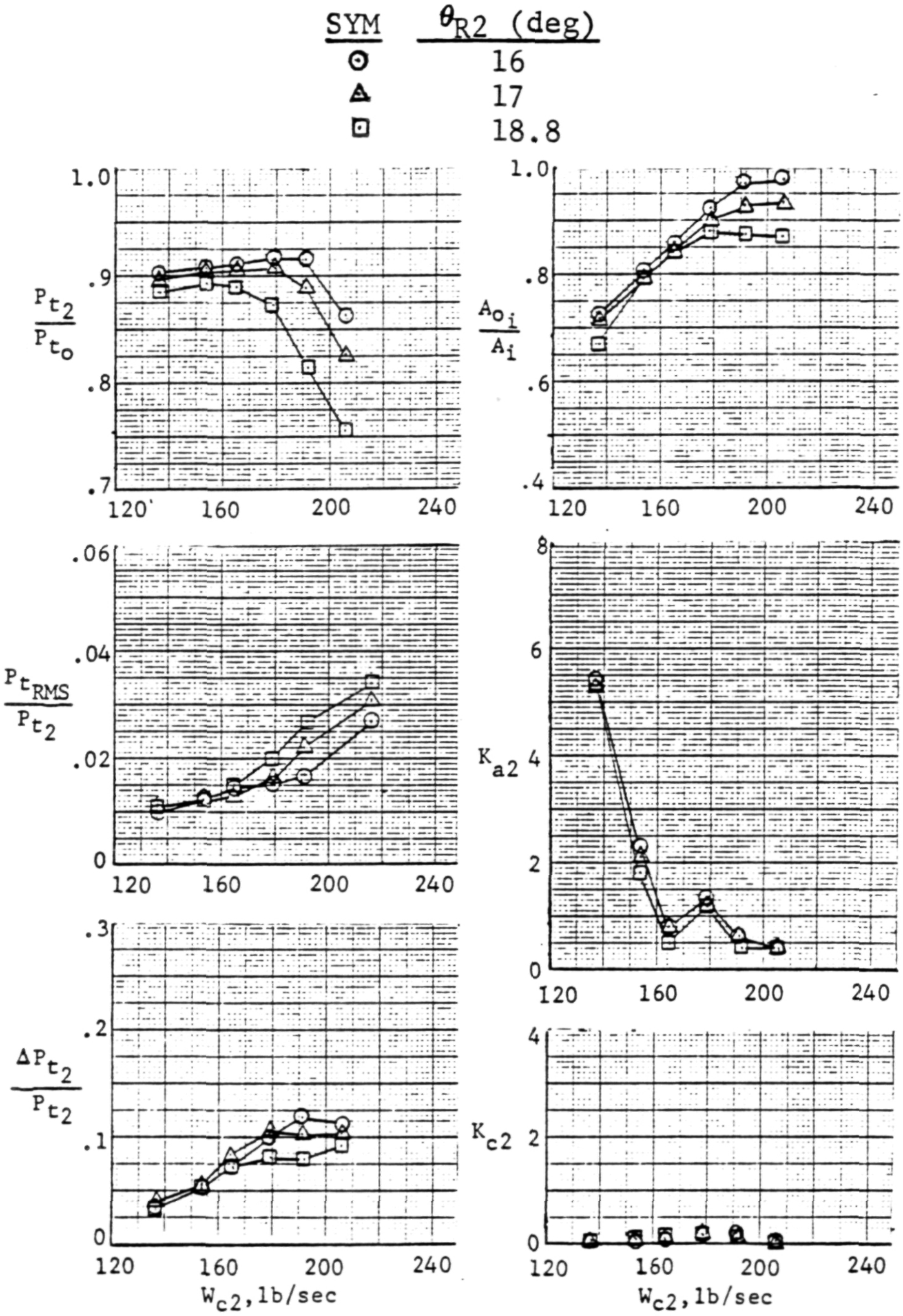

(f) $\alpha = 20^{\circ}$

Figure 7-9 (Concl)

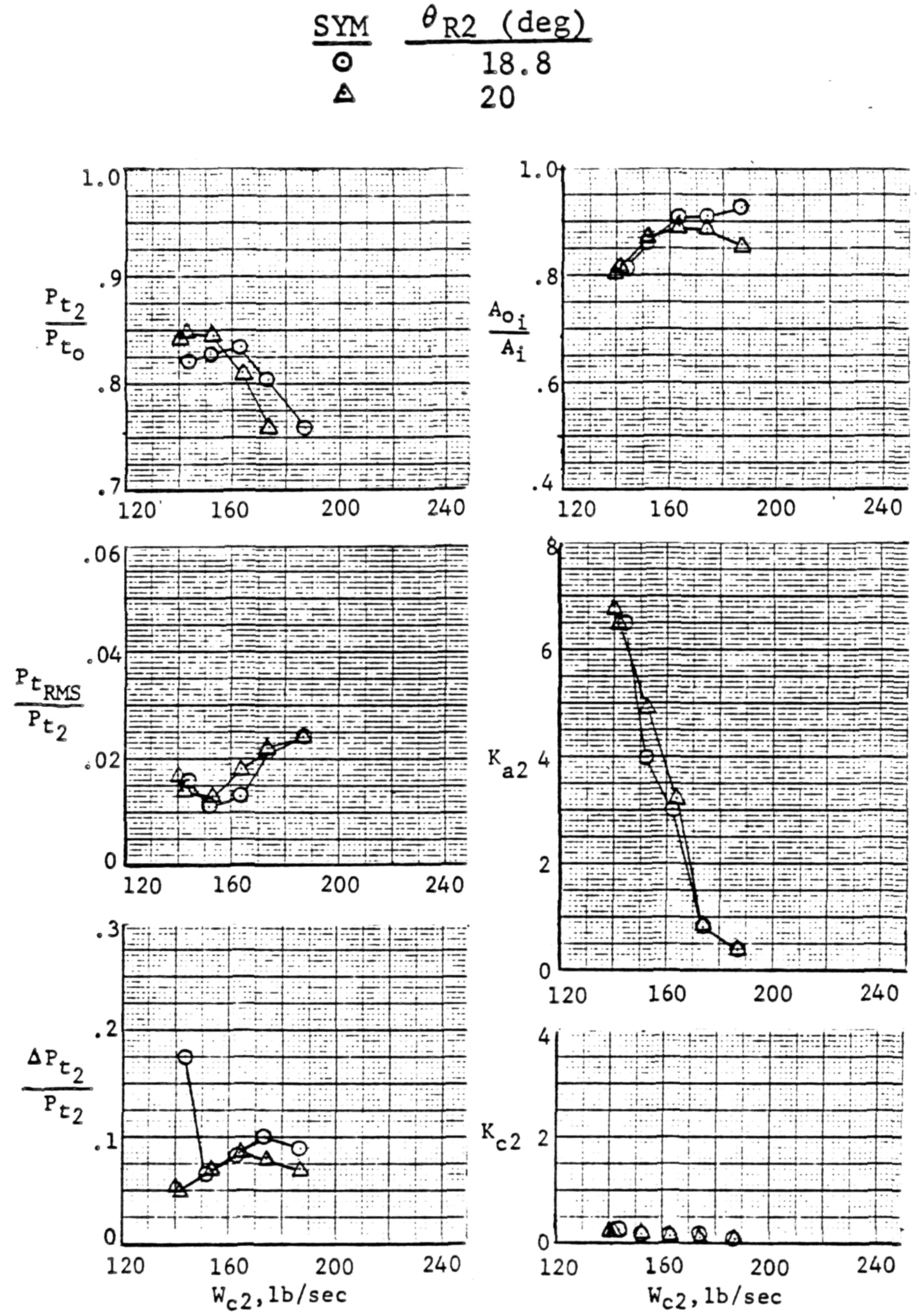

(a) $\alpha = -2^{\circ}$

Figure 7-10 Effect of Airflow on Steady-State Performance, $M_o = 2.2$, $\beta = 0^{\circ}$

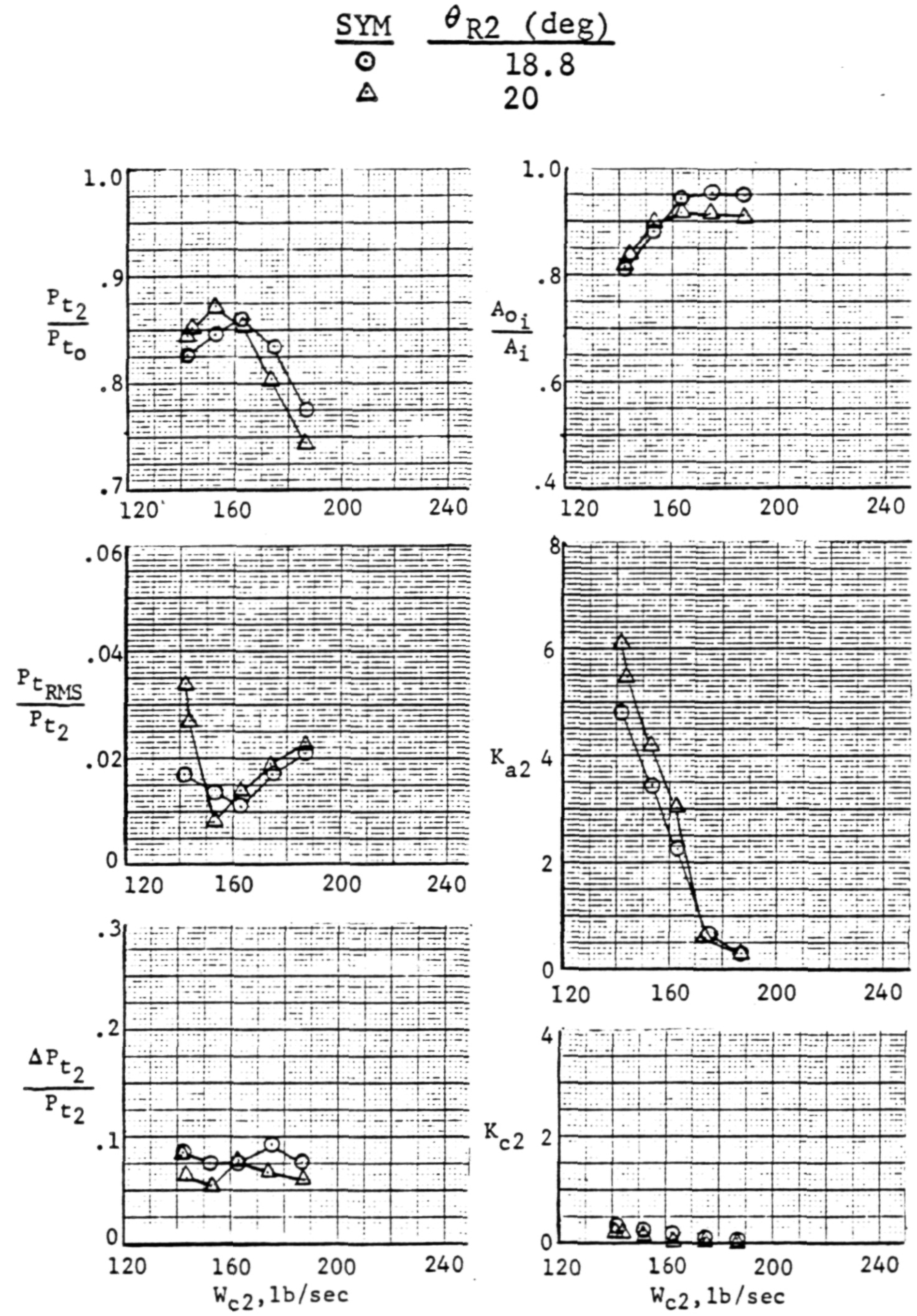

(b) $\alpha = 1^{\circ}$

Figure 7-10 (Cont'd)

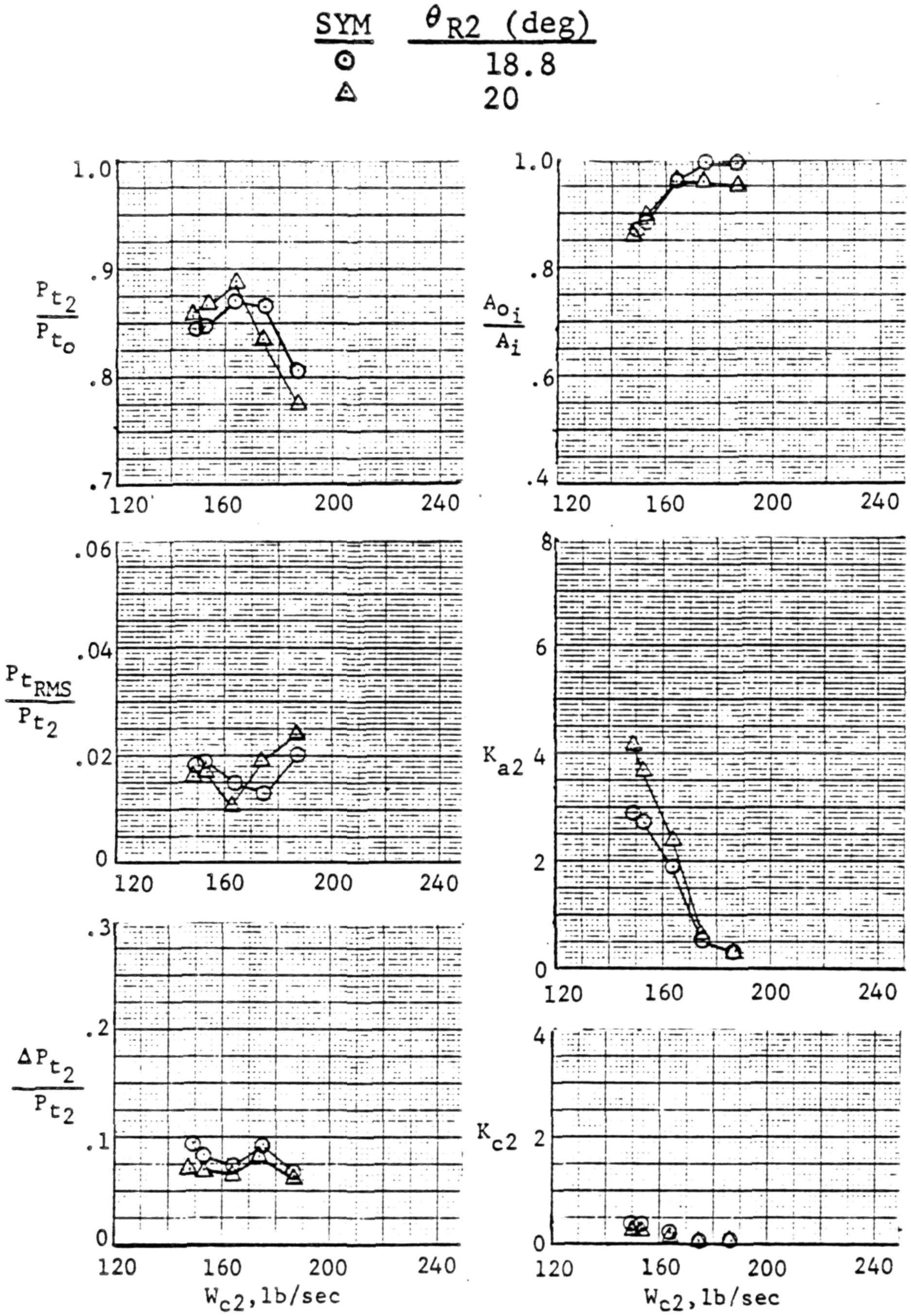

(c) $\alpha = 6^{\circ}$

Figure 7-10 (Cont'd)

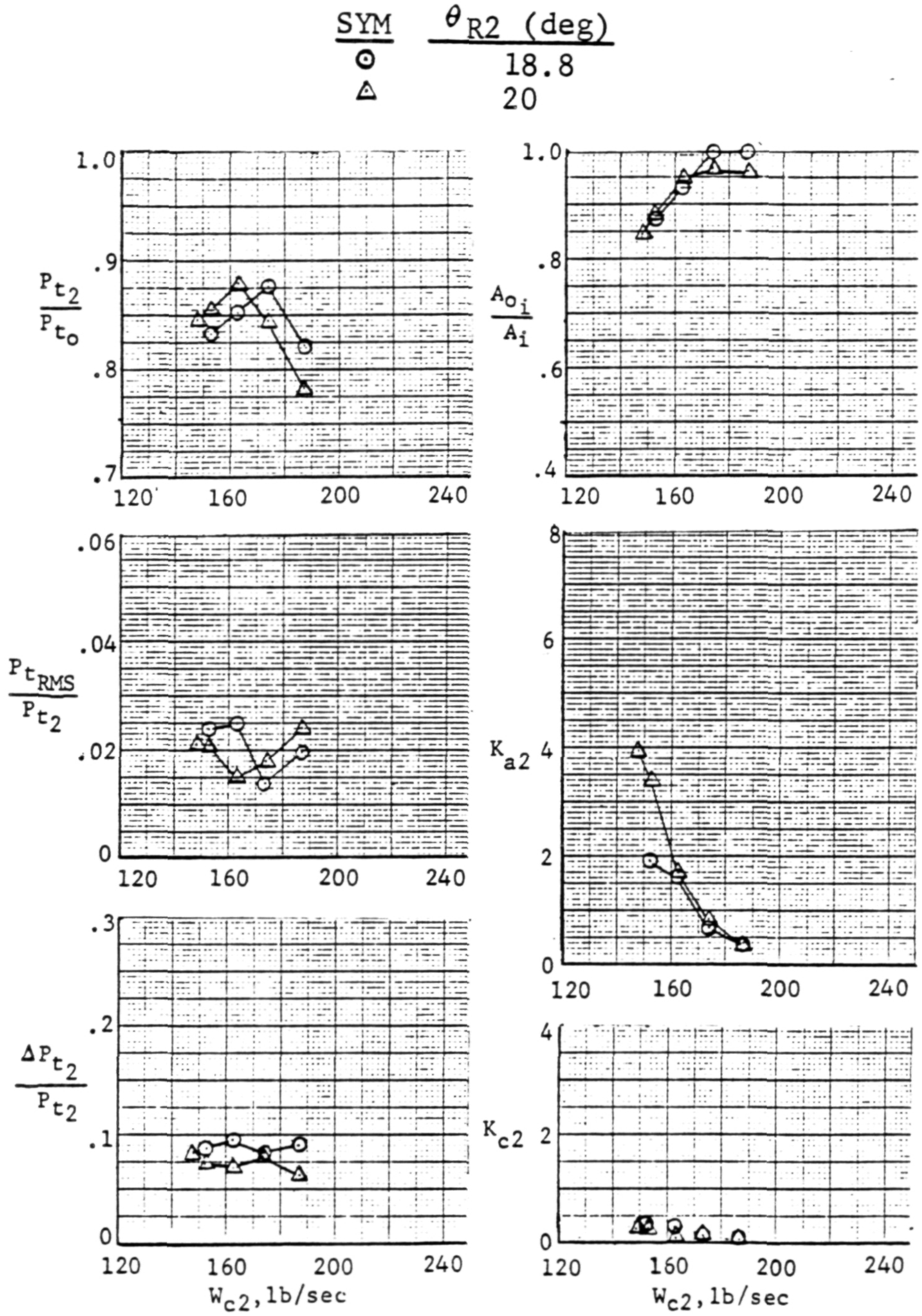

(d) $\alpha = 10^{\circ}$

Figure 7-10 (Cont'd)

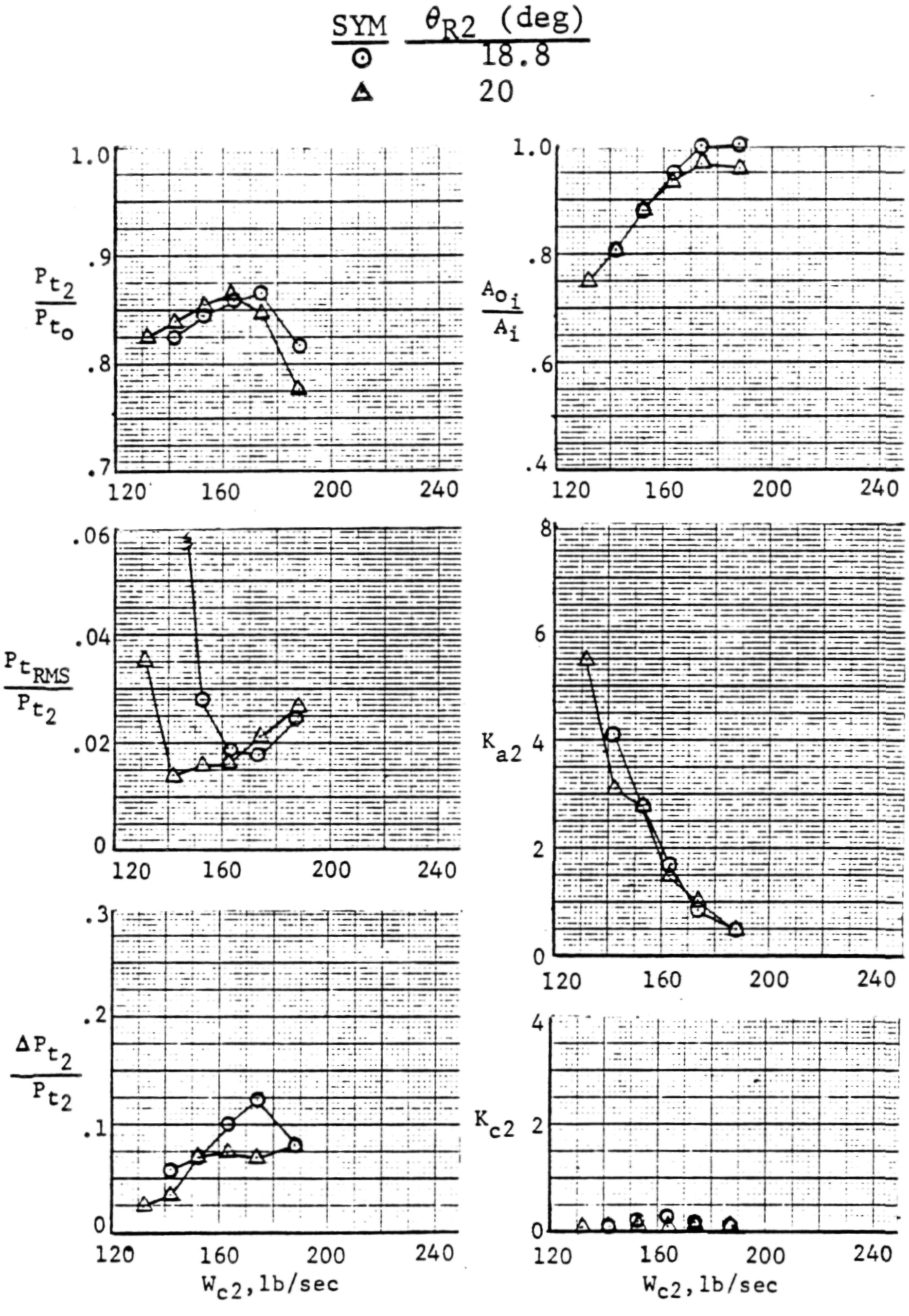

(e) $\alpha = 15^{\circ}$

Figure 7-10 (Cont'd)

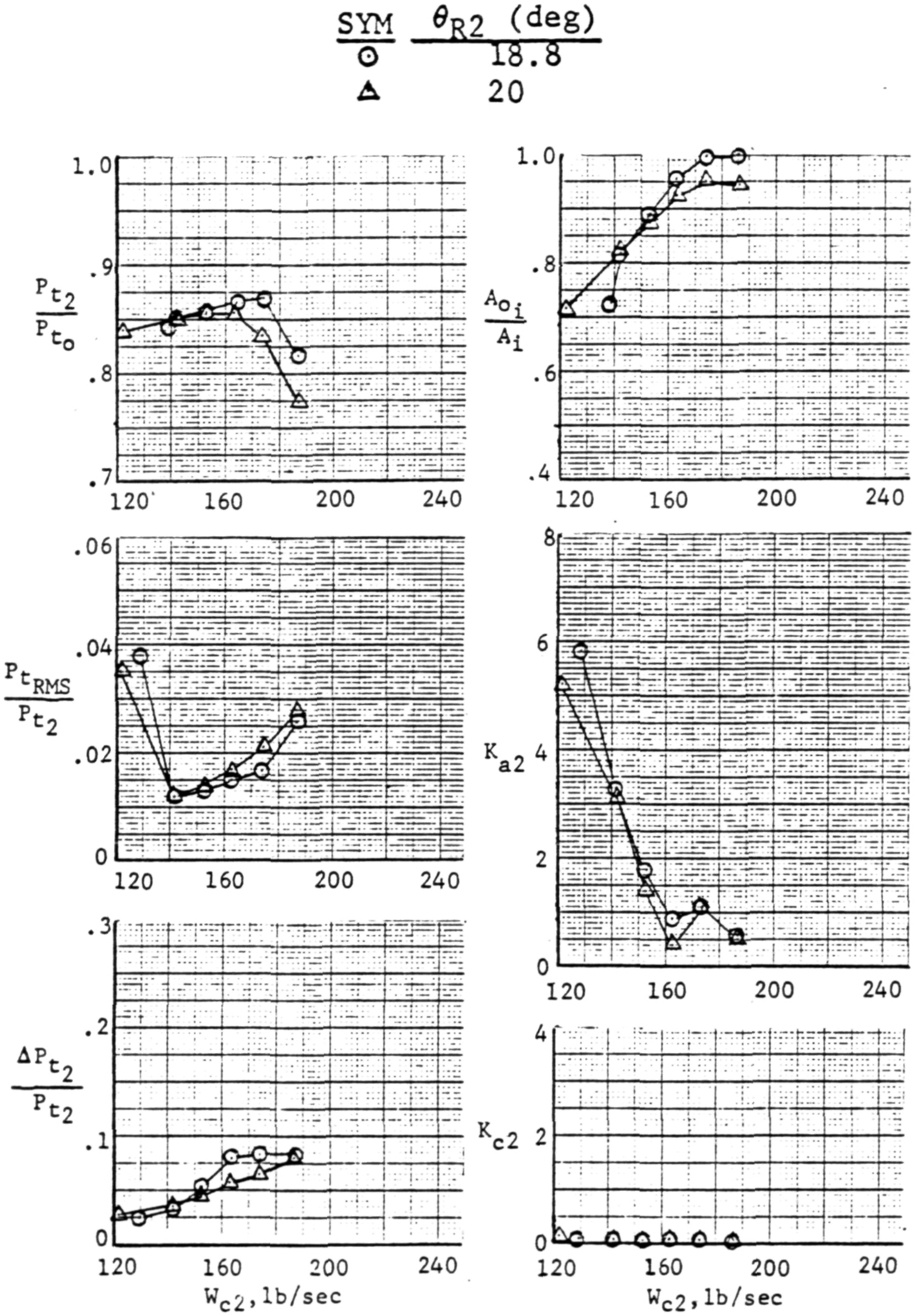

(f) $\alpha = 20^{\circ}$

Figure 7-10 (Concl)

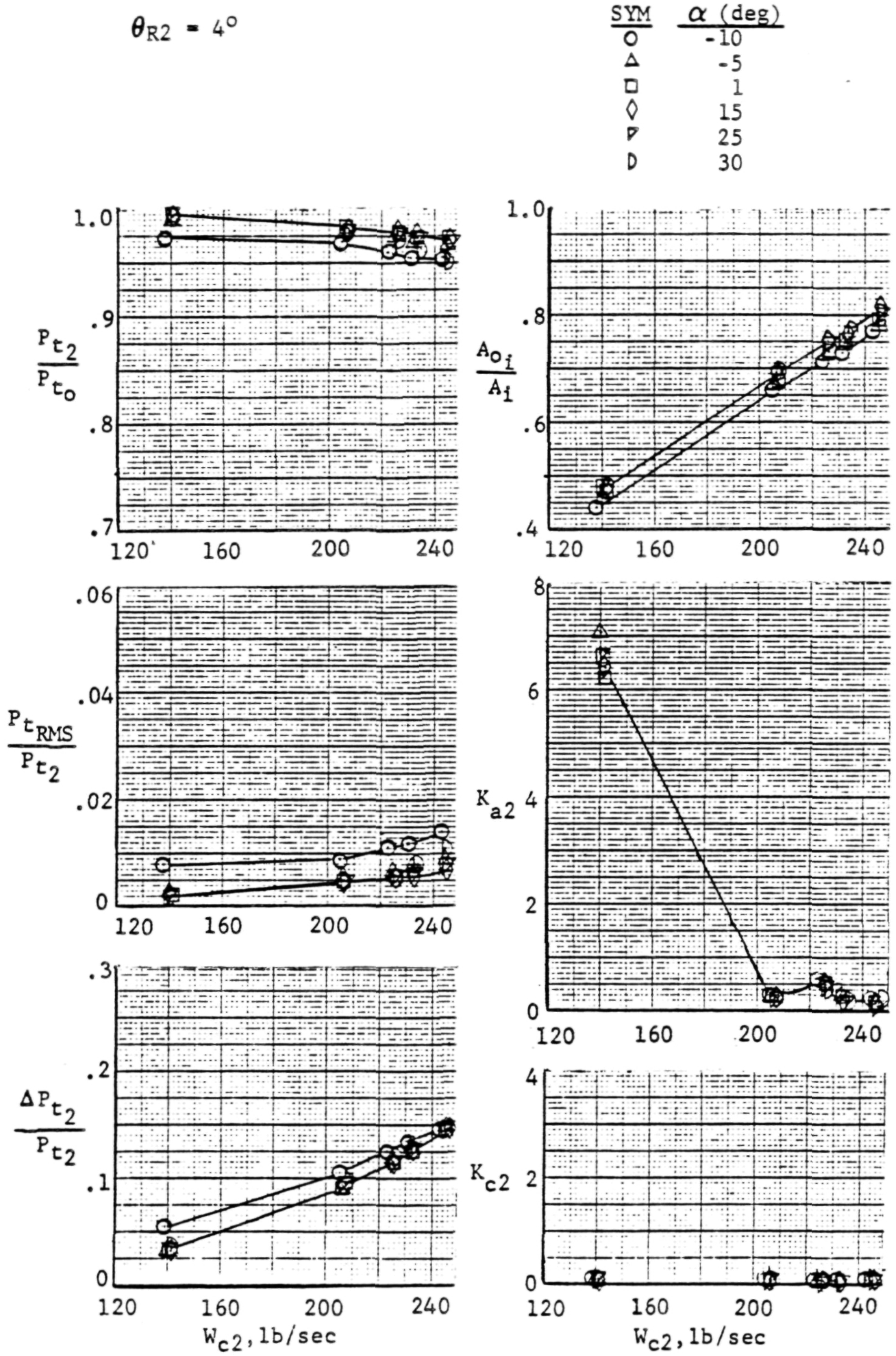

Figure 7-11 Effect of Airflow on Steady-State Performance, $M_o = 0.8$, $\beta = -5^{\circ}$

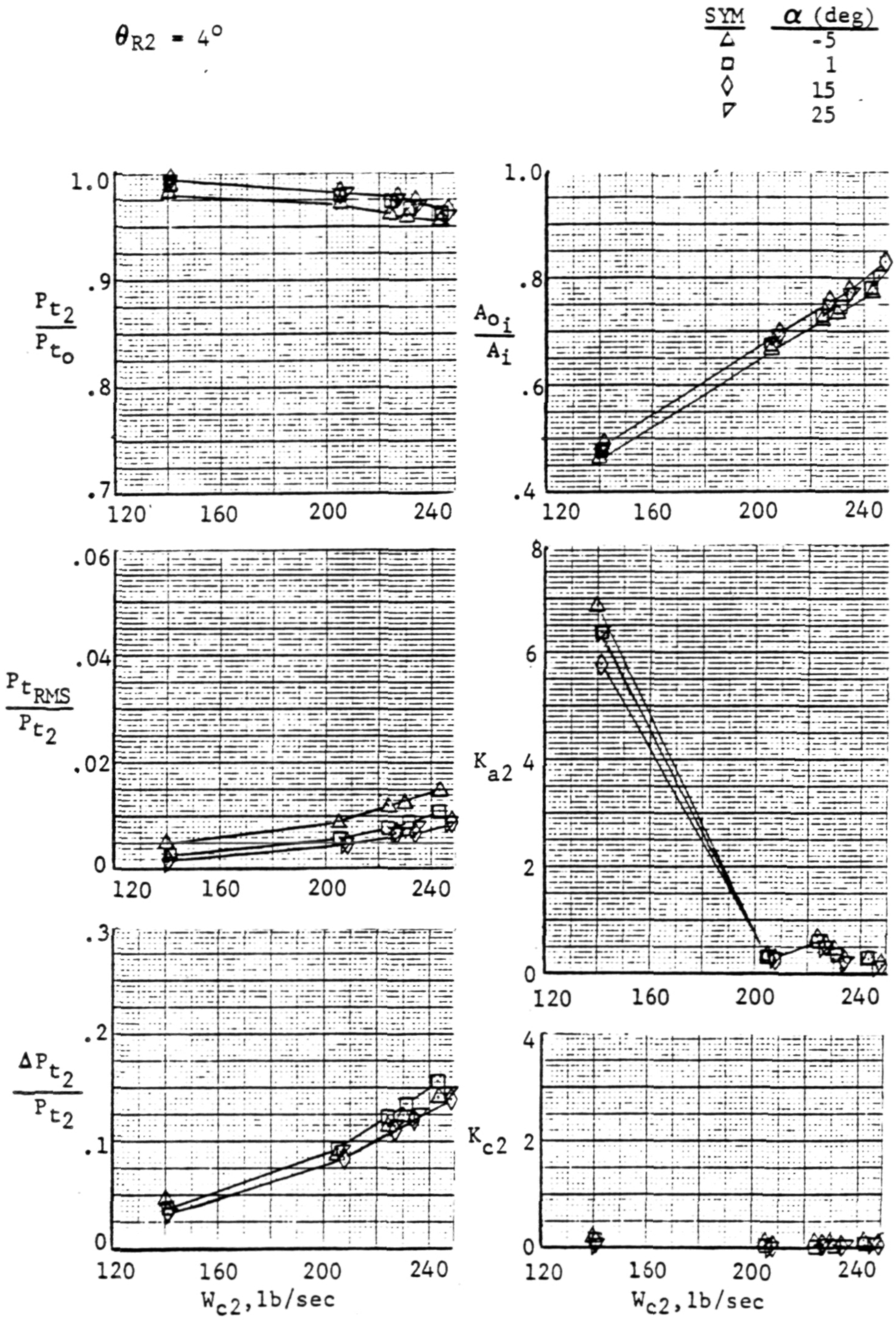

Figure 7-12 Effect of Airflow on Steady-State Performance, $M_o = 0.8$, $\beta = -10^\circ$

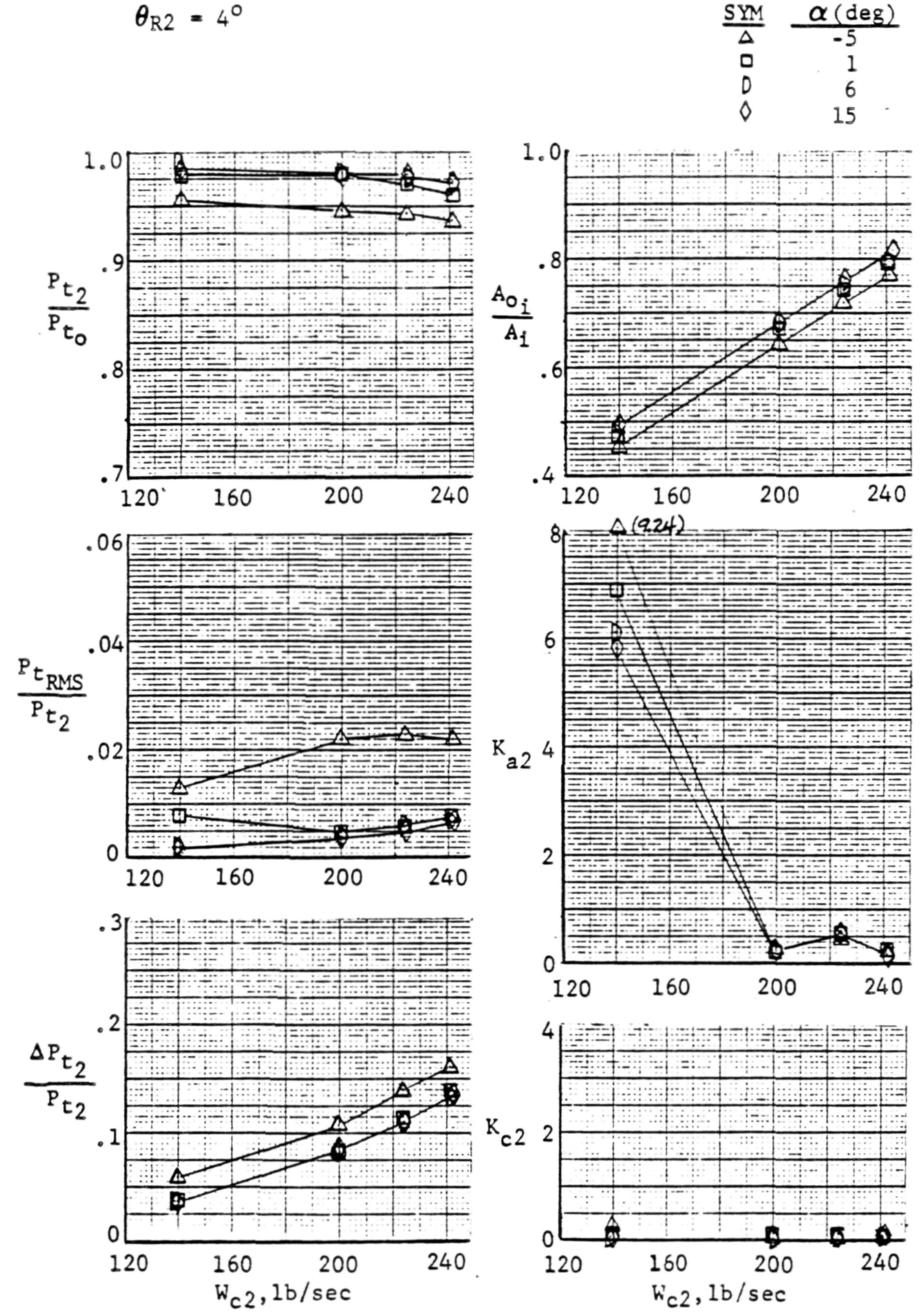

Figure 7-13 Effect of Airflow on Steady-State Performance, $M_0 = 1.3$, $\beta = -5°$

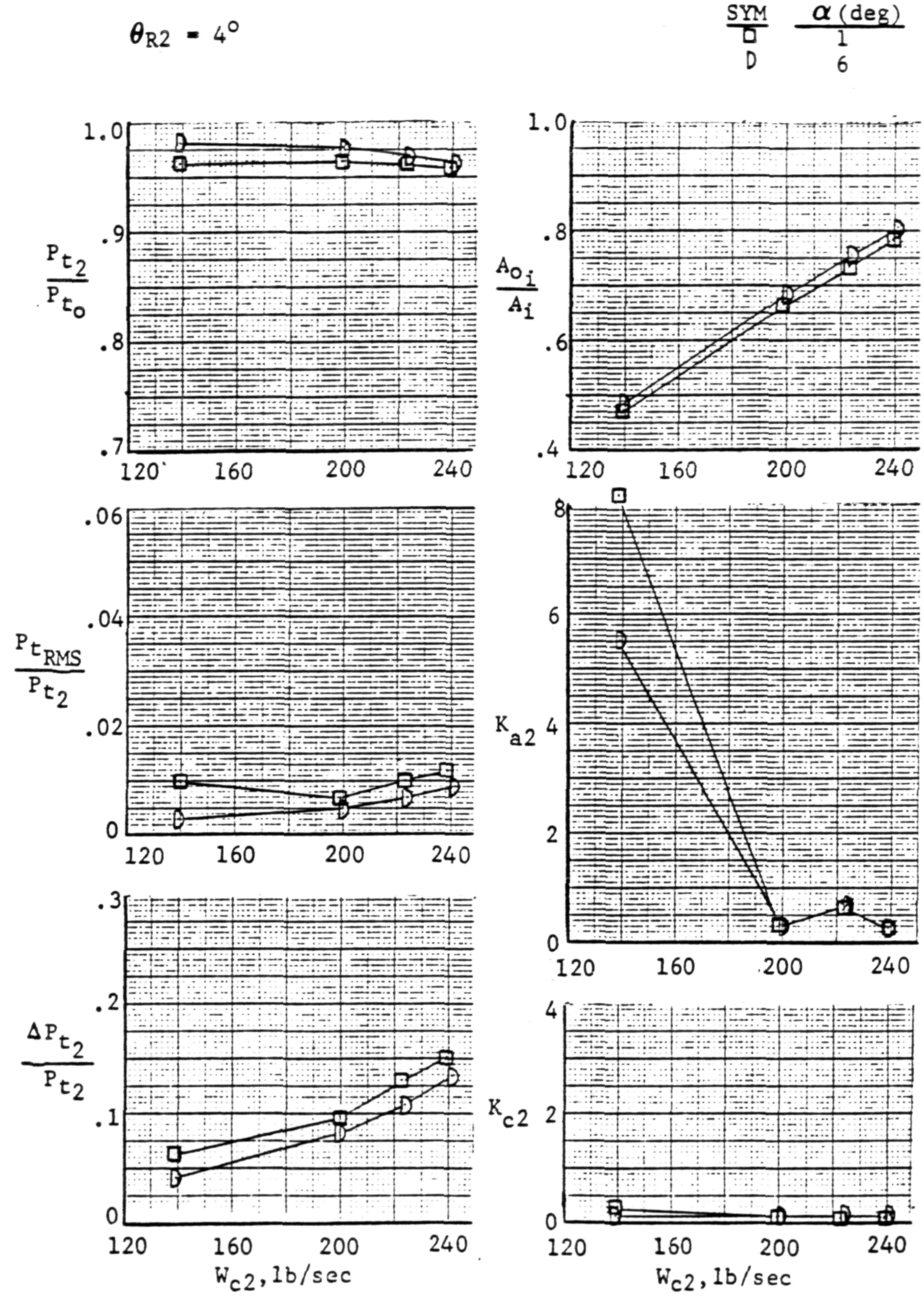

Figure 7-14 Effect of Airflow on Steady-State Performance, $M_o = 1.3$, $\beta = -10^{\circ}$

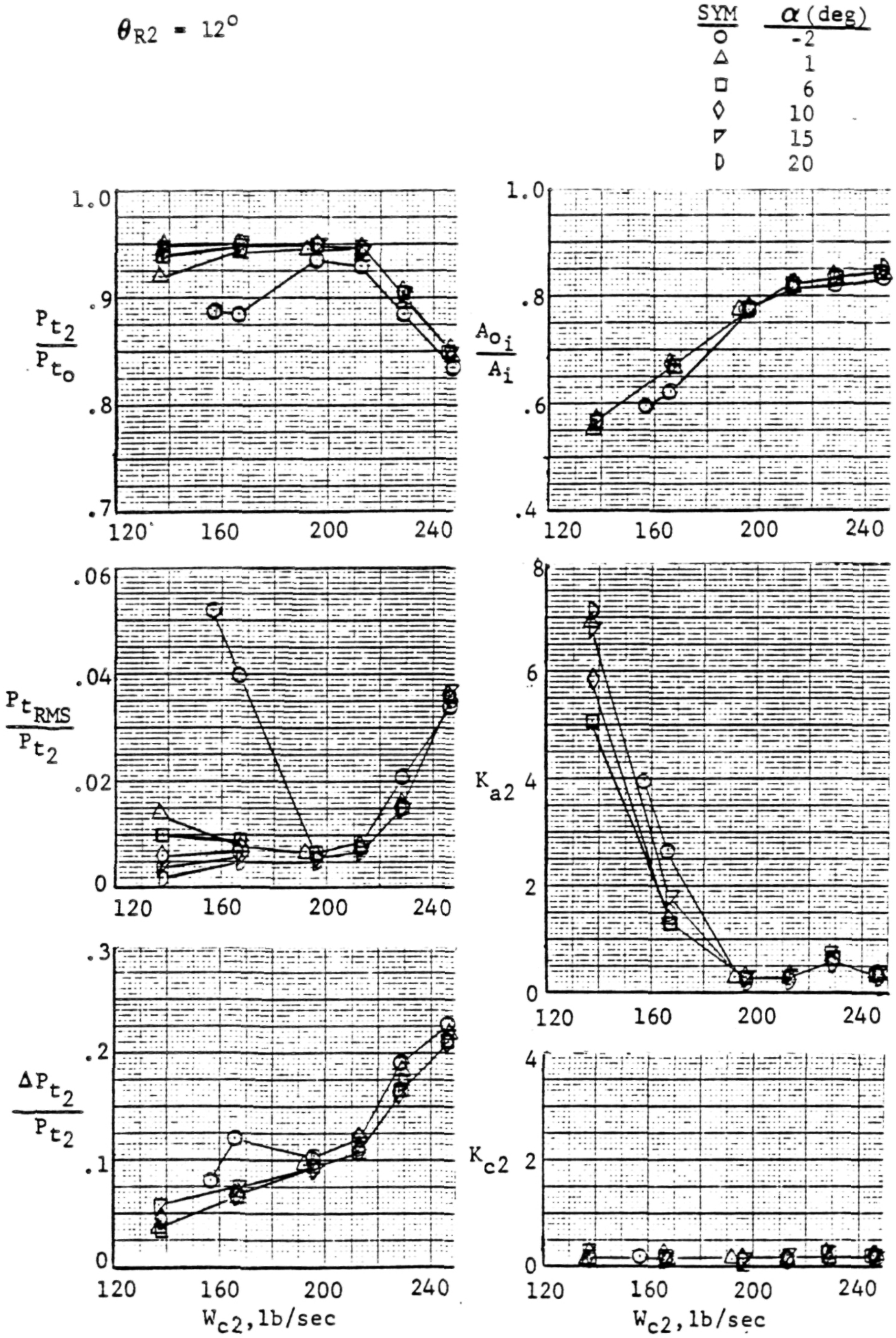

Figure 7-15 Effect of Airflow on Steady-State Performance, $M_0 = 1.6$, $\beta = -5^\circ$

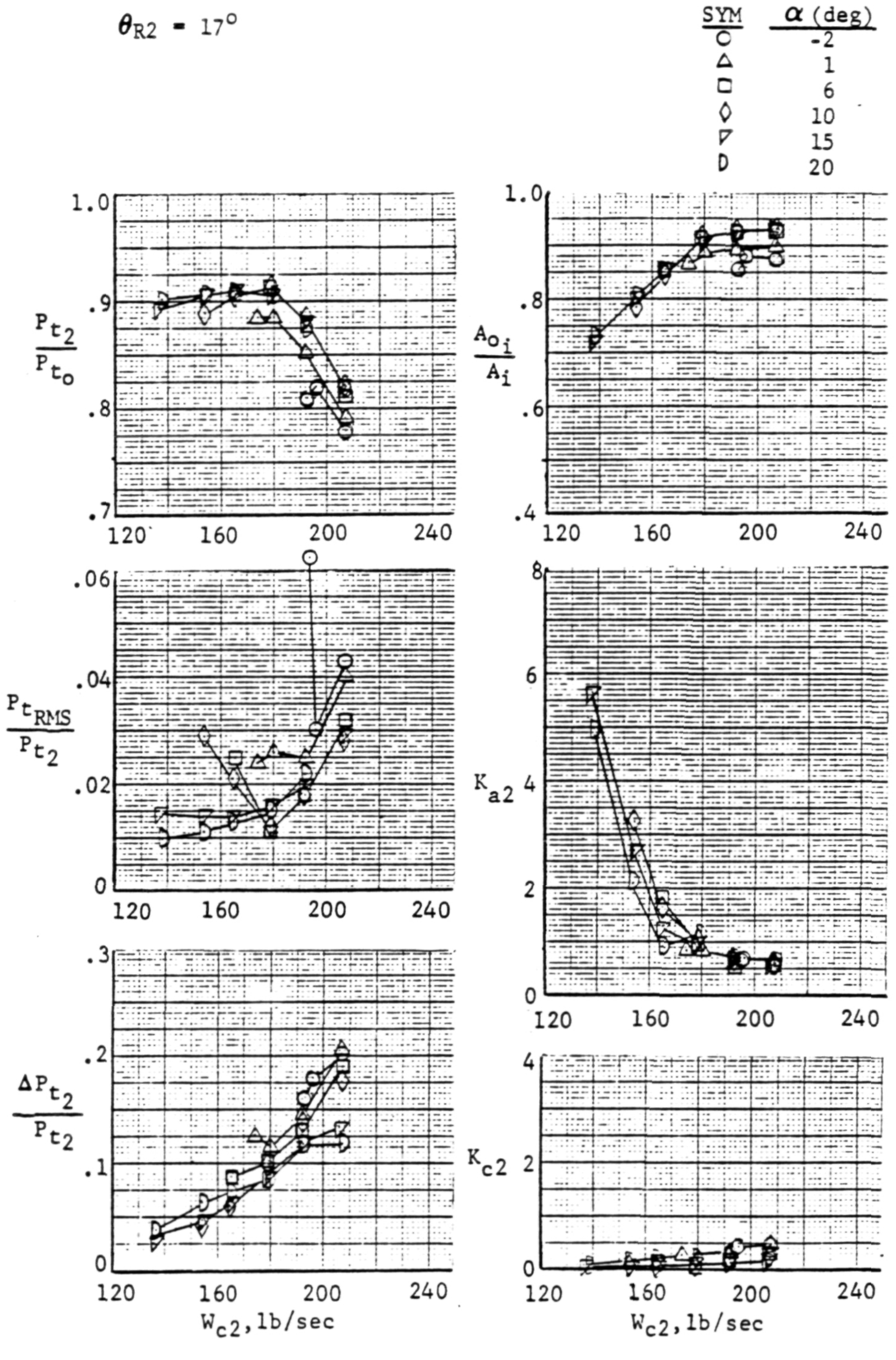

Figure 7-16 Effect of Airflow on Steady-State Performance, $M_0 = 2.0$, $\beta = -5^{\circ}$

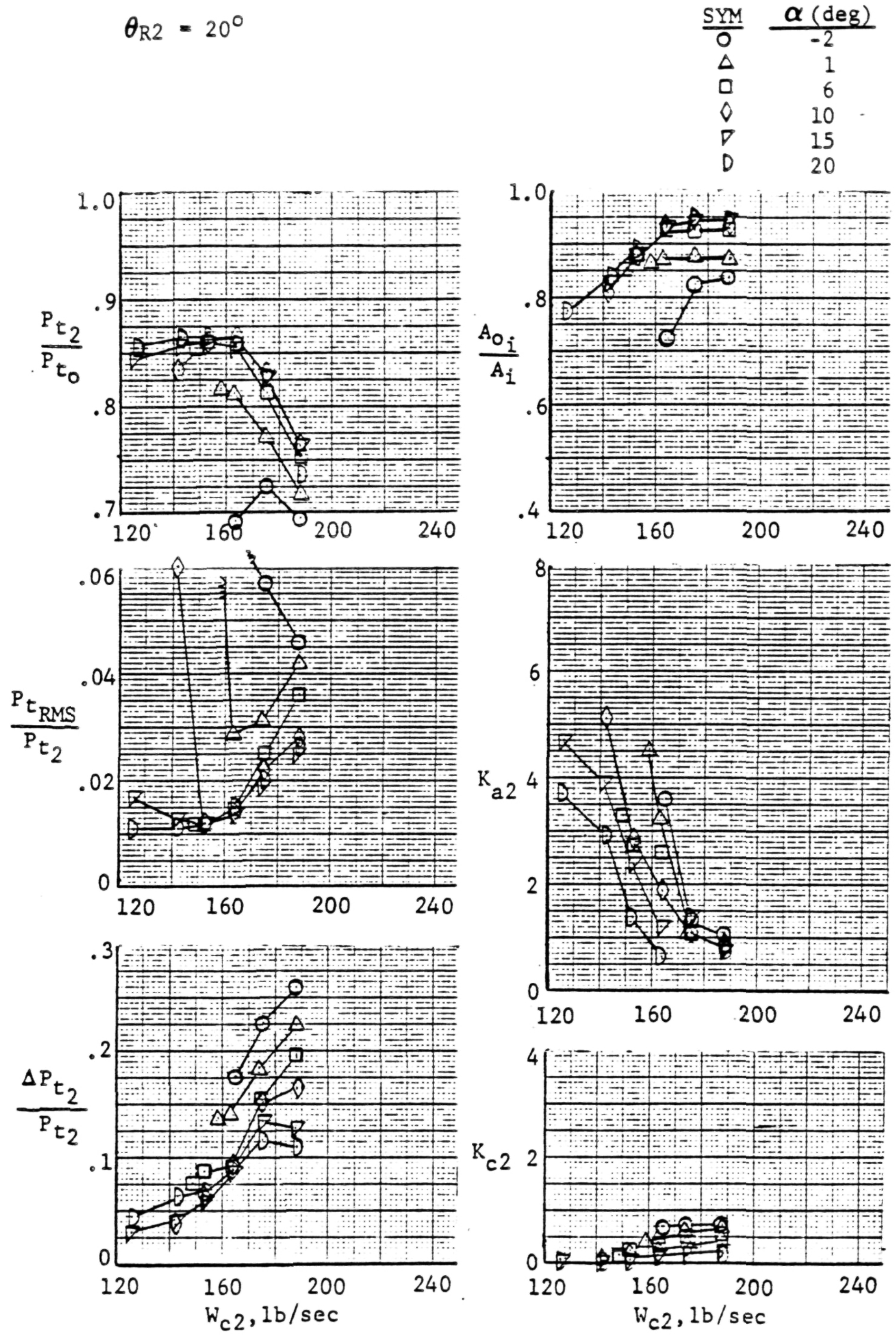

Figure 7-17 Effect of Airflow on Steady-State Performance, $M_o = 2.2$, $\beta = -5^{\circ}$

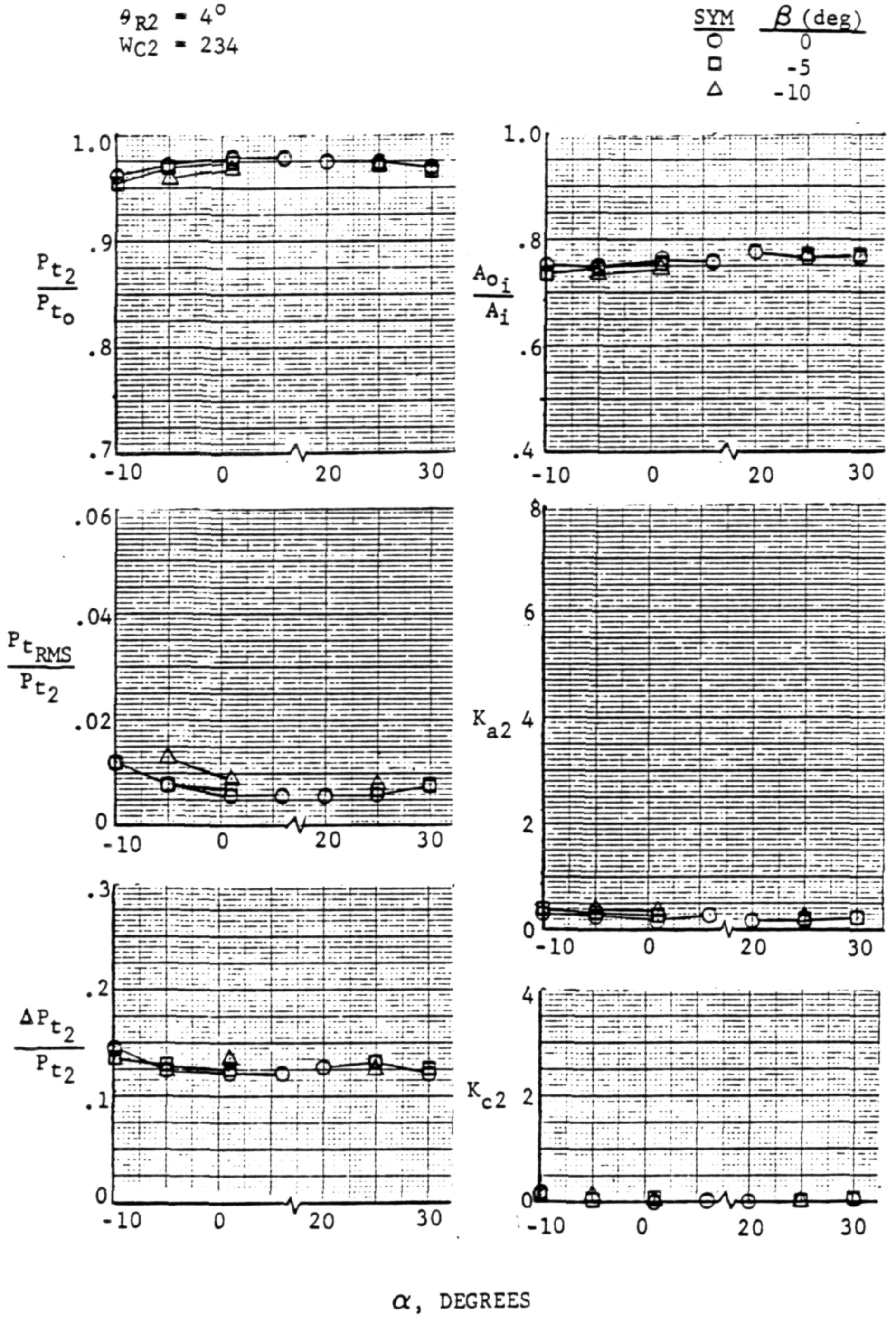

(a) $M_o = 0.8$

Figure 7-18 Effect of Angle of Attack on Steady-State Performance

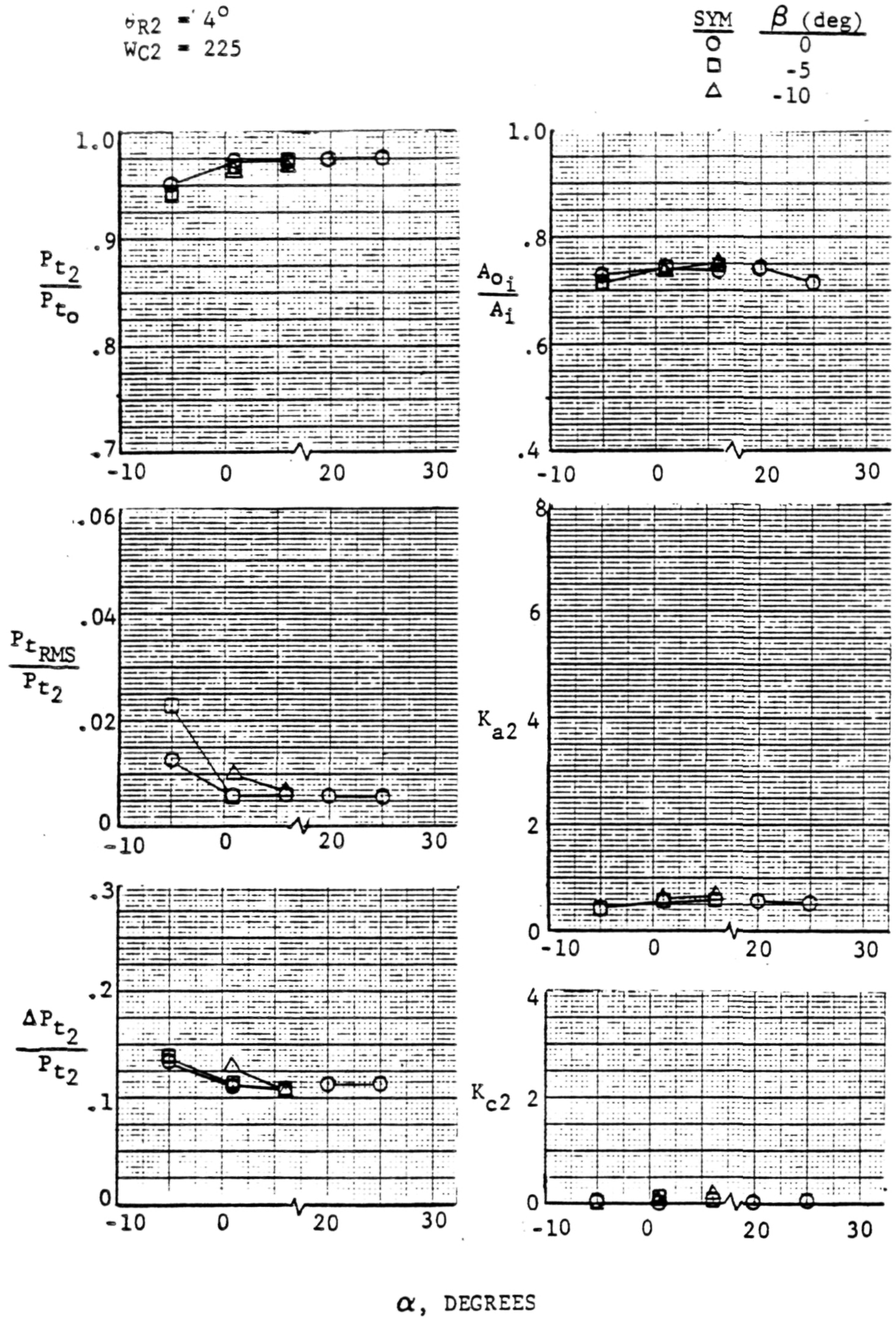

(b) $M_o = 1.3$

Figure 7-18 (Cont'd)

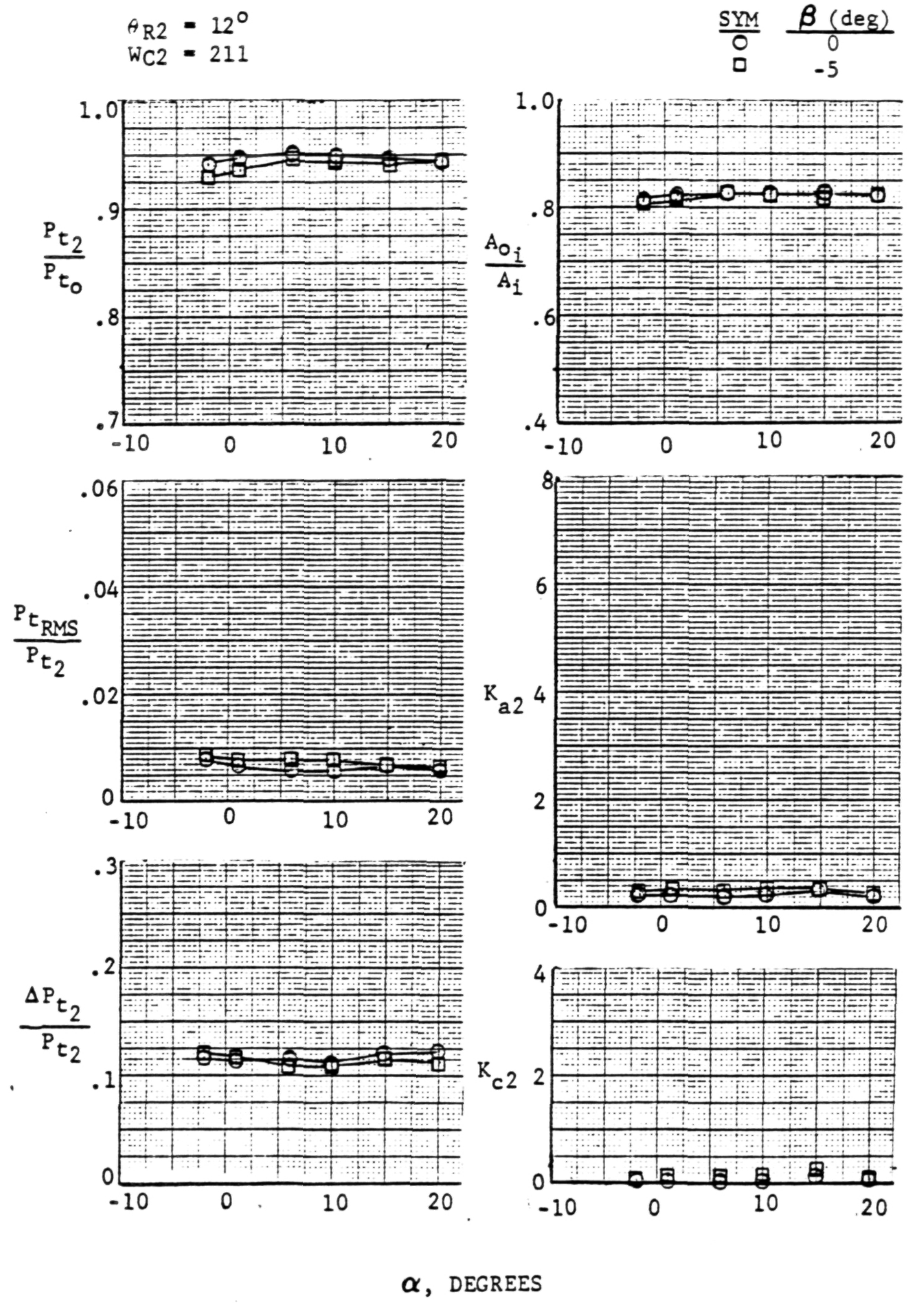

(c) $M_o = 1.6$

Figure 7-18 (Cont'd)

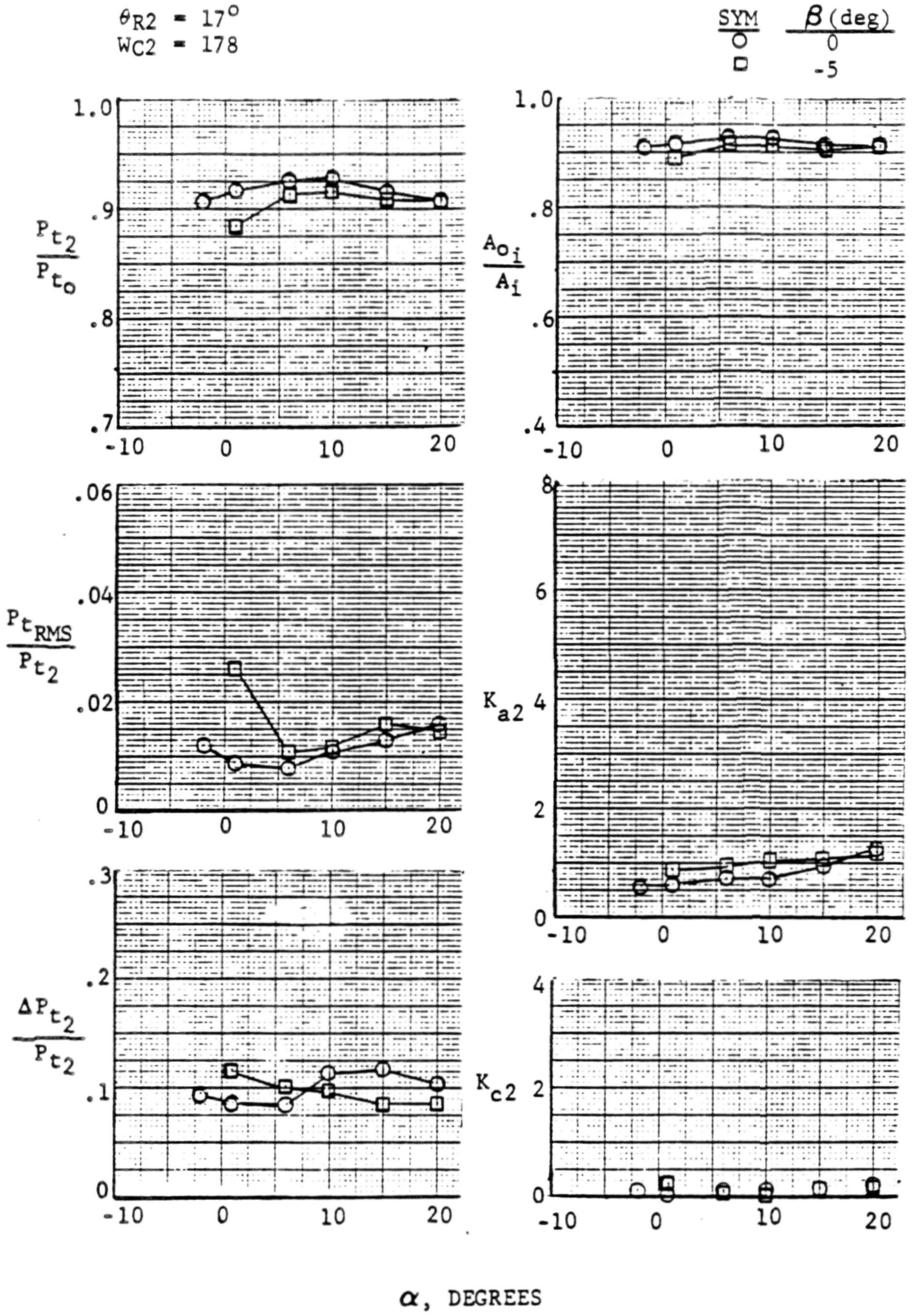

(d) $M_o = 2.0$

Figure 7-18 (Cont'd)

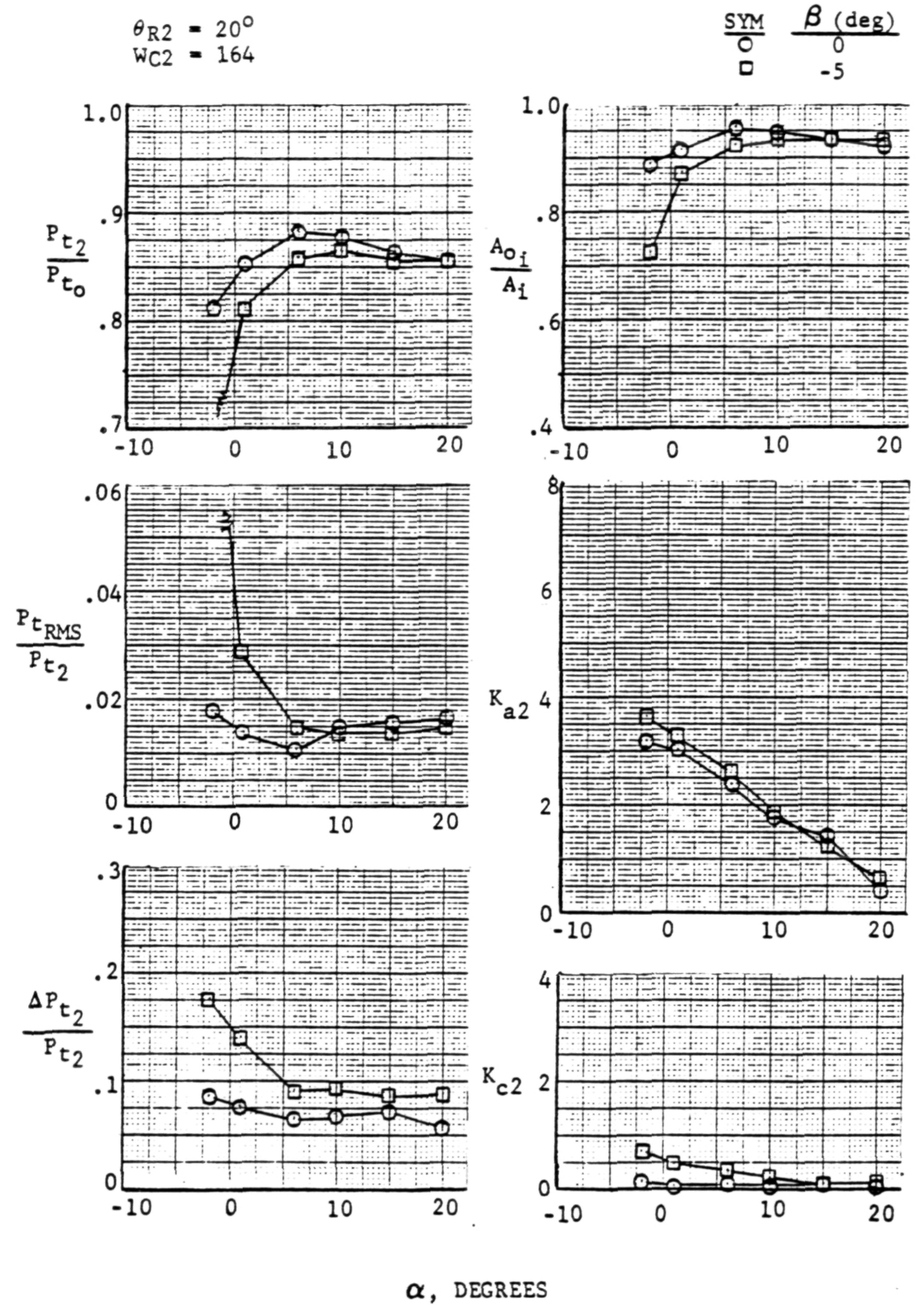

(e) $M_o = 2.2$

Figure 7-18 (Concl)

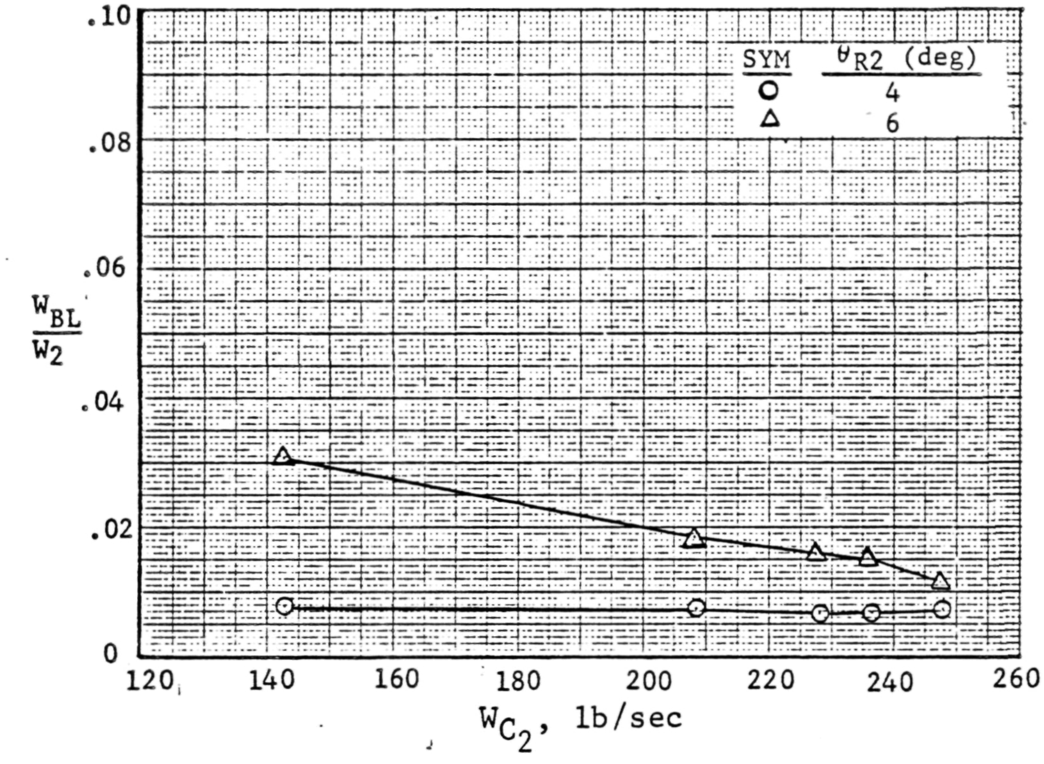

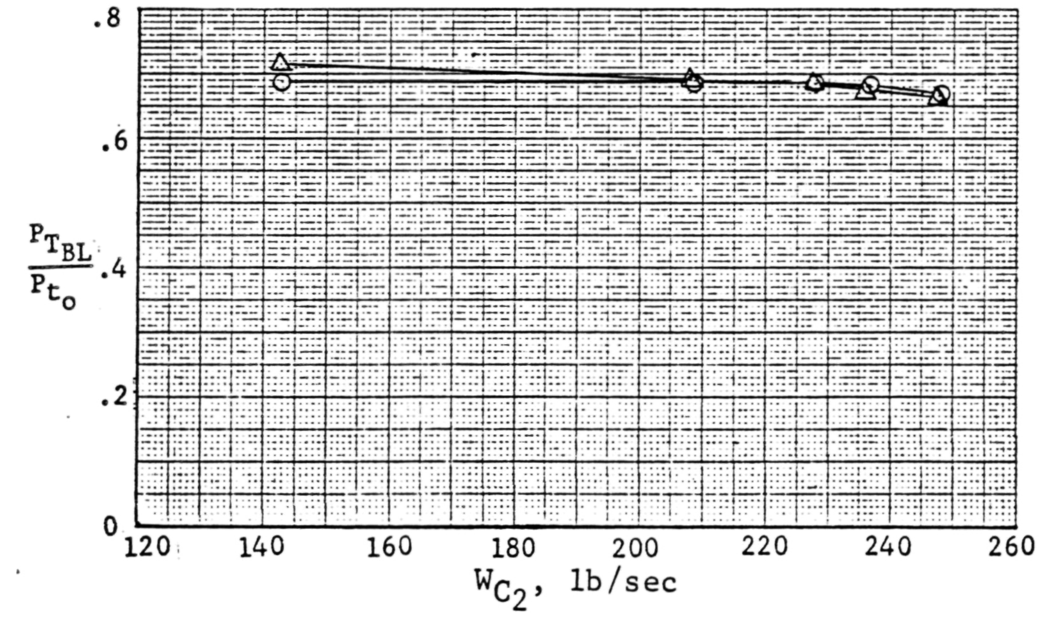

(a) $M_o = 0.8$

Figure 7-19 Effect of Engine Airflow on Bleed System Characteristics, $\alpha = 1°$, $\beta = 0°$

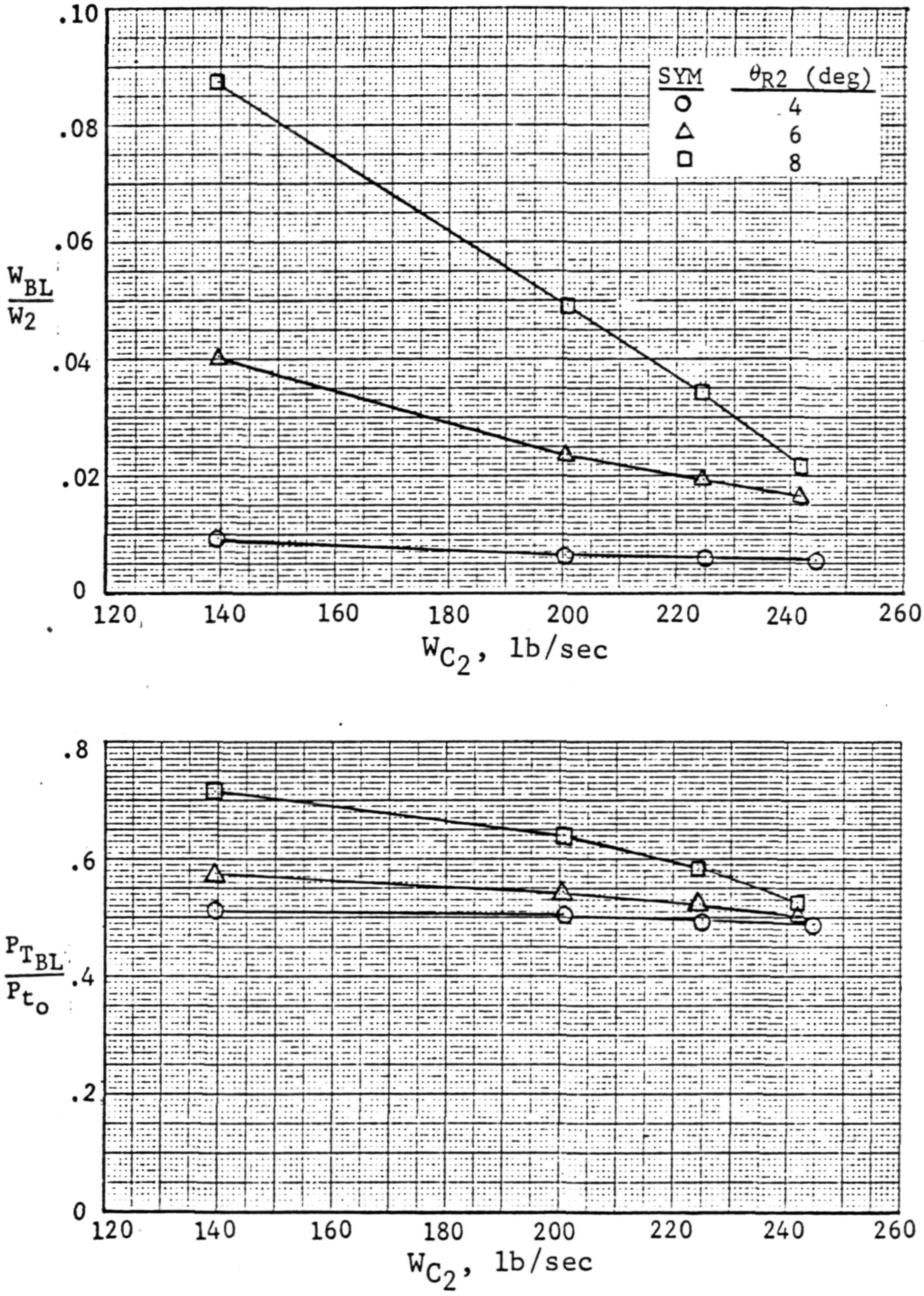

(b) $M_o = 1.3$

Figure 7-19 (Cont'd)

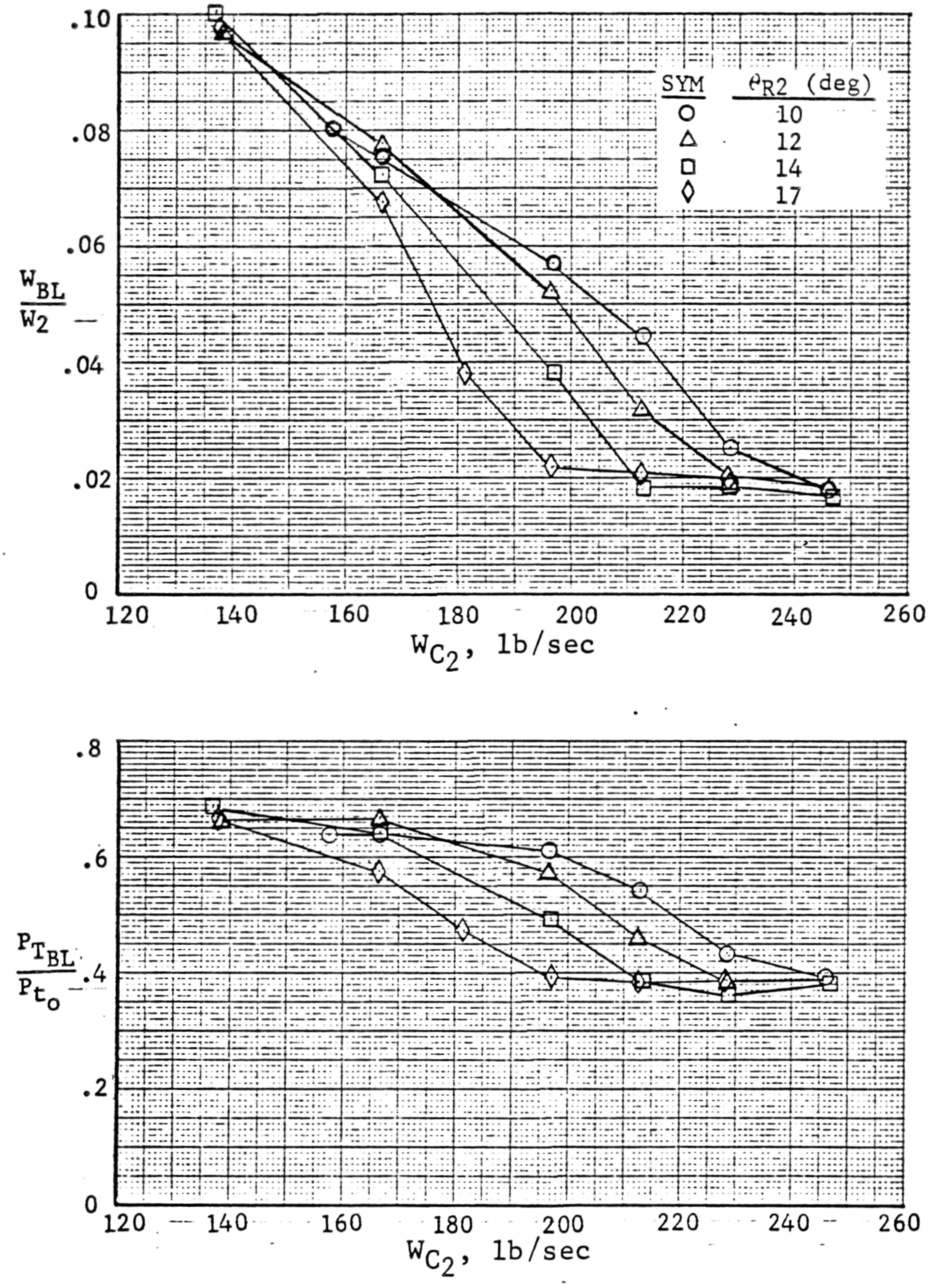

(c) $M_o = 1.6$

Figure 7-19 (Cont'd)

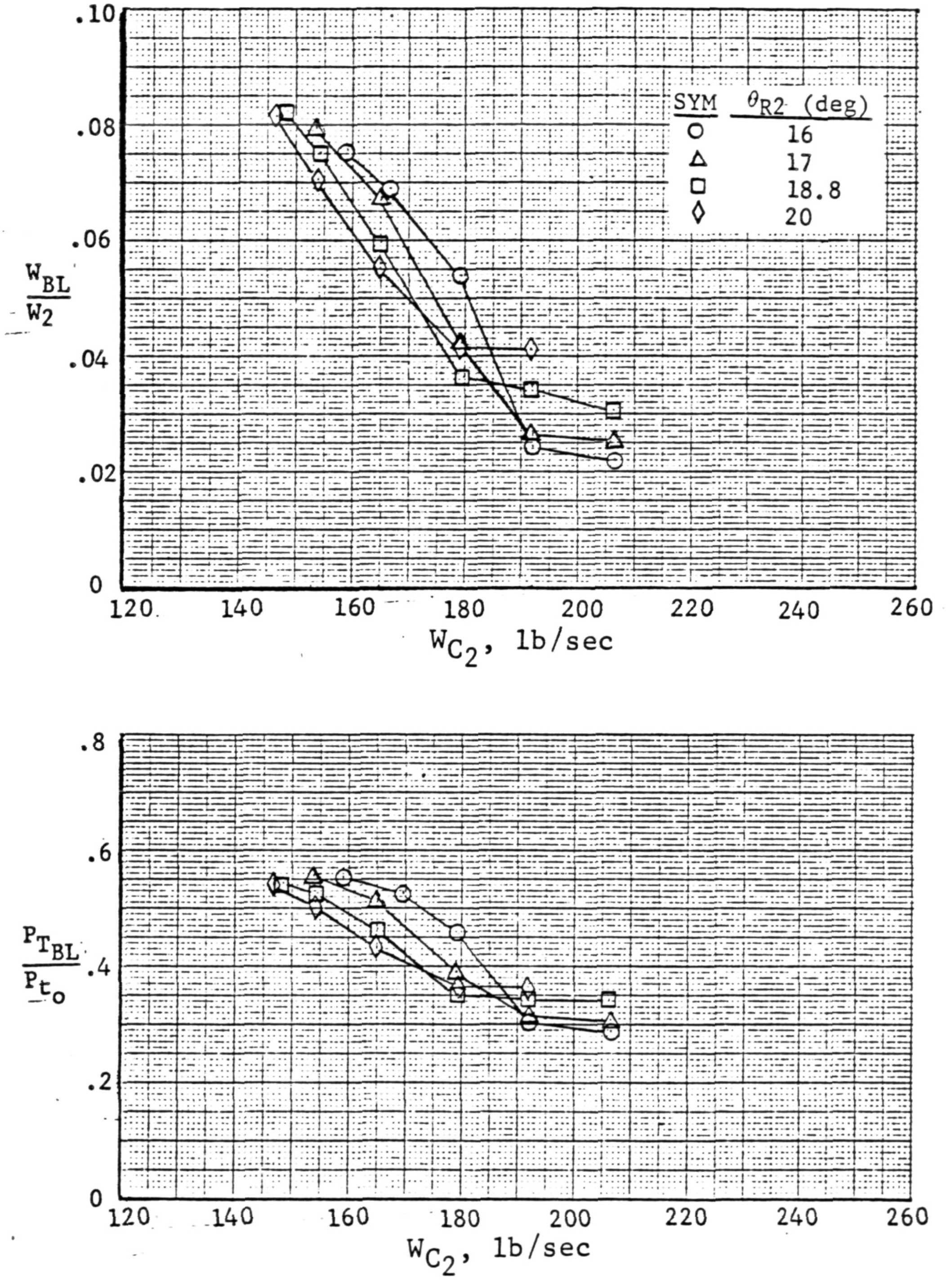

(d) $M_o = 2.0$

Figure 7-19 (Cont'd)

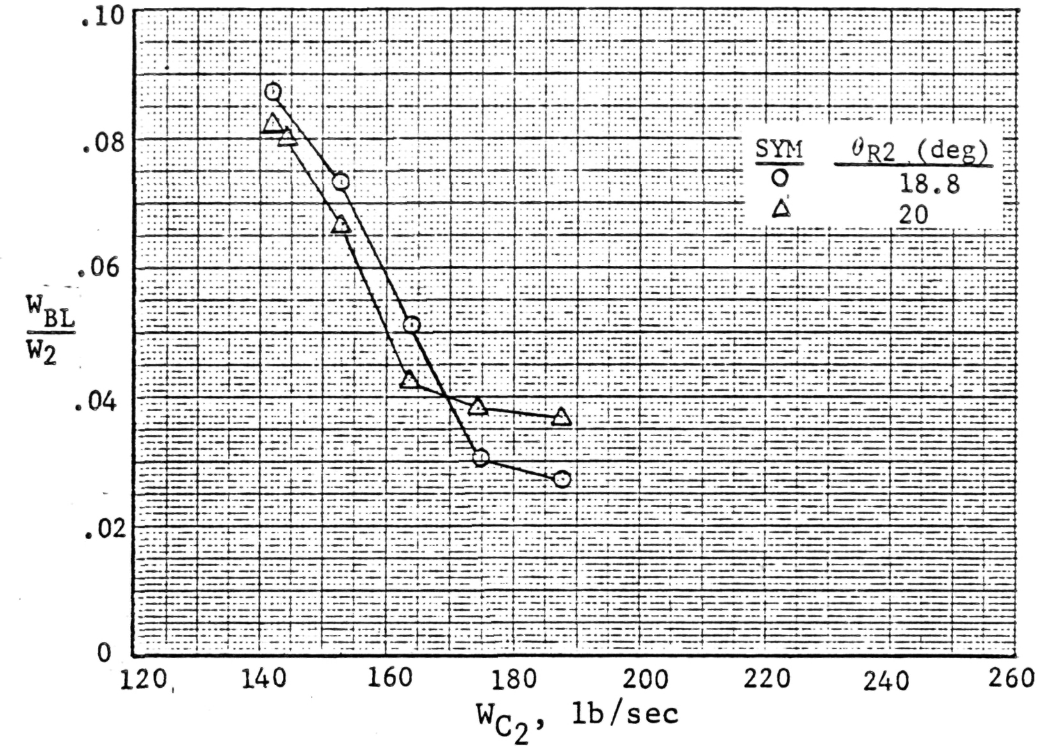

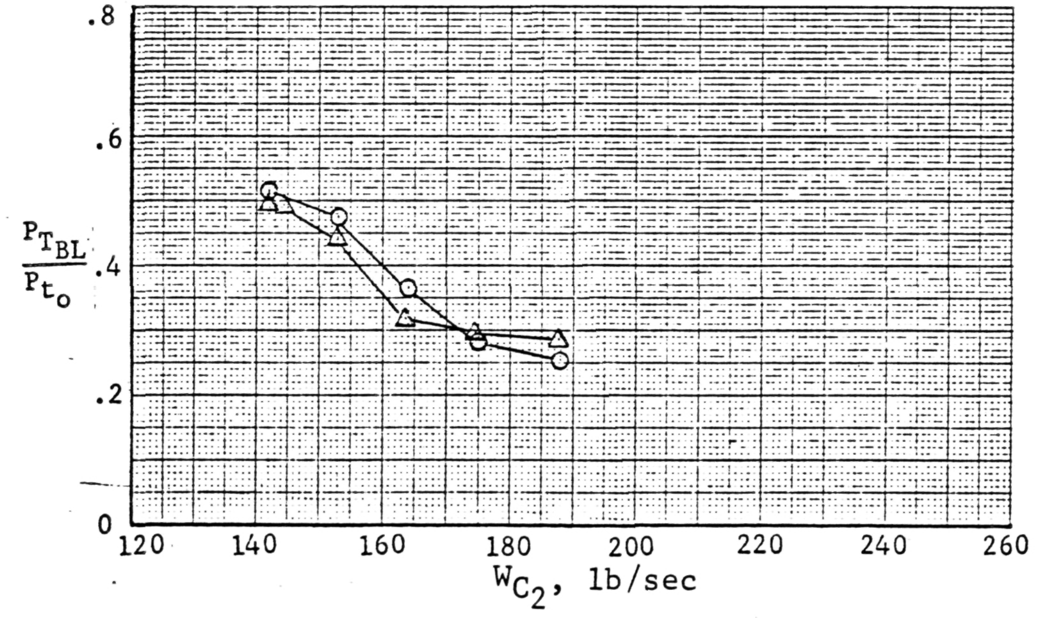

(e) $M_o = 2.2$

Figure 7-19 (Concl)

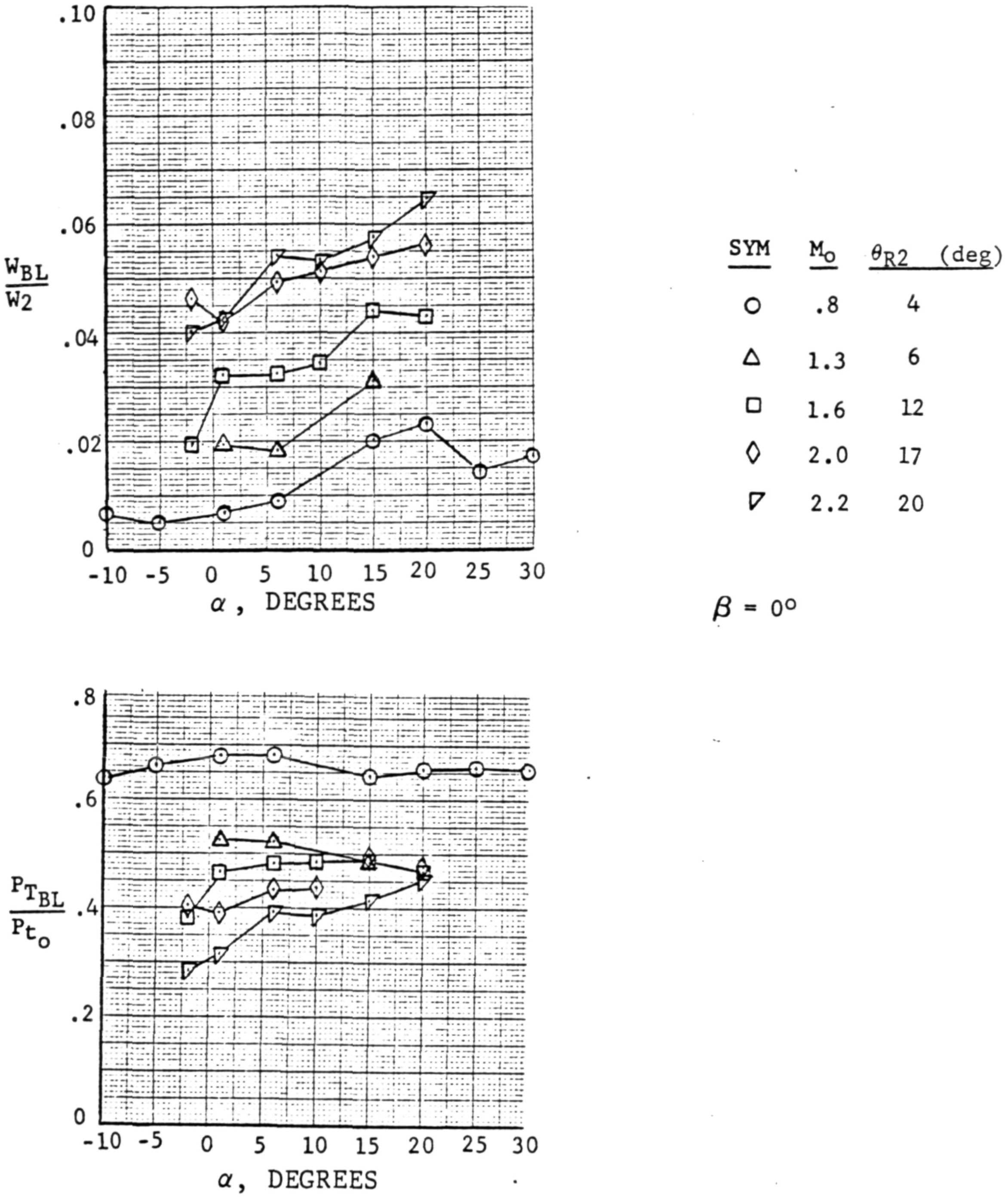

Figure 7-20 Effect of Angle of Attack on Bleed System Characteristics

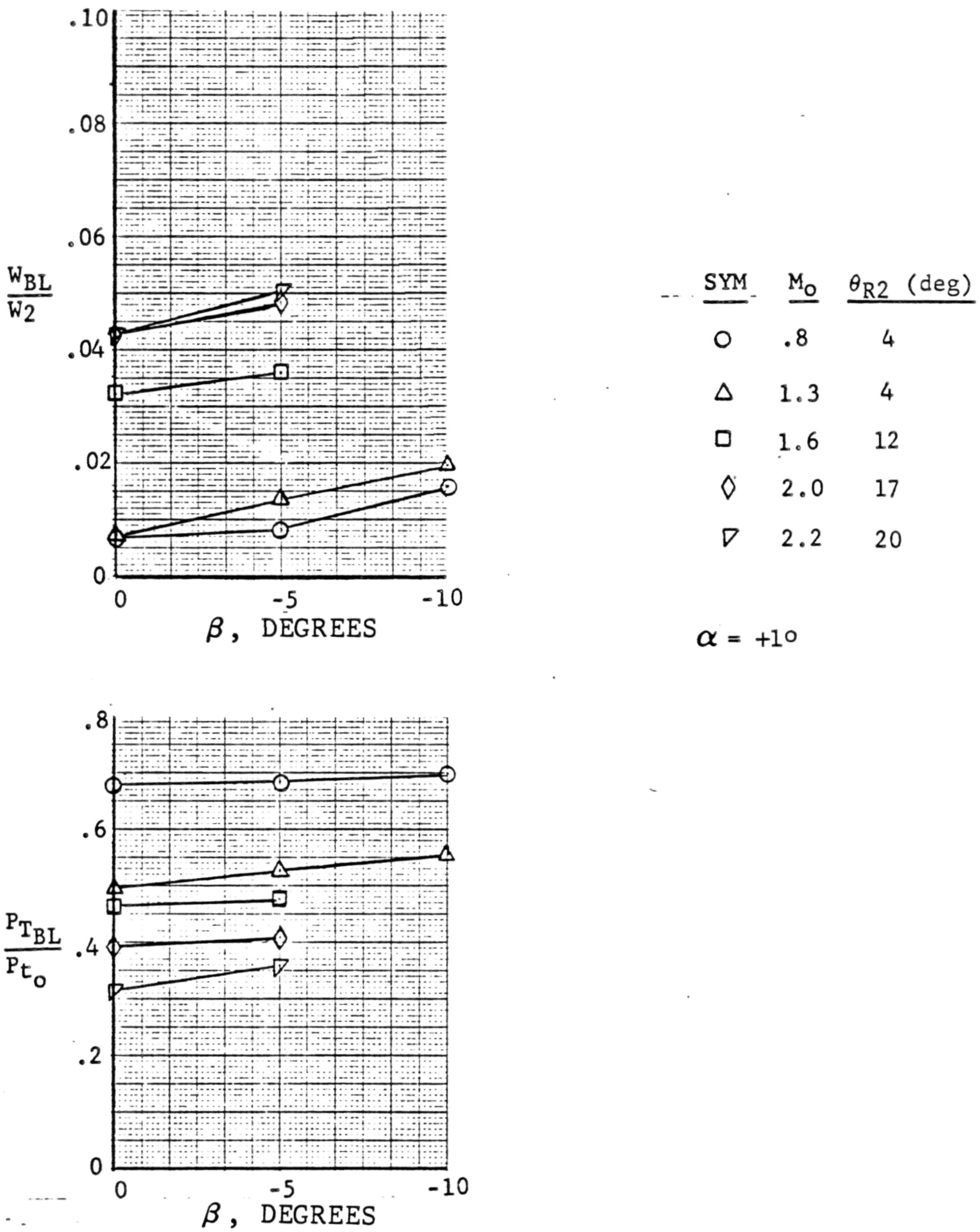

Figure 7-21 Effect of Angle of Sideslip on Bleed System Characteristics

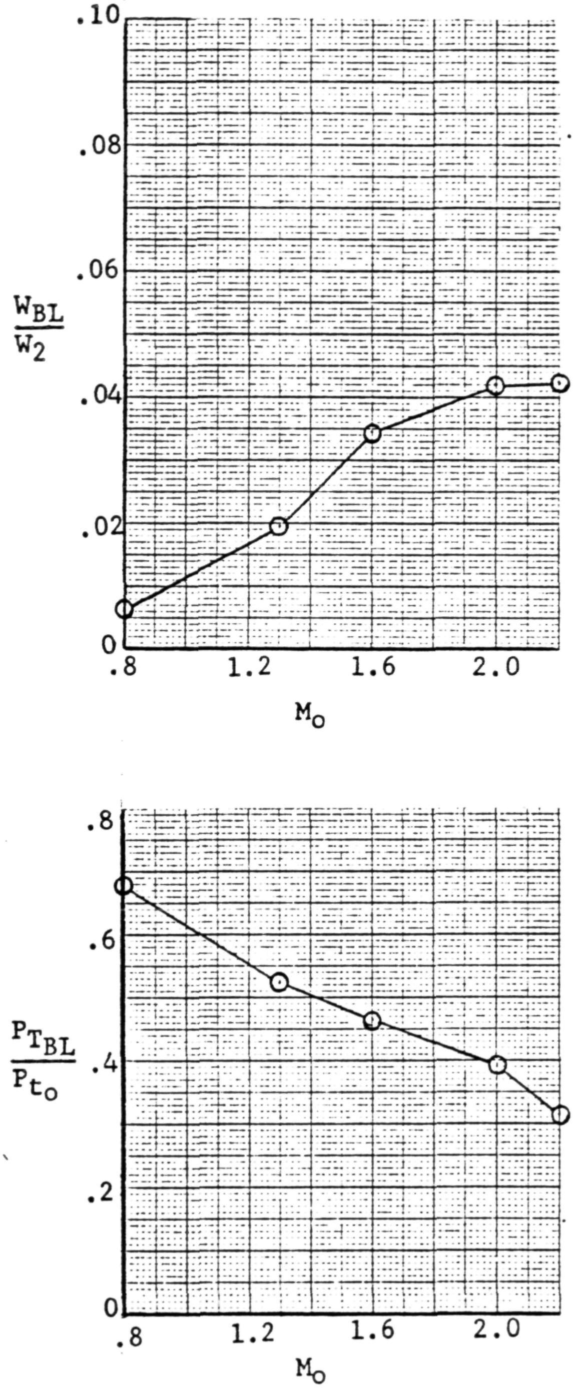

M_o	θ_{R2} (deg)
.8	4
1.3	6
1.6	12
2.0	17
2.2	20

$\alpha = 1°$

$\beta = 0°$

Figure 7-22 Effect of Mach Number on Bleed System Characteristics

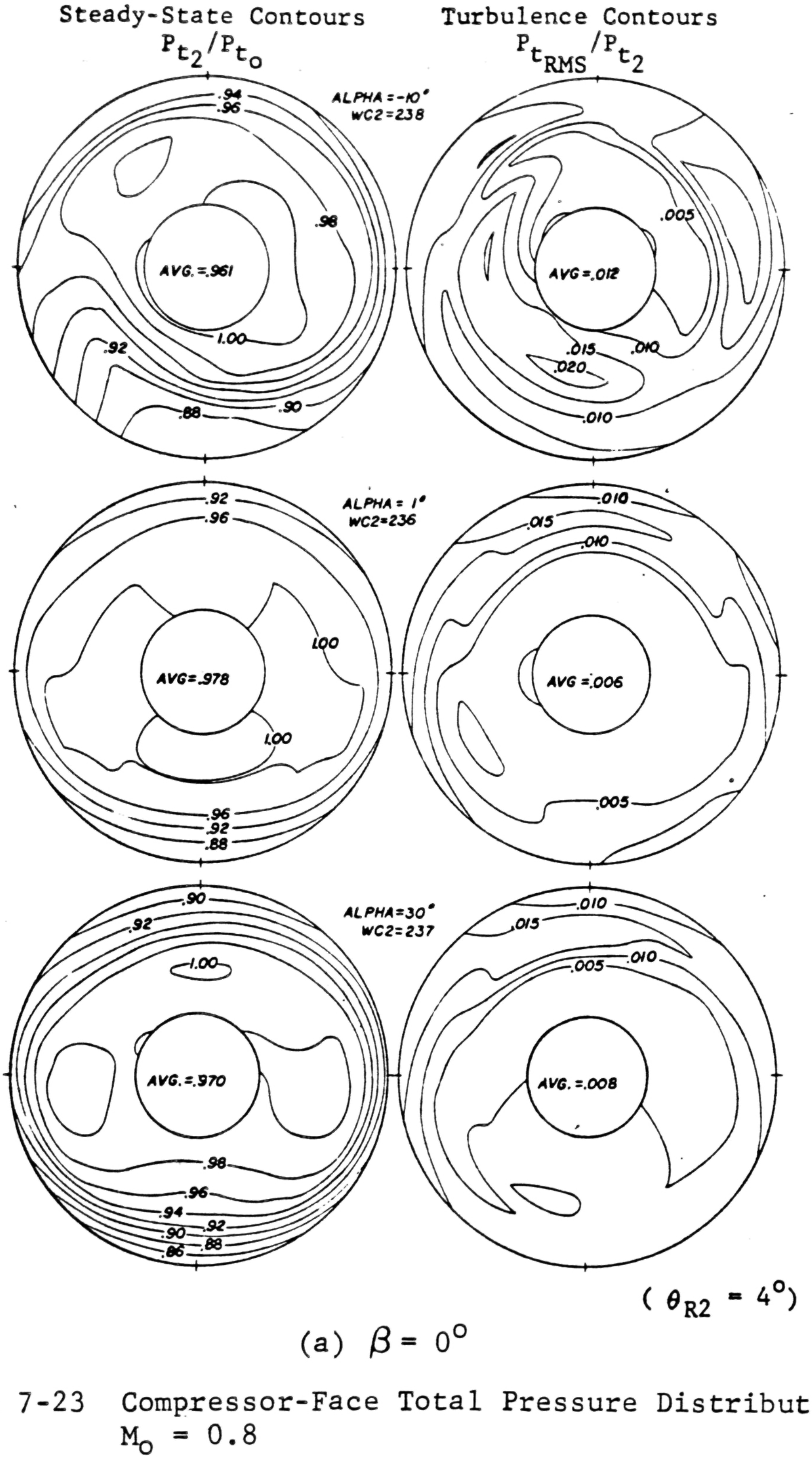

Steady-State Contours P_{t_2}/P_{t_o} Turbulence Contours $P_{t_{RMS}}/P_{t_2}$

($\theta_{R2} = 4^{\circ}$)

(a) $\beta = 0^{\circ}$

Figure 7-23 Compressor-Face Total Pressure Distribution, $M_o = 0.8$

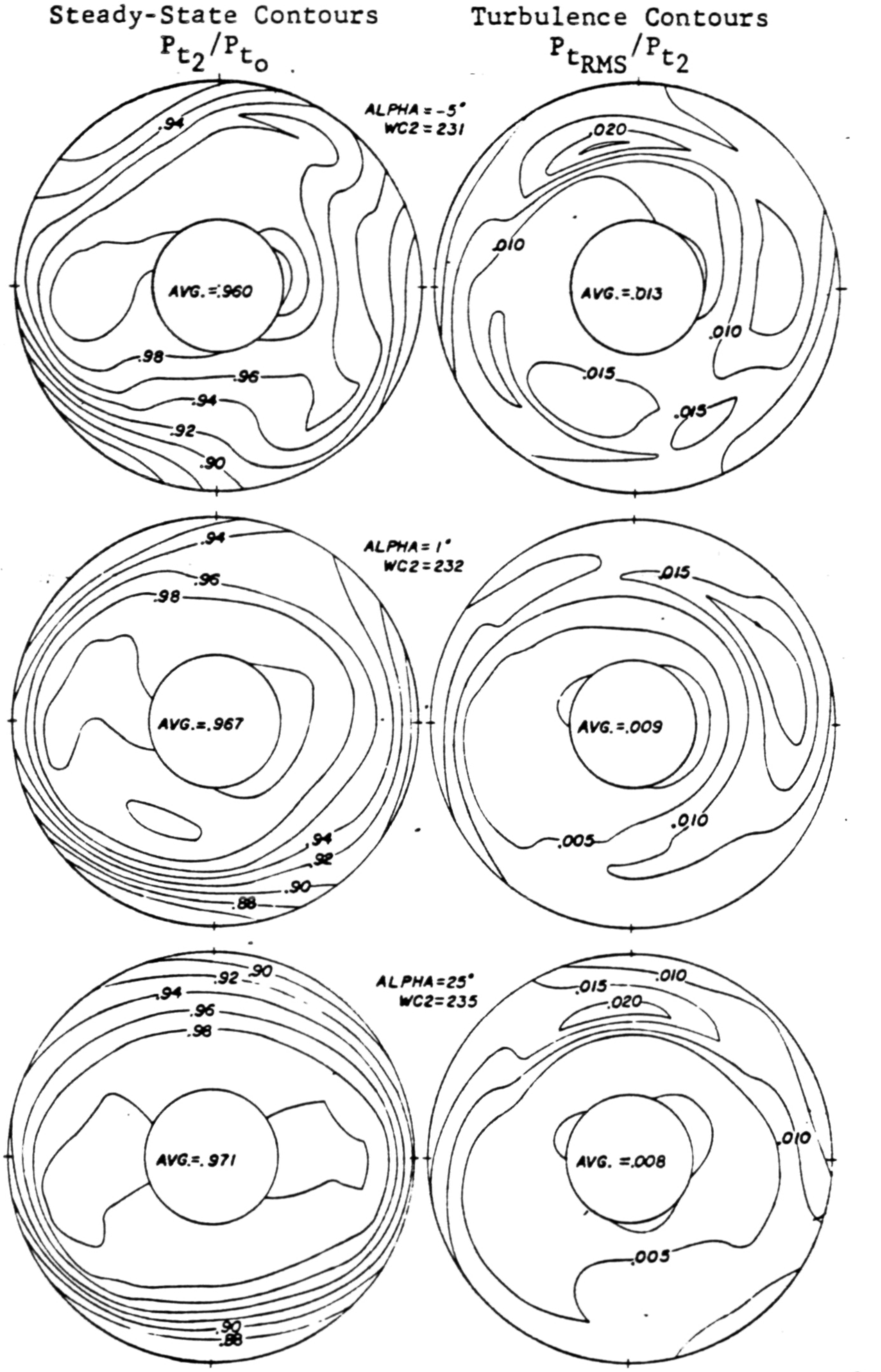
Steady-State Contours P_{t_2}/P_{t_o}

Turbulence Contours $P_{t_{RMS}}/P_{t_2}$

(θ_{R2} = 4°)

(b) $\beta = -10^\circ$

Figure 7-23 (Concl)

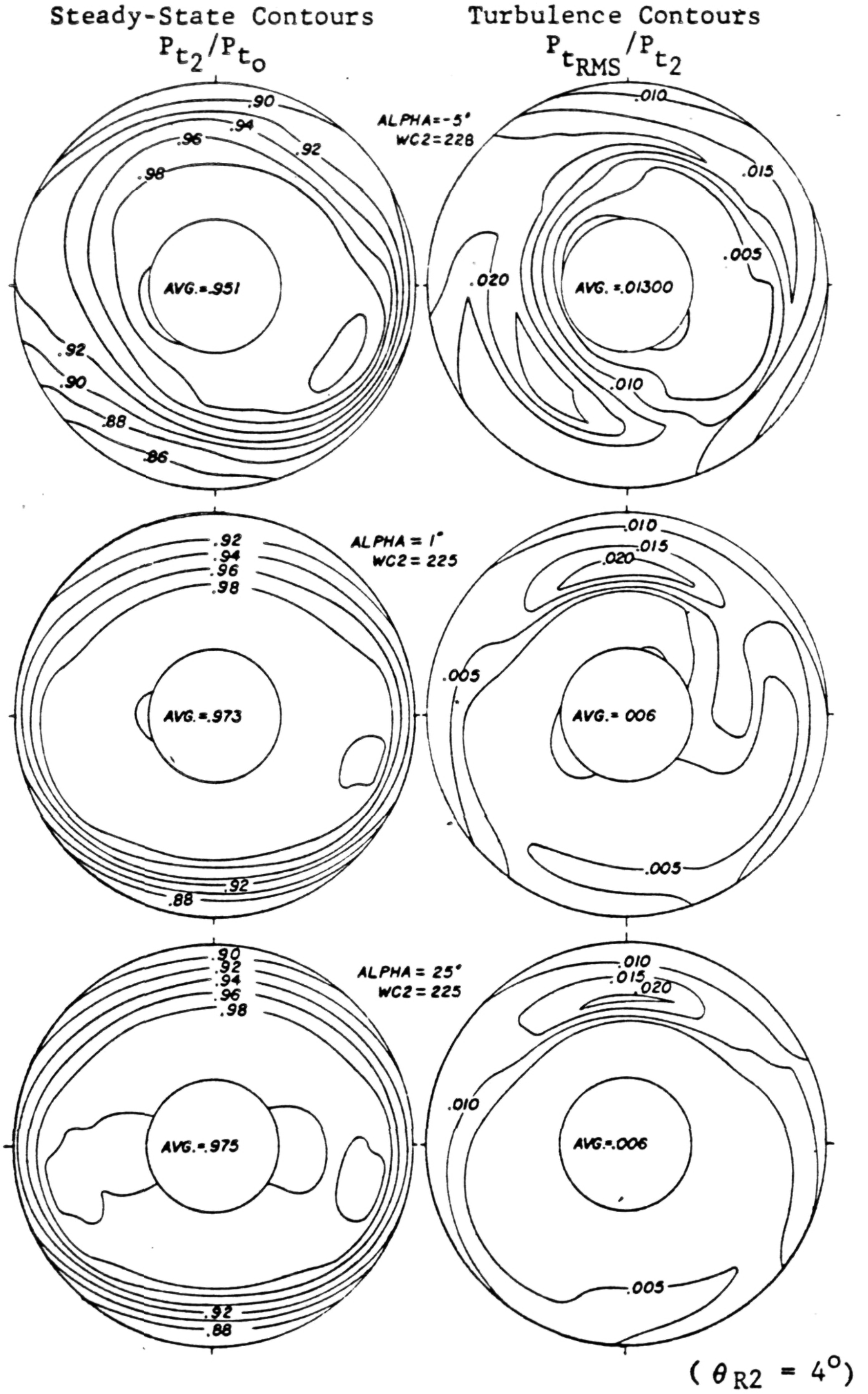

(a) $\beta = 0^{\circ}$

Figure 7-24 Compressor-Face Total Pressure Distribution, $M_o = 1.3$

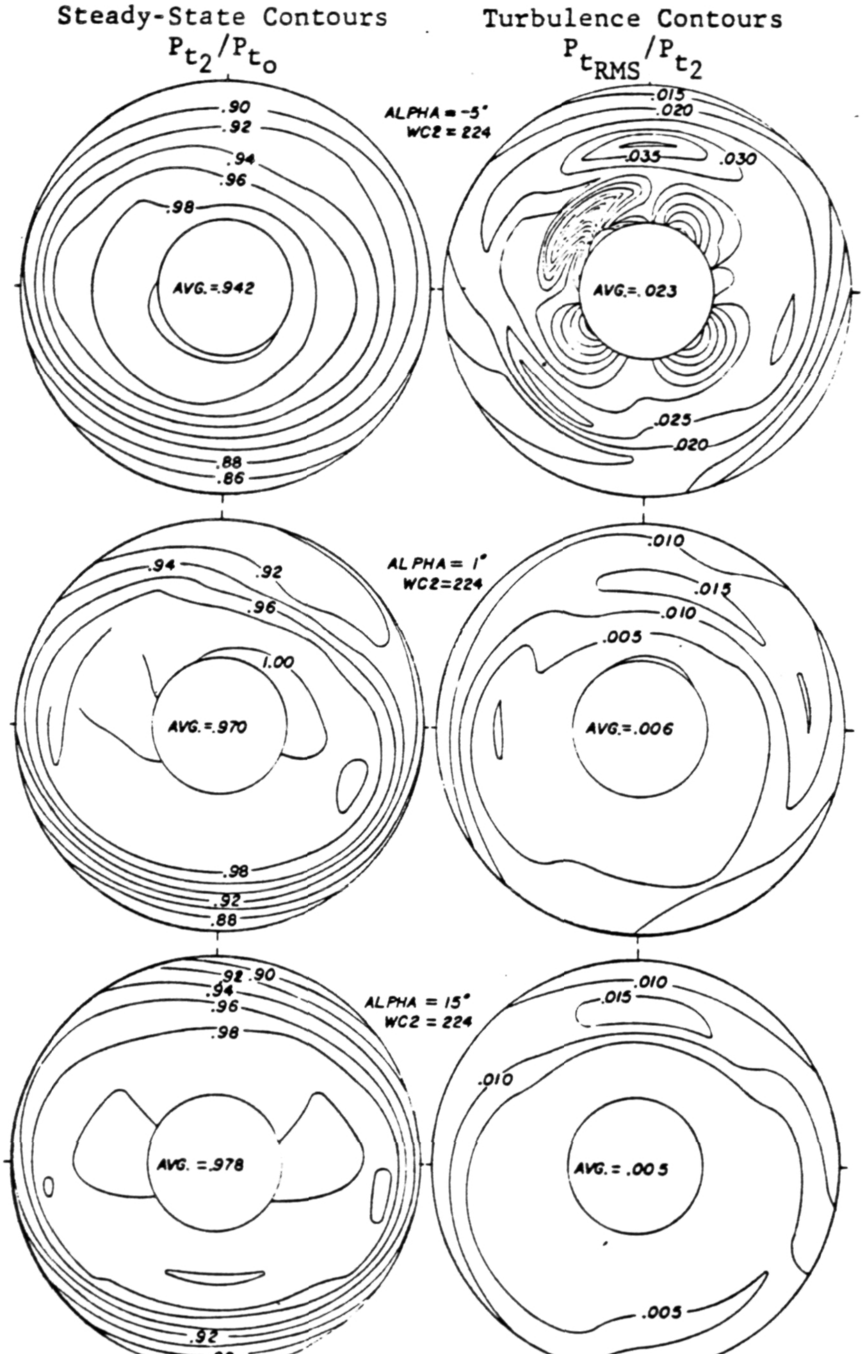

Steady-State Contours P_{t_2}/P_{t_o}

Turbulence Contours $P_{t_{RMS}}/P_{t_2}$

($\theta_{R2} = 4^\circ$)

(b) $\beta = -5^\circ$

Figure 7-24 (Concl)

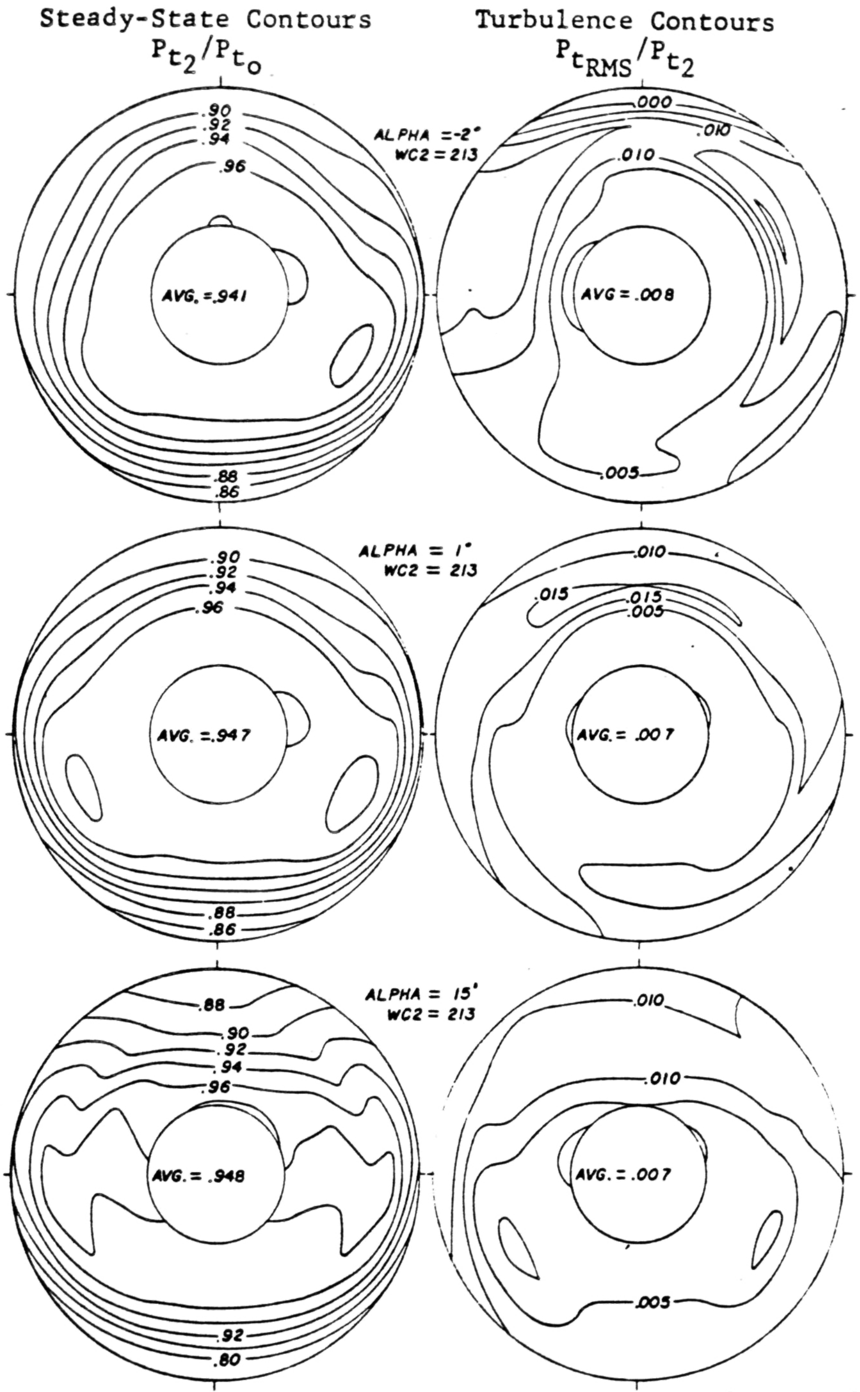

(θ_{R2} = 12°)

(a) β = 0°

Figure 7-25 Compressor-Face Total Pressure Distribution, M_o = 1.6

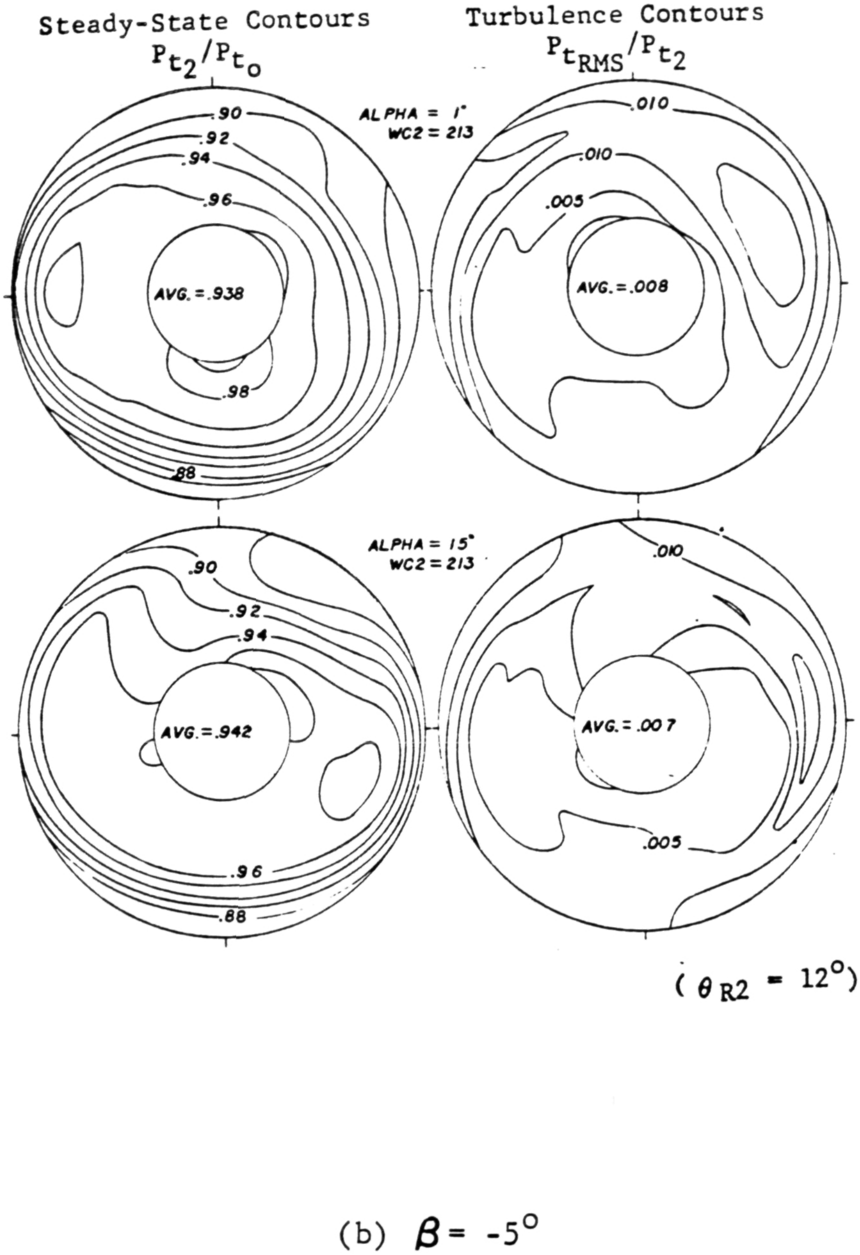

Steady-State Contours P_{t_2}/P_{t_o}

Turbulence Contours $P_{t_{RMS}}/P_{t_2}$

$(\theta_{R2} = 12^{\circ})$

(b) $\beta = -5^{\circ}$

Figure 7-25 (Concl)

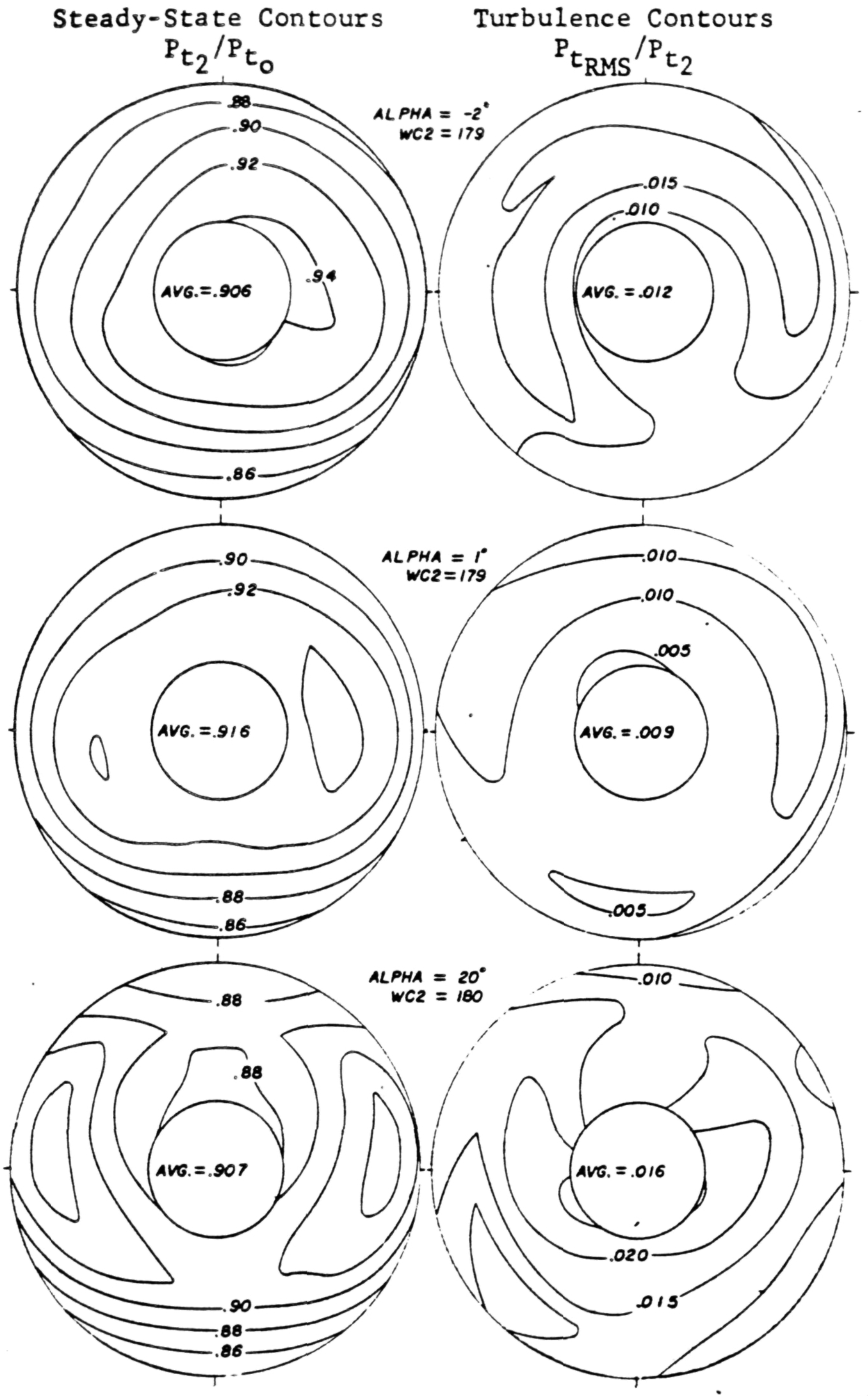

(θ_{R2} = 17°)

(a) β = 0°

Figure 7-26 Compressor-Face Total Pressure Distribution, M_o = 2.0

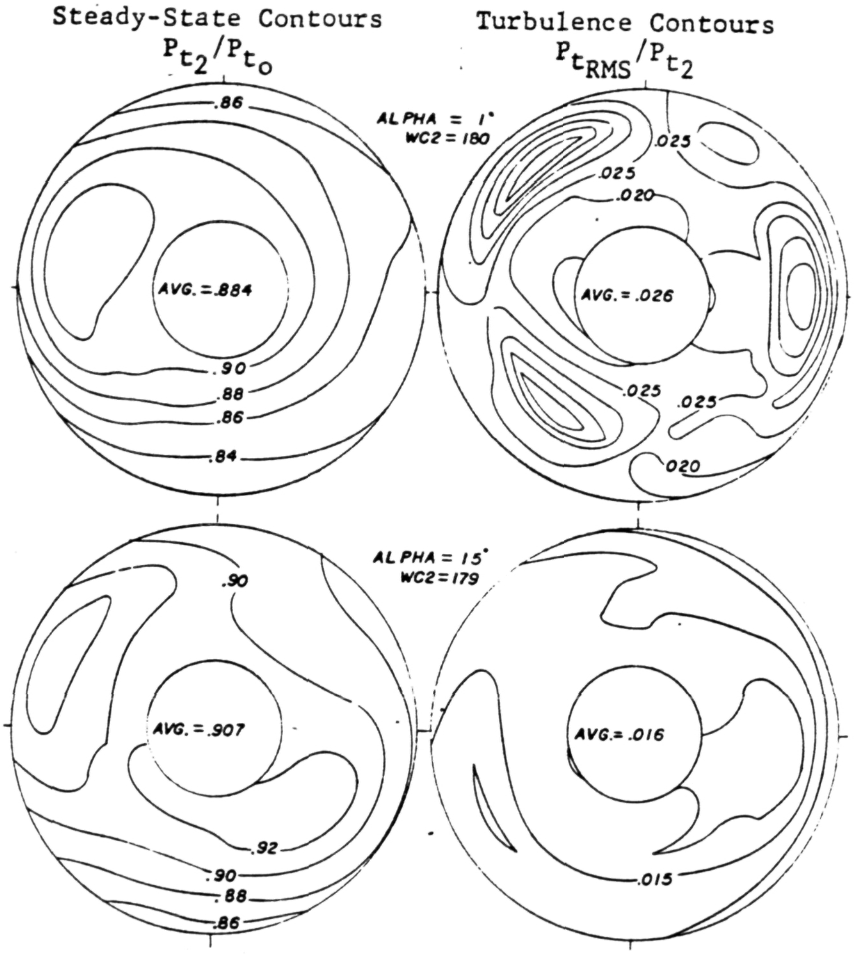

Steady-State Contours P_{t_2}/P_{t_o}

Turbulence Contours $P_{t_{RMS}}/P_{t_2}$

$(\theta_{R2} = 17^{\circ})$

(b) $\beta = -5^{\circ}$

Figure 7-26 (Concl)

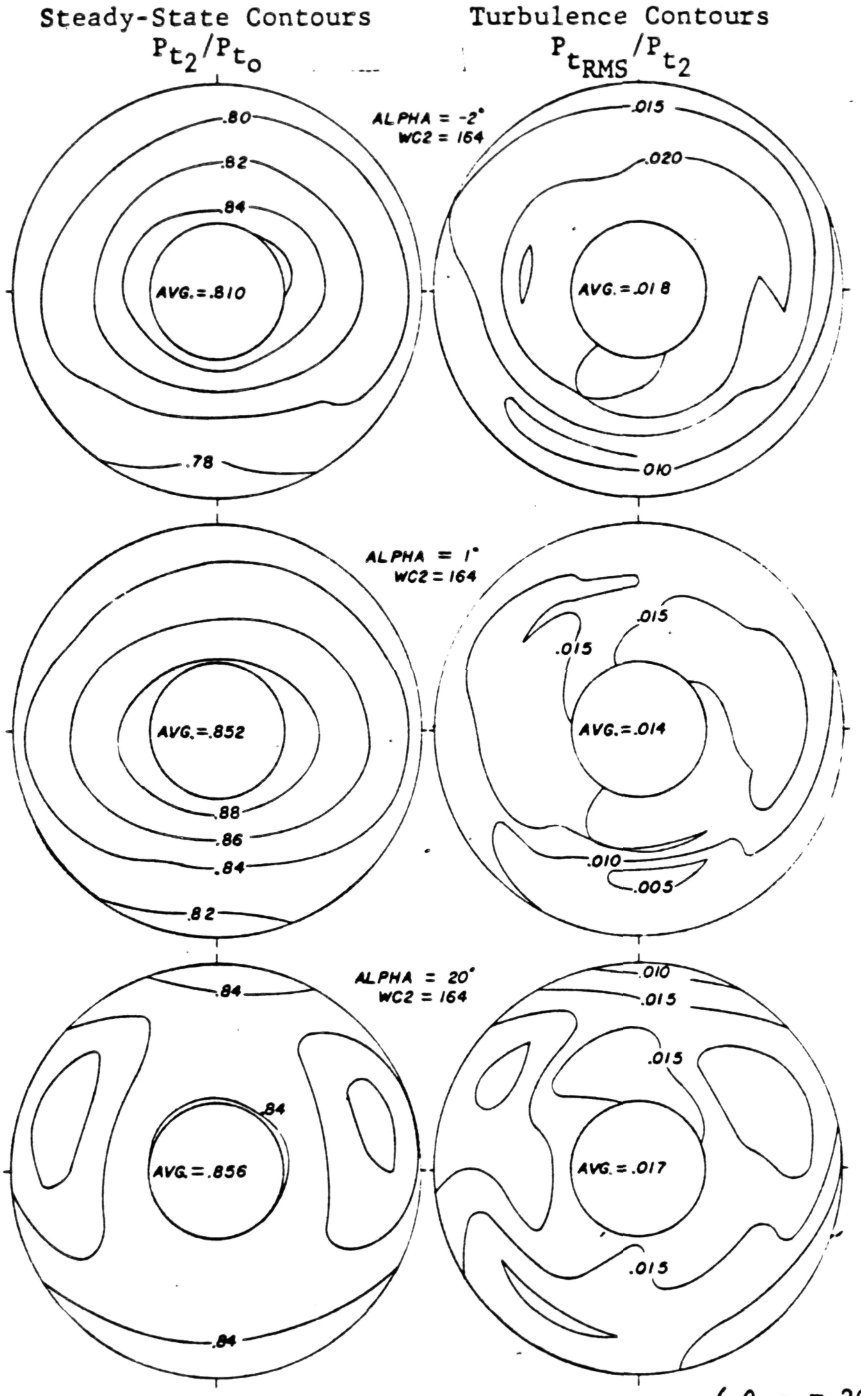

(θ_{R2} = 20°)

(a) $\beta = 0^{\circ}$

Figure 7-27 Compressor-Face Total Pressure Distribution, $M_o = 2.2$

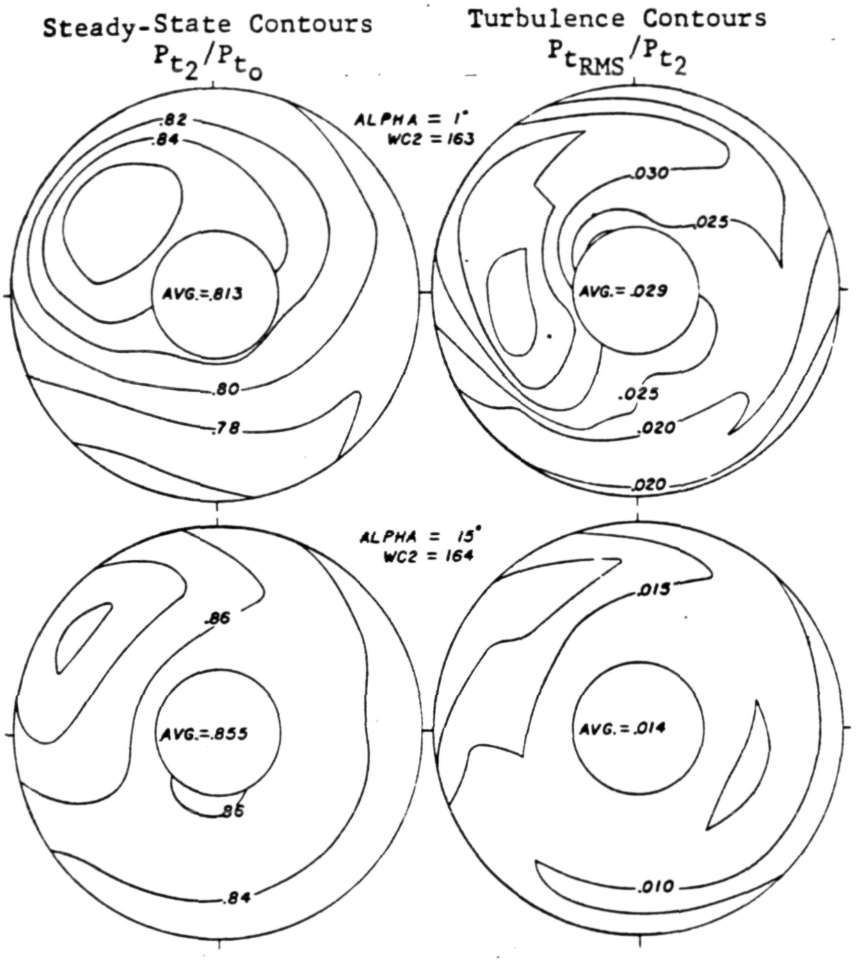 Steady-State Contours P_{t_2}/P_{t_o}

Turbulence Contours $P_{t_{RMS}}/P_{t_2}$

(θ_{R2} = 20°)

(b) $\beta = -5^{\circ}$

Figure 7-27 (Concl)

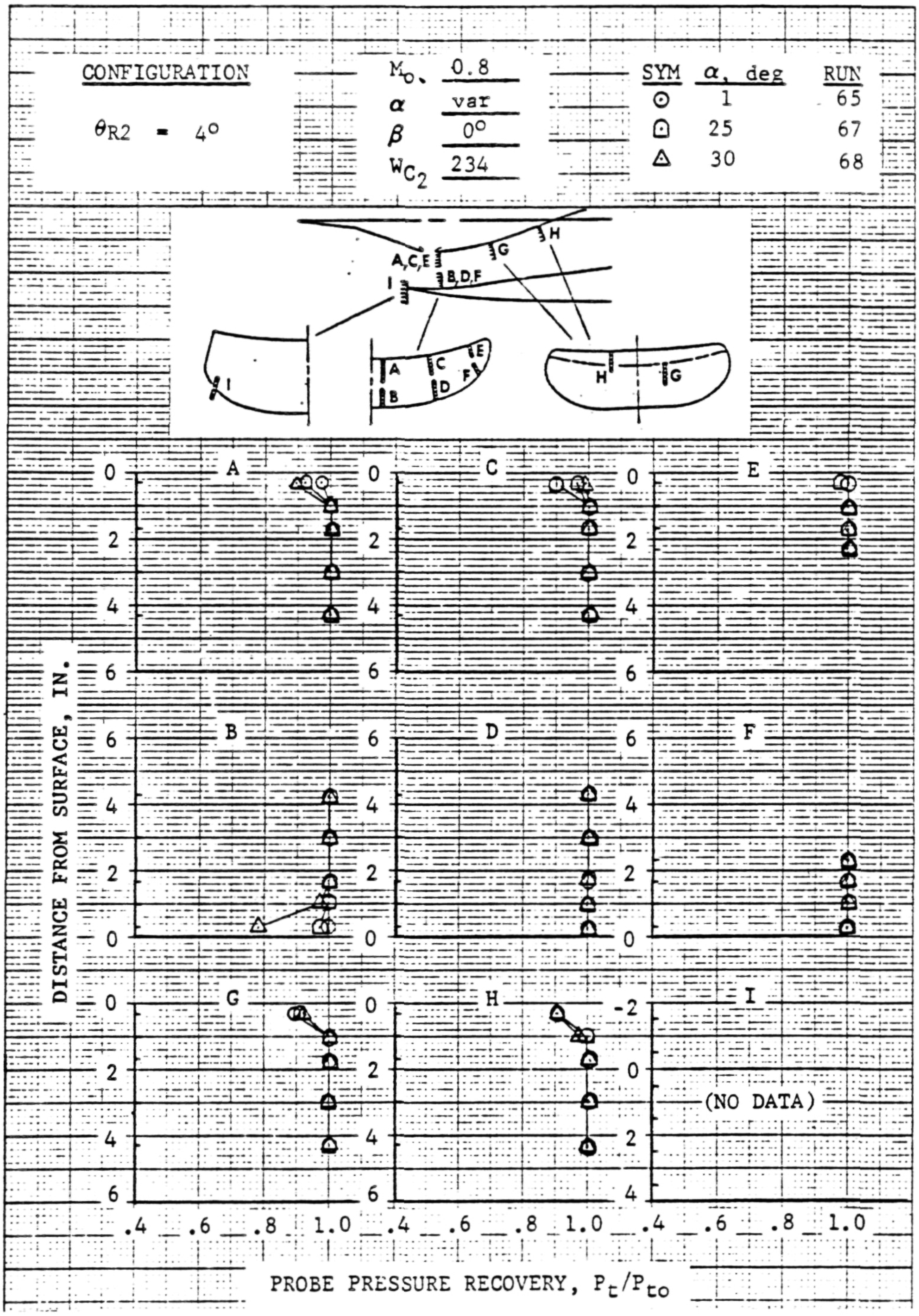

Figure 7-28 Throat Total Pressure Distribution, M_o = 0.8

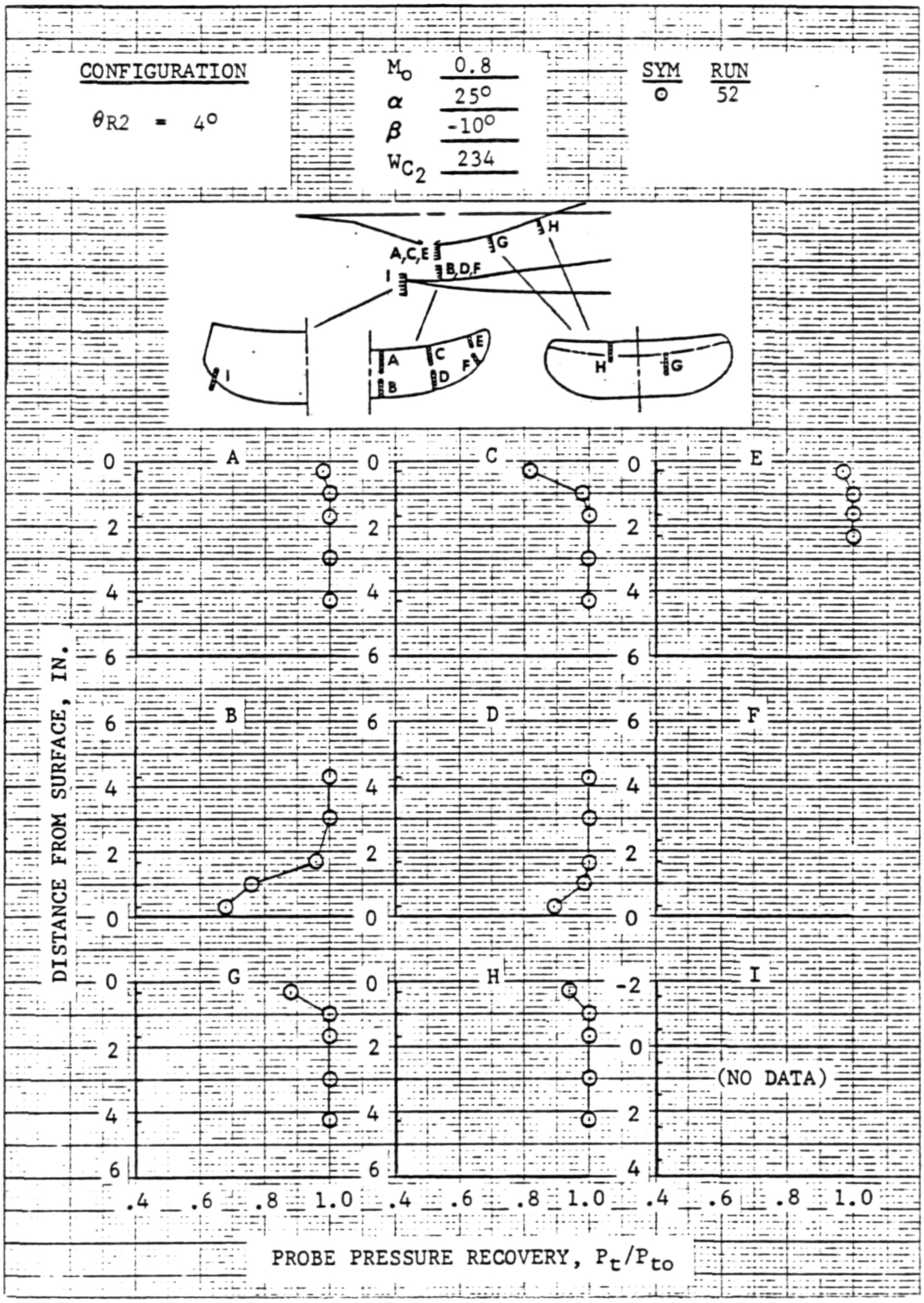

Figure 7-28 (Concl)

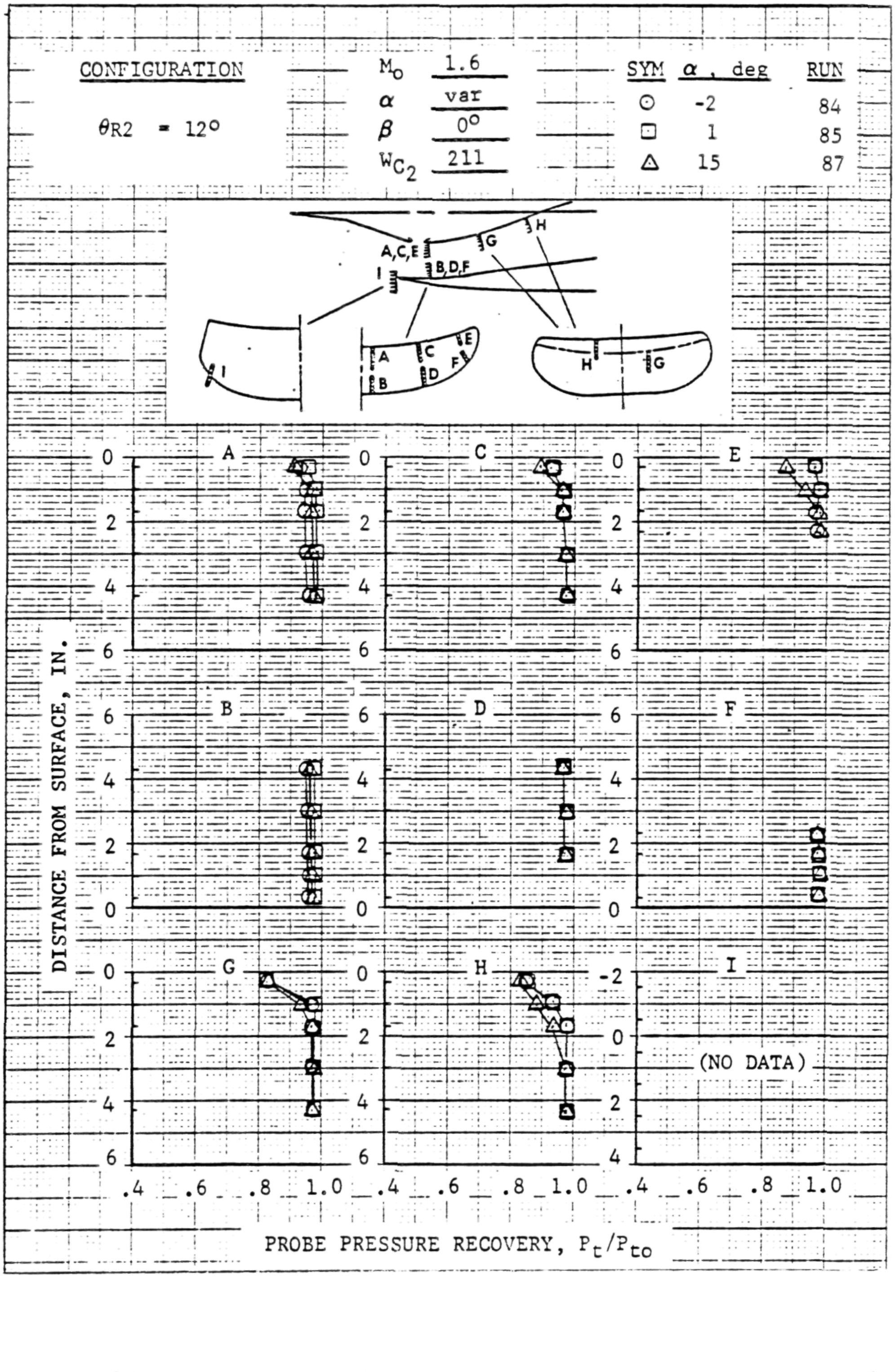

Figure 7-29 Throat Total Pressure Distribution, $M_o = 1.6$

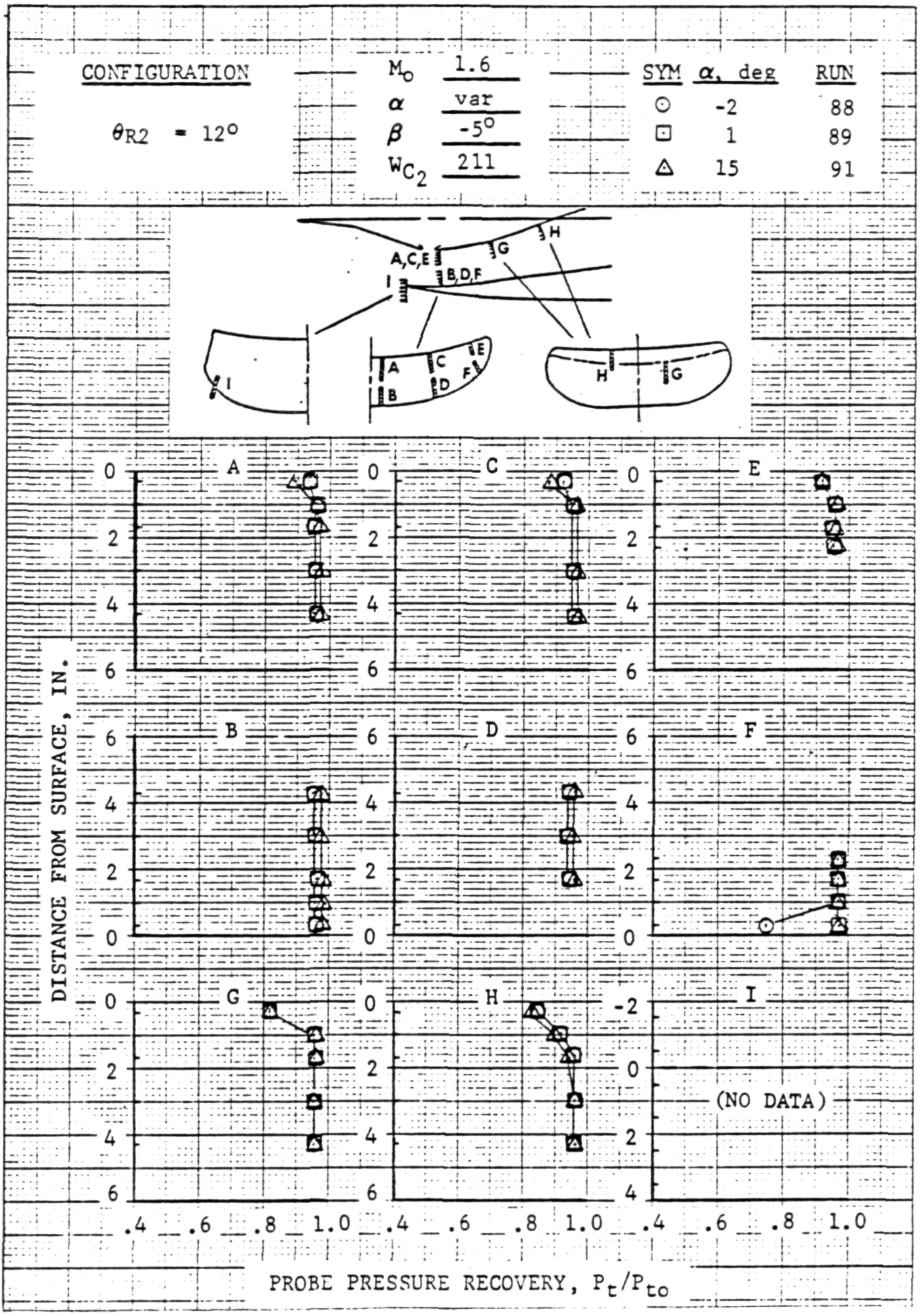

Figure 7-29 (Concl)

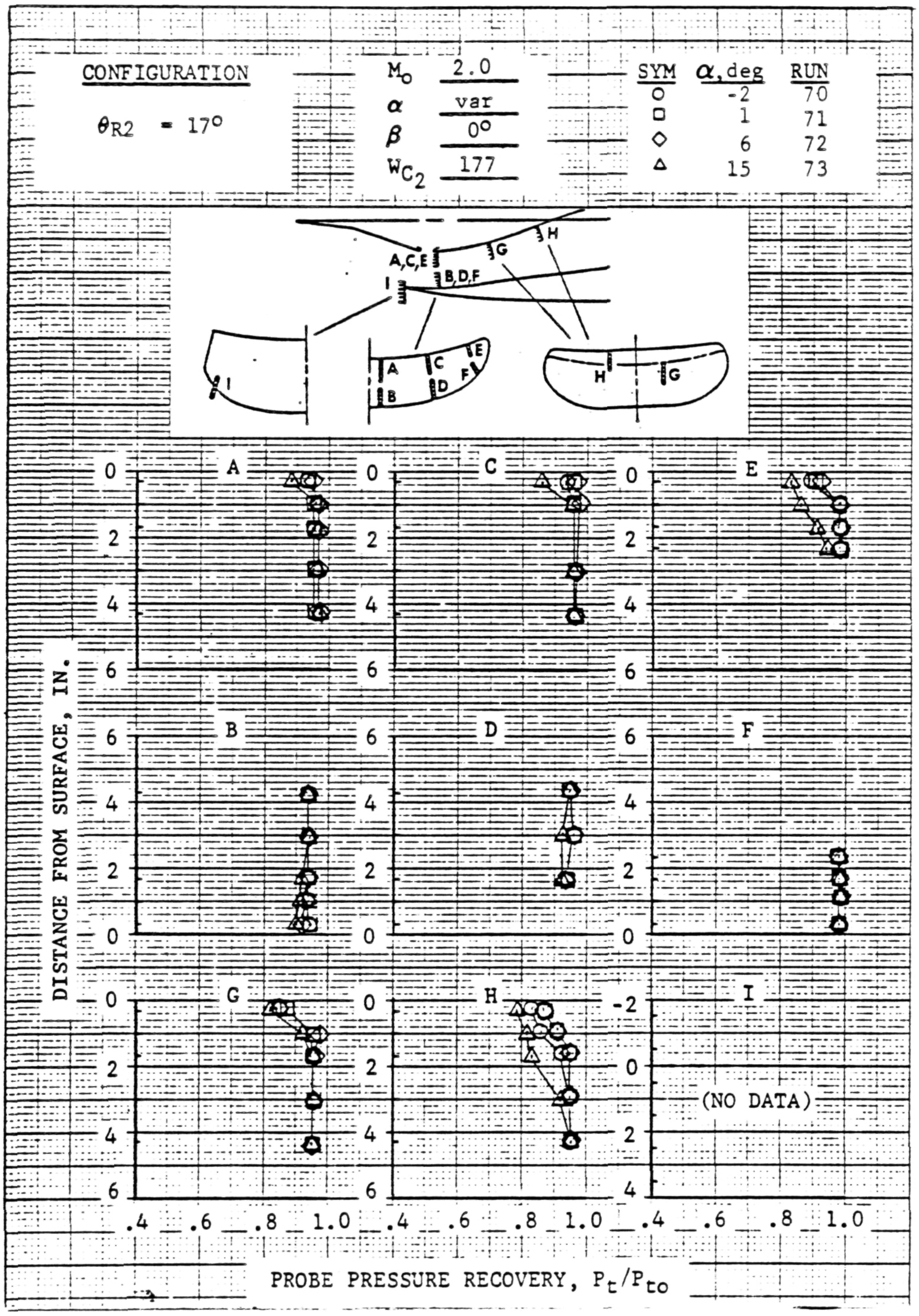

Figure 7-30 Throat Total Pressure Distribution, M_o = 2.0

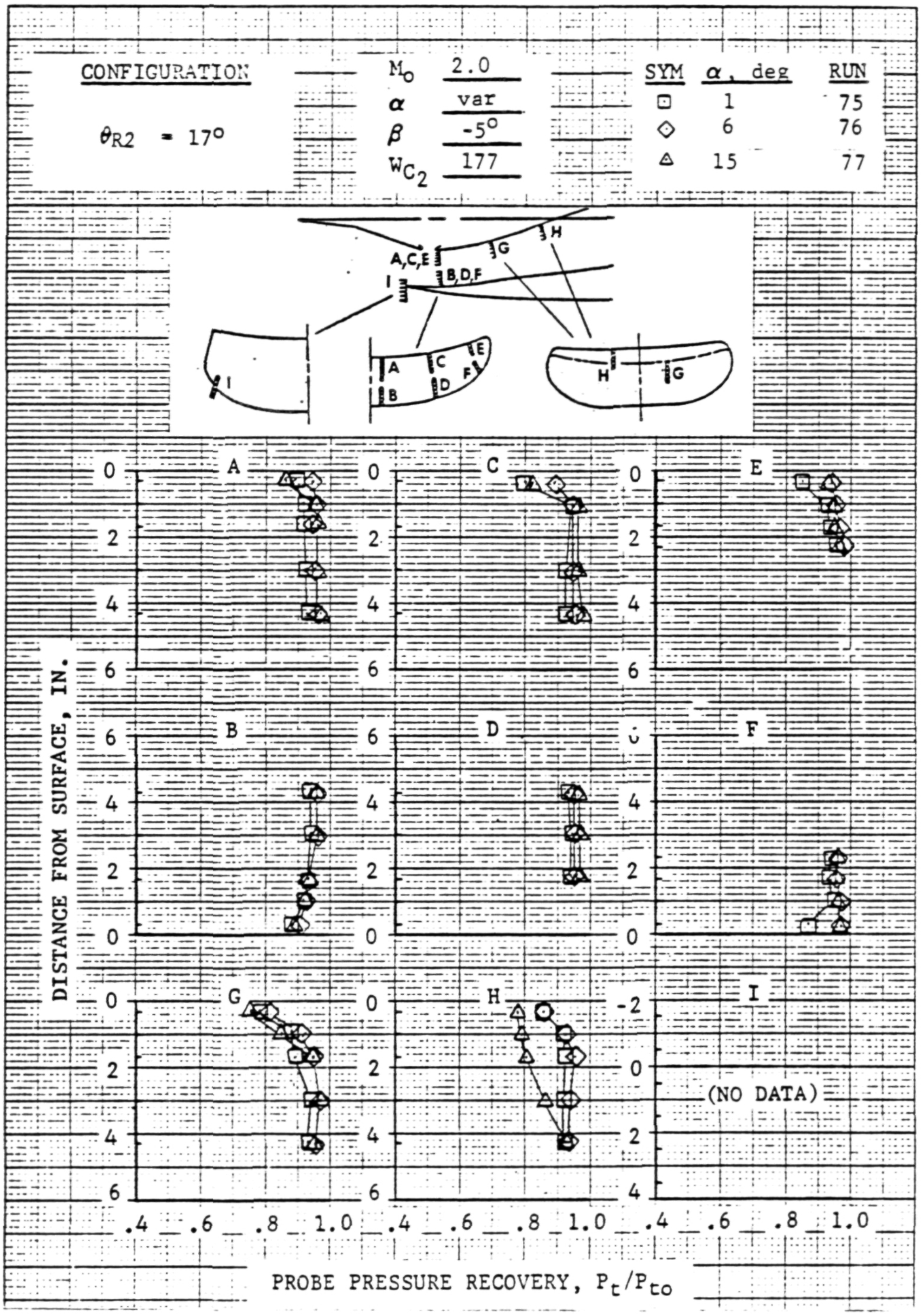

Figure 7-30 (Concl)

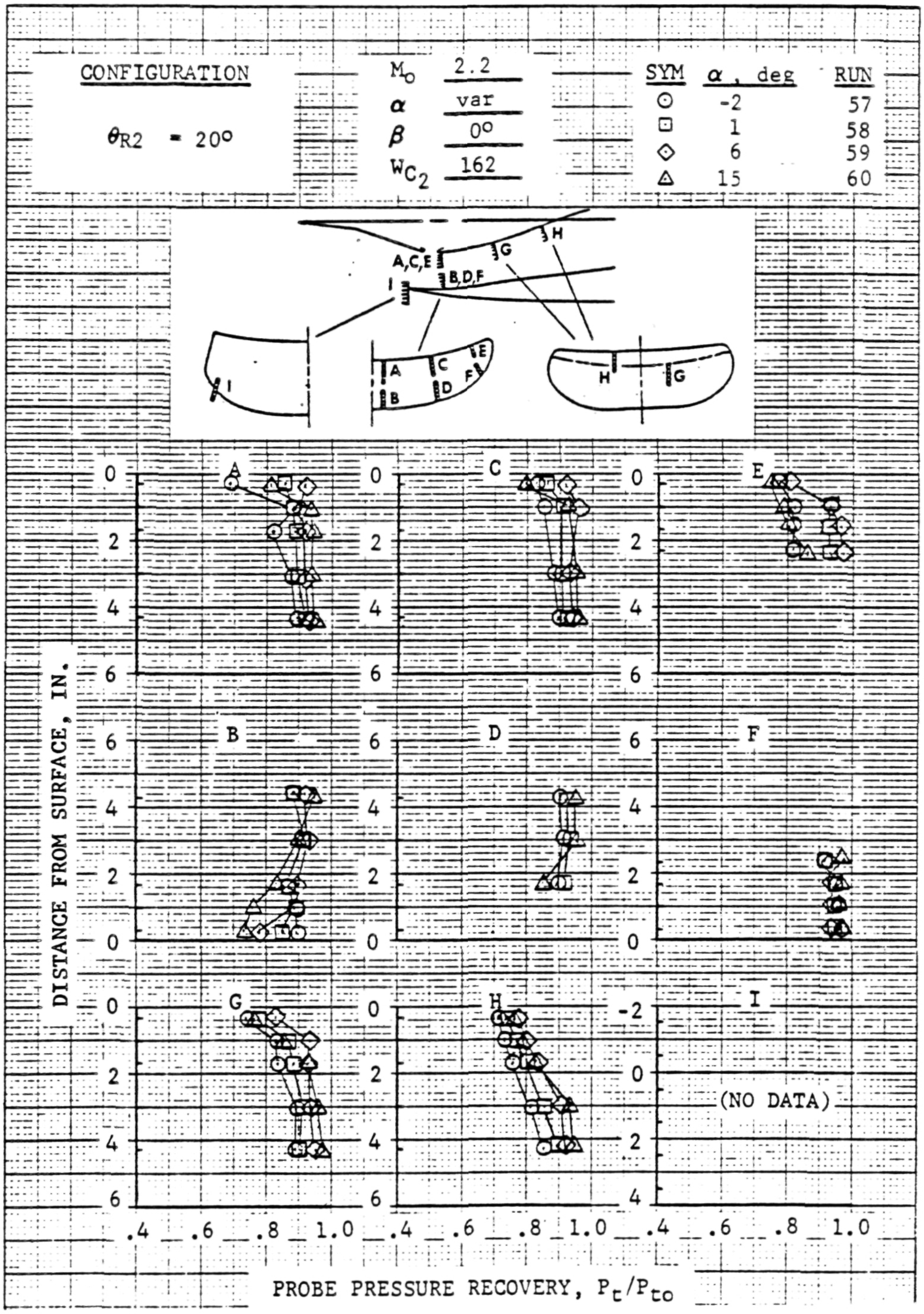

Figure 7-31 Throat Total Pressure Distribution, $M_o = 2.2$

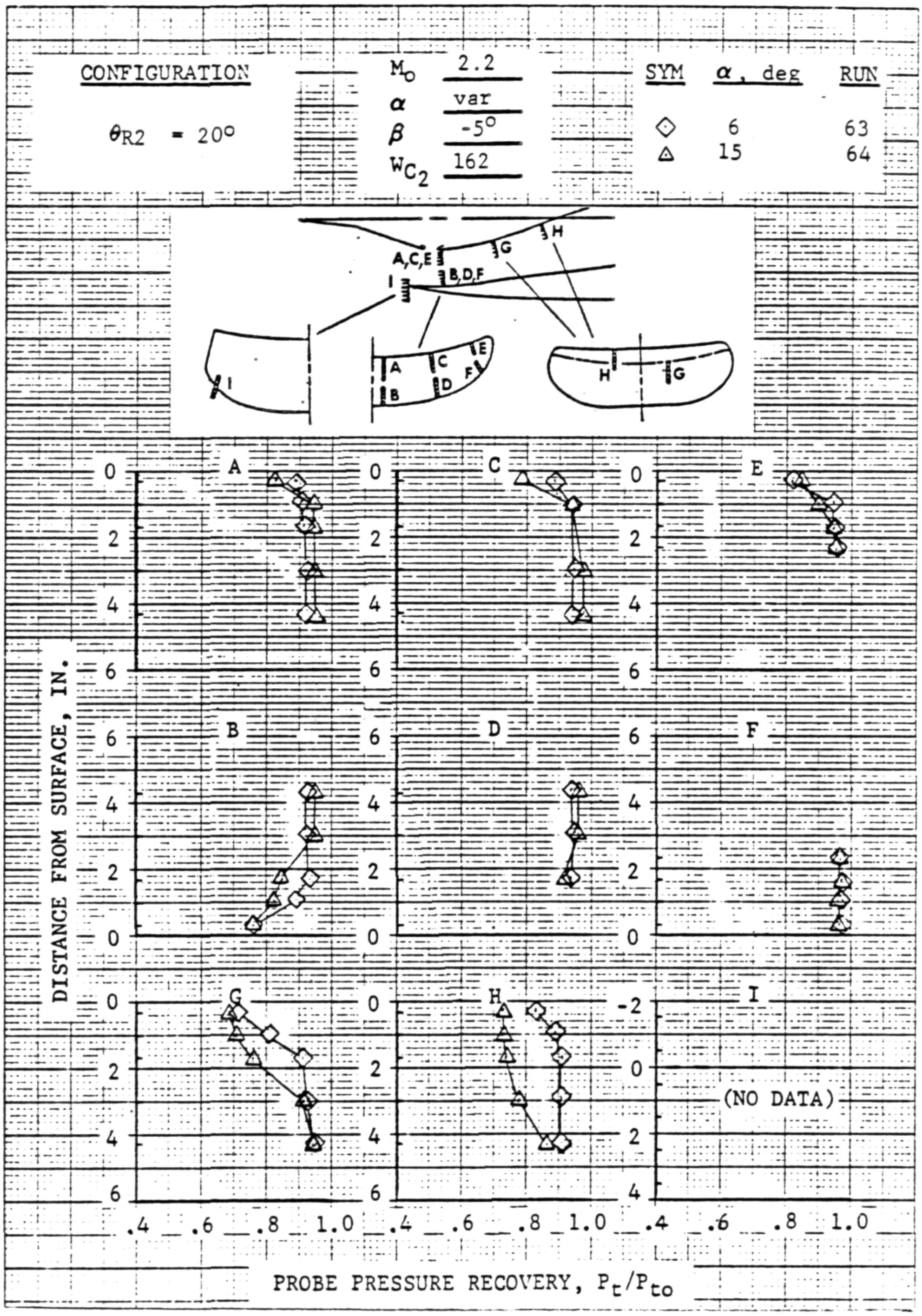

Figure 7-31 (Concl)

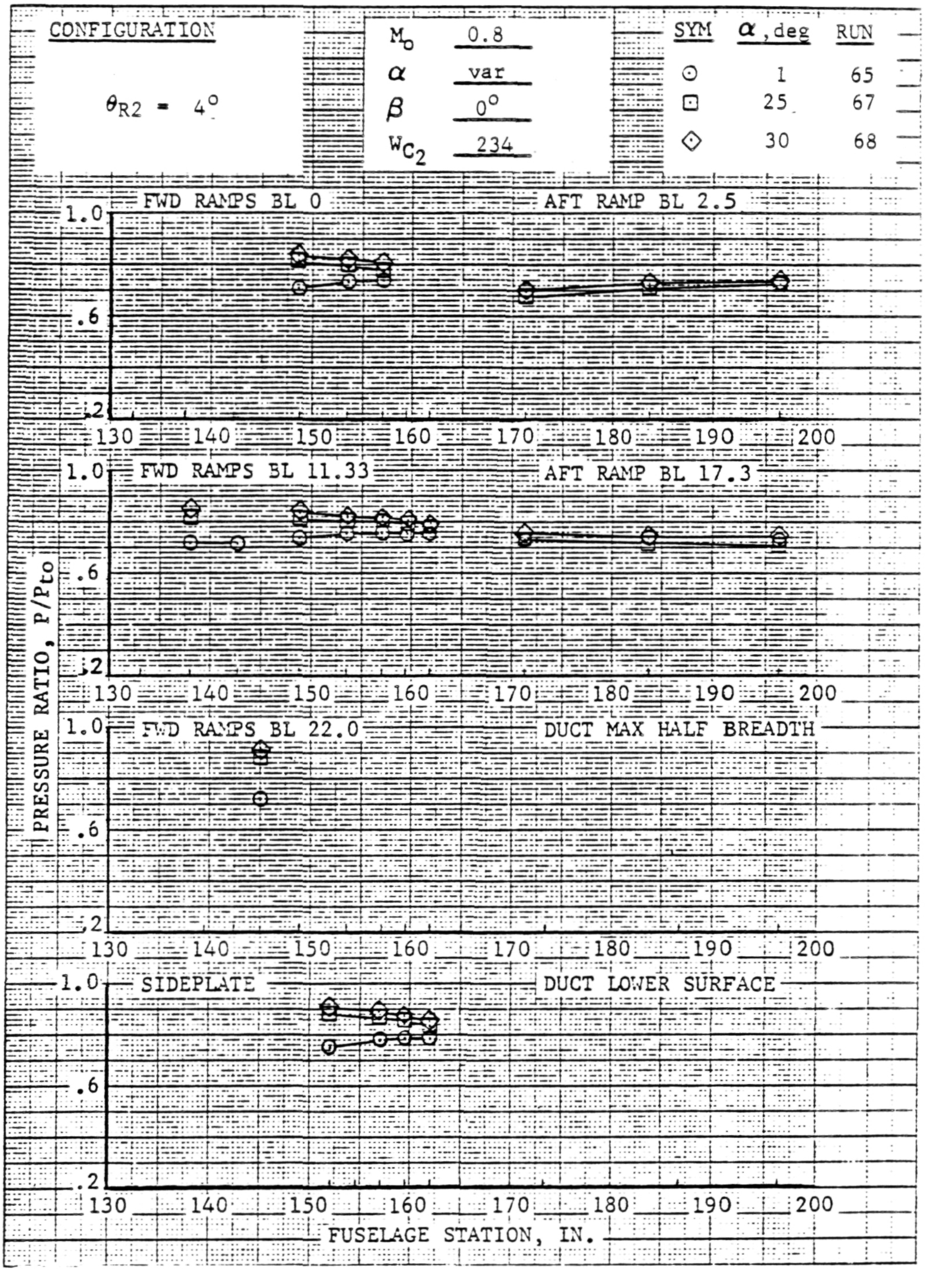

(a) M_o = 0.8

Figure 7-32 Ramp and Duct Static Pressure Distribution

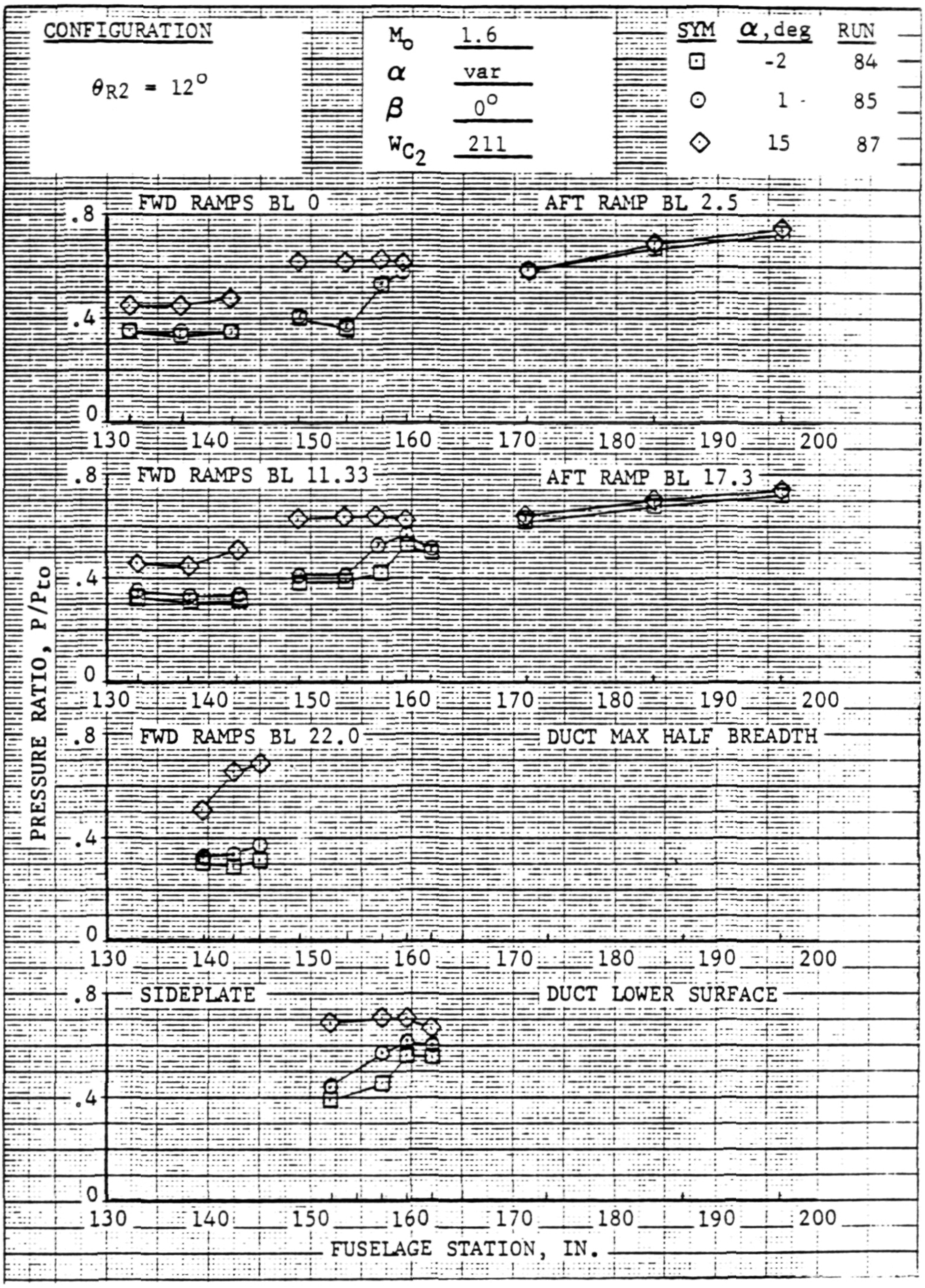

(b) M_o = 1.6

Figure 7-32 (Cont'd)

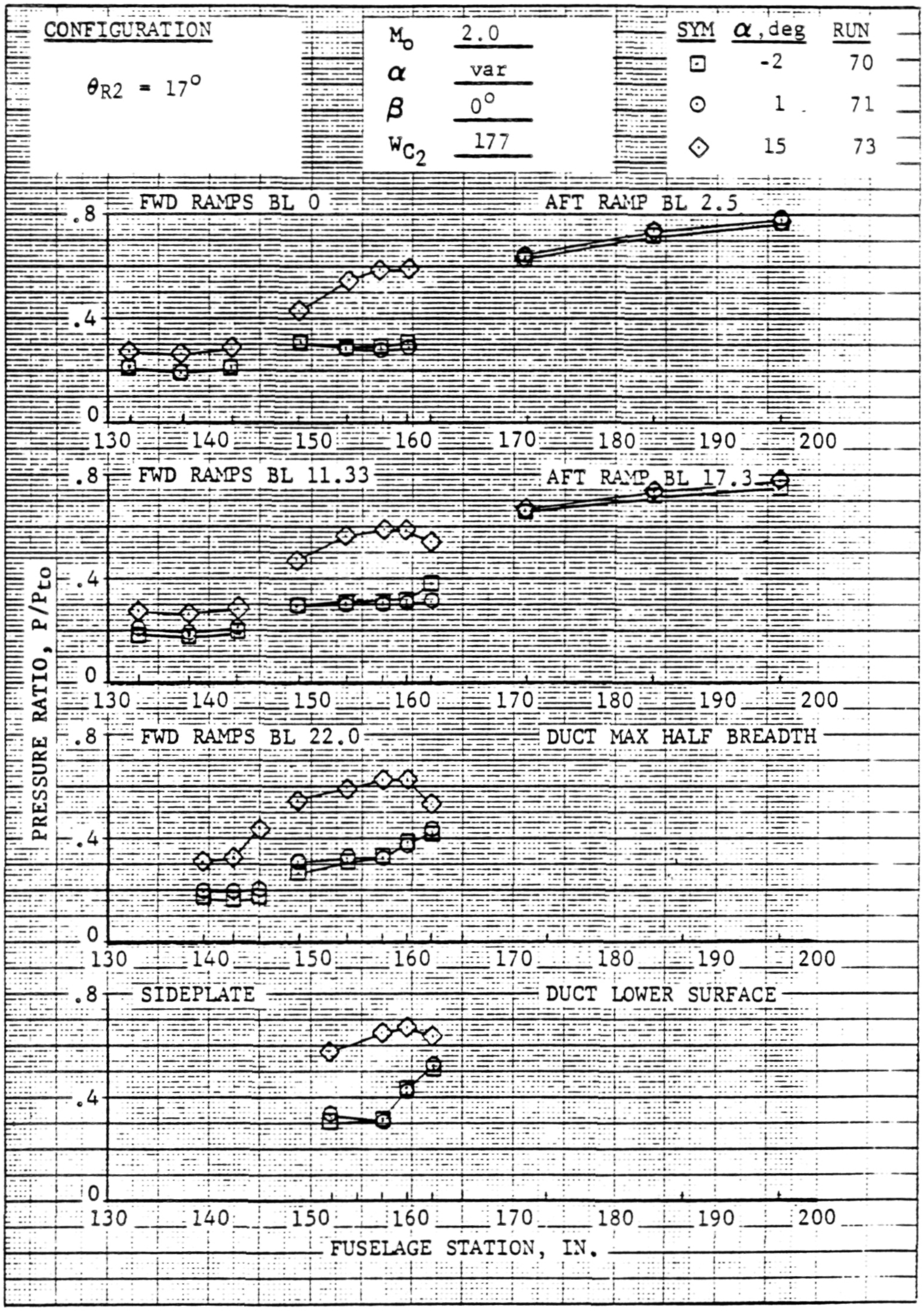

(c) $M_o = 2.0$

Figure 7-32 (Cont'd)

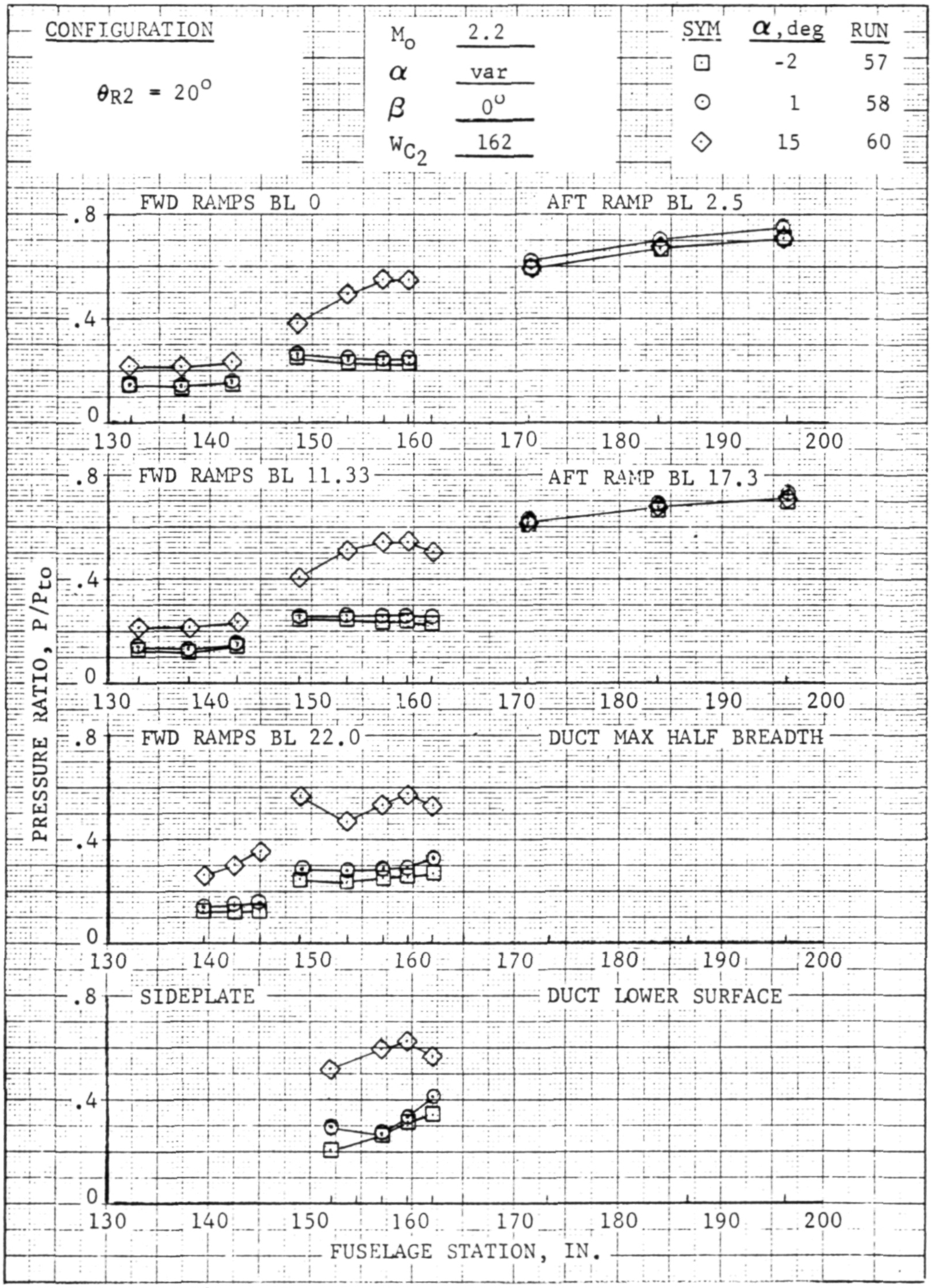

(d) M_o = 2.2

Figure 7-32 (Concl)

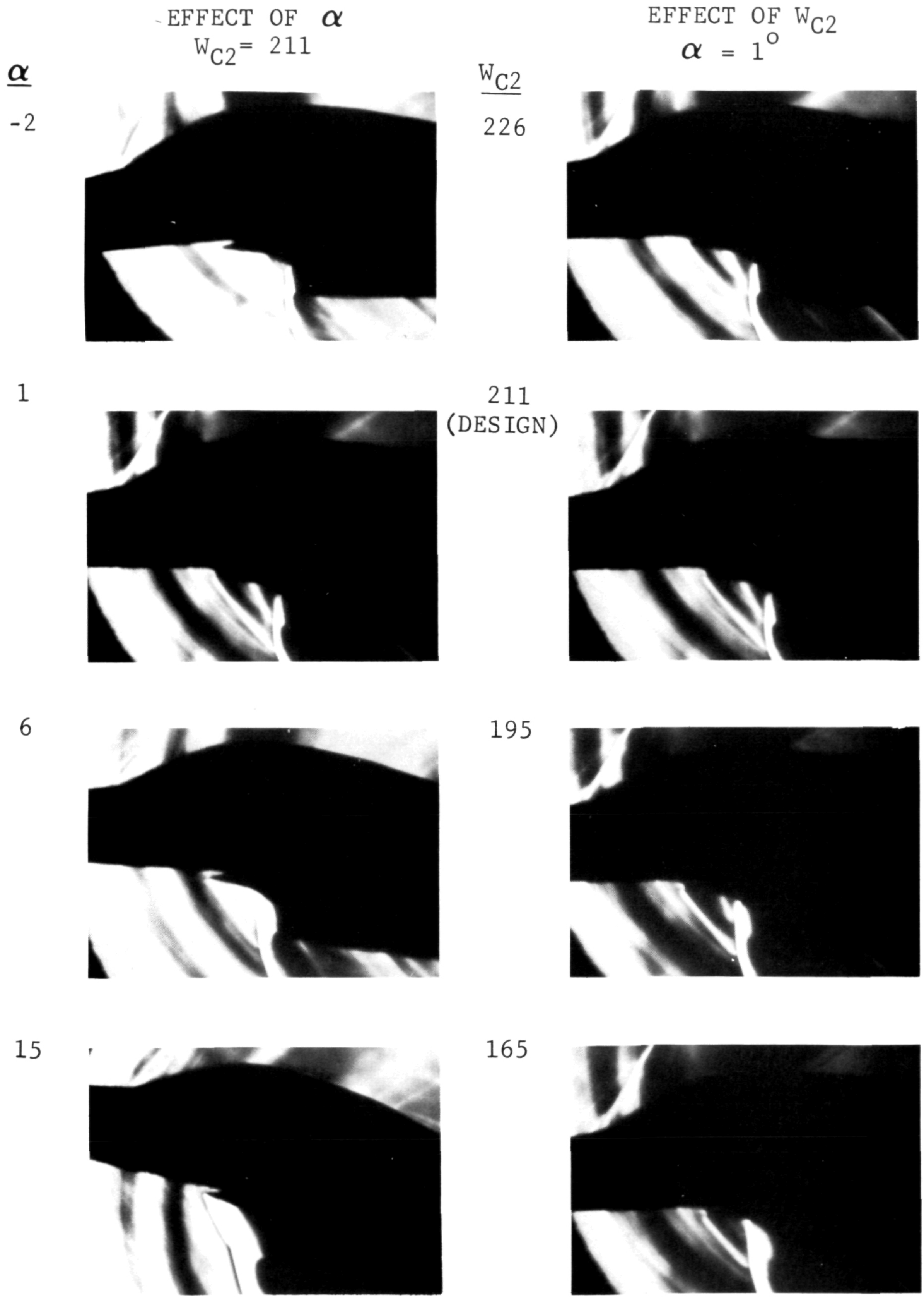

Figure 7-33 Schlieren Photographs (a) $M_o = 1.6$, $\theta_{R2} = 12^o$, $\beta = 0^o$

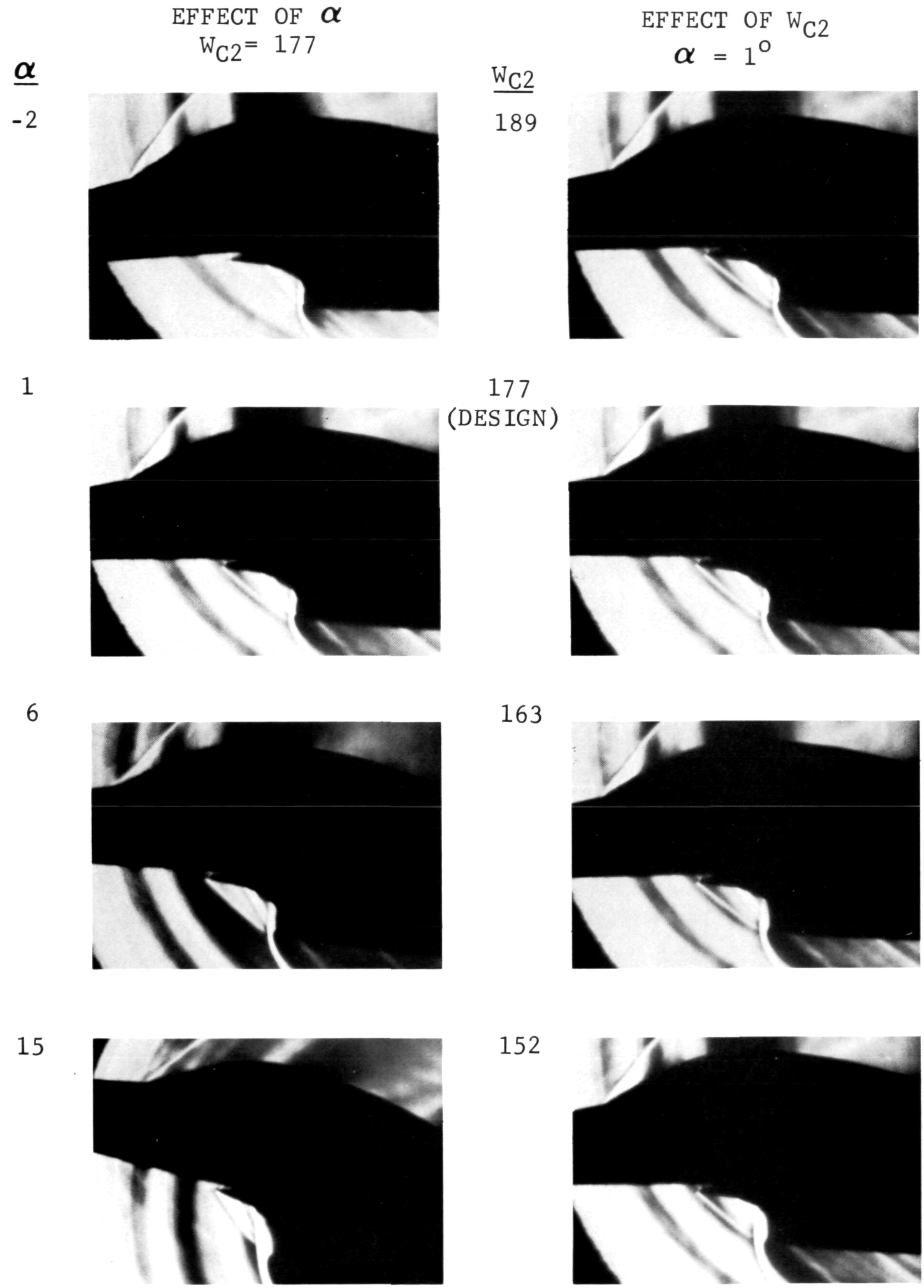

Figure 7-33 (Cont'd) (b) $M_o = 2.0$, $\theta_{R2} = 17^o$, $\beta = 0^o$

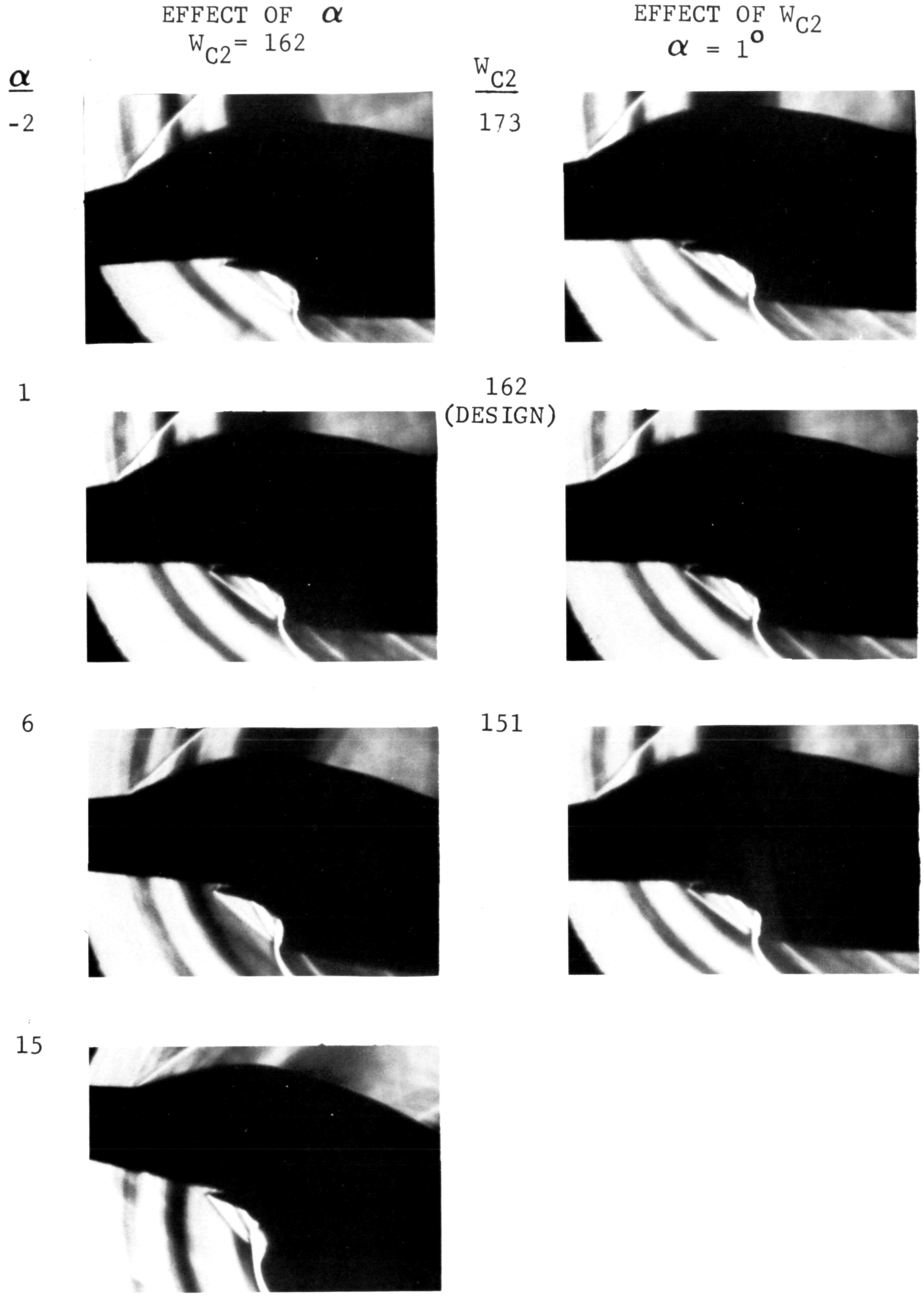

Figure 7-33 (Concl) (c) $M_o = 2.2$, $\theta_{R2} = 20°$, $\beta = 0°$

LOG OF POINTS FOR ANALOG SCREENING
NASA AMES TEST 260-1-66

RUN/SEQ.	M_o	α / β	W_{c2} Lb/Sec	θ_{R2} Deg	$\frac{\bar{P}_{t2}}{\bar{P}_{to}}$	$\frac{\bar{P}_{tRMS}}{\bar{P}_{t2}}$	$K_{a2})_{S-S}$	DYNADEC		$K_{a2})$ SCREEN LIMIT	$\frac{K_{a2})_{MAX}}{K_{a2})_{SCREEN\ LIM}}$
								FRAME NO.	Max K_{a2}		
97-6	2.2	-2/0	164	20	.811	.018	3.205	135310.295	4.812	7.30	.659
98-3		1/0	164		.853	.014	3.009	140223.160	4.158	7.30	.570
98-4		1/0	153		.872	.008	4.266	140340.104	5.376	8.05	.668
100-3		10/0	164		.879	.015	1.785	142237.527	2.886	7.30	.395
102-3		20/0			.856	.017	.445	143944.775	2.151		.295
104-3		1/-5			.813	.029	3.290	145612.539	6.755		.925
106-3		10/-5			.865	.014	1.887	152249.689	3.067		.420
107-3		15/-5			.856	.014	1.248	153029.388	2.542		.348
108-3		20/-5			.858	.015	.622	153850.988	2.380		.326
110-5		-2/0		18.8	.837	.013	3.014	092423.016	3.919		.537
111-3		1/0	164		.865	.011	2.255	093221.633	3.068		.420
111-4		1/0	153		.844	.014	3.453	093355.672	5.822	8.05	.723
111-5		1/0	142		.827	.017	4.796	093502.129	8.600	8.40	1.024
115-3		20/0	164		.865	.015	.983	102531.718	2.285	1.30	.313
116-3	2.0	-2/0	180		.854	.021	.722	103951.466	1.196	3.35	.357
116-4		-2/0	165		.891	.013	2.419	104127.666	3.422	7.20	.475
117-3		1/0	180		.877	.017	.629	104918.607	1.019	3.35	.304
117-4		1/0	165		.915	.010	2.183	105040.162	3.036	7.20	.422
121-3		20/0	180		.870	.020	1.245	112915.999	1.711	3.35	.511
121-4		20/0	165		.800	.015	.526	113029.510	1.853	7.20	.257
122-5	0.8	-10/0	230	4	.962	.011	.541	113522.013	.630	0.77	.818
124-3		1/0	228		.979	.006	.469	132638.196	.524	0.75	.699
129-3		30/0	228		.974	.007	.455	143048.320	.504	0.75	.672
130-3		-10/-5	224		.961	.011	.632	144512.604	.724	0.86	.812
135-3		30/-5	228		.973	.007	.459	182505.942	.502	0.75	.669
136-3		-5/-10	224		.963	.012	.711	183636.861	.797	0.86	.927
137-3		1/-10	225		.972	.008	.618	184452.129	.694	0.83	.835
143-4	1.3	-5/0	228		.952	.013	.467	214910.467	.603	0.75	.804
144-2		1/0	225		.974	.006	.571	215836.784	.615	0.83	.741
146-2		15/0	225		.973	.005	.575	222317.958	.619	0.83	.746
148-2		25/0	225		.976	.006	.545	224148.147	.596	0.83	.718
149-2		-5/-5	224		.942	.023	.500	225038.473	.924	0.86	1.074
150-2		1/-5	224		.971	.006	.571	225827.100	.634	0.86	.737
152-2		15/-5	224		.978	.005	.581	231234.391	.605	0.86	.703
165-5	1.6	-2/0	213	10	.942	.007	.280	212457.016	.296	1.17	.253
165-7		-2/0	167		.905	.025	1.740	212750.887	4.294	6.96	.618
166-3		1/0	213		.951	.006	.289	213521.044	.341	1.17	.291
166-4		1/0	197		.955	.006	.234	213632.169	.284	1.60	.178
169-3		15/0	213		.956	.006	.297	220123.106	.330	1.17	.282
169-4		15/0	197		.959	.006	.255	220234.006	.295	1.60	.184

Figure 7-34 Log of Points for Analog Screening

LOG OF POINTS FOR ANALOG SCREENING
NASA AMES TEST 260-1-66

RUN/SEQ.	M_o	α / β	W_{c2} Lb/Sec	θ_{R2} Deg	$\bar{P}_{t2} / \bar{P}_{to}$	$\bar{P}_{tRMS} / \bar{P}_{t2}$	$K_{a2})_{S-S}$	DYNADEC FRAME NO.	DYNADEC Max K_{a2}	$K_{a2})$ SCREEN LIMIT	$K_{a2})_{MAX} / K_{a2})_{SCREEN\ LIM}$
170-3	1.6	20/0	213	10	.949	.006	.204	221215.211	.269	1.17	.230
170-4		20/0	197	10	.952	.005	.194	221339.836	.242	1.60	.151
171-7		-2/0	167	12	.910	.025	1.774	181803.284	4.089	6.95	.588
172-5		1/0	167		.953	.005	1.563	183121.118	1.662	6.95	.239
175-3		15/0	213		.943	.007	.329	185836.312	.393	1.17	.336
178-3		1/-5	213		.937	.008	.316	192622.123	.409	1.17	.350
178-4		1/-5	197		.946	.007	.307	192738.567	.389	1.60	.243
178-5		1/-5	167		.943	.008	1.453	192859.590	1.870	6.95	.269
181-3		15/-5	213		.943	.007	.385	200033.816	.471	1.17	.403
181-4		15/-5	197		.950	.006	.310	200215.197	.395	1.60	.247
183-6		-2/0	213	14	.910	.016	.292	230306.118	.470	1.17	.402
183-8		-2/0	167		.937	.026	1.788	230552.930	3.651	6.95	.525
184-3		1/0	213		.920	.016	.301	231131.785	.504	1.17	.431
184-5		1/0	167		.957	.006	1.736	231414.588	1.888	6.95	.272
188-3		20/0	213		.904	.014	.283	185807.472	.454	1.17	.388
189-5	2.0	-2/0	180	16	.905	.012	.633	213109.618	.800	3.35	.239
190-3		1/0	180		.912	.009	.788	213805.036	.939	3.35	.280
190-4		1/0	165		.903	.013	1.571	213944.710	2.764	7.20	.384
194-3		20/0	180		.916	.015	1.381	220903.867	1.518	3.35	.453
194-4		20/0	165		.911	.014	.816	221019.997	1.827	7.20	.254
195-5		-2/0	180	17	.906	.012	.579	181508.207	.845	3.35	.252
196-3		1/0	180		.916	.009	.624	182034.112	.741	3.35	.221
196-4		1/0	165		.909	.012	1.799	182203.155	2.607	7.20	.362
200-3		20/0	180		.908	.016	1.282	190007.019	1.481	3.35	.442
200-4		20/0	165		.905	.013	.818	190128.428	1.902	7.20	.264
201-3		-2/-5	196		.820	.030	.713	190942.667	1.335	1.65	.809
205-3		15/-5	180		.908	.016	1.095	193613.211	1.450	3.35	.433
205-4		15/-5	165		.910	.014	1.380	193756.829	2.548	7.20	.354
206-3		20/-5	180		.907	.015	1.204	195416.207	1.554	3.35	.464
206-4		20/-5	165		.910	.013	.947	195542.246	2.022	7.20	.281

Figure 7-34 (Concl)

CONDITIONS AUDITED

CASE	RUN/SEQ	Mo	O R2	MATCH POINT WC2	α°/β°	AUDIT ALTITUDES/CONDITIONS
1	122-5	0.8	4°	228,225	-10/0	30K Std, 50K Std
2	124-3	0.8	4°	228,226,226	1/0	30K Std, 50K Std, 50K Cold
3	129-3	0.8	4°	228,225	30/0	30K Std, 50K Std
4	136-3	0.8	4°	228,225	-5/-10	30K Std, 50K Std
5	137-3	0.8	4°	228,225	1/-10	30K Std, 50K Std
6	143-4	1.3	4°	209,195	-5/0	30K Std, 59K Std
7	144-2	1.3	4°	210,196,226	1/0	30K Std, 59K Std, 59K Cold
8	148-2	1.3	4°	210,196	25/0	30K Std, 59K Std
9	149-2	1.3	4°	209,195	-5/-5	30K Std, 59K Std
10	150-2	1.3	4°	210,196	1/-5	30K Std, 59K Std
11*	172-3	1.6	12.°	204,202,212	1/0	30K Std, 55.5K Std, 55.5K Cold
12	175-3	1.6	12.°	204,202	15/0	30K Std, 55.5K Std
13	178-3	1.6	12.°	204,201	1/-5	30K Std, 55.5K Std
14	181-3	1.6	12.°	204,202	15/-5	30K Std, 55.5K Std
15	184-3	1.6	14.°	204,201,212	1/0	30K Std, 55.5K Std, 55.5K Cold
16	195-5	2.0	17.°	175,173	-2/0	30K Std, 60K Std
17	196-3	2.0	17.°	175,174,173,174	1/0	30K Std, 50K Std, 60K Std, 60K Cold
18	200-3	2.0	17.°	175,173	20/0	30K Std, 60K Std
19	205-3	2.0	17.°	175,173	15/-5	30K Std, 60K Std
20	117-4	2.0	18.8°	175,174,173,174	1/0	30K Std, 50K Std, 60K Std, 60K Cold
21	97-6	2.2	20.°	158,156	-2/0	36K Std, 60K Std
22	98-3	2.2	20.°	158,157,156,158	1/0	36K Std, 50K Std, 60K Std, 60K Cold
23	104-3	2.2	20.°	158,156	1/-5	36K Std, 60K Std
24	107-3	2.2	20.°	158,156	15/-5	36K Std, 60K Std

*Steady state point

Figure 7-35 Log of Points for Engine Stability Audit

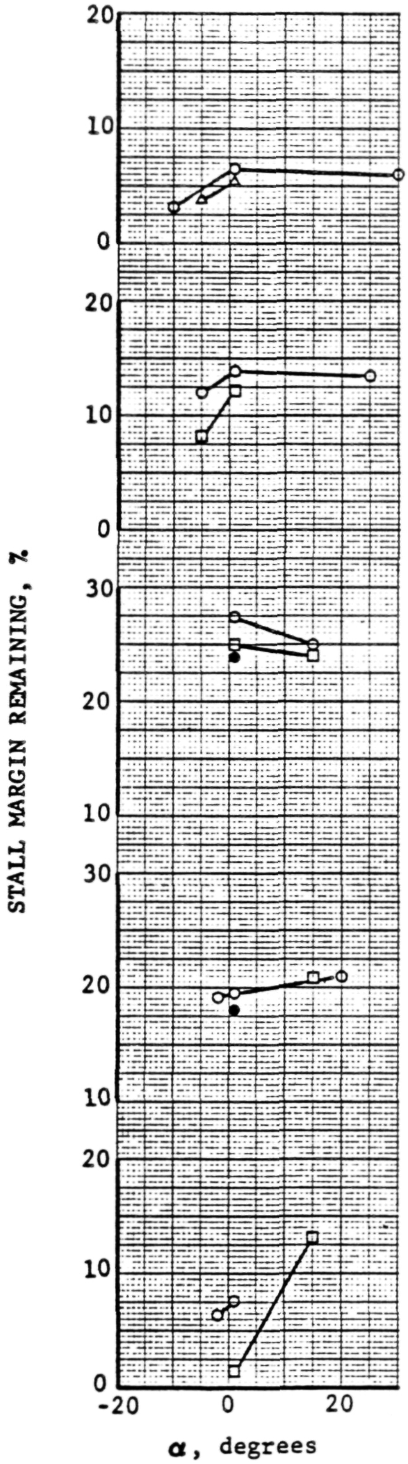

Mach	SYM	β, deg	θ_{R2}, deg	ALT, Kft
.8	○	0	4	30
	△	-10	4	30
1.3	○	0	4	30
	□	-5	4	30
1.6	○	0	12	30
	●	0	14	30
	□	-5	12	30
2.0	○	0	17	30
	●	0	18.8	30
	□	-5	17	30
2.2	○	0	20	36
	□	-5	20	36

Figure 7-36 Stall Margin Remaining, Standard Day, Intermediate Altitudes

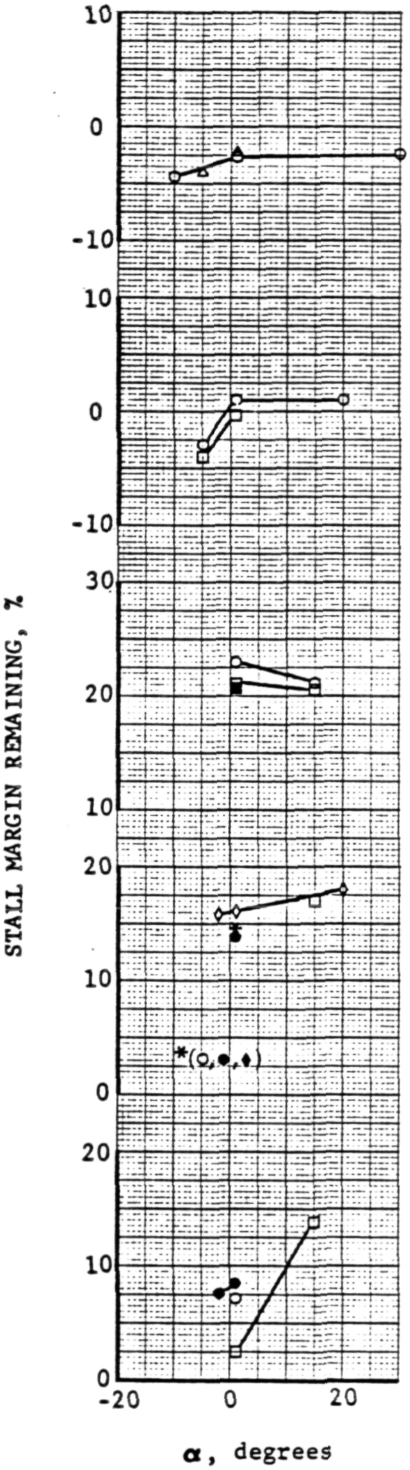

Mach	SYM	β, deg	θ_{R2}, deg	ALT, Kft
.8	○	0	4	50
	△	-10	4	50
1.3	○	0	4	59
	□	-5	4	59
1.6	○	0	12	55.5
	□	-5	12	55.5
	■	-5	14	55.5
2.0	○	0	17	50
	●	0	18.8	50
	◇	0	17	60
	◆	0	18.8	60
	□	-5	17	60
2.2	○	0	20	50
	●	0	20	60
	□	-5	20	60

Figure 7-37 Stall Margin Remaining, Standard Day, High Altitudes

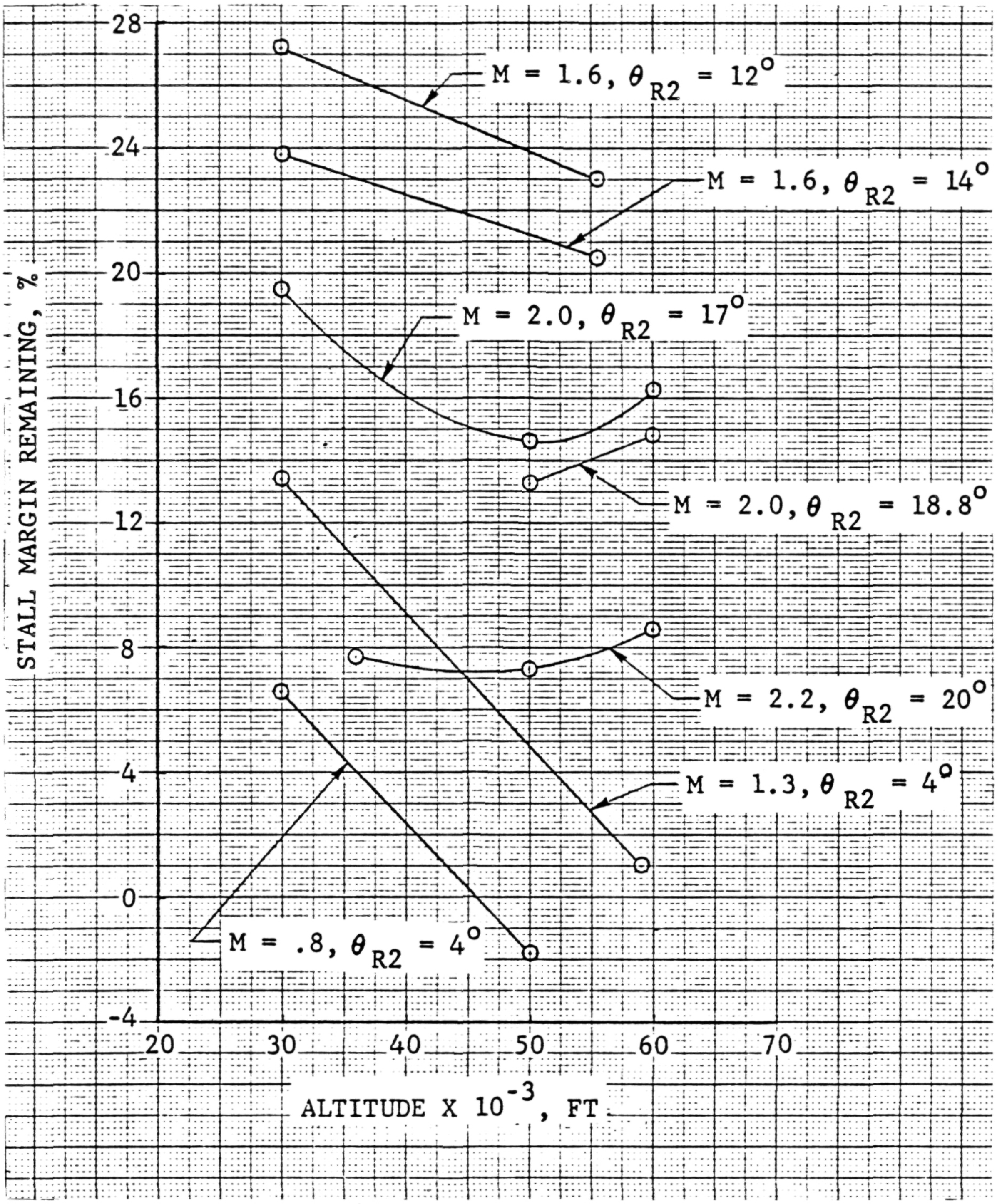

Figure 7-38 Effect of Altitude on Stall Margin Remaining, Standard Day, α = 1°, β = 0°

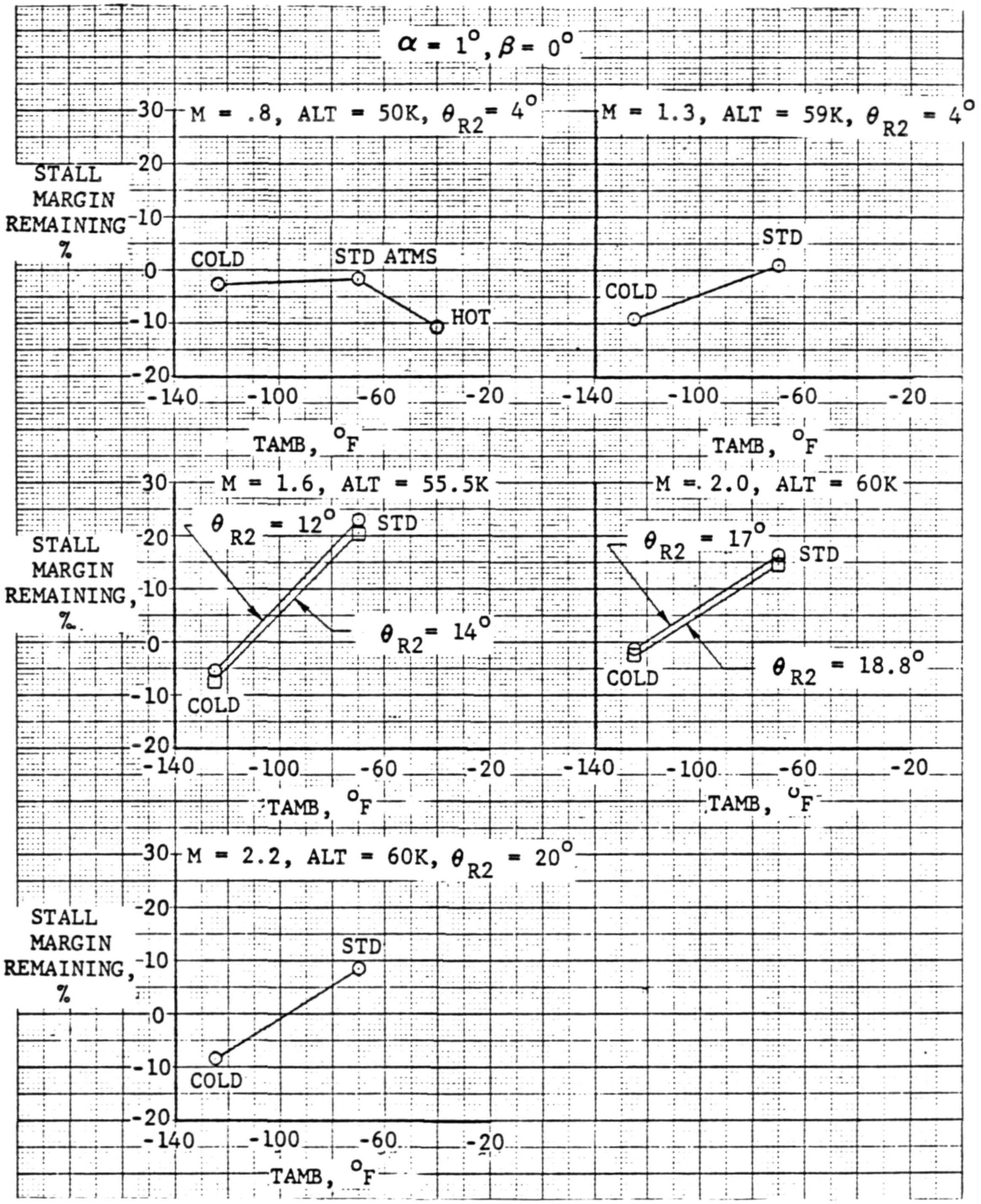

Figure 7-39 Effect of Ambient Temperature on Stall Margin Remaining, $\alpha = 1^\circ$, $\beta = 0^\circ$

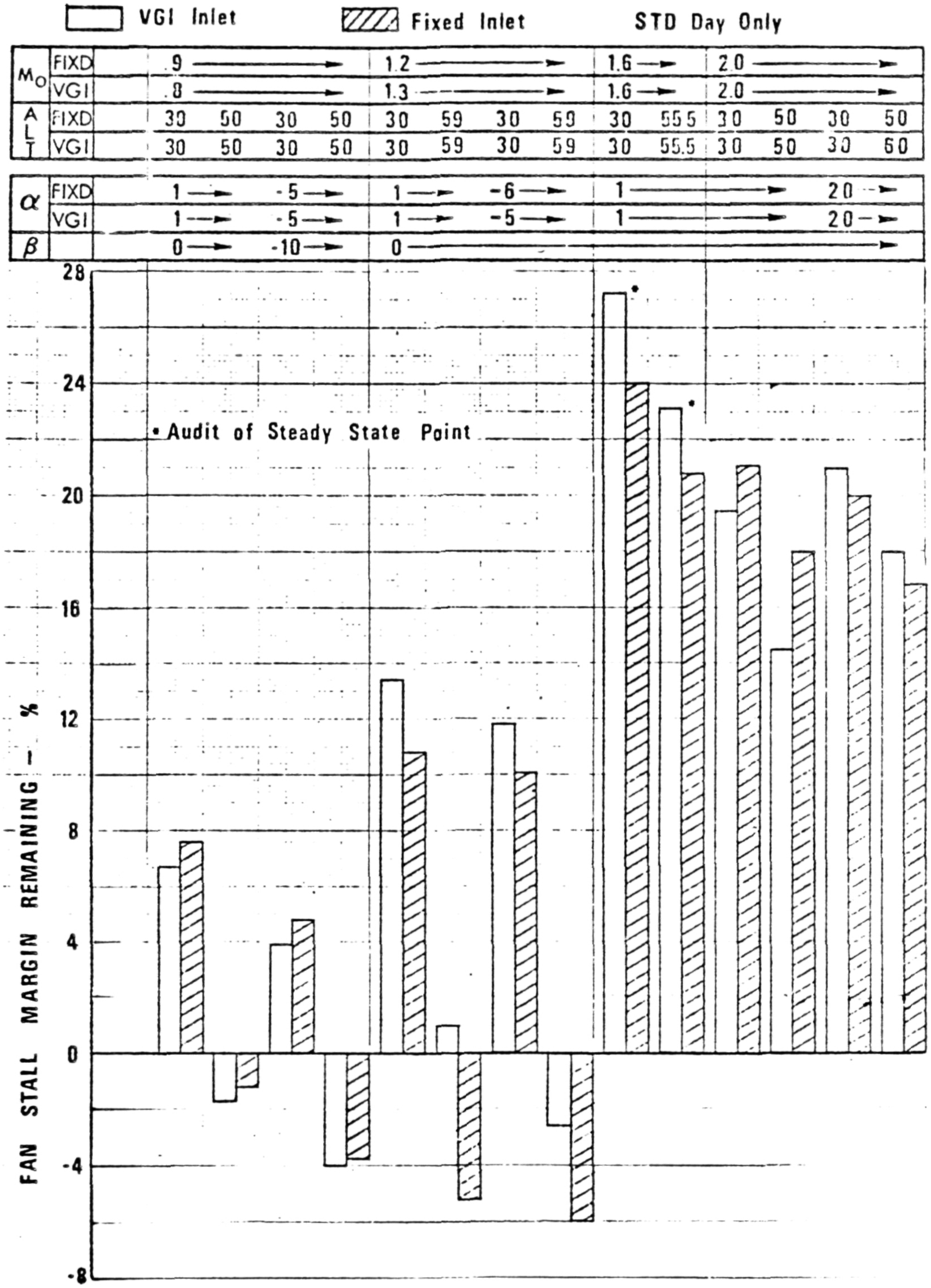

Figure 7-40 Stability Audit Comparison of the Conformal IIIB Variable-Ramp Inlet and the Basic F-16 Fixed-Geometry Inlet

F16/VGI STABILITY AUDIT GROUND RULES FOR F100(3)/LOT 4 ENGINE

Engine

As defined by P&WA Deck E7868A including Def. VI EEC schedules (0°/-25° CIVV), Lot 7 unified control schedules (Scheme IX RCVV), Improved Stability Fan, Distortion Deck CCD 1087-1.2.

Installation

F16 per PCM-75-009. Except VGI average recovery used for each pattern audited.

Destabilizing Influences

Distortion - Twenty-five worst case VGI fan face patterns and one steady state face pressure summary supplied via Coord Sheet 2005.

Segment Sequencing - "Revised May, 1974" plus 2% spike levels for 2:1 bellows 0.375" orifice, 0.009 Seg. I to II transfer fuel-air ratio. Averaged constant corrected fan speed and constant flow applications, with choked duct attenuation of spike included where applicable.

Distortion Rematch - 1% stall margin loss for fan; zero loss for compressor.

Control Tolerances - Representative of average engine (i.e., typical day to day experience)

T_{T_2} sensor: 0°F, FTIT sensor: ±15°F

Mach Number Sensor:
±.05
N1 Sensor Error
±15 rpm
N2 Sensor Error:
±15 rpm

RCVV Errors:

On Stops	±2.0°	Fan Operating Point Rematch
On Schedule Slope	±2.0°	
On Stops	±2.0°	Compressor Surge Line Loss
On Schedule Slope	±2.0°	

Reynolds Number Effects - "Wells" and "Snyder" correlations for fan and compressor except fan rig 205A is used for fan efficiency.

Engine-to-Engine Variation - 1% stall margin loss fan and compressor.

Fan Pressure Distortion Attenuation and Temperature Generation - Correlation of rig and engine data.

Compressor Lapse Rate With Thermal Distortion - AAC Rig 205 data

Figure 7-41 Stability Audit Groundrules for the Conformal IIIB Inlet and the F100(3)/Lot 4 Engine

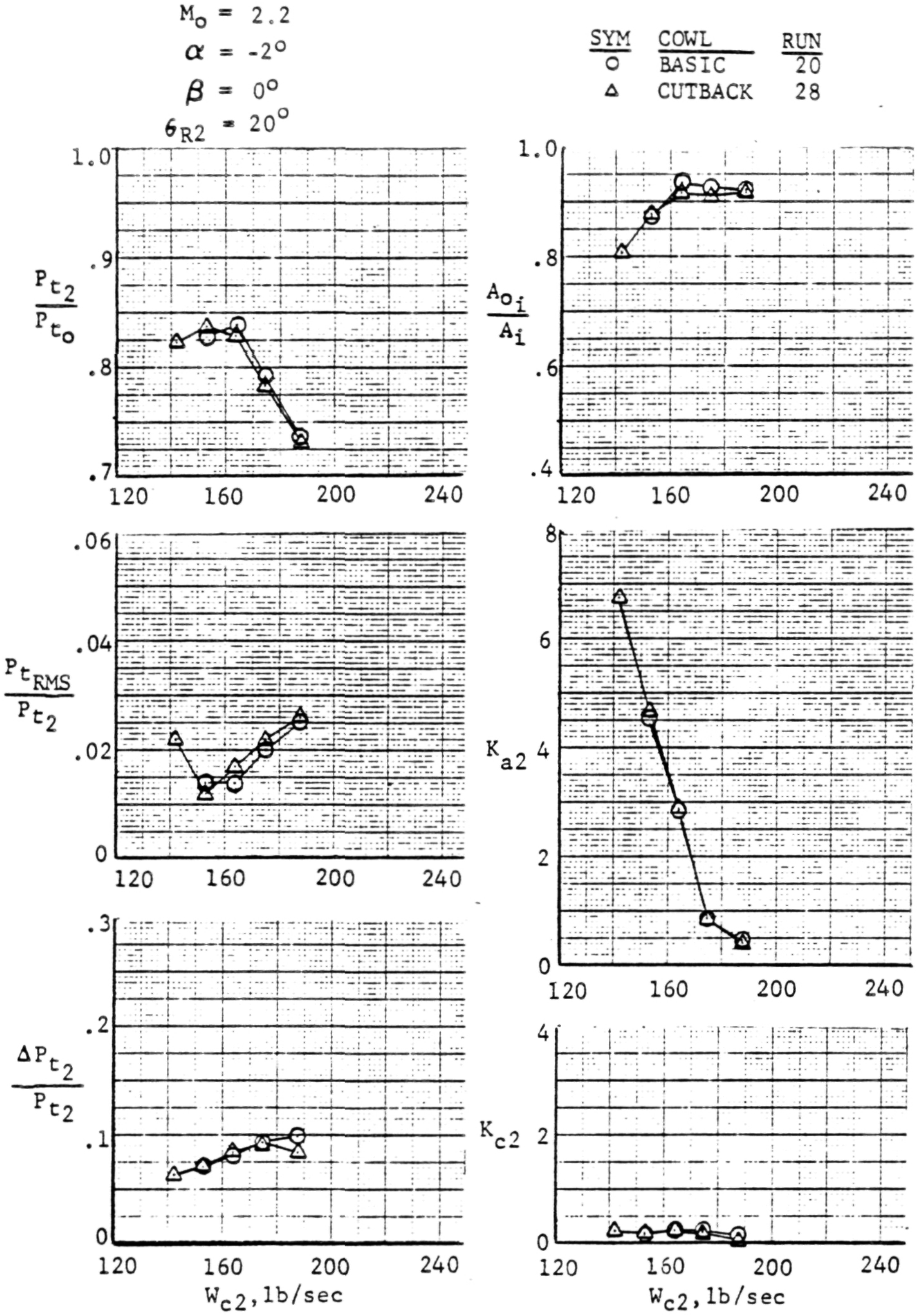

(a) α = -2°

Figure 7-42 Effect of Cowl Sidewall Cutback on Inlet Performance, Basic Lip

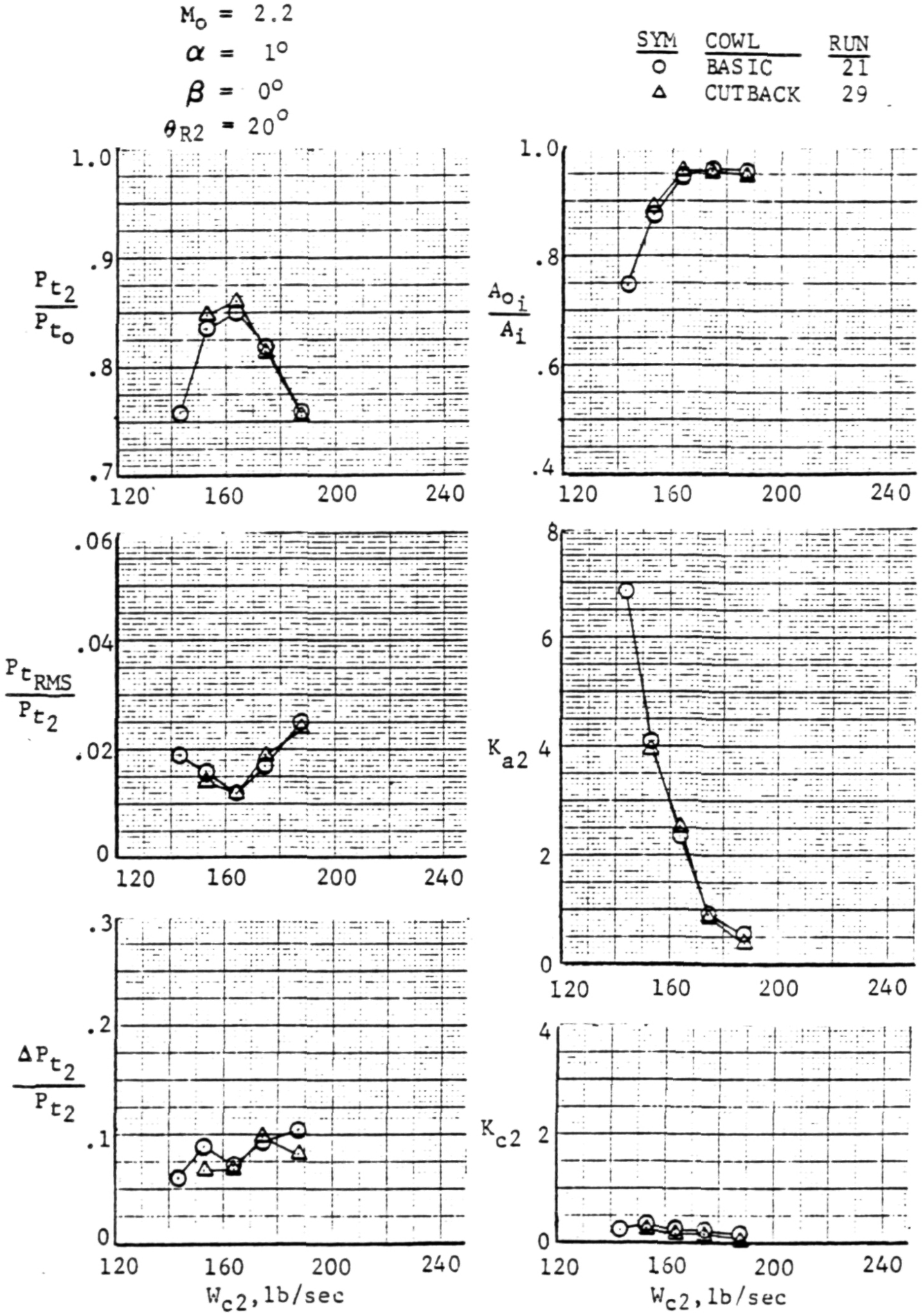

(b) α = 1°

Figure 7-42 (Concl)

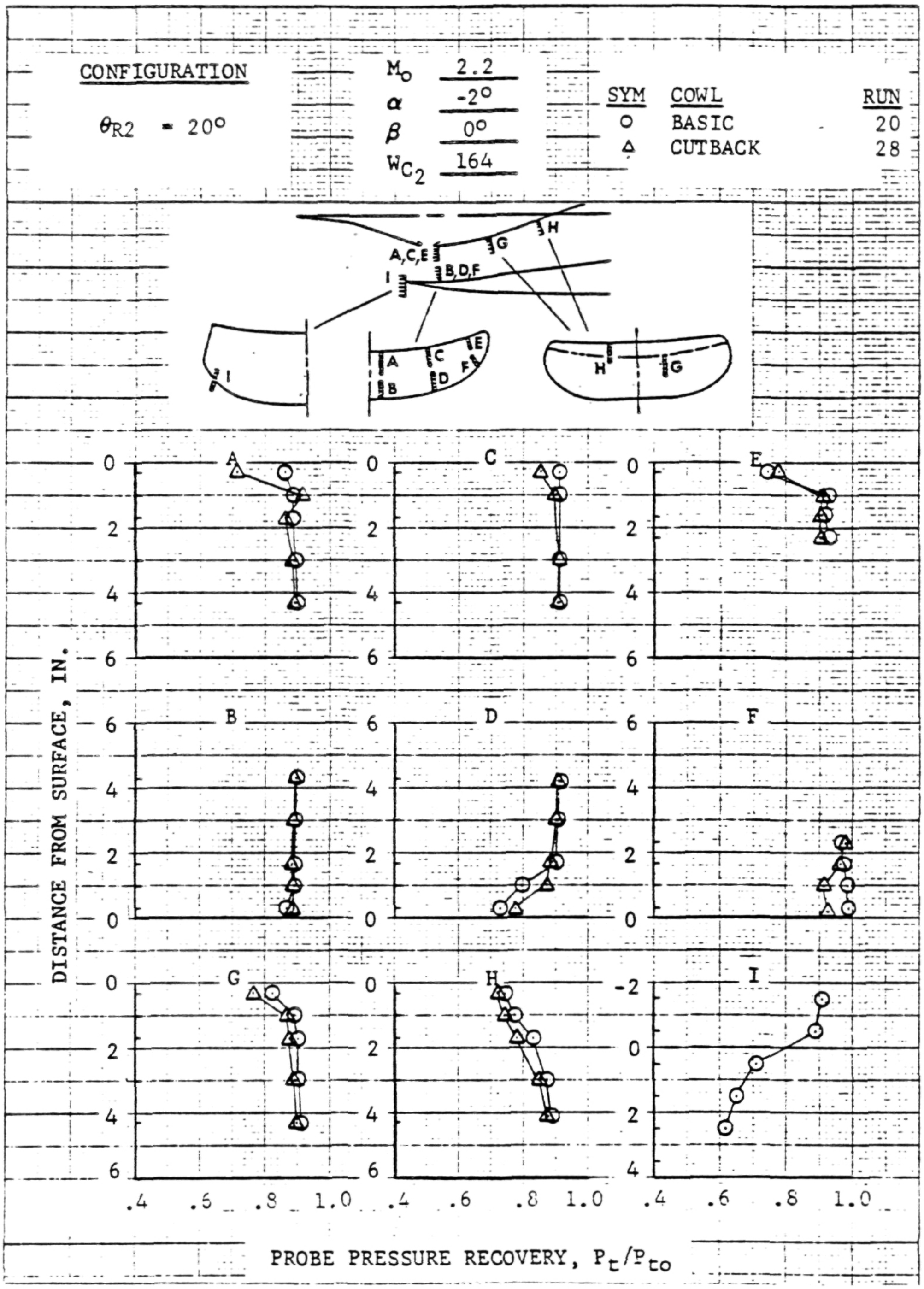

(a) $\alpha = -2^\circ$

Figure 7-43 Effect of Cowl Sidewall Cutback on Throat Total Pressures, Basic Lip

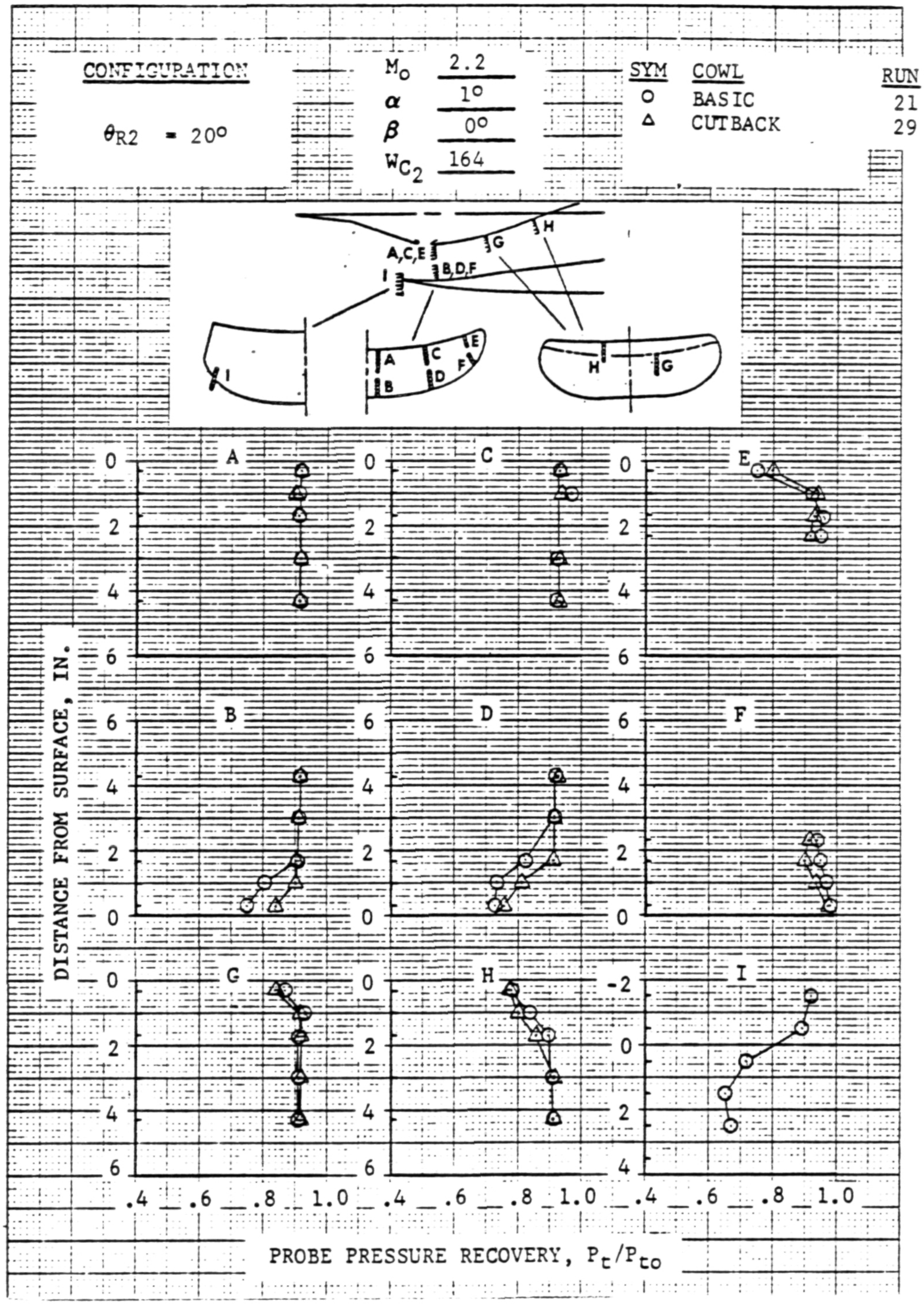

(b) α = 1°

Figure 7-43 (Concl)

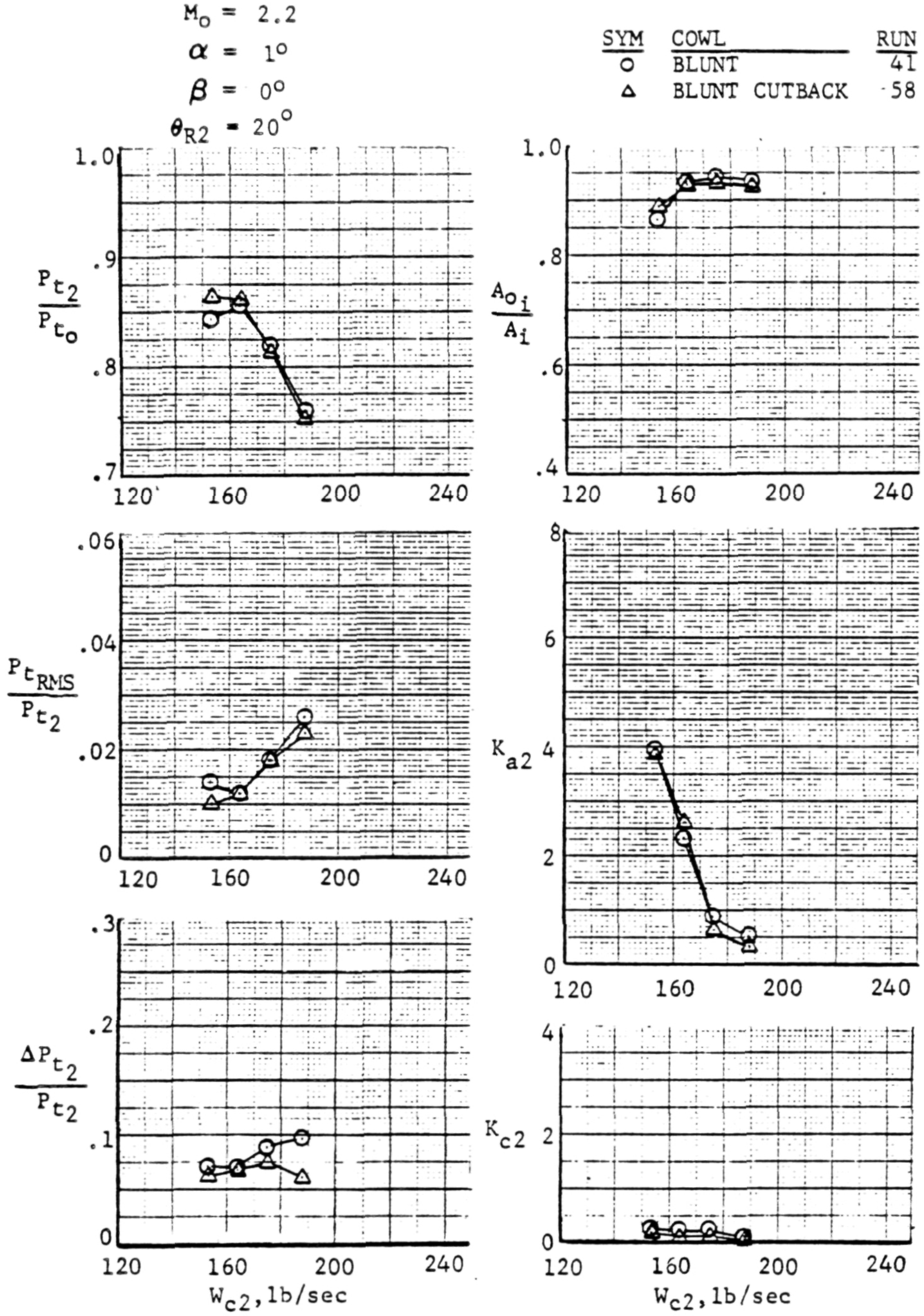

Figure 7-44 Effect of Cowl Sidewall Cutback on Inlet Performance, Blunt Lip

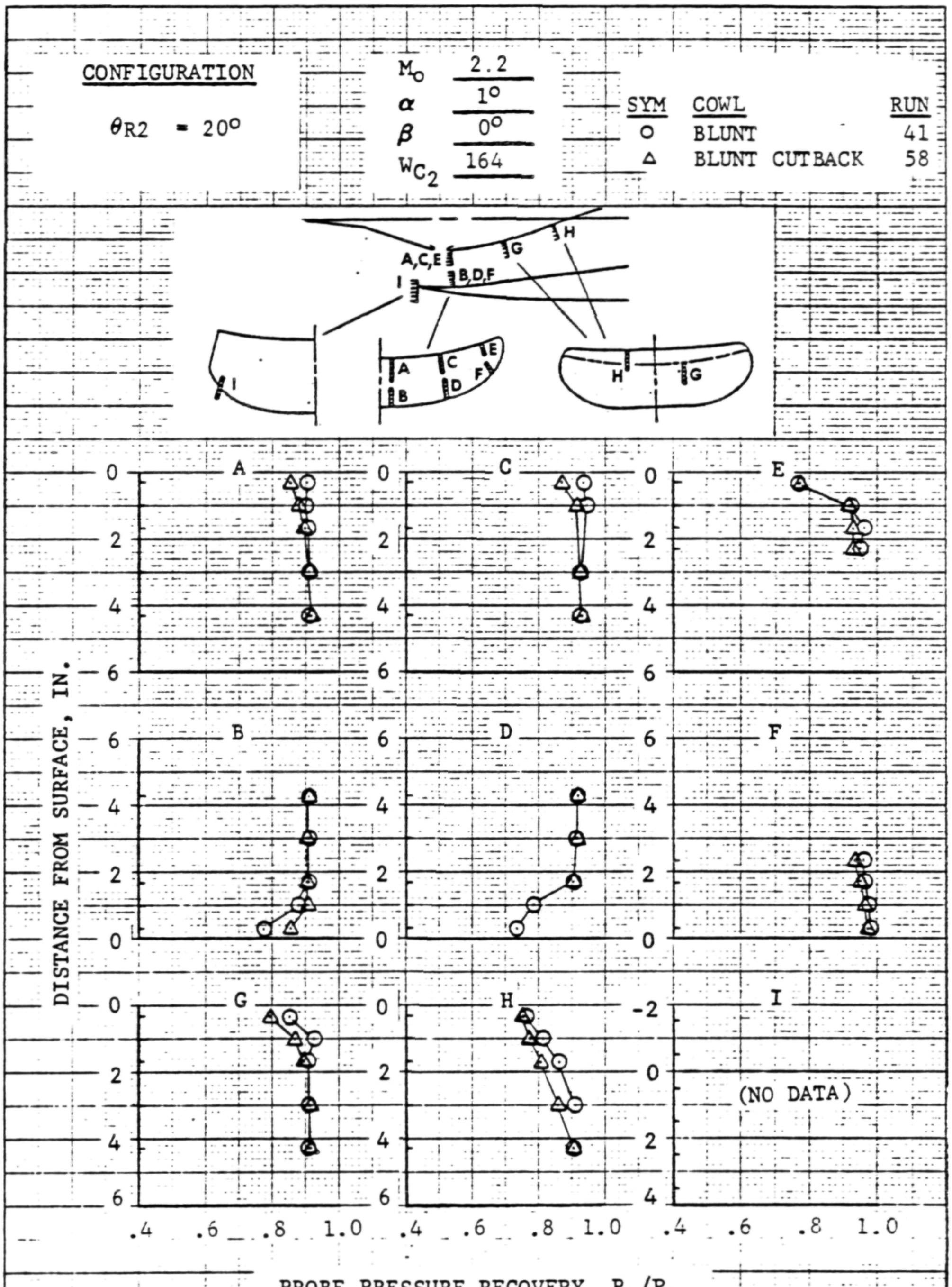

Figure 7-45 Effect of Cowl Sidewall Cutback on Throat Total Pressures, Blunt Lip

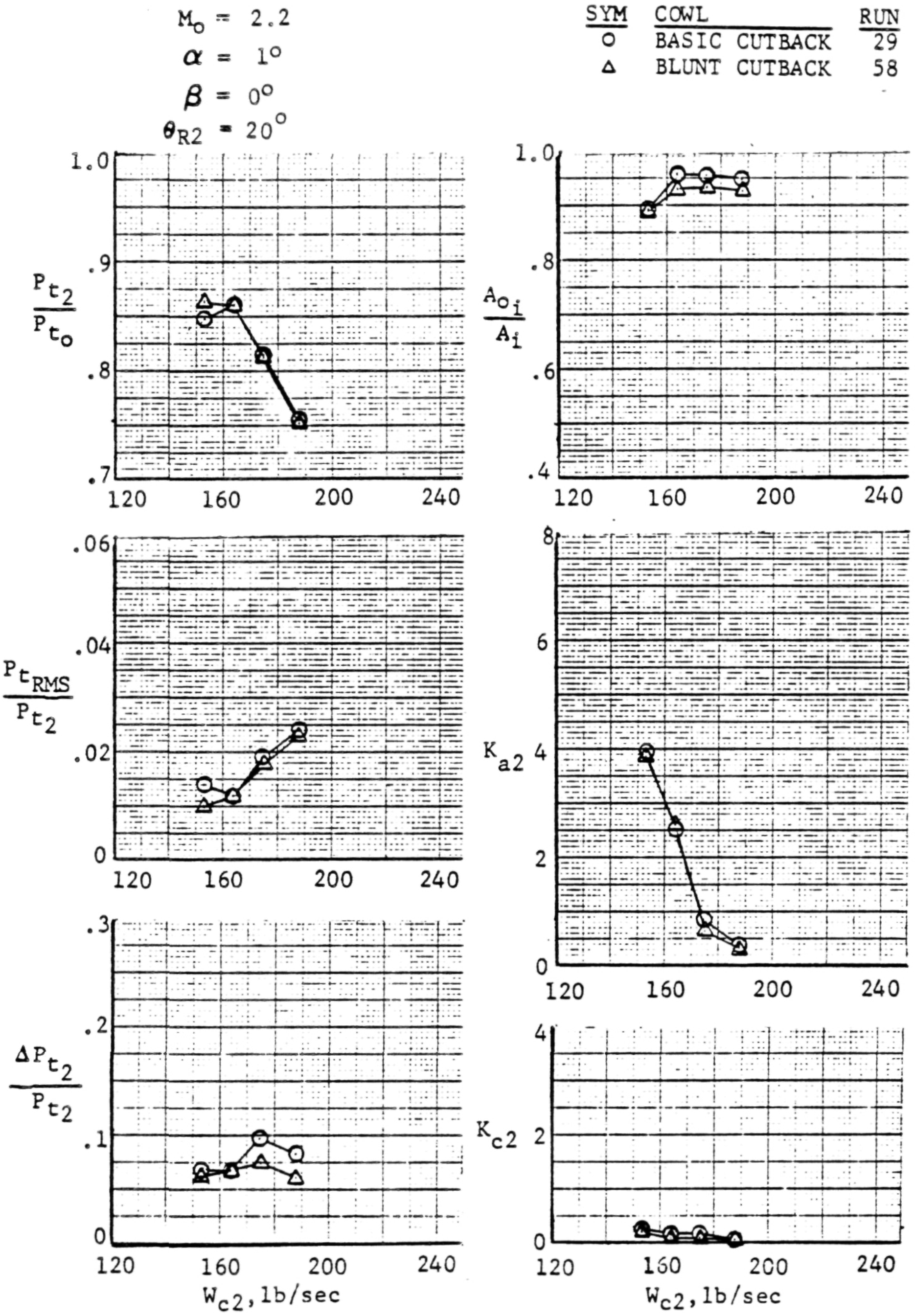

(a) $M_o = 2.2$

Figure 7-46 Effect of Cowl Lip Bluntness on Inlet Performance

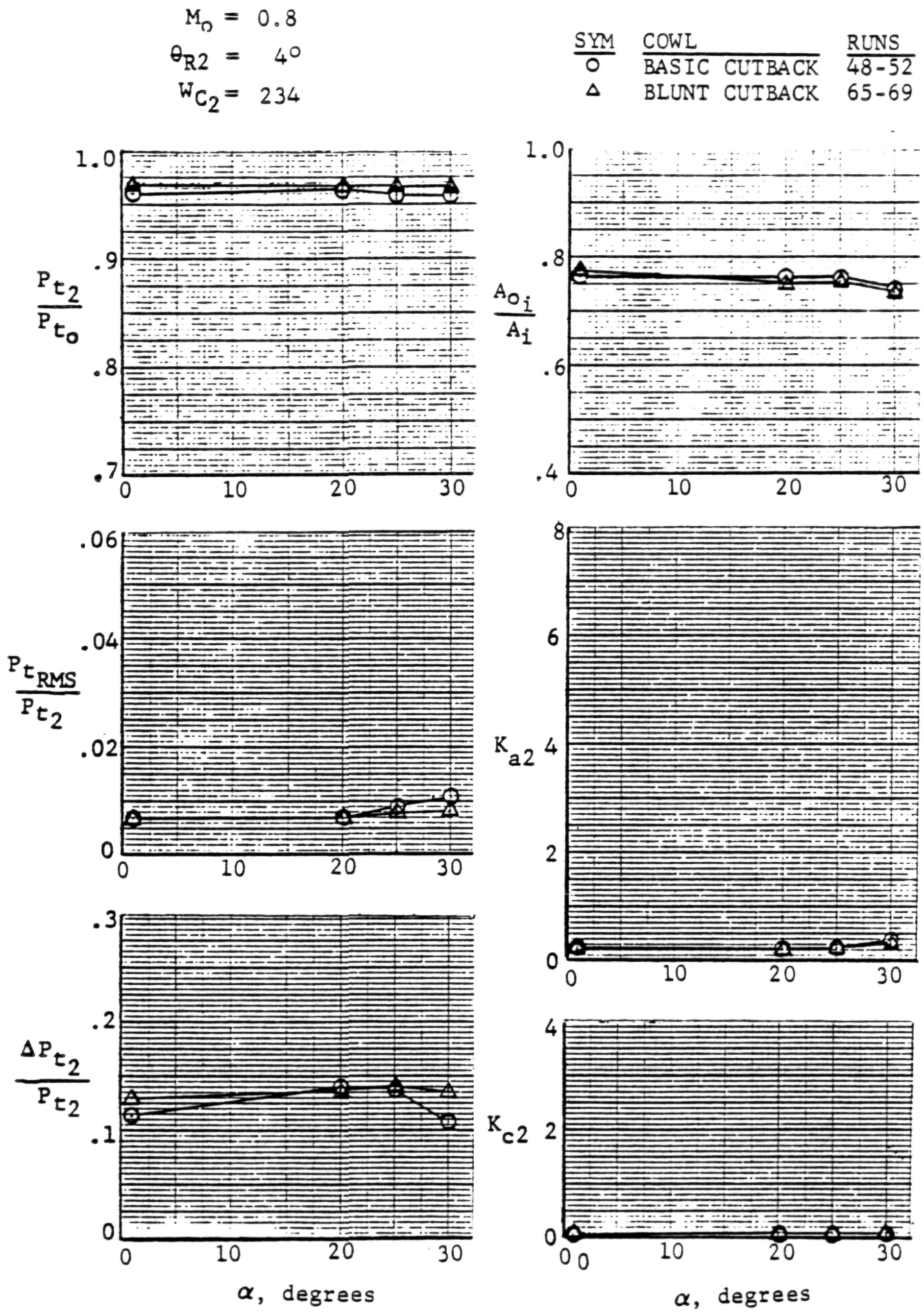

(b) M_O = 0.8

Figure 7-46 (Concl)

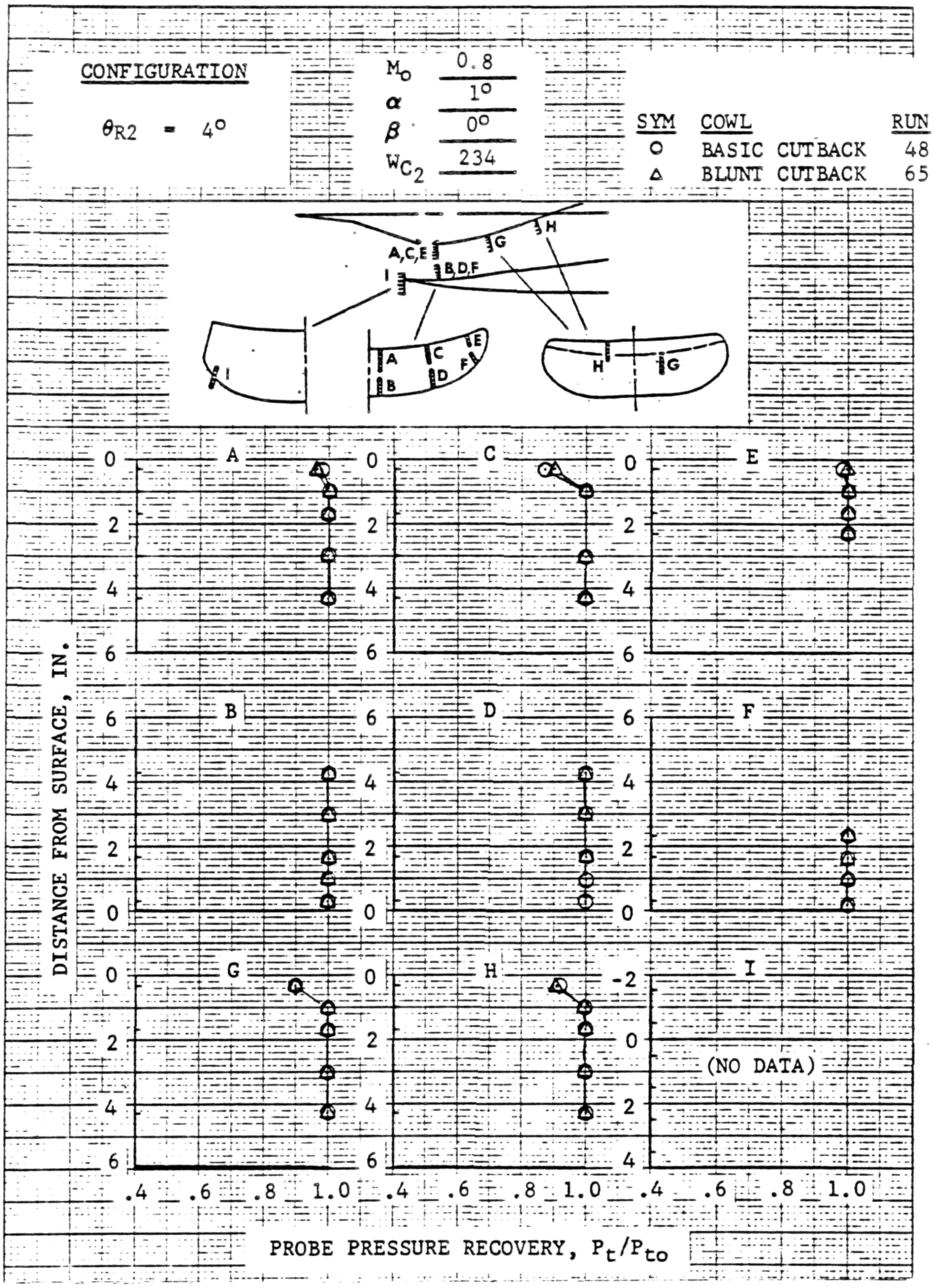

(a) $\alpha = 1°$

Figure 7-47 Effect of Cowl Lip Bluntness on Throat Total Pressures, $M_o = 0.8$

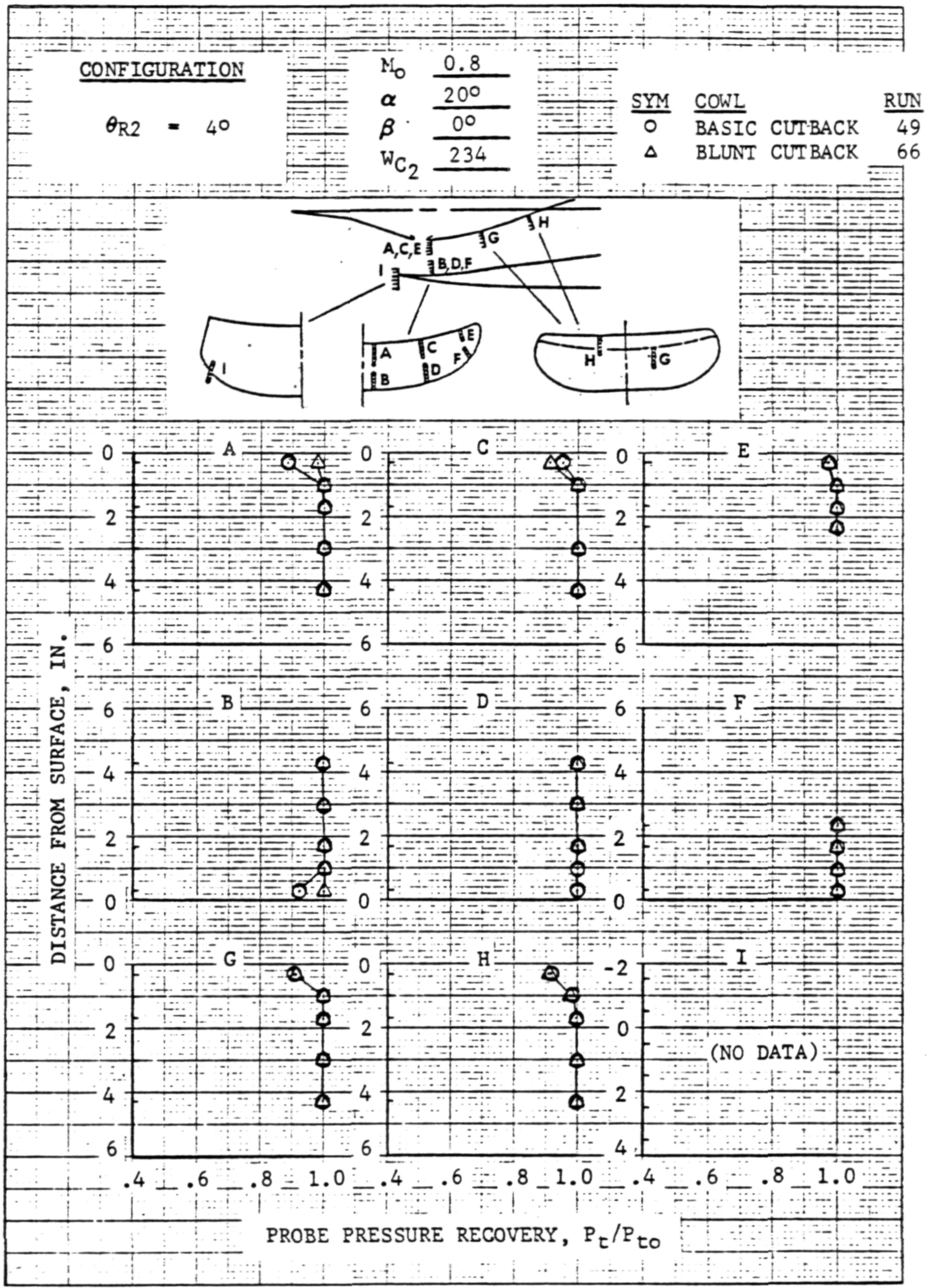

(b) $\alpha = 20^\circ$

Figure 7-47 (Cont'd)

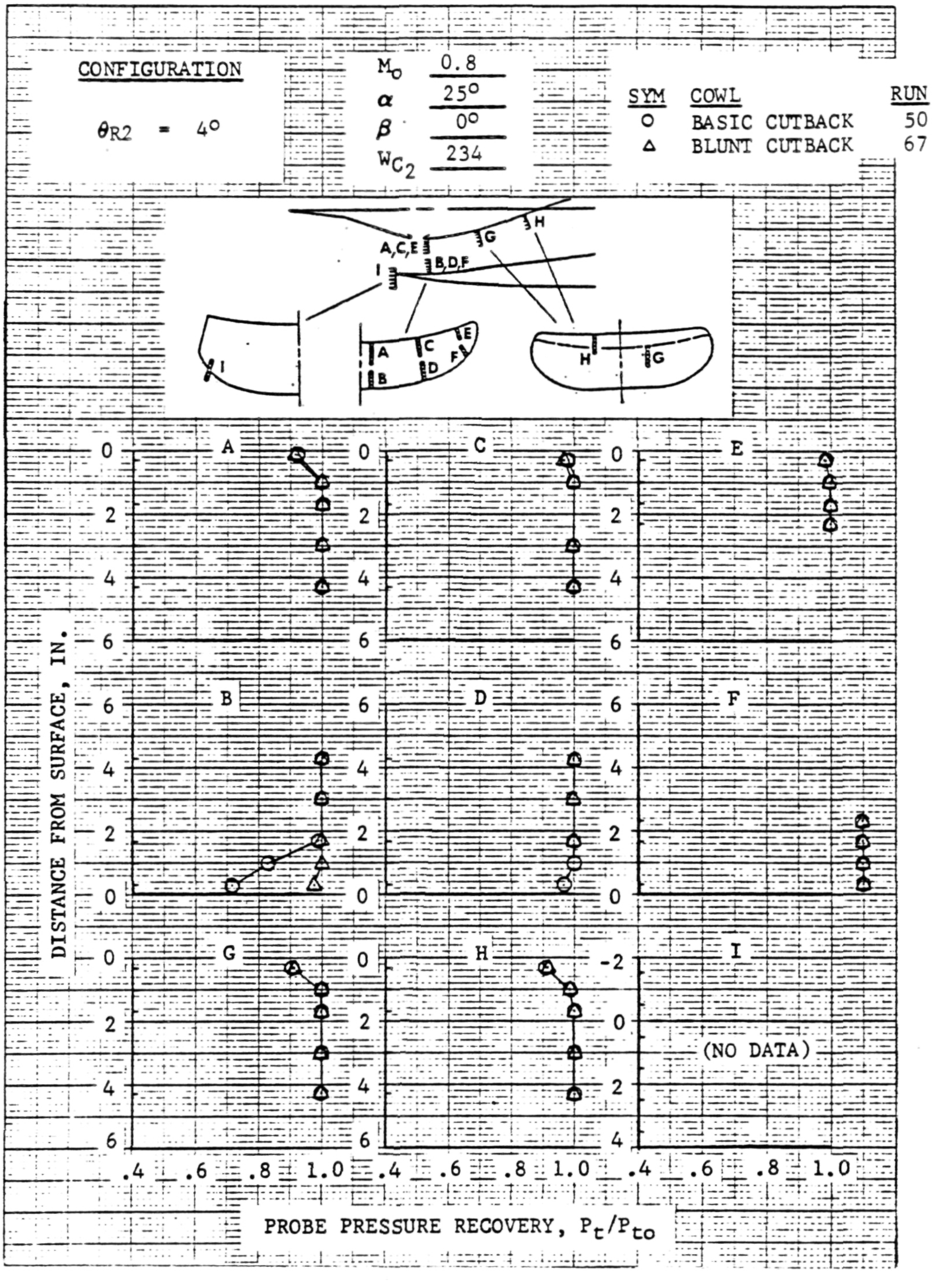

(c) $\alpha = 25^\circ$

Figure 7-47 (Cont'd)

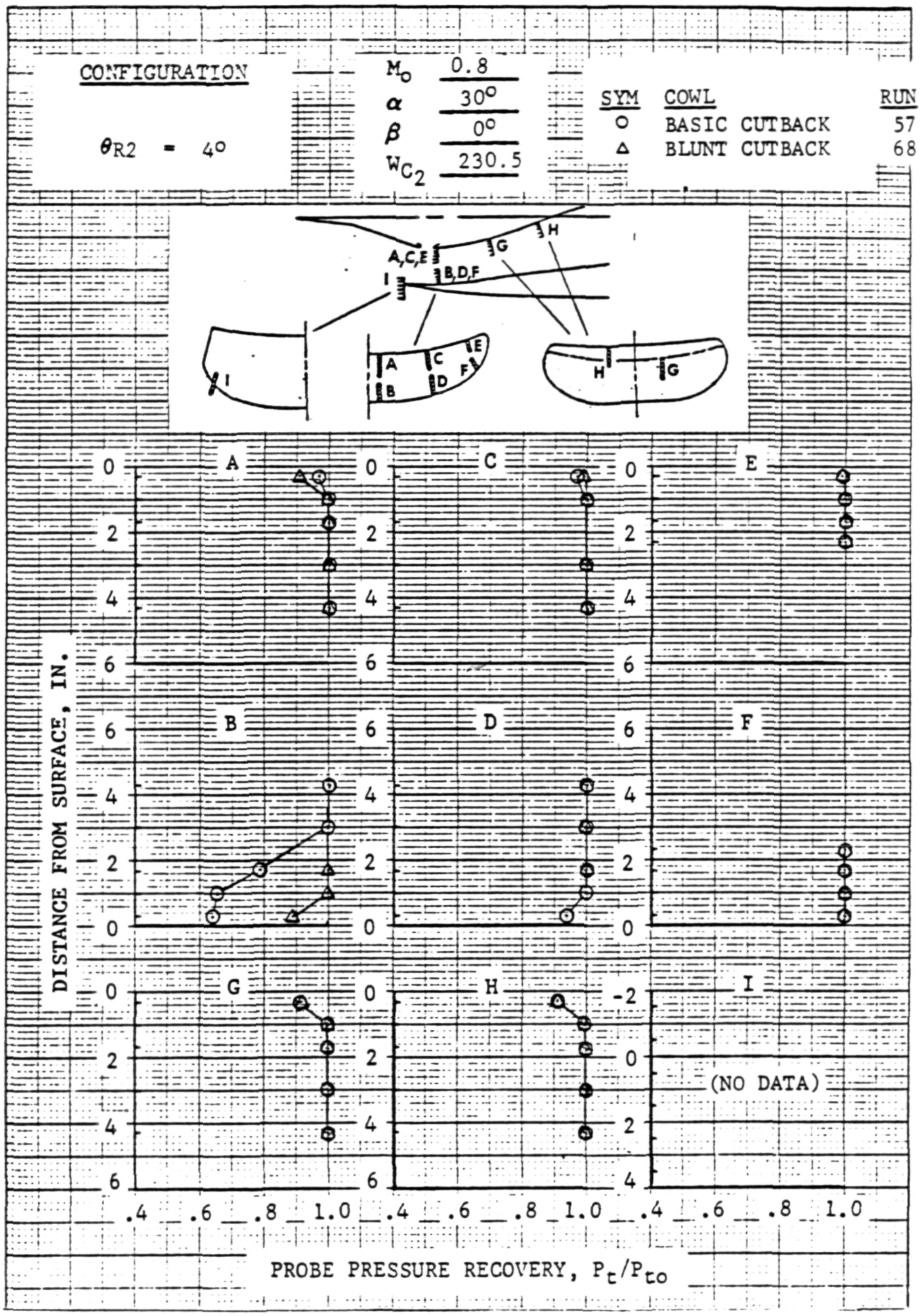

(d) $\alpha = 30^{\circ}$

Figure 7-47 (Concl)

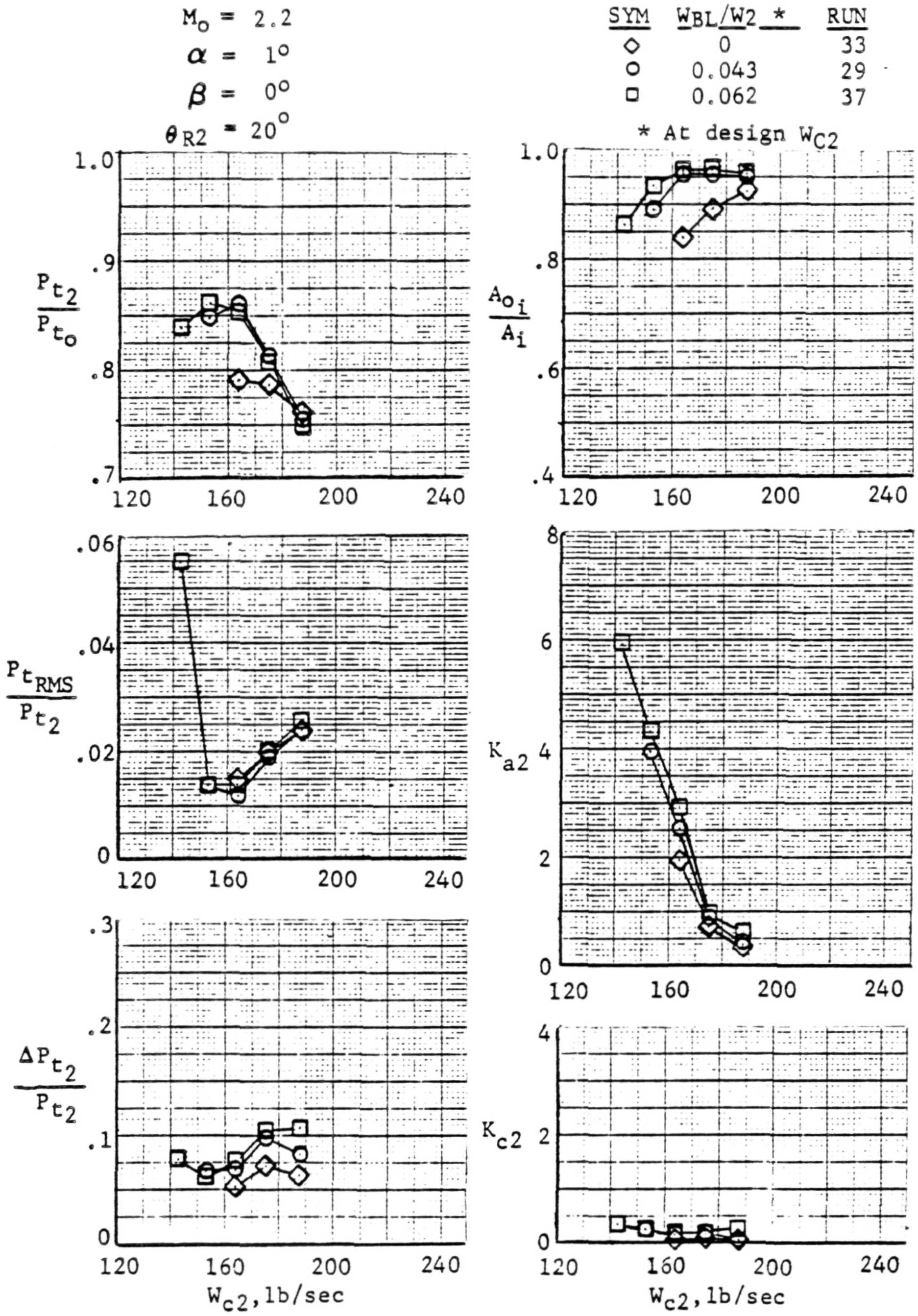

Figure 7-48 Effect of Throat Bleed on Inlet Performance

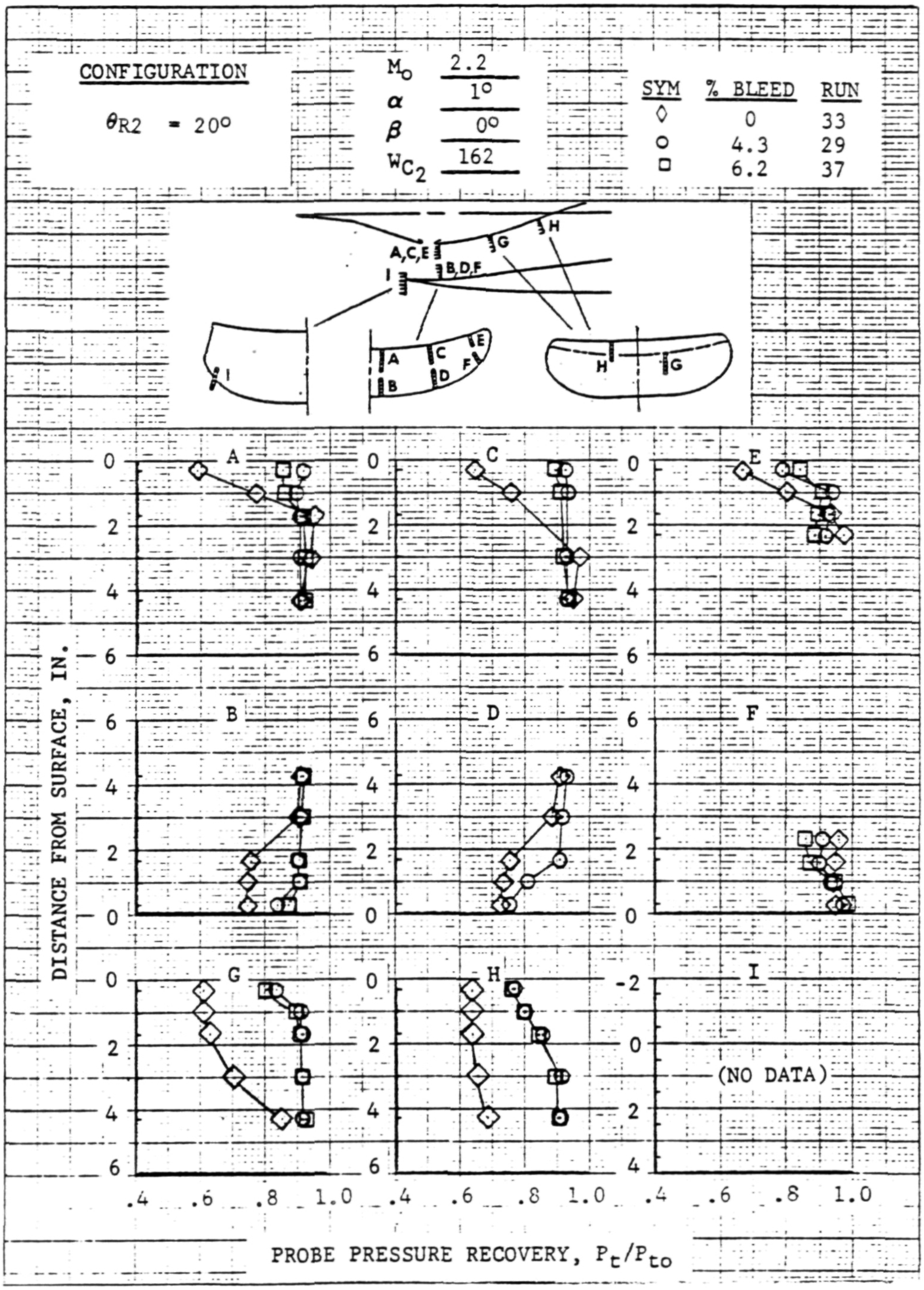

Figure 7-49 Effect of Throat Bleed on Throat Total Pressures

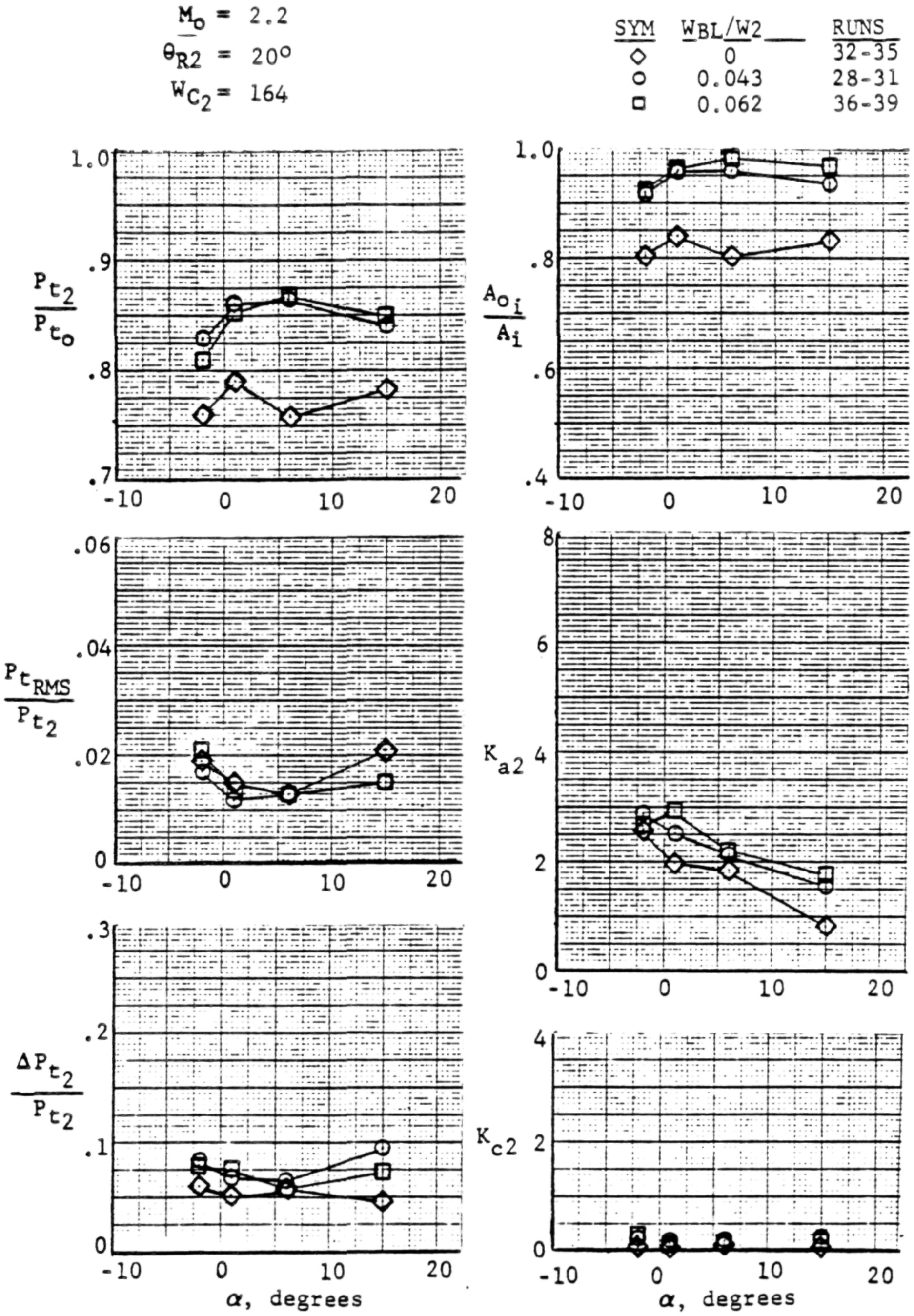

Figure 7-50 Effect of Throat Bleed at Angle of Attack

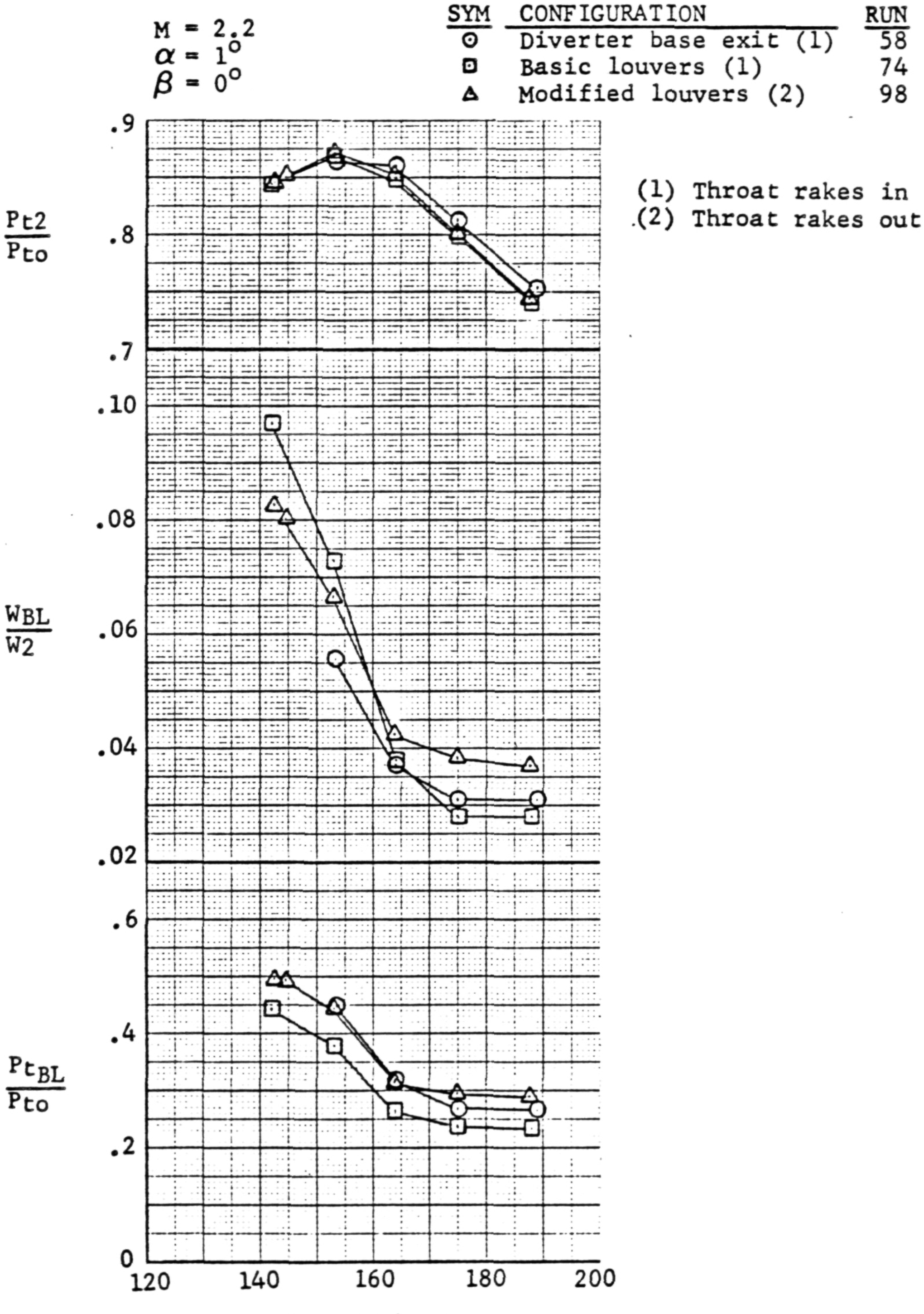

Figure 7-51 Effect of Engine Airflow on Bleed System Performance

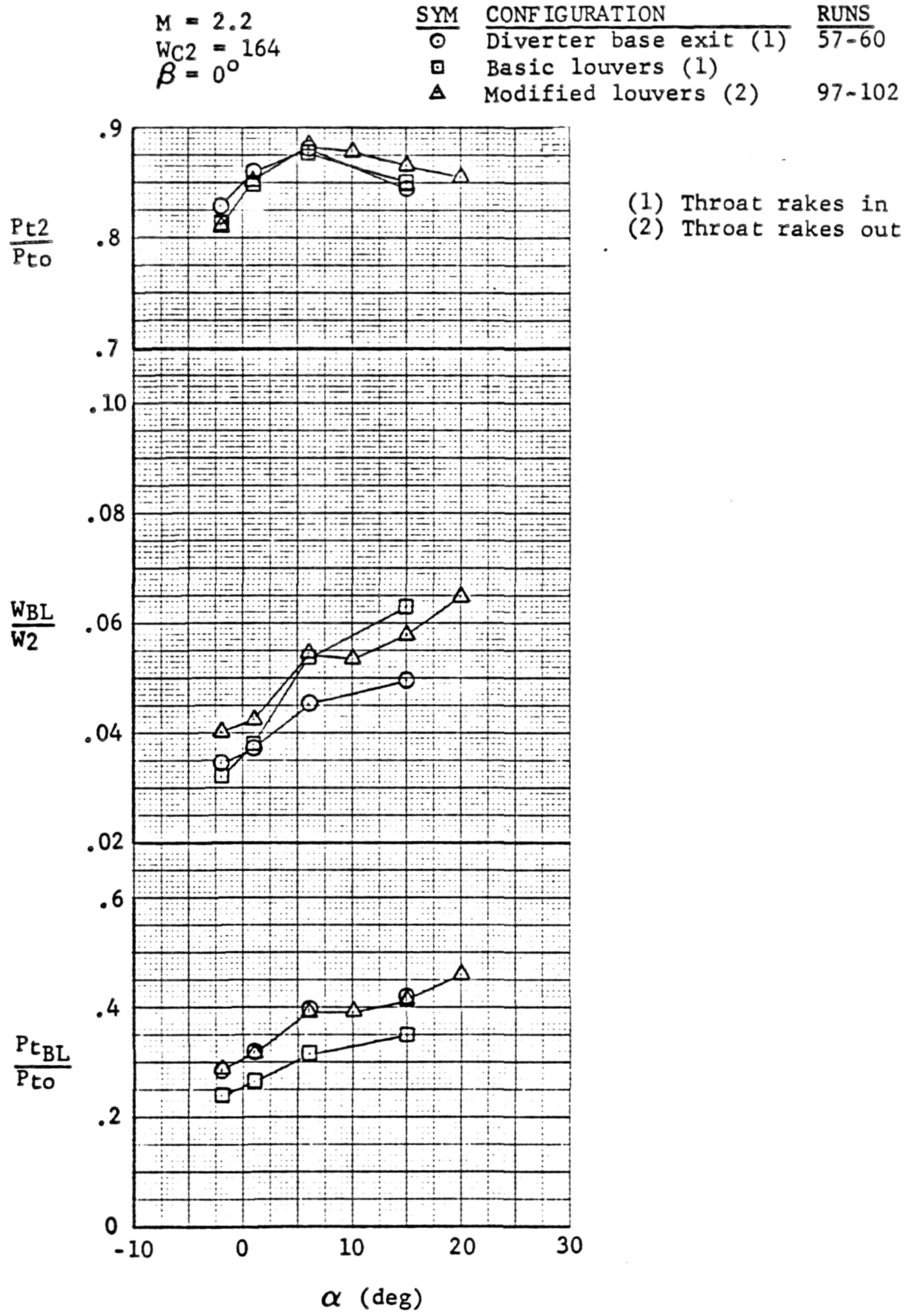

(a) β = 0°

Figure 7-52 Effect of Angle of Attack on Bleed System Performance

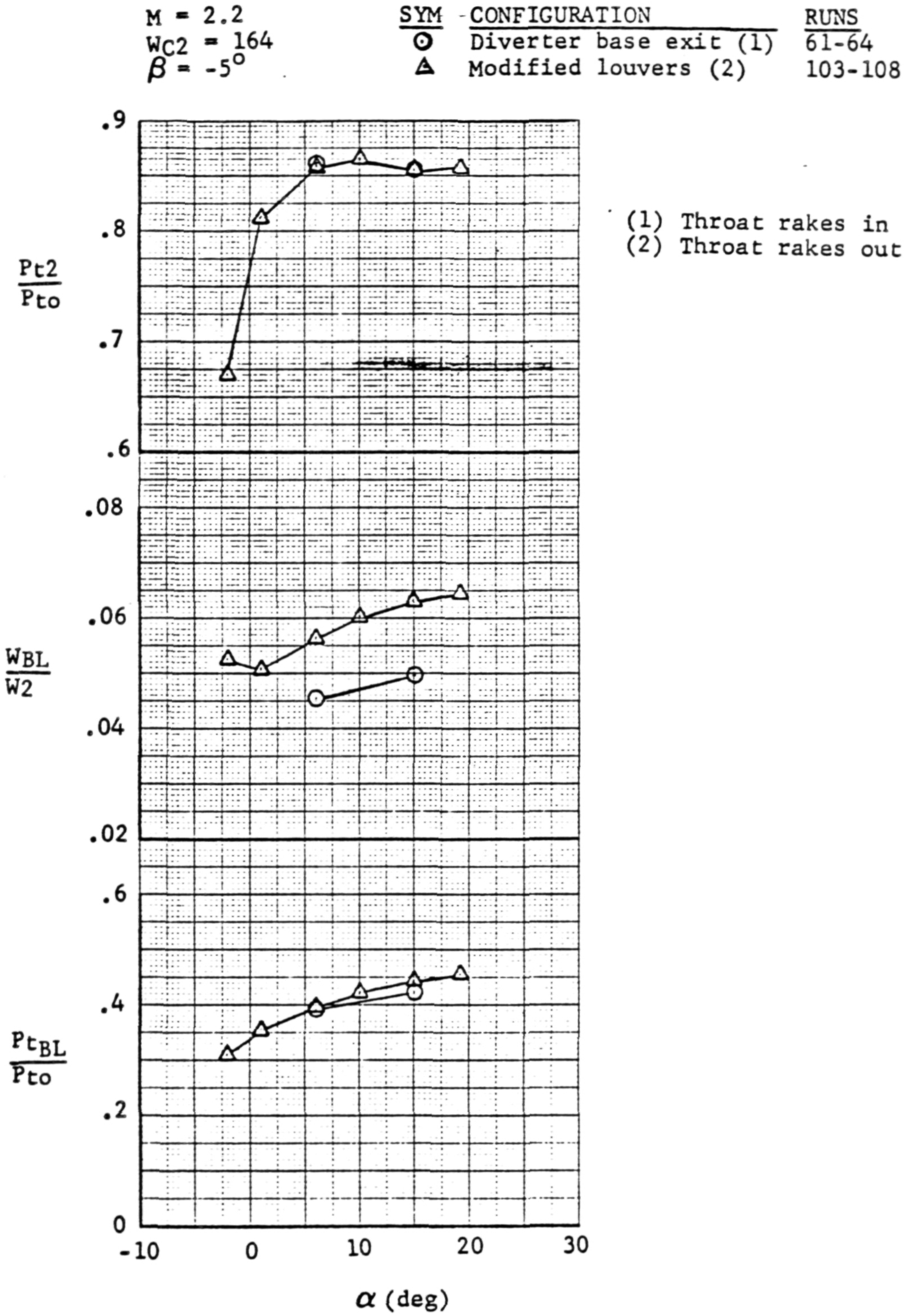

(b) β = -5°

Figure 7-52 (Concl)

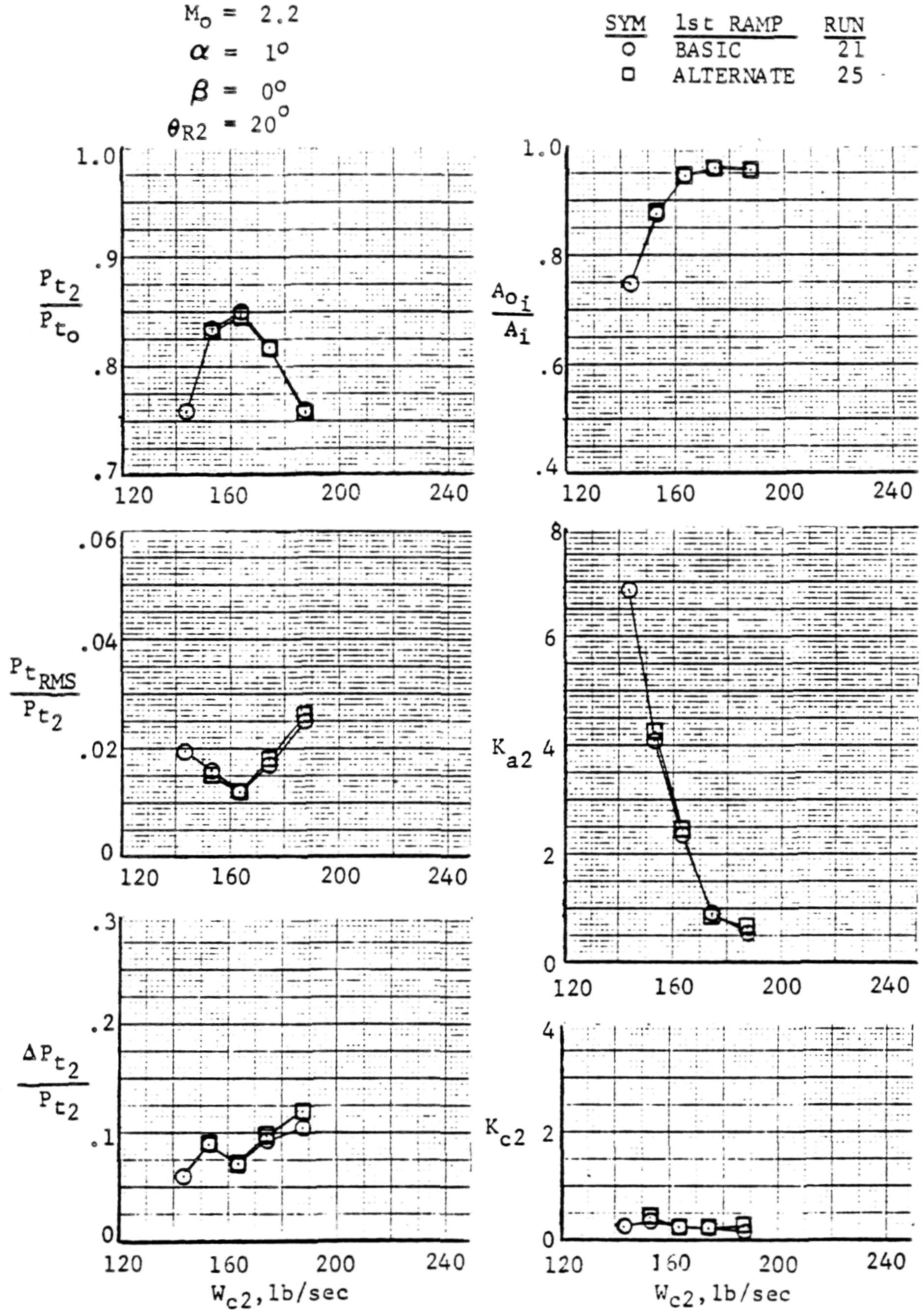

Figure 7-53 Effect of Alternate First Ramp on Inlet Performance

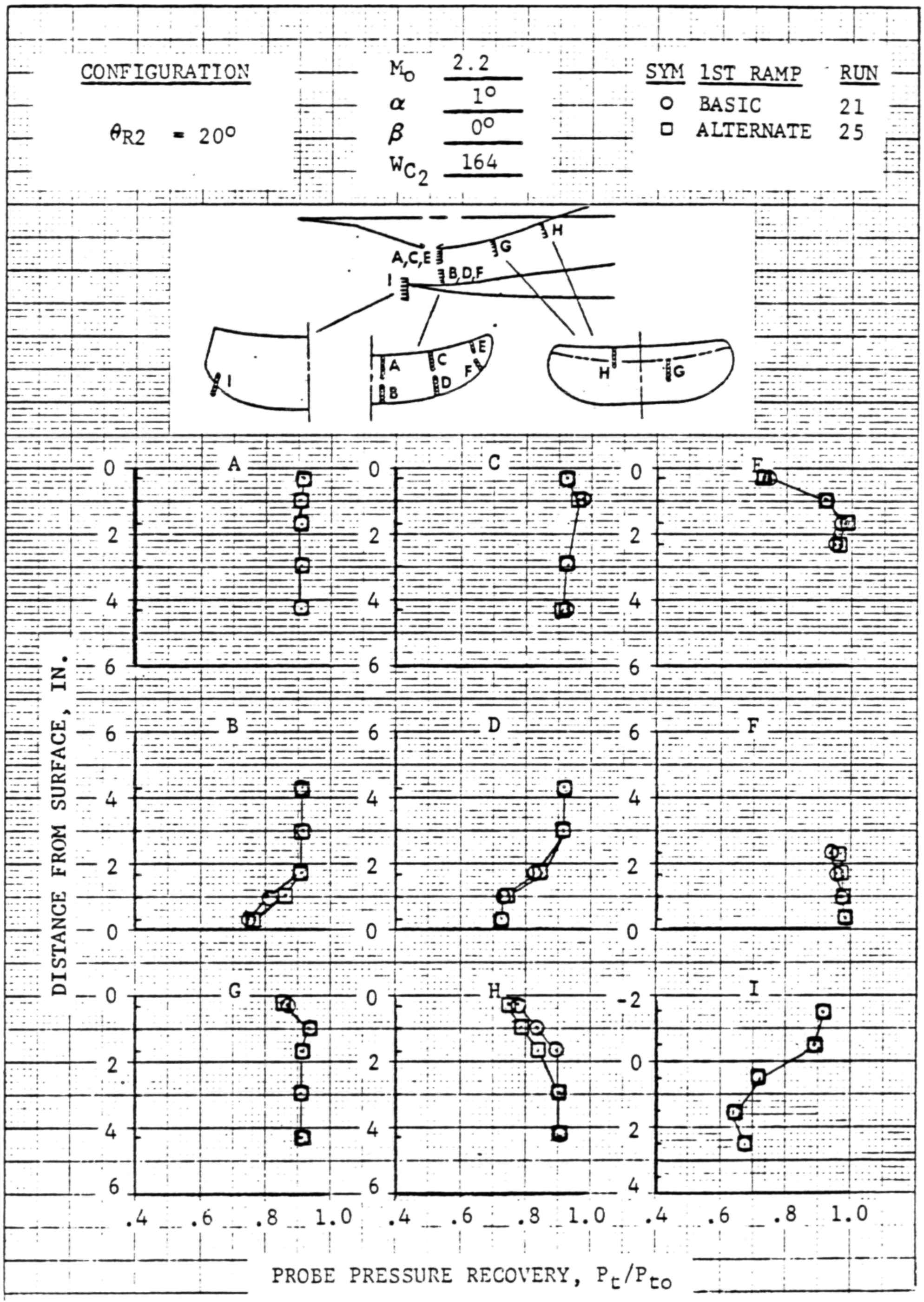

Figure 7-54 Effect of Alternate First Ramp on Throat Total Pressures

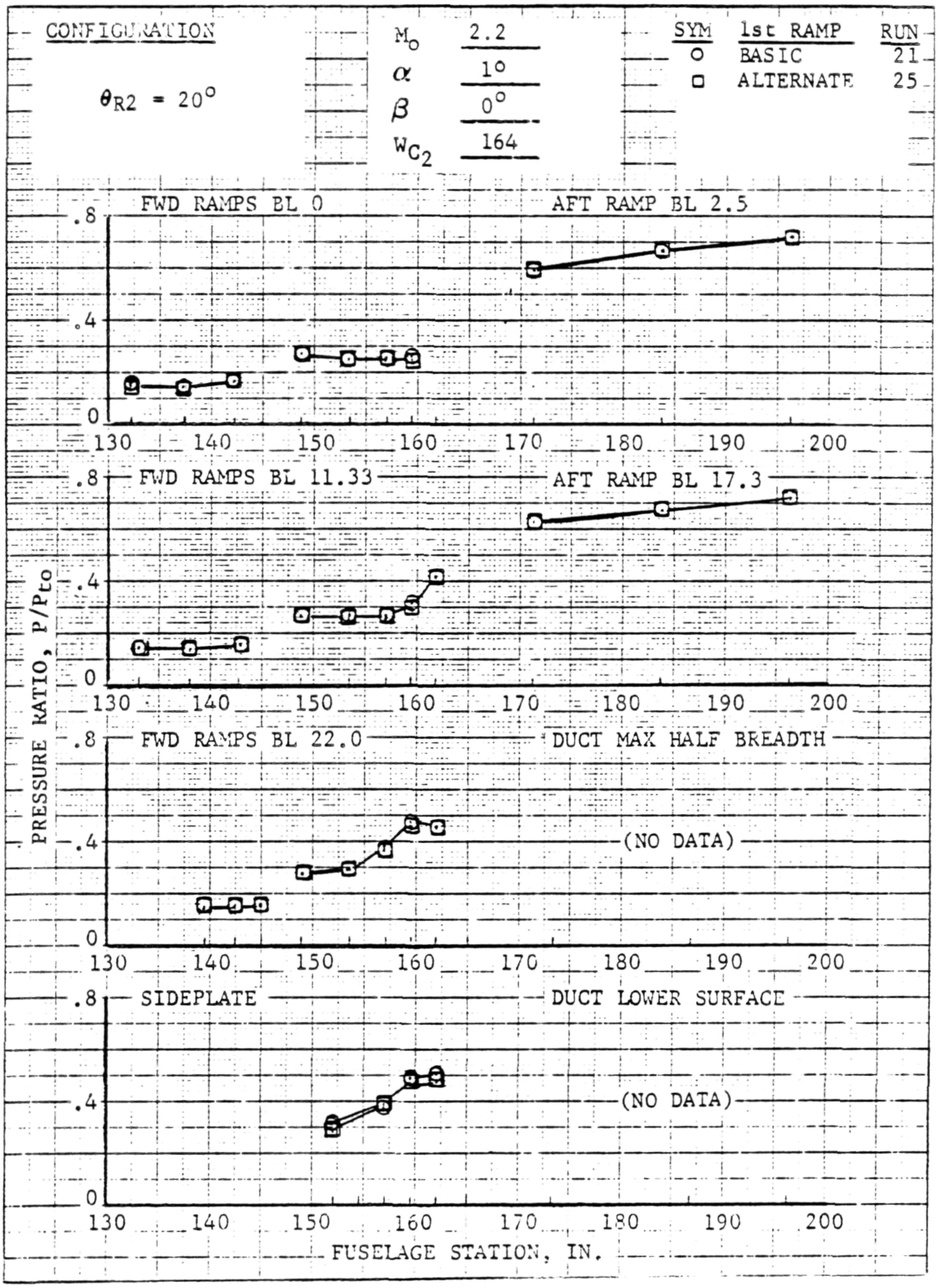

Figure 7-55 Effect of Alternate First Ramp on Ramp Static Pressures

APPENDIX A

AS-RUN TEST PROGRAM

AS-RUN TEST PROGRAM

NASA AMES TEST 260-1-66

RUNS	1ST RAMP	COWL	BLEED	INST.* CODE	θ_{R_2} (DEG)	M_o	α (DEG)	β (DEG)	W_{C_2}
1-3	Inlet and duct removed			A	-	1.6	-2,1,6,10,20	0,±5	-
4-7	↓	↓	↓	↓	-	2.0	↓	↓	-
8-10	↓	↓	↓	↓	-	2.2	↓	↓	-
11-15	Basic	Basic	2½%	B	18.8	↓	-2,1,6,15	0	A
16-19	↓	↓	↓	↓	18	↓	↓	↓	↓
20-23	↓	↓	↓	↓	20	↓	↓	↓	↓
24-27	Alternate	↓	↓	↓	↓	↓	↓	↓	↓
28-31	Basic	Basic Cutback	↓	B Minus Lip Rake	↓	↓	↓	↓	↓
32-35	↓	↓	0	↓	↓	↓	↓	↓	↓
36-39	↓	↓	5%	↓	↓	↓	↓	↓	↓
40-43	↓	Blunt Lip	2½%	↓	↓	↓	↓	↓	↓
44-47	↓	↓	↓	↓	↓	↓	↓	-5	↓
48-52	↓	Basic Cutback	0	↓	4	0.8	1,20,25,30 25	0 -10	F
53-56	↓	↓	2½%	↓	16	2.0	-2,1,6,15	0	B
57-64	↓	Blunt Cutback	↓	↓	20	2.2	↓	0,-5	A
65-69	↓	↓	0	↓	4	0.8	1,20,25,30 25	0 -10	F

AS-RUN TEST PROGRAM (Cont'd)

RUN	1ST RAMP	COWL	BLEED	INST. * CODE	θ_{R_2} (DEG)	M_o	α (DEG)	β (DEG)	W_{C_2}
70-77	Basic	Blunt Cutback	2½%	B Minus Lip Rake	17	2.0	-2,1,6,15	0,-5	B
78-81	↓	↓	↓	↓	10	1.6	↓	0	C
84-87	↓	↓	↓	↓	12	↓	↓	↓	↓
88-91	↓	↓	↓	↓	↓	↓		-5	↓
92	↓	↓	↓	↓	↓	↓	1°	0°	↓
93-96	↓	↓	2½% Louver Exits	B	20	2.2	-2,1,6,15	0	A
97-109	↓	↓	Modified Louvers	C	↓	↓	-2,1,6,10,15 20	0,-5	A+S
110-115	↓	↓	↓	↓	18.8	↓	↓	0	↓
116-121	↓	↓	↓	↓	↓	2.0	↓	0	B+S
122-129	↓	↓	↓	↓	4	0.8	-10,-5,1,6,15, 20,25,30	0	D
130-135	↓	↓	↓	↓	↓	↓	-10,-5,1,15, 25,30	-5	↓
136-139	↓	↓	↓	↓	↓	↓	-5,1,15,25	-10	↓
140-142	↓	↓	↓	↓	↓	0.6	-10,1,15,20, 25,30	0	MAX
	↓	↓	↓	↓	↓		-5,1,15,25	-5,-10	↓
143-155	↓	↓	↓	↓	↓	1.3	-5,1,6,15, 20,25	0	E
							-5,1,6,15	-5	↓
							1,6	-10	↓

AS-RUN TEST PROGRAM (Cont'd)

RUN	1ST RAMP	COWL	BLEED	INST.* CODE	θ_{R_2} (DEG)	M_o	α (DEG)	β (DEG)	W_{C_2}
156-158	Basic	Blunt Cutback	Modified Louvers	C	6	1.3	1,6,15	0	E
159-161	↓	↓	↓	↓	↓	0.8	1,20,30	0	D
162-164					8	1.3	1,6,15	0	E
165-170					10	1.6	-2,1,6,10,15,20	0	C+S
171-182					12	↓	↓	0,-5	↓
183-188					14			0	
189-194					16	2.0		0	B+S
195-206					17	↓		0,-5	↓
207					↓	1.6	1^{o}	0	C+S
208					20	2.0	1^{o}	0	B+S

<u>NOTE</u>: Runs 82 and 83 were no good.

W_{C_2} Schedules (Nominal Settings)

A	186, 173, 162, 151, 139
B	204, 189, 177, 163, 152
C	243, 226, 211, 195, 165
D	246, 234, 226, 206, 140
E	242, 226, 202, 140
F	246, 234, 226
S	Denotes stability limit

*Instrumentation codes are defined in Figure 5-10.

APPENDIX B

WORST-CASE DISTORTION PATTERNS USED FOR COMPREHENSIVE STABILITY AUDIT

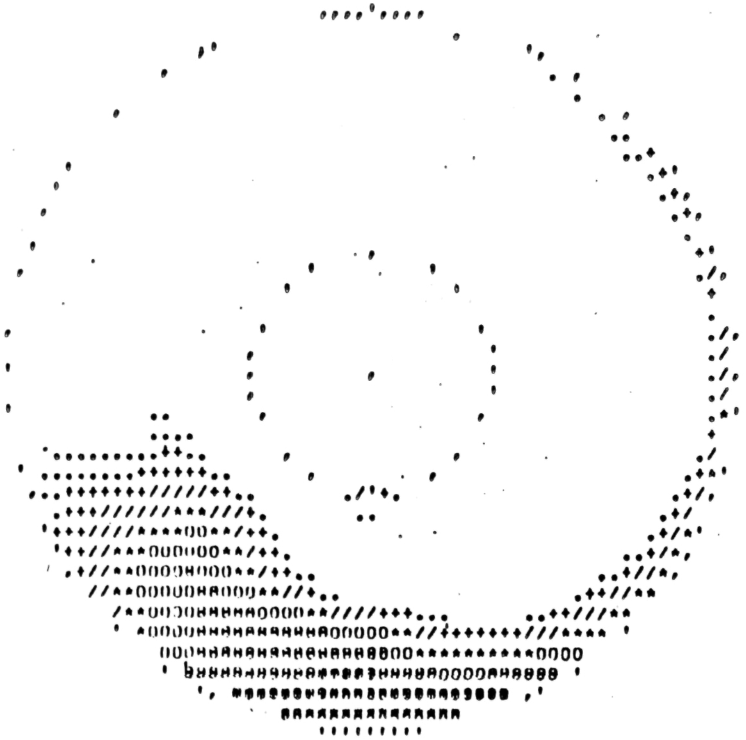

```
                    COMPRESSOR FACE TOTAL PRESSURE PROBE RECOVERIES

                                   RAKE  (DEG)

RING      0.      45.      90.     135.     180.     225.     270.     315.

.445  1.001   1.001   1.002   1.002     .963     .954     .971   1.000

.614  1.005    .998   1.001    .993     .960     .912     .961    .999

.745  1.002    .946    .991   1.002     .896     .900     .982   1.003

.856   .994    .953    .987    .940     .884     .906     .970    .998

.955   .961    .947    .934    .917     .857     .917     .968    .966


IDC1    IDC2    IDC3    IDC4    IDC5    IDCI    IDCO    IDC
.034    .069    .072    .073    .080    .051    .076    .076

IDR1    IDR2    IDR3    IDR4    IDR5    IDR
-.024   -.015   -.002   .010    .031    .031

KTHE  KRA2(3) KA2(3) KRA2(3T) KA2(3T) B1     B2      QAV    PAV
 .217   .289   .630    .113     .330  1.427  1.000   .886  5.515


             RING AVERAGES
RING1   RING2   RING3   RING4   RING5                    FACE AVERAGE
 .987    .979    .965    .954    .933                        .964


PART-POINT= 122.500          PEAK DISTORTION MAP             TIME=35  22   13


        M       8       8       8       0       *       /       +       .      BLANK
           .870    .880    .890    .900    .910    .920    .930    .940    .950
```

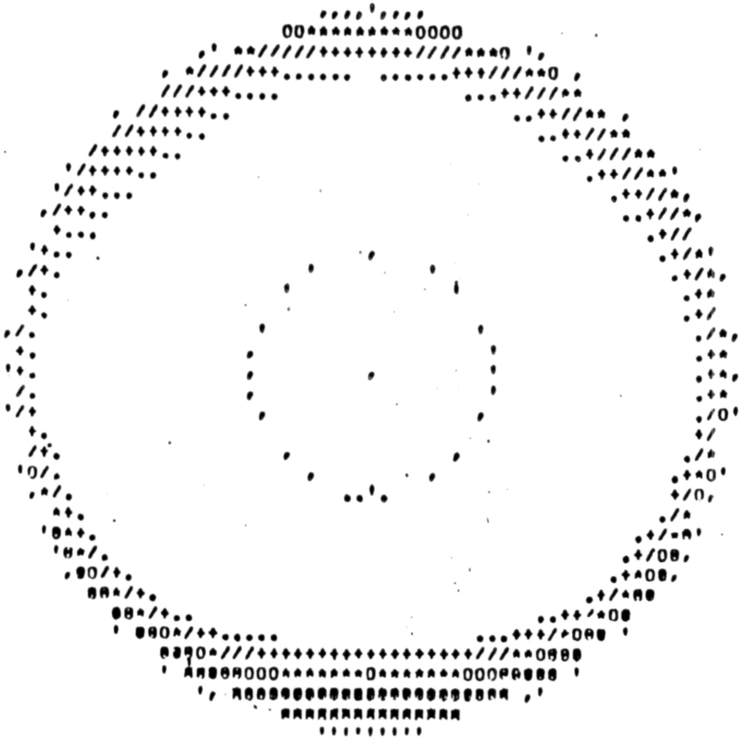

```
COMPRESSOR FACE TOTAL PRESSURE PROBE RECOVERIES

                       RAKE  (DEG)

RING      0.     45.     90.    135.    180.    225.    270.    315.

.445    .997   1.004   1.006   1.004   1.002   1.006   1.005   1.008

.614   1.002   1.003   1.009   1.003   1.006   1.009   1.007   1.002

.745   1.002   1.008   1.003   1.010    .987   1.005   1.003   1.003

.856    .985    .974   1.002    .985    .939    .988   1.006    .978

.955    .947    .955    .963    .935    .890    .929    .978    .969


IDC1    IDC2    IDC3    IDC4    IDC5    IDCI    IDCO    IDC
.007    .003    .016    .044    .056    .005    .050    .050

IDR1    IDR2    IDR3    IDR4    IDR5    IDR
-.016   -.017   -.015    .006    .042    .042

KTHE  KRA2(3) KA2(3) KRA2(3T) KA2(3T) B1      B2      QAV     PAV
 .040    .286    .524     .105      .144 1.692  1.000    .893  5.564


        RING AVERAGES
RING1  RING2  RING3  RING4  RING5              FACE AVERAGE
1.004  1.005  1.003   .982   .946                   .988
```

```
PART-POINT= 124.300          PEAK DISTORTION MAP                 TIME=26  38  196


           M       8       8       8       0       *       /       +       .      BLANK
             .910    .920    .930    .940    .950    .960    .970    .980    .990
```

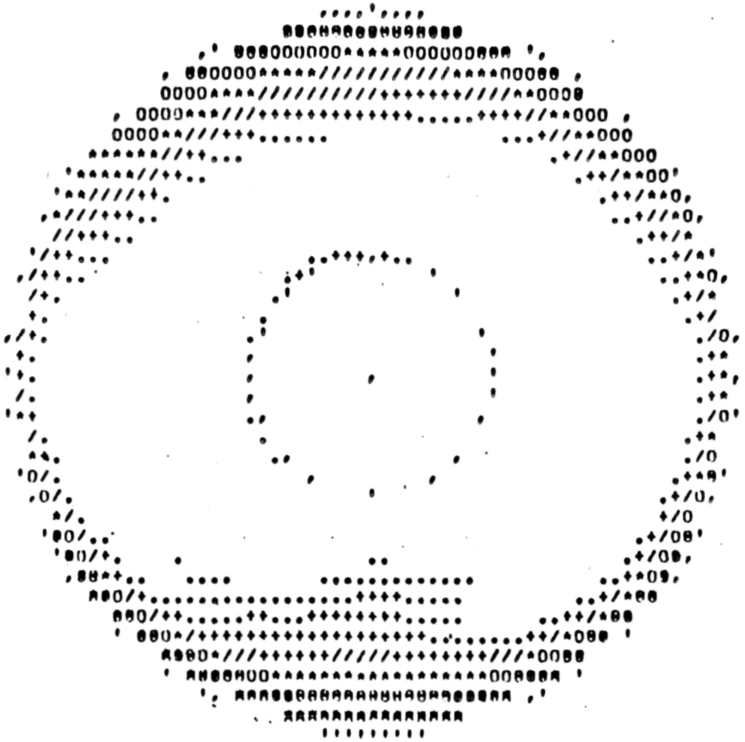

```
COMPRESSOR FACE TOTAL PRESSURE PROBE RECOVERIES

                     RAKE  (DEG)

RING     0.     45.     90.    135.    180.    225.    270.    315.

.445   .999  1.000   1.000   1.002    .986    .994    .991    .995

.614  1.002  1.002   1.004    .987    .967    .996   1.000   1.002

.745   .959   .999    .998   1.000    .958    .977    .994    .977

.856   .949   .953    .993    .973    .937    .972    .999    .945

.955   .917   .934    .951    .922    .884    .911    .969    .937


IDC1   IDC2   IDC3    IDC4    IDC5    IDCI    IDCO    IDC
.010   .029   .026    .029    .045    .019    .037    .037

IDR1   IDR2   IDR3    IDR4    IDR5    IDR
-.023  -.022  -.010   .008    .046    .046

KTHE  KRA2(3) KA2(3) KRA2(3T) KA2(3T) B1      B2       QAV     PAV
 .056   .265   .504     .131     .187 1.692  1.000    .901  5.638


         RING AVERAGES
RING1  RING2  RING3  RING4  RING5                  FACE AVERAGE
 .996   .995   .983   .965   .928                      .973
```

```
PART-POINT= 129,300          PEAK DISTORTION MAP                TIME=30  48  320


           R        8        B        8        O        *        /        +        .        BLANK
              .900     .910     .920     .930     .940     .950     .960     .970     .980
```

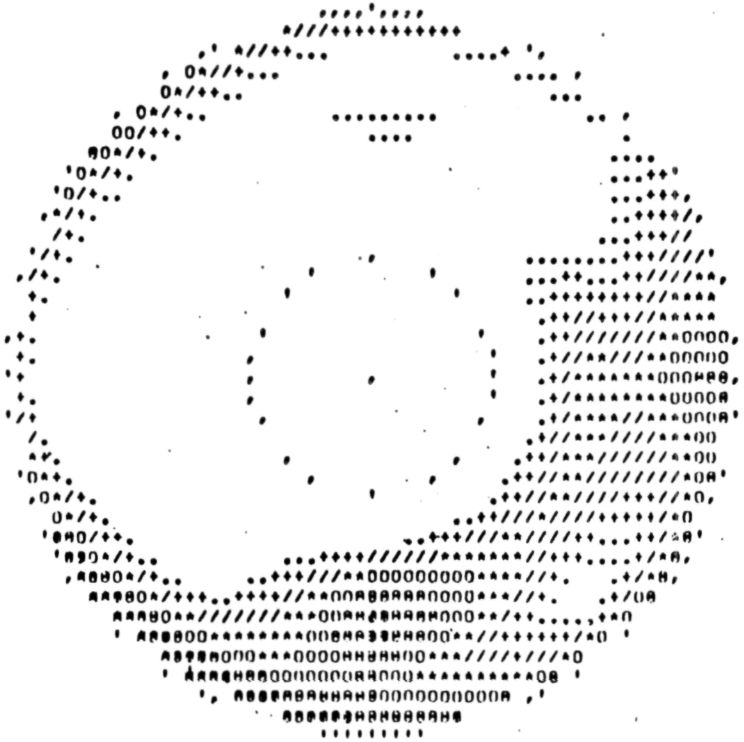

```
COMPRESSOR FACE TOTAL PRESSURE PROBE RECOVERIES

                    RAKE  (DEG)

RING      0.      45.      90.     135.     180.     225.     270.     315.

.445    .994     .989     .984     .982     .982    1.007    1.003    1.002

.614    .990     .985     .942     .950     .922    1.006    1.004    1.000

.745    .973     .993     .946     .967     .916     .986     .999    1.008

.856    .990     .986     .932     .985     .929     .943    1.004     .973

.955    .963     .980     .929     .940     .921     .887     .975     .935


IDC1    IDC2     IDC3     IDC4     IDC5     IDCI     IDCO     IDC
.011    .054     .059     .040     .056     .033     .048     .048

IDR1    IDR2     IDR3     IDR4     IDR5     IDR
-.023   -.005    -.004     .002     .030     .030

KTHE   KRA2(3) KA2(3) KRA2(3T) KA2(3T) B1       B2       QAV      PAV
 .159    .303    .797     .101       .260  2.108    1.000     .844   5.564


          RING AVERAGES
RING1   RING2    RING3    RING4    RING5                 FACE AVERAGE
.993    .975     .974     .968     .941                       .970


PART-POINT= 136.300          PEAK DISTORTION MAP                 TIME=36  36  861


             M        B        $        8        0        *        /        +        .        BLANK
                 .900     .910     .920     .930     .940     .950     .960     .970     .980
```

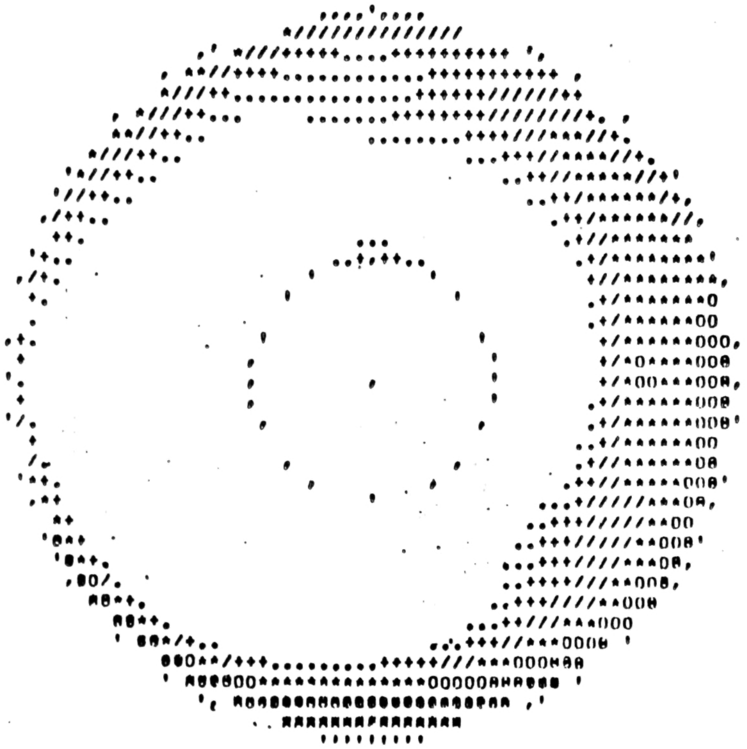

```
COMPRESSOR FACE TOTAL PRESSURE PROBE RECOVERIES

                         RAKE  (DEG)

RING      0.     45.     90.    135.    180.    225.    270.    315.

.445    .988  1.002   1.002   1.003   1.002    .999   1.004   1.003

.618    .998   .994    .977    .972   1.007   1.005   1.002   1.002

.745    .969   .959    .936    .961    .986   1.003   1.001   1.001

.856    .976   .944    .942    .952    .932    .988   1.003    .967

.955    .956   .970    .928    .933    .883    .915    .978    .947


IDC1    IDC2    IDC3    IDC4    IDC5    IDCI    IDCO    IDC
.013    .023    .042    .032    .057    .018    .044    .044

IDR1    IDR2    IDR3    IDR4    IDR5    IDR
-.026   -.020   -.003    .012    .037    .037

KTHE  KRA2(3) KA2(3) KRA2(3T) KA2(3T) B1      B2      DAV    PAV
 .117   .273    .694     .136     .253  2.115  1.000   .859  5.559


        RING AVERAGES
RING1  RING2  RING3  RING4  RING5                 FACE AVERAGE
1.000   .994   .977   .963   .939                      .975


PART-POINT= 137.300          PEAK DISTORTION MAP                 TIME=44  52  129


         M        @        B        8        0        *        /        +        .       BLANK
            .900     .910     .920     .930     .940     .950     .960     .970     .980
```

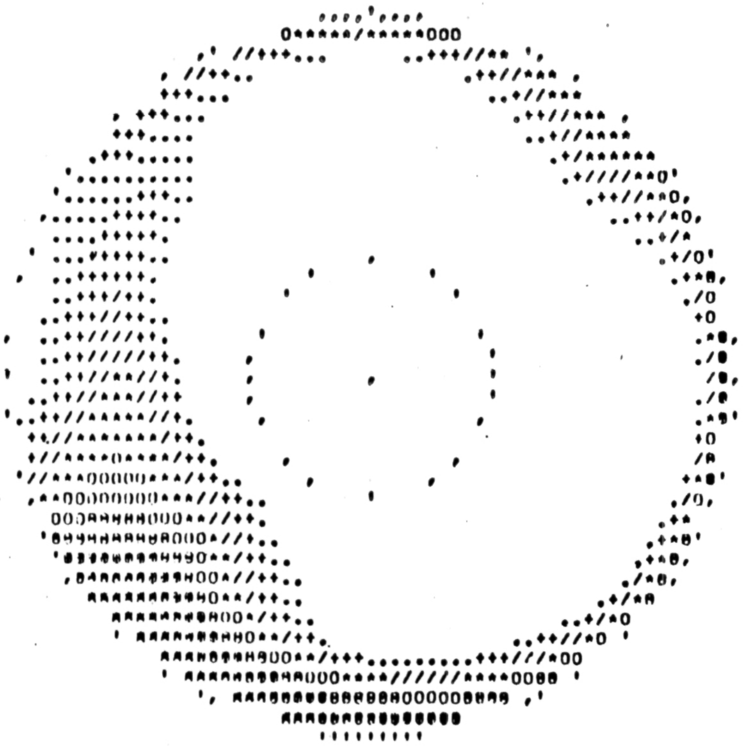

```
COMPRESSOR FACE TOTAL PRESSURE PROBE RECOVERIES

                         RAKE  (DEG)

RING      0.     45.     90.    135.    180.    225.    270.    315.

.445    .987    .994    .993    .997    .976    .948    .978    .989

.614    .990    .992    .996    .981    .973    .914    .924    .982

.745    .995    .951   1.000    .987    .959    .889    .922    .941

.856    .973    .918    .980    .954    .908    .872    .941    .941

.955    .912    .915    .900    .913    .876    .855    .962    .937


IDC1    IDC2    IDC3    IDC4    IDC5    IDCI    IDCO    IDC
.037    .058    .070    .067    .057    .047    .062    .062

IDR1    IDR2    IDR3    IDR4    IDR5    IDR
-.034   -.020   -.005    .015    .044    .044

KTHE   KRA2(3) KA2(3) KRA2(3T) KA2(3T) B1      B2      QAV     PAV
 .183    .248    .603    .162      .344  1.692  1.000    .770  4.929


        RING AVERAGES
RING1   RING2   RING3   RING4   RING5               FACE AVERAGE
 .983    .969    .956    .936    .909                   .950
```

```
PART-POINT= 143,400          PEAK DISTORTION MAP                TIME=49  10  467


       M       @       @       B       0       *       /       +       .     BLANK
          .870    .880    .890    .900    .910    .920    .930    .940    .950
```

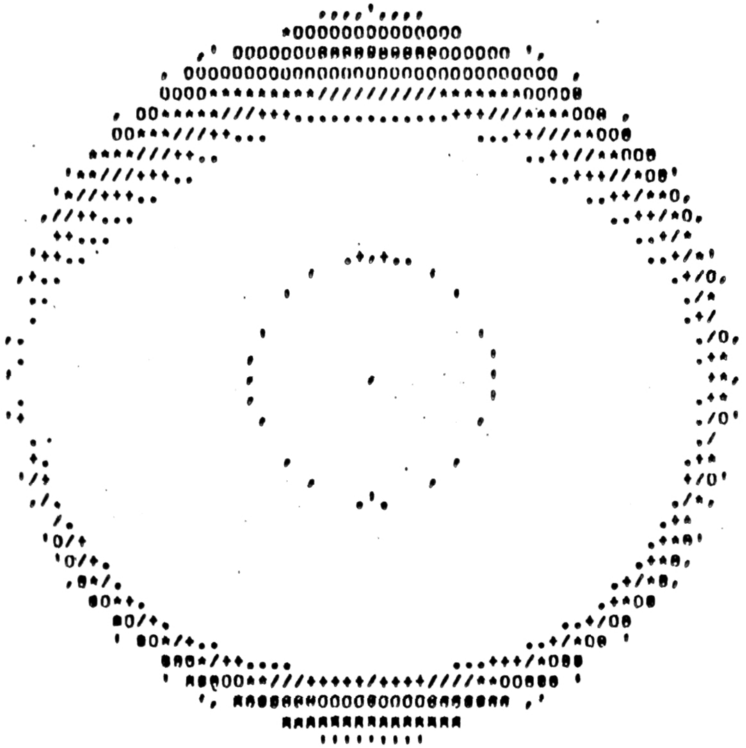

```
                         COMPRESSOR FACE TOTAL PRESSURE PROBE RECOVERIES

                                         RAKE  (DEG)

         RING       0.      45.      90.     135.     180.     225.     270.     315.

         .445     .995   1.000     .999     .999     .996    1.004    1.007    1.006

         .614    1.001    .999    1.003     .995    1.004    1.004    1.006     .997

         .745     .969    .980    1.006    1.006     .990    1.003    1.002     .981

         .856     .927    .954     .997     .982     .948     .985    1.007     .954

         .955     .936    .930     .954     .933     .883     .927     .985     .938


         IDC1     IDC2     IDC3     IDC4     IDC5     IDCI     IDCO     IDC
         .006     .006     .023     .043     .054     .006     .049     .049

         IDR1     IDR2     IDR3     IDR4     IDR5     IDR
        -.021    -.022    -.013     .011     .045     .045

         KTHE   KRA2(3) KA2(3) KRA2(3T) KA2(3T) B1       B2       QAV      PAV
          .059    .263    .615     .132       .191  2.115   1.000     .768   4.958


                     RING AVERAGES
        RING1   RING2   RING3   RING4   RING5                   FACE AVERAGE
        1.001   1.001    .992    .969    .936                       .980


PART-POINT= 144.200          PEAK DISTORTION MAP               TIME=58  36  784


                 M        @        B        8        O        *        /        +        .        BLANK
                     .900     .910     .920     .930     .940     .950     .960     .970     .980
```

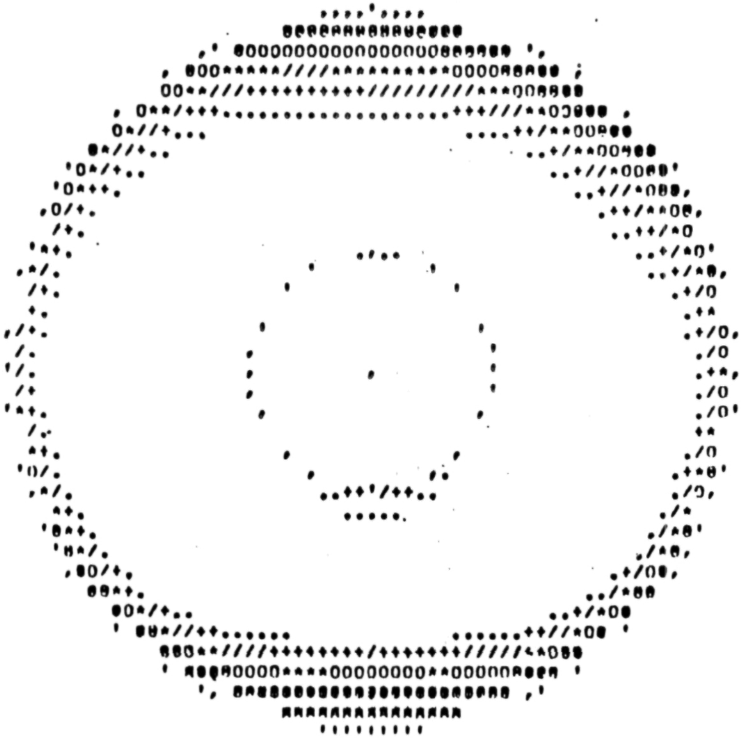

```
                    COMPRESSOR FACE TOTAL PRESSURE PROBE RECOVERIES

                                      RAKE  (DEG)

RING      0.      45.      90.     135.     180.     225.     270.     315.

.445   1.001   1.005   1.010   1.001     .996   1.007   1.010   1.011

.614   1.003   1.001   1.003   1.007   1.007   1.007   1.008   1.001

.745    .978    .991   1.002   1.006     .986   1.003   1.006   1.007

.856    .951    .952   1.001    .990     .933    .993   1.005    .984

.955    .932    .925    .960    .935     .899    .931    .974    .947


IDC1     IDC2     IDC3     IDC4     IDC5     IDCI     IDCO     IDC
.009     .004     .020     .043     .040     .006     .042     .042

IDR1     IDR2     IDR3     IDR4     IDR5     IDR
-.021    -.021    -.013     .008     .047     .047

 KTHE  KRA2(3) KA2(3) KRA2(3T) KA2(3T) B1       B2       QAV      PAV
  .035    .265    .596     .131       .166  2.115  1.000     .772  4.975


          RING AVERAGES
RING1   RING2   RING3   RING4   RING5                   FACE AVERAGE
1.005   1.005    .997    .976    .938                        .984
```

```
PART-POINT= 148.200          PEAK DISTORTION MAP                    TIME=41  48  147


            M          8          B          @          O          *          /          +          .          BLANK
                .910       .920       .930       .940       .950       .960       .970       .980       .990
```

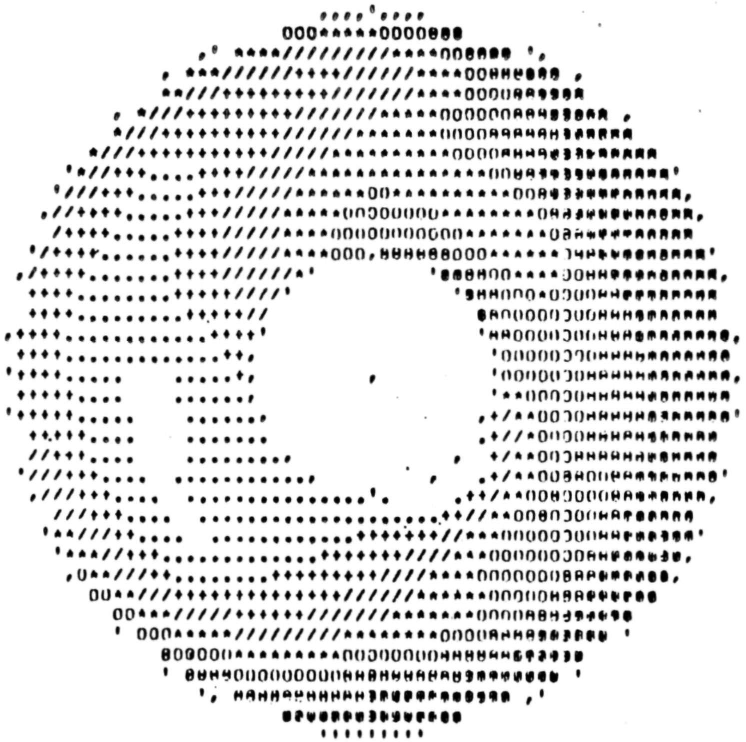

```
            COMPRESSOR FACE TOTAL PRESSURE PROBE RECOVERIES

                           RAKE  (DEG)

RING      0.      45.      90.     135.     180.     225.     270.     315.

.445     .931     .936     .927     .986     .998    1.020    1.010     .967

.614     .951     .948     .917     .918     .973    1.017    1.022     .982

.745     .964     .884     .902     .927     .945    1.012    1.014    1.004

.856     .976     .880     .864     .898     .906     .969     .999     .993

.955     .939     .845     .865     .891     .882     .931     .995     .956


IDC1     IDC2     IDC3     IDC4     IDC5     IDCI     IDCO     IDC
.047     .052     .076     .076     .072     .050     .074     .074

IDR1     IDR2     IDR3     IDR4     IDR5     IDR
-.024    -.018    -.008     .014     .037     .037

KTHE   KRA2(3) KA2(3) KRA2(3T) KA2(3T) B1       B2       QAV      PAV
 .379    .258    .924      .134       .513  2.108    1.000     .738   4.973


           RING AVERAGES
RING1    RING2    RING3    RING4    RING5                  FACE AVERAGE
 .972     .966     .956     .936     .913                       .949
```

```
PART-POINT= 149.200          PEAK DISTORTION MAP                 TIME=50   38   473


           M        H        W        8        O        *        /        +        .        BLANK
              .860     .880     .900     .920     .940     .960     .980    1.000    1.020
```

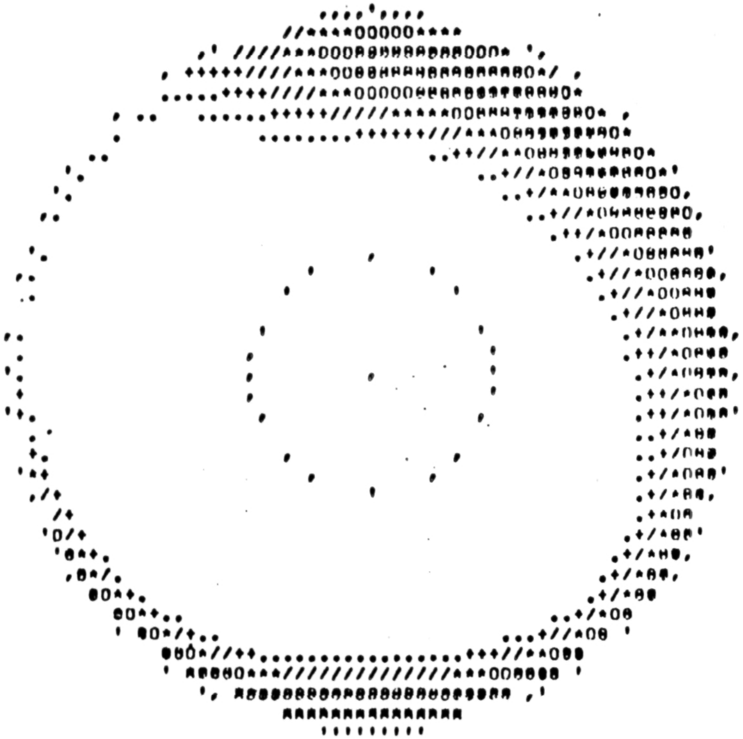

```
                    COMPRESSOR FACE TOTAL PRESSURE PROBE RECOVERIES

                                      RAKE  (DEG)

 RING       0.      45.      90.     135.     180.     225.     270.     315.

 .445     .999   1.004    1.003    1.001    1.001    1.005    1.009    1.010

 .614     .986    .980    1.003    1.002    1.006    1.004    1.006    1.000

 .745     .945    .939     .969    1.005     .993     .999    1.003    1.006

 .856     .924    .913     .943     .975     .940     .985    1.007    1.001

 .955     .940    .942     .908     .928     .884     .925     .979     .979


 IDC1     IDC2    IDC3     IDC4     IDC5     IDC1     IDC0     IDC
 .005     .018    .044     .049     .053     .012     .051     .051

 IDR1     IDR2    IDR3     IDR4     IDR5     IDR
-.028    -.023   -.006     .016     .042     .042

 KTHE   KRA2(3) KA2(3) KRA2(3T) KA2(3T) B1       B2       QAV      PAV
  .126    .241    .634     .154     .280  2.108  1.000     .761   4.973


          RING AVERAGES
RING1   RING2   RING3   RING4   RING5               FACE AVERAGE
1.004    .998    .982    .961    .936                   .976



PART-POINT= 150,200          PEAK DISTORTION MAP               TIME=58  27  100


        M       8       B       0       O       *       /       +       .      BLANK
          .900    .910    .920    .930    .940    .950    .960    .970    .980
```

```
TITLE - F-16 VGI TEST AT NASA/AMES, AUG & SEPT 1977, S-S COMPRESSOR-FACE PRESSURES

                  RAKE 1     RAKE 2     RAKE 3     RAKE 4     RAKE 5     RAKE 6     RAKE 7     RAKE 8

*** STEADY-STATE COMPRESSOR-FACE TOTAL-PRESSURE RATIOS FOR PART =   172 POINT =      3 ***
                       *** TUNNEL TOTAL-PRESSURE =   5.189 PSIA ***
RING 1          0.96290    0.97720    0.97720    0.97600    0.96840    0.97310    0.97290    0.97560
RING 2          0.96600    0.96960    0.97430    0.97930    0.96810    0.97190    0.97550    0.97380
RING 3          0.94540    0.92780    0.97410    0.97610    0.93910    0.97340    0.97580    0.94340
RING 4          0.91430    0.91090    0.96940    0.94930    0.90380    0.94480    0.96910    0.91330
RING 5          0.88970    0.90190    0.91590    0.90000    0.87210    0.90000    0.92240    0.89950
```

$\overline{P}_{t2}/P_{to}$ = .947, $\overline{P}_{trms}/\overline{P}_{t2}$ = .007, W_{C2} = 213 lb_m/sec

K_θ = .0422, K_{RA2} = .1075, b = 1.6571, K_{A2} = .221

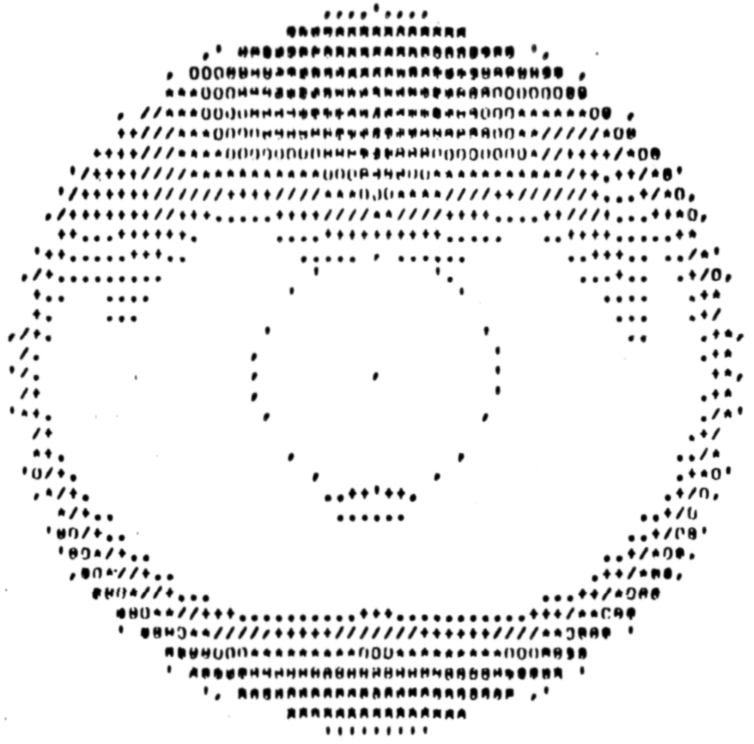

```
                 COMPRESSOR FACE TOTAL PRESSURE PROBE RECOVERIES

                                  RAKE  (DEG)

RING      0.      45.      90.     135.     180.     225.     270.     315.

.445    .936     .976     .980     .982     .972     .980     .982     .980

.614    .902     .966     .983     .978     .971     .982     .983     .969

.745    .892     .942     .975     .981     .937     .981     .979     .941

.856    .882     .957     .981     .952     .904     .950     .985     .947

.955    .878     .923     .946     .907     .872     .908     .953     .951


IDC1    IDC2     IDC3     IDC4     IDC5     IDCI     IDCO     IDC
.039    .068     .065     .066     .048     .054     .057     .057

IDR1    IDR2     IDR3     IDR4     IDR5     IDR
-.023   -.016    -.002    .007     .035     .035

KTHE  KRA2(3) KA2(3) KRA2(3T) KA2(3T) B1  -  B2      QAV    PAV
 .113   .169   .393    .133      .247  1.657 1.000   .708  5.308


           RING AVERAGES
RING1   RING2   RING3   RING4   RING5                  FACE AVERAGE
 .973    .967    .953    .945    .917                       .951
```

```
PART-POINT= 175.300          PEAK DISTORTION MAP                TIME=58  36  312


              M        B        8        @        O        *        /        +        .        BLANK
                  .890     .900     .910     .920     .930     .940     .950     .960     .970
```

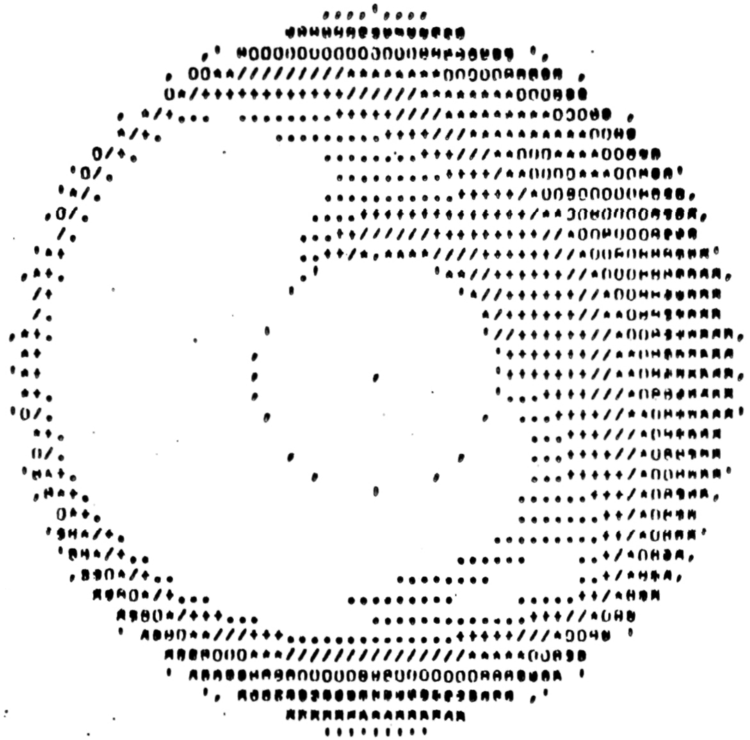

```
                 COMPRESSOR FACE TOTAL PRESSURE PROBE RECOVERIES

                                RAKE  (DEG)

RING      0.     45.     90.    135.    180.    225.    270.    315.

.445    .946    .942    .946    .973    .962    .971    .971    .969

.614    .955    .939    .935    .956    .958    .969    .975    .972

.745    .941    .908    .912    .962    .947    .969    .970    .975

.856    .918    .923    .881    .944    .899    .938    .976    .975

.955    .895    .898    .862    .895    .875    .884    .935    .931


IDC1    IDC2    IDC3    IDC4    IDC5    IDCI    IDCO    IDC
.019    .023    .042    .054    .037    .021    .046    .046

IDR1    IDR2    IDR3    IDR4    IDR5    IDR
-.022   -.020   -.010   .007    .045    .045

KTHE   KRA2(3) KA2(3) KRA2(3T) KA2(3T) B1     B2      QAV    PAV
 .169    .145    .409     .144      .314  1.657  1.000    .702  5.292


            RING AVERAGES
RING1   RING2   RING3   RING4   RING5                FACE AVERAGE
 .960    .957    .948    .932    .897                    .939
```

```
PART-POINT= 178.300          PEAK DISTORTION MAP                TIME=26  22  123


            M         B         8         0         O         *         /         +         .         BLANK
               .880      .890      .900      .910      .920      .930      .940      .950      .960
```

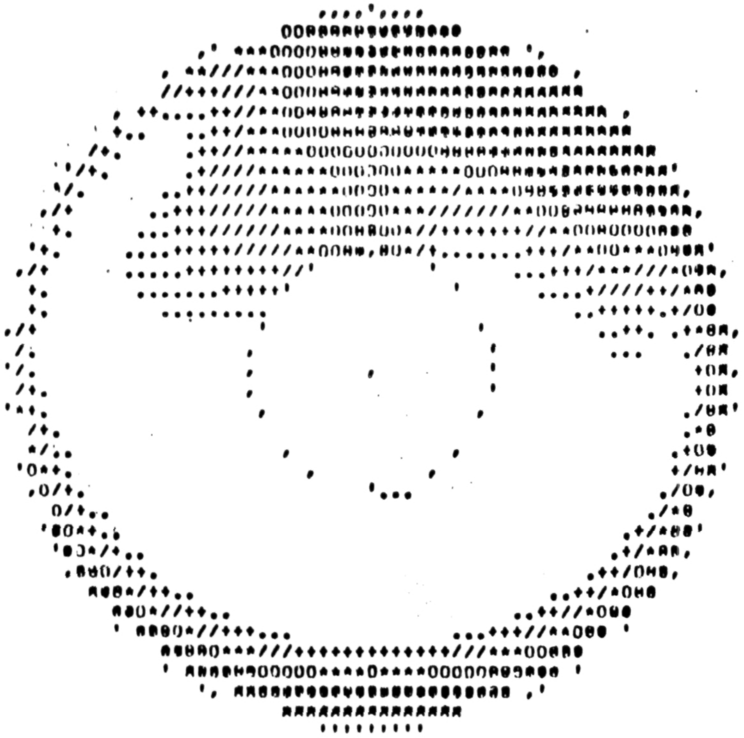

```
                              COMPRESSOR FACE TOTAL PRESSURE PROBE RECOVERIES

                                               RAKE  (DEG)

                              RING      0.     45.     90.    135.    180.    225.    270.    315.

                              .445    .920    .974    .979    .978    .974    .984    .983    .948

                              .614    .922    .936    .982    .983    .975    .970    .982    .949

                              .745    .902    .896    .972    .983    .970    .977    .978    .963

                              .856    .901    .883    .979    .952    .918    .952    .981    .982

                              .955    .909    .882    .901    .914    .877    .900    .953    .957


                              IDC1    IDC2    IDC3    IDC4    IDC5    IDCI    IDCO    IDC
                              .050    .043    .063    .064    .037    .046   ,.051    .051

                              IDR1    IDR2    IDR3    IDR4    IDR5    IDR
                             -.021   -.015   -.008    .005    .039    .039

                              KTHE  KRA2(3) KA2(3) KRA2(3T) KA2(3T) B1      B2      QAV     PAV
                               .192   .168   .471     .125     .317 1.657 1.000    .712  5.337


                                       RING AVERAGES
                             RING1   RING2   RING3   RING4   RING5              FACE AVERAGE
                              .967    .963    .955    .943    .911                   .948



PART-POINT= 181.300         PEAK DISTORTION MAP                 TIME= 0  33  816


           M       B       8       0       O       *       /       +       .      BLANK
             .890    .900    .910    .920    .930    .940    .950    .960    .970
```

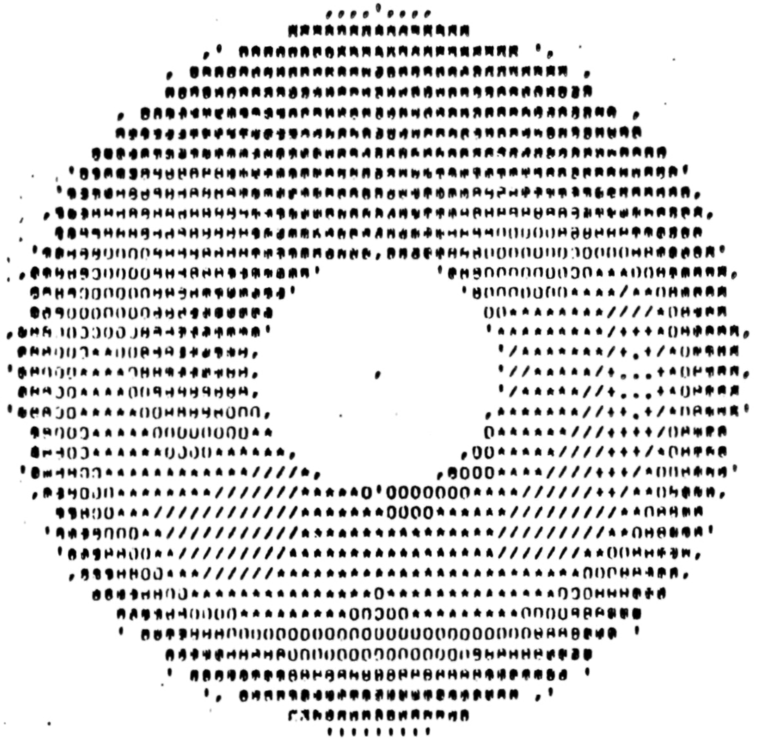

```
COMPRESSOR FACE TOTAL PRESSURE PROBE RECOVERIES

                    RAKE  (DEG)

RING      0.     45.     90.    135.    180.    225.    270.    315.

.445    .886    .945    .978    .967    .962    .990    .916    .916

.614    .887    .934    .987    .988    .959    .991    .928    .928

.745    .880    .894   1.029    .975    .945    .982    .967    .928

.856    .879    .886    .931    .940    .921    .935    .954    .915

.955    .865    .886    .875    .910    .882    .891    .921    .899


IDC1    IDC2    IDC3    IDC4    IDC5    IDCI    IDCO    IDC
.063    .068    .075    .044    .029    .066    .036    .066

IDR1    IDR2    IDR3    IDR4    IDR5    IDR
-.015   -.020   -.020   .012    .043    .043

KTHE   KRA2(3) KA2(3) KRA2(3T) KA2(3T) B1      B2      QAV     PAV
 .264    .145   .504     .130     .394 1.657  1.000    .689  5.293


        RING AVERAGES
RING1   RING2   RING3   RING4   RING5                FACE AVERAGE
 .945    .950    .950    .920    .891                    .931


PART-POINT= 184.300        PEAK DISTORTION MAP               TIME=11  31  785


      M       #       8       H       0       *       /       +       .      BLANK
         .880    .900    .920    .940    .960    .980   1.000   1.020   1.040
```

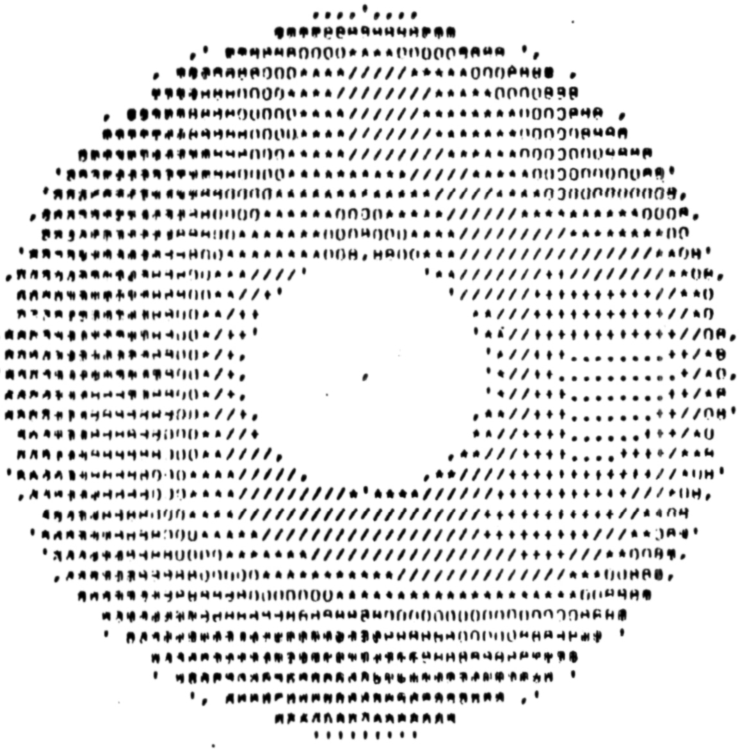

```
COMPRESSOR FACE TOTAL PRESSURE PROBE RECOVERIES

                      RAKE  (DEG)

RING     0.      45.      90.     135.     180.     225.     270.     315.

.445    .917    .935    .939    .937    .934    .932    .923    .928

.614    .932    .930    .956    .944    .920    .923    .895    .906

.745    .935    .916    .956    .938    .892    .908    .899    .889

.856    .931    .911    .948    .917    .885    .898    .887    .891

.955    .899    .905    .916    .898    .873    .888    .868    .894


IDC1    IDC2    IDC3    IDC4    IDC5    IDCI    IDCO    IDC
.015    .033    .030    .026    .027    .024    .026    .026

IDR1    IDR2    IDR3    IDR4    IDR5    IDR
-.017   -.012   -.002   .007    .024    .024

KTHE  KRA2(3) KA2(3) KRA2(3T) KA2(3T) B1      B2      QAV     PAV
 .205   .188    .845     .143      .348 3.400  1.000    .550  6.191

          RING AVERAGES
RING1  RING2  RING3  RING4  RING5                  FACE AVERAGE
 .931   .926   .917   .908   .893                       .915


PART-POINT= 195.500         PEAK DISTORTION MAP              TIME=15   8  207


         M        B        ■        H        O        *        /        +        .        BLANK
           .880     .890     .900     .910     .920     .930     .940     .950     .960
```

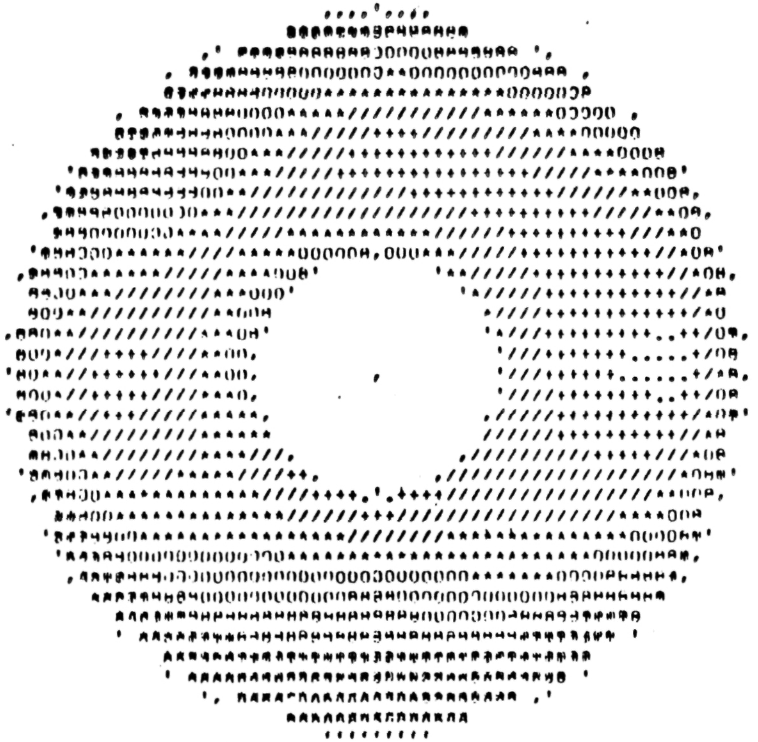

```
                    COMPRESSOR FACE TOTAL PRESSURE PROBE RECOVERIES

                                    RAKE  (DEG)

RING       0.       45.       90.      135.      180.      225.      270.      315.

.445     .933      .937      .938      .936      .931      .932      .924      .926

.614     .944      .941      .949      .930      .908      .921      .942      .927

.745     .933      .937      .952      .921      .898      .916      .946      .904

.856     .916      .922      .949      .903      .882      .901      .931      .900

.955     .898      .912      .908      .900      .868      .874      .908      .889


IDC1     IDC2      IDC3      IDC4      IDC5      IDCI      IDCO      IDC
.009     .027      .030      .034      .029      .018      .032      .032

IDR1     IDR2      IDR3      IDR4      IDR5      IDP
-.014    -.014     -.007     .007      .027      .027

KTHE   KRA2(3) KA2(3) KRA2(3T) KA2(3T) H1      B2       QAV     PAV
 .127    .181    .741    .134       .261  3.400  1.000     .556  6.191


          RING AVERAGES
RING1   RING2   RING3   RING4   RING5                  FACE AVERAGE
 .932    .933    .926    .913    .895                       .920
```

```
PART-POINT= 196.300          PEAK DISTORTION MAP                TIME=20  34  112


       A          H          #          B          0          *          /          +          .          BLANK
            .880       .890       .900       .910       .920       .930       .940       .950       .960
```

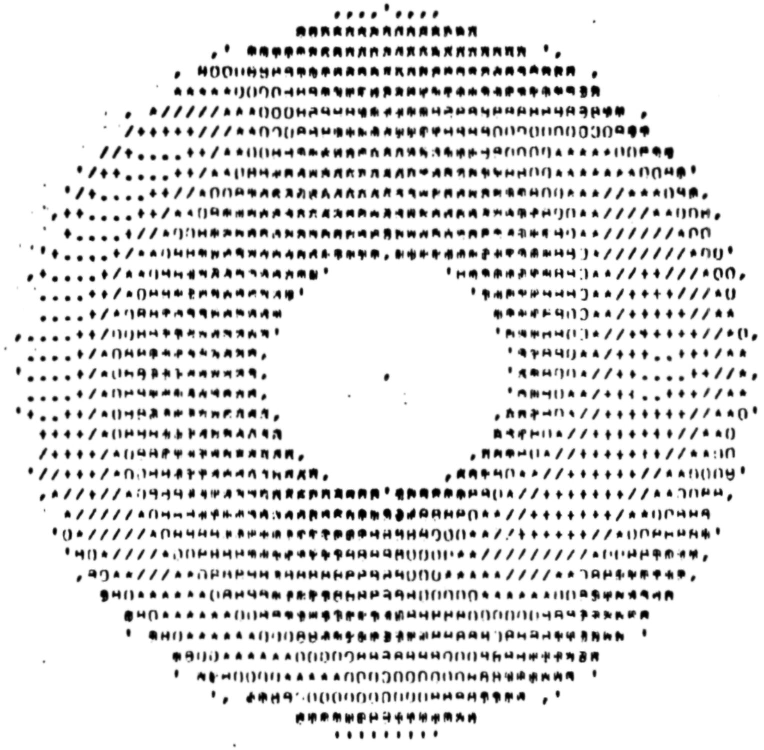

```
                                         COMPRESSOR FACE TOTAL PRESSURE PROBE RECOVERIES

                                                    RAKE  (DEG)

                                        RING    0.      45.     90.     135.    180.    225.    270.    315.

                                        .445    .882    .892    .905    .917    .904    .873    .886    .882

                                        .614    .878    .899    .941    .947    .904    .898    .897    .895

                                        .745    .893    .927    .953    .929    .893    .912    .916    .937

                                        .856    .870    .922    .944    .891    .918    .929    .951    .954

                                        .955    .862    .895    .929    .882    .896    .898    .958    .937


                                        IDC1    IDC2    IDC3    IDC4    IDC5    IDCI    IDCO    IDC
                                        .021    .032    .030    .057    .050    .027    .054    .054

                                        IDR1    IDR2    IDR3    IDR4    IDR5    IDR
                                        .019    .003   -.011   -.014    .003    .019

                                        KTHE  KRA2(3) KA2(3) KRA2(3T) KA2(3T) B1      B2       QAV     PAV
                                         .196   .378  1.481     .135      .331  3.400  1.000    .563   6.322

                                                RING AVERAGES
                                       RING1  RING2  RING3  RING4  RING5                FACE AVERAGE
                                        .893   .908   .920   .923   .907                      .910


PART-POINT= 200.300          PEAK DISTORTION MAP                     TIME= 0    7   19


          ■       ■       ●       ■       0       *       /       +       .       BLANK
            .880    .890    .900    .910    .920    .930    .940    .950    .960
```

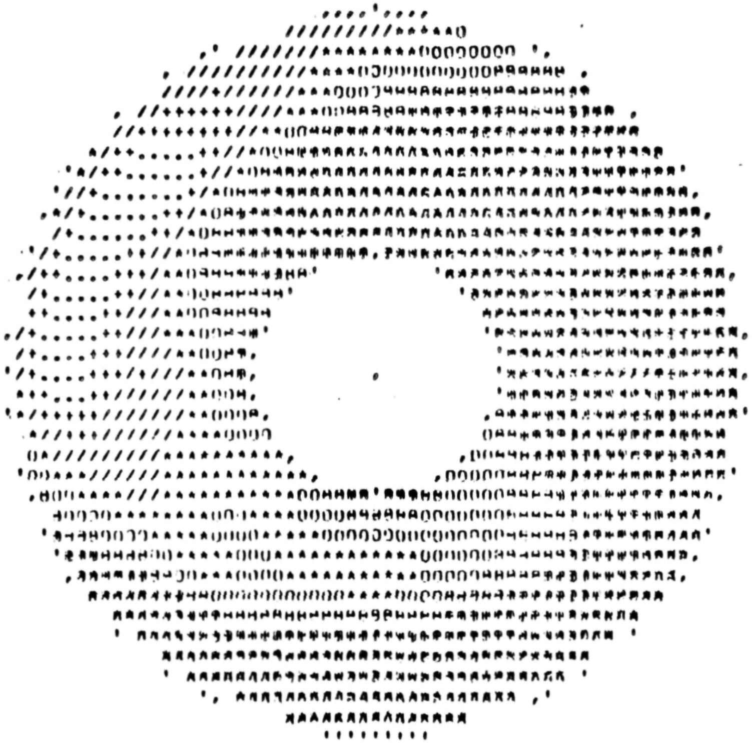

```
              COMPRESSOR FACE TOTAL PRESSURE PROBE RECOVERIES

                              RAKE  (DEG)

RING      0.       45.      90.     135.     180.     225.     270.     315.

.445     .878     .894     .893     .924     .925     .934     .927     .905

.614     .882     .891     .891     .915     .931     .928     .951     .920

.745     .917     .890     .899     .909     .897     .931     .953     .964

.856     .930     .903     .905     .900     .889     .899     .968     .963

.955     .943     .897     .890     .886     .880     .886     .949     .944


IDC1     IDC2     IDC3     IDC4     IDC5     IDCI     IDCO     IDC
.034     .035     .033     .033     .033     .035     .033     .035

IDR1     IDR2     IDR3     IDR4     IDR5     IDR
.005     .001    -.006    -.006     .006     .006

KTHE  KRA2(3) KA2(3) KRA2(3T) KA2(3T) B1      B2       QAV     PAV
 .338   .327  1.450     .046      .384 3.400  1.000     .561  6.309

         RING AVERAGES
RING1   RING2   RING3   RING4   RING5                FACE AVERAGE
 .910    .914    .920    .920    .909                     .915
```

```
PART-POINT= 205.300          PEAK DISTORTION MAP                TIME=36  13  211


           M       [illegible]       [illegible]       8       0       *       /       +       .       BLANK
              .890      .900      .910      .920      .930      .940      .950      .960      .970
```

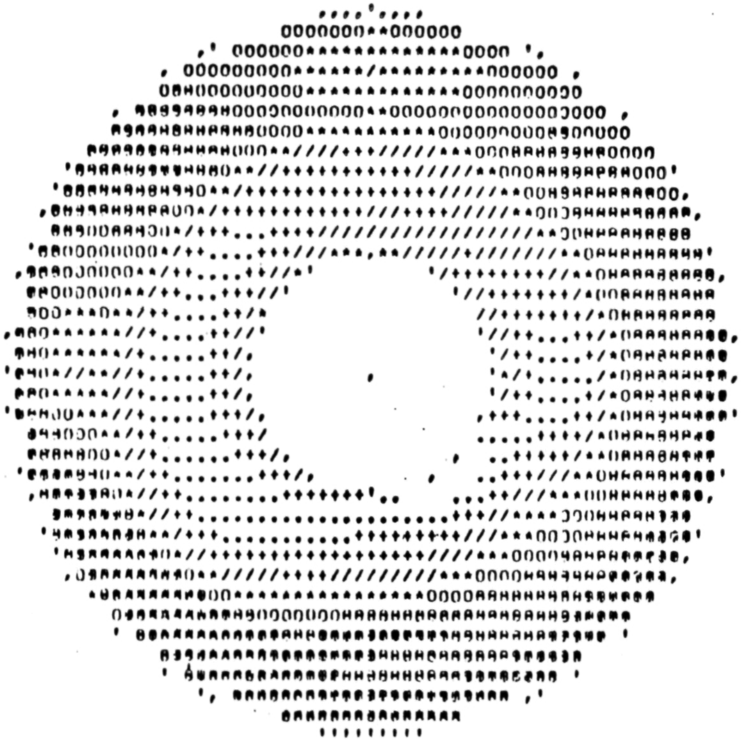

```
COMPRESSOR FACE TOTAL PRESSURE PROBE RECOVERIES

                      RAKE  (DEG)

RING     0.     45.     90.    135.    180.    225.    270.    315.

.445   .920   .920   .930   .931   .930   .934   .928   .929

.614   .921   .906   .929   .901   .906   .930   .930   .920

.745   .900   .885   .884   .889   .871   .901   .907   .879

.856   .911   .887   .883   .879   .884   .845   .907   .880

.955   .898   .898   .875   .874   .857   .883   .877   .885


IDC1   IDC2   IDC3   IDC4   IDC5   IDCI   IDCO   IDC
.009   .019   .020   .044   .027   .014   .036   .036

IDR1   IDR2   IDR3   IDR4   IDR5   IDR
-.031  -.020  .012   .017   .021   .021

KTHE  KRA2(3) KA2(3) KRA2(3T) KA2(3T) B1      B2     QAV    PAV
 .125   .361  3.036    .295      .420 8.056 1.000   .477  6.442


          RING AVERAGES
RING1  RING2  RING3  RING4  RING5              FACE AVERAGE
 .928   .918   .889   .884   .881                  .900


PART-POINT= 117.400        PEAK DISTORTION MAP              TIME=50  40  162
```

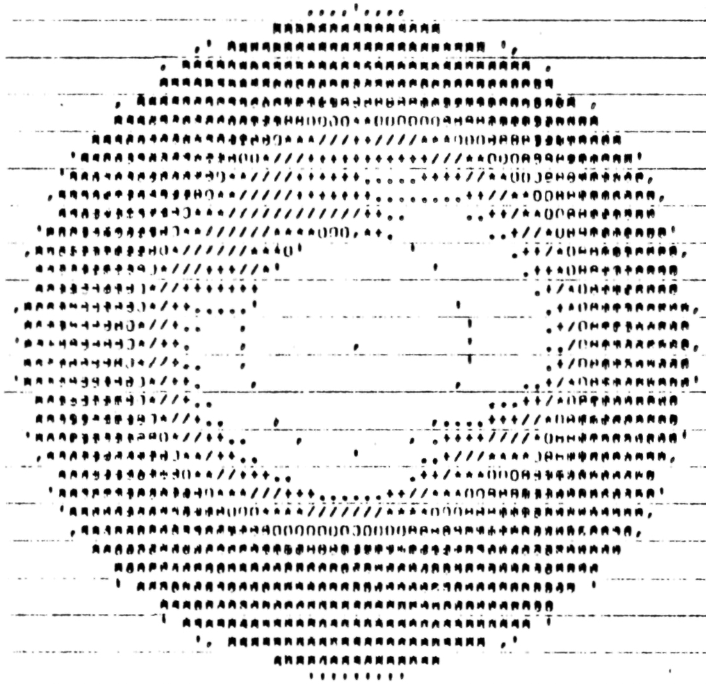

```
COMPRESSOR FACE TOTAL PRESSURE PROBE RECOVERIES

                         RAKE  (DEG)

RING      0.     45.     90.    135.    180.    225.    270.    315.
.445    .845    .876    .879    .836    .857    .856    .865    .830
.614    .840    .833    .846    .808    .798    .817    .830    .820
.745    .796    .809    .793    .788    .778    .791    .801    .761
.856    .770    .796    .787    .785    .776    .787    .802    .786
.955    .771    .781    .784    .784    .767    .778    .775    .772

IDC1    IDC2    IDC3    IDC4    IDC5    IDC1    IDCO    IDC
.031    .032    .016    .020    .011    .032    .016    .032

IDR1    IDR2    IDR3    IDR4    IDR5    IDR
-.061   -.022   .019    .026    .037    .037

KTHE  KRA2(3) KA2(3) KRA2(3T) KA2(3T) B1      B2      QAV    PAV
 .133   .555  4.812     .532     .666  8.426  1.000    .439  6.756

           RING AVERAGES
RING1   RING2   RING3   RING4   RING5              FACE AVERAGE
.855    .824    .791    .786    .777                   .807

PART-POINT=  97.600          PEAK DISTORTION MAP                TIME=53  10  295

             M        A        #        B        0        *        /        +        .        BLANK
                 .780     .790     .800     .810     .820     .830     .840     .850     .860
```

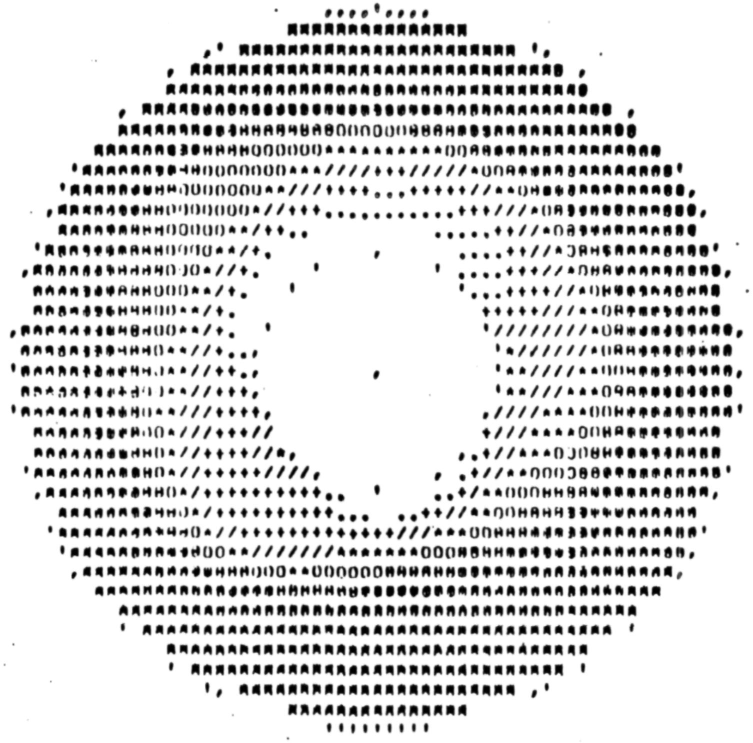

```
                    COMPRESSOR FACE TOTAL PRESSURE PROBE RECOVERIES

                                  RAKE  (DEG)

RING      0.     45.     90.    135.    180.    225.    270.    315.

.445    .909    .905    .881    .880    .893    .895    .889    .904

.614    .879    .876    .875    .849    .846    .889    .864    .861

.745    .843    .833    .847    .839    .822    .845    .844    .860

.856    .826    .827    .844    .832    .818    .826    .839    .836

.955    .825    .832    .838    .828    .812    .817    .836    .818


IDC1    IDC2    IDC3    IDC4    IDC5    IDCI    IDCO    IDC
.017    .025    .023    .016    .016    .021    .016    .026

IDR1    IDR2    IDR3    IDR4    IDR5    IDR
-.050   -.018   .012    .025    .031    .031

KTHE  KRA2(3) KA2(3) KRA2(3T) KA2(3T) B1      B2      QAV     PAV
 .118   .479  4.158    .440      .559 8.426  1.000    .462  6.776


           RING AVERAGES
RING1   RING2   RING3   RING4   RING5               FACE AVERAGE
.895    .867    .842    .831    .826                    .852
```

```
PART-POINT=  98,300          PEAK DISTORTION MAP                 TIME= 2  23  160


         R       B       8       H       O       *       /       +       '     BLANK
           .830    .840    .850    .860    .870    .880    .890    .900    .910
```

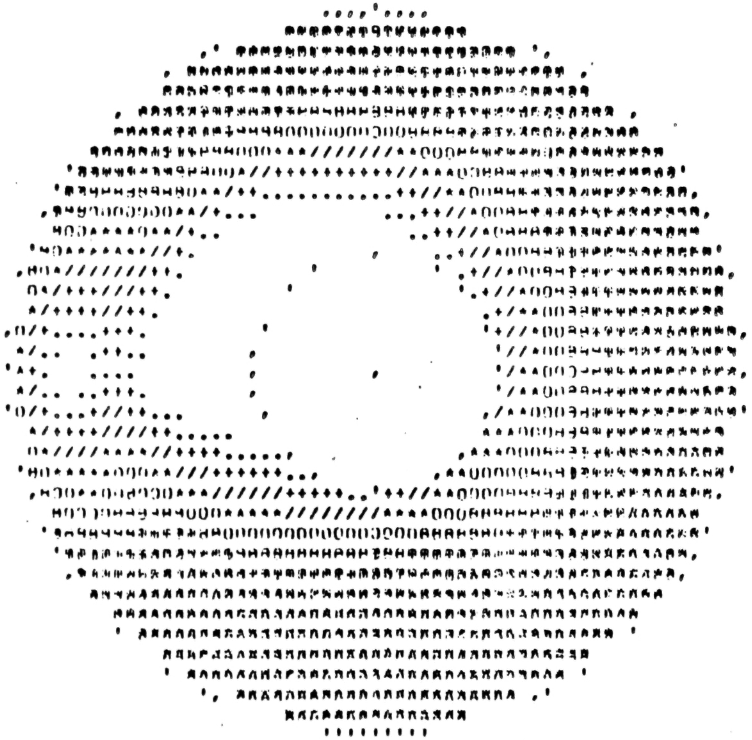

```
                   COMPRESSOR FACE TOTAL PRESSURE PROBE RECOVERIES

                                  RAKE  (DEG)

RING      0.      45.      90.     135.     180.     225.     270.     315.

.445    .903     .838     .825     .807     .808     .860     .934     .935

.614    .847     .771     .780     .774     .740     .798     .911     .876

.745    .779     .751     .751     .749     .726     .741     .883     .790

.856    .765     .751     .743     .730     .728     .735     .914     .760

.955    .704     .750     .747     .741     .722     .743     .948     .741


IDC1    IDC2     IDC3     IDC4     IDC5     IDCI     IDC0     IDC
.071    .091     .057     .048     .047     .081     .047     .081

IDR1    IDR2     IDR3     IDR4     IDR5     IDR
-.087   -.022    .029     .036     .044     .044

KTHE  KRA2(3) KA2(3) KRA2(3T) KA2(3T) H1      H2       QAV      PAV
 .853   .700  6.755     .724    1.577  8.426  1.000     .442   6.801

           RING AVERAGES
RING1   RING2   RING3   RING4   RING5                  FACE AVERAGE
 .864    .812    .771    .766    .760                      .795


PART-POINT= 104.300          PEAK DISTORTION MAP                 TIME=56  12  539


          M        8        $        A        0        *        /        +        .        BLANK
              .740     .760     .780     .800     .820     .840     .860     .880     .900
```

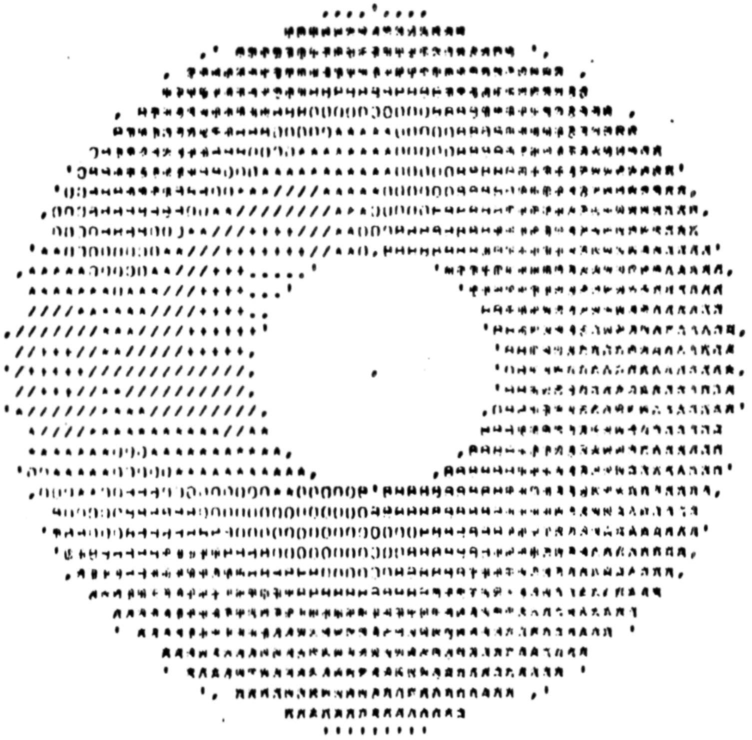

```
COMPRESSOR FACE TOTAL PRESSURE PROBE RECOVERIES

                       RAKE  (DEG)

RING      0.     45.     90.    135.    180.    225.    270.    315.

.445    .868    .848    .842    .853    .863    .870    .849    .902

.614    .874    .845    .823    .844    .856    .857    .889    .876

.745    .867    .839    .829    .832    .834    .843    .884    .847

.856    .846    .838    .820    .823    .833    .846    .897    .838

.955    .837    .833    .815    .820    .822    .829    .891    .851


IDC1    IDC2    IDC3    IDC4    IDC5    IDCI    IDCO    IDC
.029    .041    .021    .026    .026    .035    .026    .035

IDR1    IDR2    IDR3    IDR4    IDR5    IDR
-.019   -.009   .004    .009    .015    .015

KTHF   KRA2(3) KA2(3) KRA2(3T) KA2(3T) B1       B2       UAV      PAV
 .350    .260  2.542     .177      .527  8.426  1.000    .482  7.036


          RING AVERAGES
RING1   RING2   RING3   RING4   RING5                  FACE AVERAGE
.867    .858    .847    .842    .837                        .850


PART-POINT= 107.300          PEAK DISTORTION MAP                  TIME=30  29  388


          M         A         B         H         O         *         /         +         .         BLANK
              .830      .840      .850      .860      .870      .880      .890      .900      .910
```

Page intentionally left blank

Page intentionally left blank

APPENDIX C

PRATT AND WHITNEY DISTORTION METHODOLOGY

The P&WA distortion calculation procedure produces two primary distortion indices, K_{a_2} and K_{c_2}. K_{a_2} is the engine fan distortion index and consists of both radial, K_{ra_2}, and circumferential, K_θ, distortion. In equation form

$$K_{a_2} = K_\theta + bK_{ra_2}$$

where b is a factor that permits the fan circumferential and fan radial distortion to be considered on a common basis. K_{c_2} is the engine high-compressor distortion index and is a measure of the circumferential distortion of the core air that passes through the high compressor. The radial distortion in the inlet flow is attenuated as it passes through the fan and the flow entering the high-compressor has no radial distortion; hence, K_{c2} has no radial component.

The calculation procedure for each of the distortion indices (K_θ, K_{ra_2}, K_{a_2}, K_{c_2}) is described below. The steady-state data used in these calculations are obtained with 40 (8 rakes x 5 rings) compressor-face total-pressure probes located on centroids of equal area as shown in Figure C-1. The nomenclature given in Figure C-1 is used in the following description.

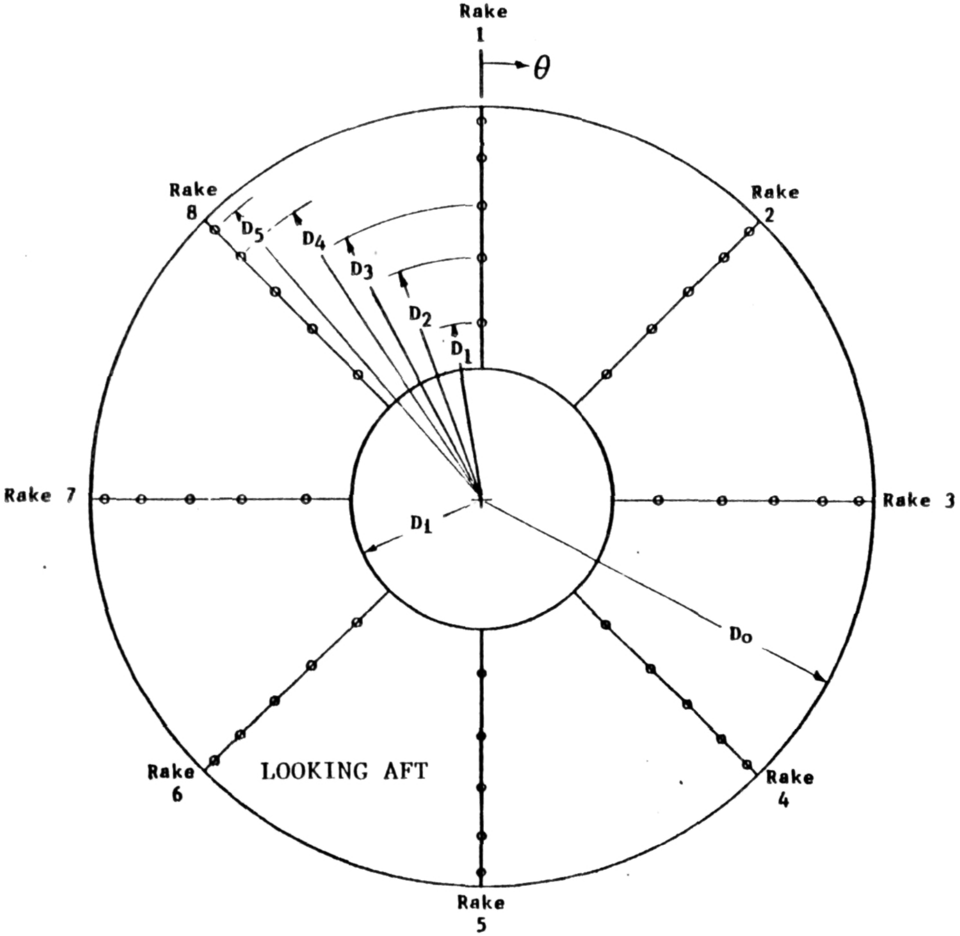

I	P&WA Distortion Computation Plane D_I (Inches)
1	2.325
2	3.204
3	3.888
4	4.470
5	4.983
D_o	5.220
D_i	1.728
AREA	19.056 in.^{2}

Figure C-1 Computation Plane Nomenclature

Fan Circumferential Distortion, K_θ

The P&WA engine specification requires the evaluation of the first 10 Fourier coefficients for calculating circumferential distortion. However, the following will be a rapid procedure evaluating only the first 3 coefficients.

1. For each test point, the 40 compressor-face pressures are obtained. Starting with Ring 1, form the products $(P_{t2}/P_{to})\cos\theta$ and $(P_{t2}/P_{to})\sin\theta$ for each probe in the ring. θ is the rake angle measured from Rake 1. Note that θ is always an integer multiple of 45°.

2. Use the products of Step 1 to obtain the Fourier coefficients a_1 and b_1:

$$\frac{a_1}{P_{t_o}} = 1/4 \sum_{I=1}^{8} \left(\frac{P_{t2}}{P_{to}}\right)_I \cos\theta_I$$

$$\frac{b_1}{P_{to}} = 1/4 \sum_{I=1}^{8} \left(\frac{P_{t2}}{P_{to}}\right)_I \sin\theta_I$$

where I is the rake designation.

3. Then

$$\frac{A_1}{P_{to}} = \left[\left(\frac{a_1}{P_{to}}\right)^2 + \left(\frac{b_1}{P_{to}}\right)^2\right]^{\frac{1}{2}}$$

4. Repeat Steps 1 and 2 substituting $N\theta$ (i.e., 2θ and 3θ) for θ to obtain a_2, b_2 and a_3, b_3. Then compute A_N/P_{to} as done in Step 3 (where previously, $N = 1$). Divide the quantity A_N/P_{to} by N^2 to yield A_N/N^2P_{to}. The largest value of A_N/N^2P_{to} for the ring is designated $A_N/N^2P_{to})_{max}$ and retained.
5. Repeat Steps 1 through 4 for each ring.
6. For each ring form the product $A_N/N^2P_{to})_{max}\left(1/D\right)$ and sum over all rings to obtain

$$\sum_{J=1}^{5} \left[\left(\frac{A_N}{N^2 P_{to}} \right)_{max} \right]_J \frac{1}{D_J}$$

   where J is the ring designation and values for D_J are presented in Figure C-1.
7. Obtain the sum of $1/D_J$ to obtain

$$\sum_{J=1}^{5} \frac{1}{D_J}$$

8. Obtain the average pressure for each ring

$$\bar{P}_{t_{2_r}}/P_{to})_J = 1/8 \sum_{I=1}^{8} (P_{t_2}/P_{to})_{I,J}$$

   and the average pressure for the compressor-face

$$\bar{P}_{t_2}/P_{to} = 1/5 \sum_{J=1}^{5} (\bar{P}_{t_{2_r}}/P_{to})_J$$

9. Calculate the percent corrected airflow

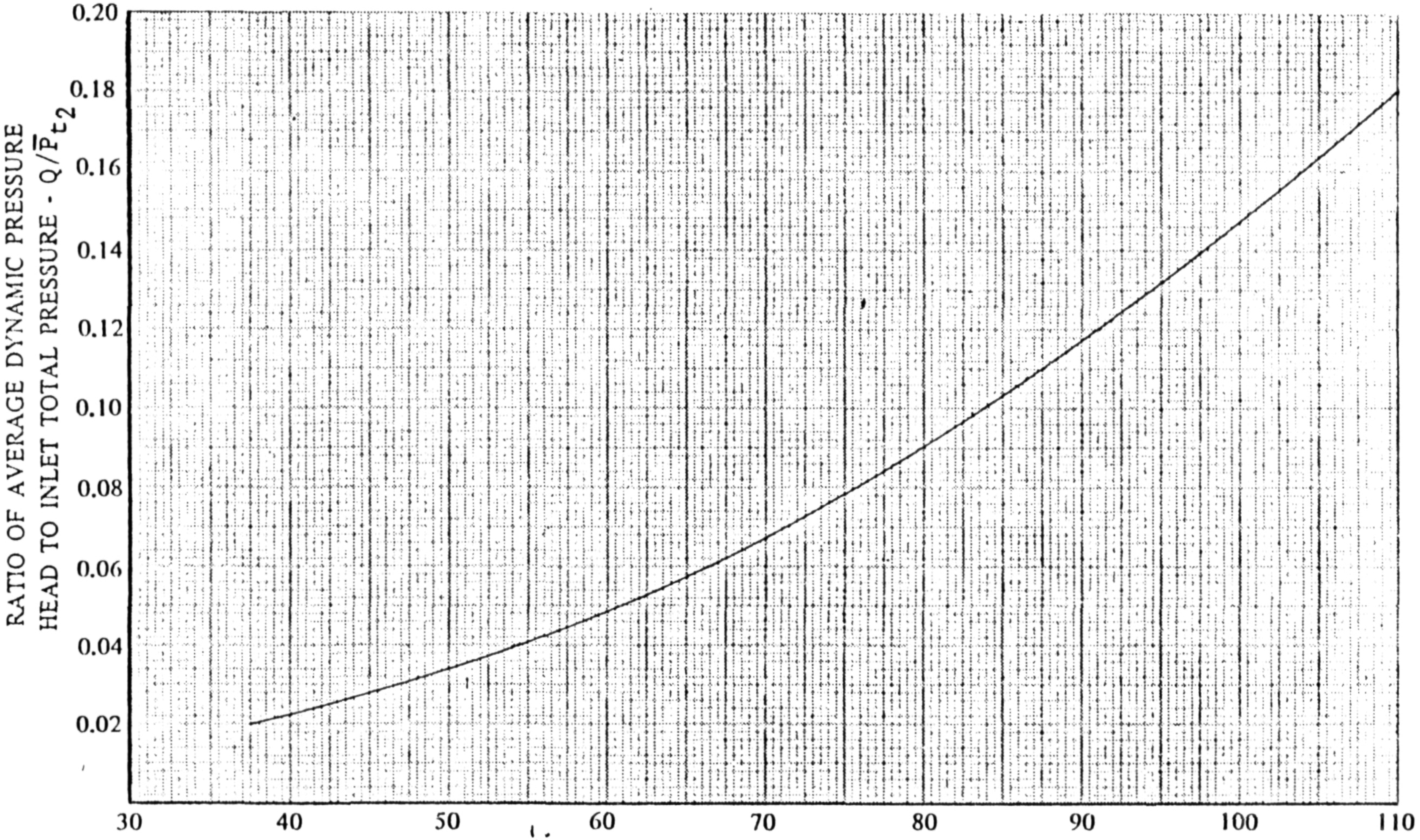

% Engine Airflow, $\%W_{c2} = \frac{W\sqrt{\theta_{t2}}}{\delta_{t2}} \left(\frac{100}{217}\right)$

Figure C-2 Estimated Variation in Ratio of Average Dynamic Pressure Head to Inlet Total-Pressure

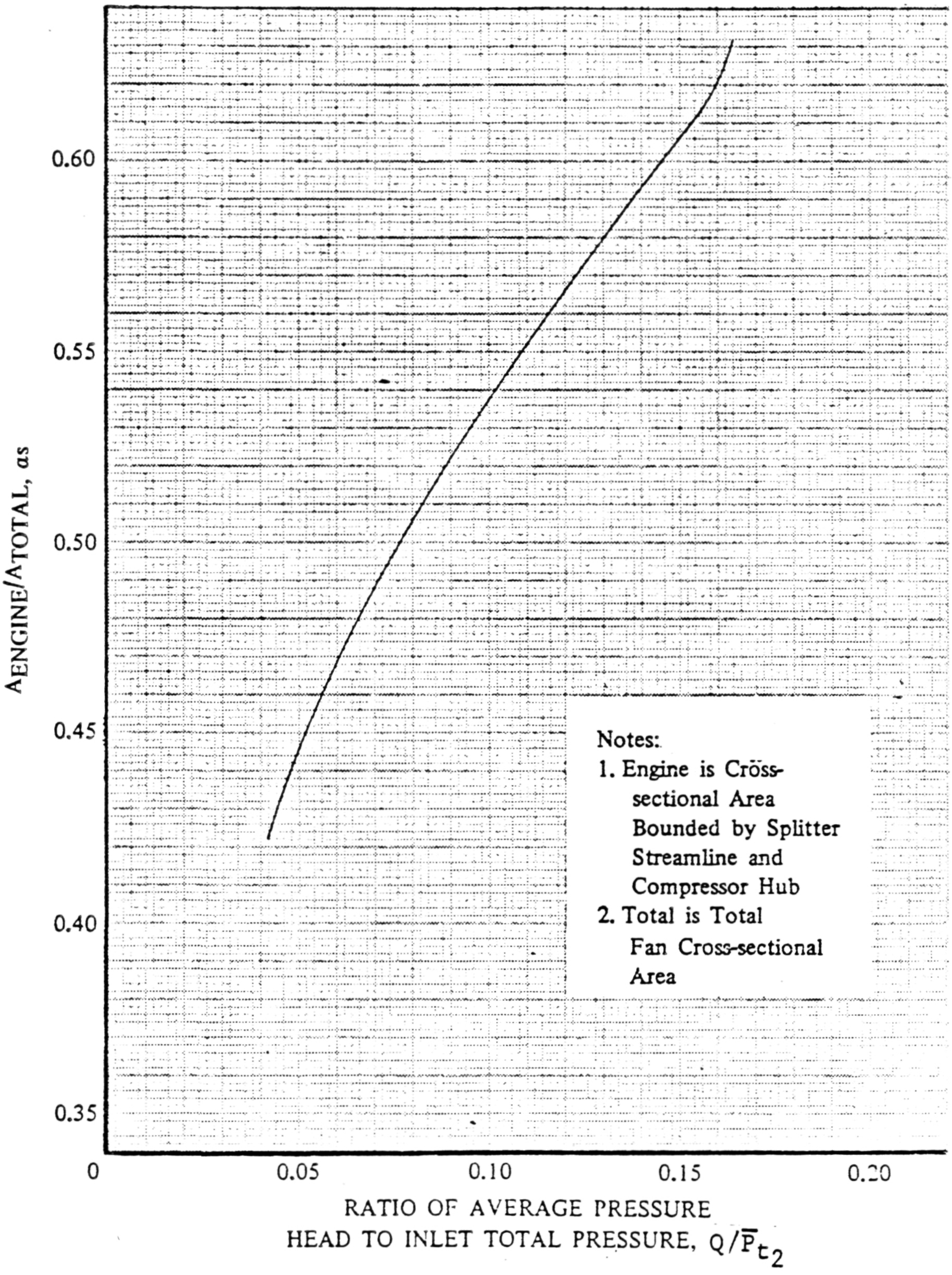

Notes:
1. Engine is Cross-sectional Area Bounded by Splitter Streamline and Compressor Hub
2. Total is Total Fan Cross-sectional Area

Figure C-3 Ratio of High-Compressor Airflow to Total Engine Airflow

$$\%W_{c_2} = W_{c_2} \left(\frac{100}{217}\right)$$

Enter Figure C-2 with $\%W_{c_2}$ to obtain $Q/\bar{P}_{t2}$.

10. Calculate K_θ using the results of Steps 6 through 9:

$$K_\theta = \frac{\sum_{J=1}^{5} \left[\left(\frac{A_N}{N^2 P_{to}} \right)_{MAX} \right]_J \frac{1}{D_J}}{\left[\frac{\bar{P}_{t2}}{P_{to}} \right] \left(\frac{Q}{\bar{P}_{t2}} \right) \sum_{J=1}^{5} \frac{1}{D_J}}$$

High-Compressor Circumferential Distortion, K_{c_2}

11. Using $Q/\bar{P}_{t_2}$, obtain α_s from Figure C-3. Then calculate the splitter diameter

$$D_S = \left[\alpha_s \left(D_o^2 - D_i^2\right) + D_i^2 \right]^{\frac{1}{2}}$$

where D_i and D_o are given in Figure C-1.

12. Calculate K_{θ_S} using values for only those rings having a diameter less than or equal to the splitter diameter, D_S:

$$K_{\theta_S} = \frac{\sum_{J=1}^{S} \left[\left(\frac{A_N}{N^2 P_{to}} \right)_{\text{max within S}} \right]_J \frac{1}{DJ}}{\left[\frac{1}{S} \sum_{J=1}^{S} \left(\frac{\bar{P}_{t2_r}}{P_{to}} \right)_J \right] \frac{Q}{\bar{P}_{t_2}} \left[\sum_{J=1}^{S} \frac{1}{D_J} \right]}$$

where S = number of rings having a diameter less than or equal to the splitter diameter.

13. For each ring having a diameter less than or equal to D_S, normalize each pressure in the ring with the ring average:

$$\left.\frac{P_{t_2}}{\bar{P}_{t_{2_r}}}\right)_{I,J} = \left.\frac{P_{t_2}}{P_{to}}\right)_{I,J} \Bigg/ \left.\bar{P}_{t_{2_r}}/P_{to}\right)_J$$

14. Linearly curve fit $\left.P_{t_2}/\bar{P}_{t_{2_r}}\right)_{I,J}$ vs. θ for each ring whose diameter is less than or equal to D_S. Obtain θ^- for each ring. θ^- is equal to the greatest circumferential extent where $\left.P_{t_2}/\bar{P}_{t_{2_r}}\right)_{I,J} \leq 1.0$.

    If there are two regions of low $\left.P_{t_2}/\bar{P}_{t_{2_r}}\right)_{I,J}$ separated by 25° or less, they are to be treated as one low-pressure region.

15. Using the largest value of θ^- from the applicable rings, K_{c_2} is computed as

$$K_{c_2} = K_{\theta_S} \left(\frac{180^\circ}{\theta^-}\right)$$

Fan Radial Distortion, K_{ra_2}

16. Normalize each ring average pressure by the compressor face average to establish the radial profile.

$$\left.\frac{\bar{P}_{t2_r}}{P_{t2}}\right)_J = \left.\frac{\bar{P}_{t_{2_r}}}{P_{t_o}}\right)_J \div \frac{\bar{P}_{t_2}}{P_{t_o}}$$

17. Enter Table C-1 with $\%W_{c_2}$ to obtain the base-radial-profile, $\left.P_{t_{2_r}}/\bar{P}_{t_2}\right)_{\text{base } J}$, for each ring.

18. For each ring, compute

$$\left| \left.\frac{\bar{P}_{t2_r}}{\bar{P}_{t2}}\right)_J - \left.\frac{\bar{P}_{t_{2_r}}}{\bar{P}_{t_2}}\right)_{\text{base } J} \right| \frac{1}{\left.\bar{P}_{t2_r}/\bar{P}_{t_2}\right)_{\text{base } J}} \frac{1}{D_J}$$

19. Then compute K_{ra_2},

$$K_{ra_2} = \frac{\displaystyle\sum_{J=1}^{5} \left| \left.\frac{\bar{P}_{t2_r}}{\bar{P}_{t2}}\right)_J - \left.\frac{\bar{P}_{t2_r}}{\bar{P}_{t_2}}\right)_{\text{base } J} \right| \frac{1}{\left.\bar{P}_{t_2}/\bar{P}_{t_2}\right)_{\text{base } J}} \frac{1}{D_J}}{\left(Q/\bar{P}_{t_2}\right) \displaystyle\sum_{J=1}^{5} \frac{1}{D_J}}$$

Table C-1

CIVV, B, AND BASE-RADIAL-PROFILE FROM
P&WA TIME-VARIANT DISTORTION DECK CCD 1087-1.2
(Page 1 of 3)

D_1 - inner ring
D_5 - outer ring

			- BASE-RADIAL-PROFILE -				
$\%W_{c_2}$	CIVV ANGLE	B	D_1	D_2	D_3	D_4	D_5
63.0	-25.0	23.5123	0.9831	0.9923	1.0108	1.0103	1.0057
63.5	-25.0	22.8148	0.9829	0.9923	1.0108	1.0103	1.0057
64.0	-25.0	22.1173	0.9828	0.9923	1.0108	1.0103	1.0057
64.5	-25.0	21.4198	0.9827	0.9923	1.0108	1.0103	1.0057
65.0	-25.0	22.7222	0.9826	0.9923	1.0108	1.0102	1.0056
65.5	-25.0	20.0247	0.9825	0.9923	1.0108	1.0102	1.0056
66.0	-25.0	19.3272	0.9824	0.9924	1.0108	1.0102	1.0056
66.5	-25.0	18.6296	0.9823	0.9924	1.0108	1.0102	1.0056
67.0	-25.0	17.9321	0.9822	0.9924	1.0108	1.0102	1.0055
67.5	-25.0	17.3225	0.9821	0.9924	1.0108	1.0102	1.0055
68.0	-25.0	16.7130	0.9820	0.9924	1.0108	1.0102	1.0055
68.5	-25.0	16.1034	0.9821	0.9925	1.0108	1.0102	1.0054
69.0	-25.0	15.4938	0.9822	0.9926	1.0109	1.0101	1.0054
69.5	-25.0	14.8843	0.9823	0.9927	1.0109	1.0101	1.0051
70.0	-25.0	14.2747	0.9824	0.9928	1.0110	1.0100	1.0050
70.5	-25.0	13.6651	0.9824	0.9930	1.0109	1.0100	1.0049
71.0	-25.0	13.0556	0.9824	0.9932	1.0107	1.0100	1.0047
71.5	-25.0	12.5224	0.9824	0.9934	1.0106	1.0099	1.0046
72.0	-25.0	11.9893	0.9825	0.9936	1.0105	1.0099	1.0045
72.5	-25.0	11.4562	0.9825	0.9937	1.0105	1.0098	1.0046
73.0	-25.0	10.9231	0.9826	0.9938	1.0105	1.0097	1.0047
73.5	-25.0	10.4237	0.9827	0.9940	1.0105	1.0096	1.0049
74.0	-25.0	9.9467	0.9828	0.9941	1.0105	1.0095	1.0050
74.5	-25.0	9.4697	0.9837	0.9946	1.0101	1.0093	1.0042
75.0	-25.0	8.9927	0.9846	0.9951	1.0097	1.0090	1.0035
75.5	-25.0	8.5185	0.9855	0.9956	1.0094	1.0087	1.0027
76.0	-25.0	8.0556	0.9865	0.9961	1.0090	1.0085	1.0020
76.5	-25.0	7.1930	0.9867	0.9962	1.0089	1.0082	1.0018
77.0	-25.0	6.5000	0.9870	0.9963	1.0087	1.0080	1.0017
77.5	-25.0	5.8947	0.9872	0.9964	1.0086	1.0078	1.0016

Table C-1

CIVV, B, AND BASE-RADIAL-PROFILE FROM P&WA TIME-VARIANT DISTORTION DECK CCD 1087-1.2

(Page 2 of 3)

D_1 - inner ring
D_5 - outer ring

$\%W_{c_2}$	CIVV ANGLE	B	- BASE-RADIAL-PROFILE -				
			D_1	D_2	D_3	D_4	D_5
78.0	-25.0	5.4250	0.9875	0.9966	1.0085	1.0075	1.0015
78.5	-25.0	4.9012	0.9892	0.9985	1.0095	1.0050	0.9980
79.0	-25.0	4.4696	0.9910	1.0005	1.0105	1.0025	0.9945
79.5	-25.0	4.1245	1.0035	1.0120	1.0154	0.9950	0.9722
80.0	-25.0	3.8558	1.0160	1.0235	1.0204	0.9875	0.9498
80.5	-25.0	3.6943	1.0215	1.0260	1.0229	0.9811	0.9486
81.0	-25.0	3.6173	1.0270	1.0285	1.0254	0.9746	0.9474
81.5	-25.0	3.6957	1.0289	1.0295	1.0261	0.9727	0.9453
82.0	-25.0	6.2927	1.0299	1.0306	1.0268	0.9708	0.9432
82.5	-25.0	4.0035	1.0289	1.0298	1.0261	0.9717	0.9447
83.0	-24.8	3.2497	1.0273	1.0285	1.0250	0.9731	0.9470
83.5	-24.4	2.9708	1.0256	1.0270	1.0237	0.9748	0.9498
84.0	-23.9	2.8316	1.0241	1.0257	1.0225	0.9765	0.9524
84.5	-23.4	2.7409	1.0233	1.0250	1.0219	0.9773	0.9536
85.0	-22.9	2.7168	1.0226	1.0246	1.0215	0.9779	0.9545
85.5	-22.4	2.7016	1.0223	1.0244	1.0213	0.9783	0.9550
86.0	-22.0	2.5097	1.0225	1.0247	1.0215	0.9780	0.9544
86.5	-21.5	2.6609	1.0218	1.0242	1.0210	0.9787	0.9554
87.0	-21.0	2.6500	1.0214	1.0240	1.0208	0.9791	0.9560
87.5	-20.5	2.6266	1.0210	1.0237	1.0205	0.9795	0.9566
88.0	-20.0	2.6015	1.0206	1.0235	1.0202	0.9800	0.9571
88.5	-19.6	2.5759	1.0208	1.0236	1.0203	0.9798	0.9568
89.0	-19.1	2.5480	1.0208	1.0238	1.0204	0.9798	0.9566
89.5	-18.6	2.5138	1.0208	1.0240	1.0204	0.9798	0.9565
90.0	-18.1	2.4821	1.0208	1.0243	1.0205	0.9798	0.9564
90.5	-17.6	2.4480	1.0210	1.0244	1.0205	0.9796	0.9562
91.0	-17.1	2.4139	1.0211	1.0245	1.0205	0.9796	0.9560
91.5	-16.6	2.3677	1.0210	1.0244	1.0206	0.9797	0.9560
92.0	-16.0	2.3410	1.0206	1.0241	1.0206	0.9801	0.9562
92.5	-15.6	2.3222	1.0212	1.0247	1.0211	0.9795	0.9545

Table C-1
CIVV, B, AND BASE-RADIAL-PROFILE FROM P&WA TIME-VARIANT DISTORTION DECK CCD 1087-1.2
(Page 3 of 3)

D_1 - inner ring
D_5 - outer ring

$\%W_{c_2}$	CIVV ANGLE	B	- BASE-RADIAL-PROFILE -				
			D_1	D_2	D_3	D_4	D_5
93.0	-15.1	2.3238	1.0219	1.0254	1.0217	0.9788	0.9535
93.5	-14.7	2.2884	1.0226	1.0261	1.0223	0.9781	0.9521
94.0	-14.2	2.2730	1.0233	1.0268	1.0230	0.9774	0.9507
94.5	-13.7	2.2116	1.0251	1.0279	1.0226	0.9759	0.9488
95.0	-13.2	2.1276	1.0268	1.0289	1.0221	0.9742	0.9468
95.5	-12.7	2.0261	1.0285	1.0299	1.0217	0.9727	0.9449
96.0	-12.2	1.9267	1.0303	1.0309	1.0216	0.9715	0.9429
96.5	-11.7	1.8468	1.0344	1.0320	1.0213	0.9702	0.9409
97.0	-11.2	1.7738	1.0381	1.0332	1.0212	0.9690	0.9386
97.5	-10.7	1.7355	1.0412	1.0348	1.0216	0.9681	0.9356
98.0	-10.1	1.6694	1.0442	1.0363	1.0218	0.9672	0.9327
98.5	- 9.5	1.6387	1.0486	1.0376	1.0226	0.9639	0.9307
99.0	- 8.9	1.6083	1.0529	1.0391	1.0236	0.9600	0.9278
99.5	- 8.2	1.5906	1.0567	1.0410	1.0251	0.9555	0.9236
100.0	- 7.6	1.5319	1.0605	1.0436	1.0274	0.9511	0.9185
100.5	- 6.9	1.5098	1.0624	1.0454	1.0288	0.9494	0.9150
101.0	- 6.1	1.5746	1.0643	1.0469	1.0299	0.9478	0.9120
101.5	- 5.3	1.8660	1.0661	1.0478	1.0301	0.9466	0.9101
102.0	- 4.4	2.1176	1.0679	1.0482	1.0294	0.9458	0.9093
102.5	- 3.5	2.0926	1.0694	1.0475	1.0307	0.9448	0.9083
103.0	- 2.4	2.09442	1.0709	1.0481	1.0322	0.9433	0.9061
103.5	- 1.0	2.1291	1.0725	1.0507	1.0344	0.9410	0.9021
104.0	0	2.0926	1.0743	1.0536	1.0359	0.9386	0.8980
104.5	0	1.8973	1.0745	1.0537	1.0359	0.9382	0.8980
105.0	0	1.7234	1.0747	1.0538	1.0359	0.9379	0.8979
105.5	0	1.5677	1.0749	1.0538	1.0359	0.9376	0.8979
106.0	0	1.4275	1.0751	1.0539	1.0359	0.9373	0.8978
106.5	0	1.2656	1.0751	1.0539	1.0359	0.9373	0.8978
107.0	0	1.1202	1.0751	1.0539	1.0359	0.9373	0.8978
107.5	0	0.9793	1.0751	1.0539	1.0359	0.9373	0.8978
108.0	0	0.8519	1.0751	1.0539	1.0359	0.9373	0.8978
108.5	0	0.7381	1.0751	1.0539	1.0359	0.9373	0.8978

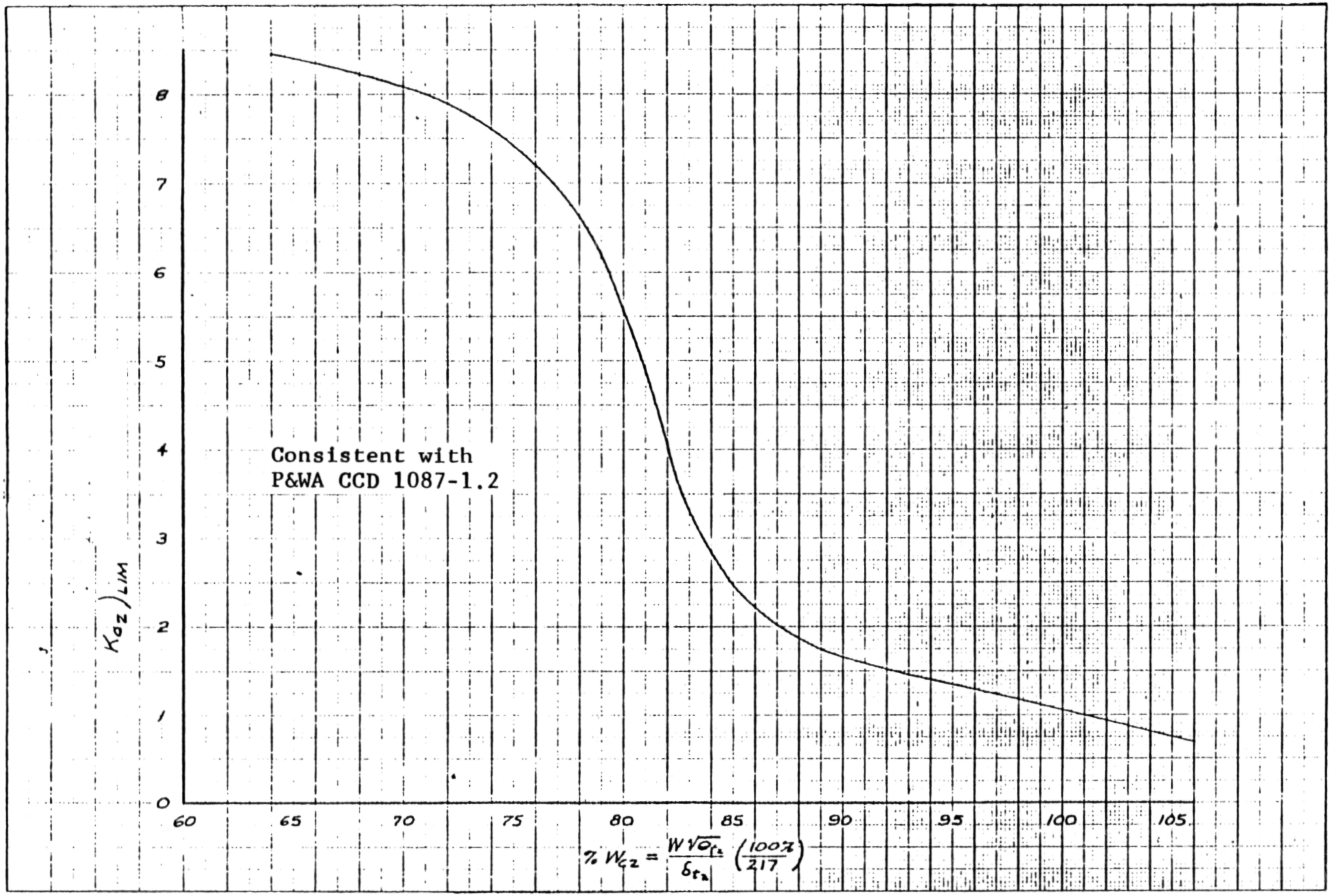

Figure C-4 K_{a_2} Screening Limit for P&WA Distortion Calculations

20. Enter Table C-1 with $\%W_{c2}$, obtain b, and compute K_{a2}.

$$K_{a_2} = K_\theta + bK_{ra_2}$$

21. Normalize K_{a2} from Step 20 by $K_{a2})_{limit}$ from Figure C-4 to obtain D_{x1}:

$$D_{x1} = \frac{K_{a_2}}{K_{a2})_{limit}}$$

22. Likewise normalize K_{c_2} from Step 15 by $K_{c_2})_{limit}$ from Table C-2 to obtain D_{x2}:

$$D_{x_2} = \frac{K_{c_2}}{K_{c_2})_{limit}}$$

Although the inlet/engine compatibility data is being obtained at the plane passing through the tip of the hub, the data is transferred on a one-for-one basis to centroids of equal area located at the leading edge of the inlet guide vanes. The correct diameters to be used in the foregoing distortion calculations are given in Figure C-1.

In the case that some probes are not working, it will be necessary to substitute values for the steady-state total pressures during the P&WA distortion computations. This is to be accomplished as follows:

1. If the missing value is associated with Rings 2, 3, or 4, then the average of the four surrounding probes is used.

2. If the missing value is associated with Rings 1 or 5, then the average of the three surrounding probes is used.
3. If two adjacent values are missing, then starting in a clockwise direction (looking aft) and working from the inner ring to the outer ring, use the adjacent 2 probes for Rings 1 and 5 and the adjacent 3 probes for Rings 2, 3, and 4.

Table C-2

HIGH-COMPRESSOR DISTORTION SCREENING LIMIT FOR F100(3)

Ref: P&WA Spec 2903B of 11-7-73, SCN 679

M_o	$K_{c_2})_{LIM}$
0	2.47
.2	2.24
.3	2.29
.4	2.10
.6	1.76
.9	1.47
1.2	1.80
1.4	1.85
1.6	1.90
1.8	2.37
2.0	3.13
2.2	4.05
2.3	4.25

REFERENCES

1. Cawthon, J. A.; Truax, P. P.; and Savage, T. M.: Advanced Inlet Study (Tailor-Mate II). Air Force Flight Dynamics Laboratory Report AFFDL-TR-73-72, June 1973.

2. Ammann, V. R.: Model and Test Information Report, 0.15-Scale F-16 Composite Inlet Model (Configuration VGI-Conformal IIIA), Test in NASA Ames Research Center 6- x 6-Foot Supersonic Wind Tunnel, July 1977. General Dynamics Fort Worth Division Report FZT-302, July 1977.

3. Garner, J. E.; and Lawrence, W. G.: High-Response Data Plan for the 0.15-Scale F-16 Variable-Geometry Inlet Test in the NASA/Ames 6- x 6-Foot Wind Tunnel. General Dynamics Fort Worth Division Report MR-P-389, 25 May 1977.

4. Savage, T. M.; and Ketter, F. C.: F-16 Internal Aerodynamic Design Data Report (USAF DI-S-3581/M). General Dynamics Fort Worth Division Report 16PR278, 15 April 1976.

2
10/15/81 ~~Myron Jaich 343/32/3647~~7
~~Post 260~~

16 JAN 86

11/7/88 Victoria Vernaw 069D/111/1/1831

MAR 13 1989

GENERAL DYNAMICS
Fort Worth Division

P.O. Box 748, Fort Worth, Texas 76101

McDONNELL DOUGLAS
RESEARCH & ENGINEERING LIBRARY
ST. LOUIS, MISSOURI

1100 13 OCT RECD